Investigation of delayed fluorescence phenomena in conjugated molecules using time-resolved laser spectroscopy

MURAT AYDEMIR

INVESTIGATION OF DELAYED FLUORESCENCE PHENOMENA IN CONJUGATED MOLECULES USING TIME-RESOLVED LASER SPECTROSCOPY

Murat Aydemir

Organic Electroactive Materials Research Group Department of Physics

University of Durham

A Thesis Submitted to the Faculty of Science for the Degree of Doctor of Philosophy

August 2016

INVESTIGATION OF DELAYED FLUORESCENCE PHENOMENA IN CONJUGATED MOLECULES USING TIME-RESOLVED LASER SPECTROSCOPY

Murat Aydemir

ABSTRACT

This thesis reports structure-property relationships in a range of conjugated molecules where the nature of the delayed fluorescence (DF) is used as a powerful diagnostic tool in order to gain insight into the nature of the molecules. All the investigations revolve around using three spectroscopic methods; steady state, single-photon counting and particularly time-resolved nanosecond spectroscopy.

The rarely observed optically generated geminate electron-hole (e-h) pair recombination is designated as the origin of DF in Rhodamine 6G and its derivative ATTO-532 molecules. The DF shows a strong dependence on excitation energy, which is due to emission arising from higher energy excited dimeric states.

In addition, the complex excited-state nature of the polyspirobifluorene (PSBF) polymer is investigated in both dilute solutions and spin-coated films. According to investigations carried out in dilute solutions, solvent polarity and temperature dependent charge transfer (CT) state formation is observed as arising from the “inter/intrachain” interaction phenomena. The stabilisation of the intra- CT state at low temperatures exhibits the presence of both triplet-triplet annihilation (TTA) and monomolecular processes. These findings are used to interpret the up-conversion data of PSBF in thin films, clearly revealing that both TTA and thermally activated delayed fluorescence (TADF) are involved in indirect singlet generation. The same mixed contribution is also confirmed in anthracene based, small molecule, thin films. Consequentially, these findings highlight the investigated system as one of the desirable alternative molecular systems through which high efficiencies in organic light emitting device (OLED) applications can be attained.

Finally, an understanding of novel anthracene based novel acceptor molecule is developed through the use of a sensitizer based up-conversion experimental method, in which the question of how the side groups (having different electron affinities) affect the TTA efficiency and triplet energy transfer efficiency is clarified. Lastly, the investigations show that novel pyridine derivatives have solvent polarity and viscosity dependent excited state configurations, which are designated as twisted/wagged intramolecular charge transfer states. The DF, in this case, predominantly originates from monomolecular recombination of the geminately bound e-h pairs. It is believed that this can be a major loss mechanism for quantum yield in ICT systems.

Murat Aydemir, August, 2016

INVESTIGATION OF DELAYED FLUORESCENCE PHENOMENA IN CONJUGATED MOLECULES USING TIME-RESOLVED LASER SPECTROSCOPY

by

Murat Aydemir

A Thesis submitted to the Faculty of Science, Durham University, for the Degree of Doctor of Philosophy

Organic Electroactive Materials Research Group Department of Physics

University of Durham

August 2016

Dedicated to My beloved Family…

To my mum, Ümmühan

To my dad, Hilmi

And to my lovely brother, Mehmet

DECLARATION

The work in this thesis based on research carried out at the organic electroactive materials (OEM) research group at Durham University, UK. No part of this thesis submitted elsewhere for any other degree or qualification and it is all my work unless referenced to the contrary in the text.

ACKNOWLEDGEMENTS

Many people have helped and supported me during the course of my PhD, both in UK and Turkey. First of all, I would like to thank my supervisor Prof. Dr. Andy Monkman for the advice and guidance he has provided me throughout my studies. I can easily say that without his support it would have been difficult to progress my PhD, therefore, I am very grateful to have such a friendly supervisor. I would also like to thank my second supervisor Dr. Fernando B Dias who was all the time happy to help me whenever I needed him. In addition, my friends in OEM group, VJ, Hameed, Heather, Marc, Przemyslaw, Chunyong, Khalid, Chris M, Chris C, David, Paloma, Roberto, Javan, Gareth and Piotr, who really shared their personal experiences and thoughts with me, and we had a lot of good memories together. It was enjoyable to live the moments with you guys. I hope we can make good collaborations at next future.

Rabbime şükürler olsun ki yıllarca hasretliklerini çektiğim aileme bu tezi ithaf etmek nasip oldu. Hayatımın her safhasında her zaman maddi ve manevi desteklerinizle yanımda oldunuz, bunun için her ne kadar şükretsem azdır. Bu tezi oğlunuzdan bir hediye olarak kabul etmenizi istiyorum.

Özellikle bu zamana kadar desteklerini esirgemeyen, İsmail ve Nurettin hocalarıma sonsuz saygılarımı sunuyorum.

Gurbette ki hiç bir arkadaşımı unutmam mümkün değil özellikle Malik, Melih, Çiğdem, Mehmet, Mustafa Onur, İlker, Ahmet, Mümin Mehmet. Sizlerle tanıştığıma son derece memnunum. Bu arkadaşların yanısıra tez sürecinde her zaman vakitli vakitsiz demeden evlerini açan Hatice-Bünyamin, Cangül-Samet ve özellikle Nihan-Mustafa çiftlerine sonsuz teşekkürlerimi sunuyorum.

Ayrica, tez yazma sürecinde yanımda olamasada varlığını herdaim hissettiren Hilal'ime sonsuz teşekkürlerimi sunuyorum.

CONTENTS

LIST OF TABLES

LIST OF FIGURES

LIST OF ABBREVIATIONS

CT- Charge transfer

DF- Delayed fluorescence, DOS- Density of states, DCM- Dichloromethane, DMSO-dimethyl sulfoxide

EQE- External quantum efficiency, EtOH-Ethanol

GP- Geminate pair

FRET-Förster energy transfer

HOMO- Highest occupied molecular orbital

iCCD- Intensified charged coupled device, IC-Internal conversion, ICT-Intramolecular charge transfer, ISC-intersystem crossing

LUMO- Lowest unoccupied molecular orbital, LED-Light emitting device, LE-Locally excited

MCH- Methyl cyclohexane

Nd:YAG- Neodymium doped yttrium aluminium gamet

(P)OLED- (polymer) organic light emitting diode

PF- Prompt fluorescence, PH-Phosphorescence, PL-Photoluminescence, PLQY-Photoluminescence quantum yield, PSBF-polyspirobifluorene, PtOEP- Platinium-octaethylporphyrin, PVA-Poly-vinyl-alcohol

rISC- Reverse intersystem crossing, Rh6G-Rhodamine 6G, RT-Room temperature

SSA-Singlet-singlet annihilation, SSL- Solid state lighting, STA-Singlet-triplet annihilation

TTA- triplet-triplet annihilation, TADF-Thermally activated delayed fluorescence, TF- Triplet fusion, TTE- Triplet-triplet energy, TCSPC- Time-correlated single photon counting, TICT- Twisted intramolecular charge transfer

UC-DF- Up-converted delayed fluorescence

WICT- Wagged intramolecular charge transfer

2-MeTHF- 2-methyltetrahyrafuran

CHAPTER 1: INTRODUCTION

In the context of this thesis, organic conjugated molecules are the centre of attention due to their potential applications in today's lighting technologies. Artificial lighting technologies cover a wide spectrum of our daily life from illumination of places, i.e. houses, offices, parks, etc. to electronic devices, i.e. television, computers, phones, etc. which show evidence of how strongly human beings depend on artificial lighting. However, that addiction gives rise to a high amount of inevitable energy consumption in our daily life. To reduce this energy consumption, one of the methods is to take advantage of sunlight by means of delaying the nominal time of sunset and sunrise ± 1 hour, which is considered to reduce energy consumption. However, according to researchers in India, this method increased the overall residential electricity consumption by 1% to 4% in the period of between 2006 to 2008.[1] In Great Britain, a report estimates that the daylight saving method in the winter-term prevented a ~2% increase in average daily electricity consumption between 2001 and 2006.[2] Similarly in the U.S., a report undertaken between 2007 to 2008, showed extension of daylight saving time resulted in a negligible decrease (~ 0.5 %) in electricity usage excluding the amount of energy used for heating.[3] Besides energy consumption effects, changing the clocks also has significant effects on the economies of many countries and the health of people, details of which can be found elsewhere.[4,5] Consequentially, the daylight saving method needs to be investigated in depth by each country prior to being directly accepted as an alternative energy saving methods. Furthermore, another good example with regard to energy consumption was reported in the U.S., where according to the U.S. Department of Energy in 2001, on average each year lighting consumes ~765 TW hour of electricity, which is equal to 8.3% of total energy consumption and costs around $58 million per a year.[6] Therefore, in 2003, the U.S. Department of Energy initiated a competition between industry partners to develop energy-saving alternative methods for artificial lighting, offering a $10 million prize.

The world-wide problem is limited energy resources, therefore, any ideas that offer an alternative solution to reduce overall energy consumption becomes the centre of interest for governments and researchers. For instance, recently the U.S. Department of Energy has invested in companies and universities to develop alternative energy-saving projects in solid-state lighting (SSL) including light-emitting diodes (LEDs) and organic-light emitting diodes (OLEDs), which are alternative illumination sources that are expected to substitute incandescent bulbs, etc. By switching to SSL technologies, the U.S. Department of Energy estimates to reduce energy costs by $120m within twenty years, as well as reducing electricity consumption by one fourth. In addition, this new-technology will have a significant effect on the climate in terms of avoiding approximately 246 million metric tons of carbon emission, which prevents man-made climate change.

OLEDs are simply organic LEDs structured by using organic (carbon-based) materials, i.e. either conjugated polymers or small molecules, as the active emissive electroluminescence layers in which, charge recombination takes place between electrons and holes. The organic layer emits photons with energy corresponding to the unique emission spectrum of the conjugated molecules. Actually, the absorption spectrum of the organic molecules is the crucial parameter that gives more insight into the light it produces. The invention of OLED technology was made by Tang *et al.*,[7] it was inspired by LEDs. Instead of using inorganic crystal layers as in LEDs, OLEDs are made-up of nicely organized emissive multiple thin films (layers) that result in remarkably brighter light while consuming less energy compared with LED technology.

The benefits and drawbacks of LEDs and OLEDs can be summarised:

- Both of them are energy conversion devices where electricity is converted to the form of light.
- OLEDs are more flexible (i.e due to using plastic substrates), lighter and thinner than LEDs. In essence, easy deposition on flexible substrates makes the OLEDs more attractive for new technological designs (Fig. 1.1). This feature also makes OLEDs durable for long-lasting applications.

- In applications, OLEDs are brighter than LEDs, because the active layers are produced from very thin layers of the solid organic materials. However, LEDs have liquid crystal layers (which help to switch on/off the pixels by means of (un)twisting by electricity), and glass is commonly used as a substrate which leads to additional light absorption and makes the LEDs heavier.
- The production of OLEDs is quite easy, but still expensive, and they are preferentially used for large size flat-panels, whereas, LEDs are not practically convenient for large area lighting applications, because it is more difficult to grow and lay down many liquid crystals.

  The external quantum efficiency of the OLEDs is still a problem, and it needs to be increased to produce highly efficient OLEDs.

Figure 1.1 Recent OLED applications are announced for television and smart-phone screen technologies by Samsung and LG companies. The pictures adapted from online.[8,9]

Nowadays, many research groups focus on increasing the external quantum efficiency of OLEDs, where the term represents the amount of injected charge carriers that are converted into photons. The high-efficiency of this conversion is one of the most crucial processes in OLEDs. However, it is not that easy to measure photon generation rates within the active layers of OLED architectures. Therefore, the quantum efficiency is commonly described by the external quantum efficiency (EQE) term, which gives us

the ratio between the number of emitted photons and the number of charges injected. The expression can be written as,[10]

$$\mathbf{EQE} = \eta_{\mathbf{ext}}\Phi_{\mathbf{fl}}\,\boldsymbol{\gamma}\eta_{\mathbf{fr}} \qquad \mathbf{(1.1)}$$

where η_{ext} represents the light out-coupling factor, and its estimated value is about 0.2-0.3.[11] Φ_{fl} represents the fluorescence quantum yield of the material (internal quantum yield), γ is the charge-balance factor, which particularly shows the fraction of total current giving rise to charge recombination. η_{fr} is the emissive excited state contribution upon EQE. Theoretical calculations of the maximum EQE were estimated as ~0.05 where spin statistics dictates that singlet (a quantum state with a spin of zero) and triplet (a quantum state with a spin of one) states are formed in the ratio of 1:3 (0.25 singlet, 0.75 triplet). Since, classically only the excited singlet state makes a contribution to the EQE as an emissive state, η_{fr} is considered to be ~0.25 for fluorescent devices and ~1 (unity) for phosphorescent devices, then the maximum value of EQE for fluorescent devices is equal to 0.05. However, many research groups have reported EQE's substantially exceeding this value of 0.05, suggesting that a number of secondary processes where the triplets can be converted into emissive singlets by means of triplet harvesting mechanisms are involved. In the literature, these secondary processes are called delayed fluorescence (DF) and lead to the population of emissive states. In this way the quantum yield of the emissive states can be increased. The possible DF mechanisms can be categorised as triplet-triplet annihilation (TTA)[11,12] and thermally activated delayed fluorescence (TADF)[5,6] where triplets follow bimolecular and monomolecular pathways to form an excited singlet state, from which subsequent DF originates. Consequentially, the potential value of EQE strongly depends on existing photo-physical mechanisms in the materials which may result in higher EQE values than the theoretically calculated value of 0.05.

In addition, Adachi *et al.*[15] overcame the spin statistics limitation (0.05-singlet generation) by using phosphorescent heavy metal complexes, where the emissive state

has triplet characteristics (multiplicity). These phosphorescent OLEDs increase the emission yield to ~100% by means of enhancing the spin-orbit coupling giving rise to an increased intersystem crossing rate from the singlet state to triplet states (hence, the value of η_{fr} can be assumed to be ~1) then the system emits from triplet states. By using this method, it is likely to achieve 100% internal quantum efficiency through the use of red, green and blue phosphorescent heavy metal complexes in white OLED applications.[16] However, using heavy metal complexes has some drawbacks, for instance, these metals (generally Ir(III) or Pt(II)) are quite expensive and rare, besides which, this method is still inconvenient for deep blue phosphor emitters which also require high triplet level host materials to avoid possible quenching. Finding a host material with a triplet energy level higher than the emitter is a challenge for blue-emitting phosphorescent materials, as well as their possible degradation problems, which create serious restrictions on performance, stability and lifetimes of blue-emitting phosphorescent OLEDs. Therefore, phosphorescent OLEDs do not seem to be an alternative option for achieving efficient full-colour rendering white OLEDs. Therefore, the most promising alternatives for full-colour rendering and high efficiency of devices are fluorescence-based OLEDs, where a great portion of non-emissive triplet excitons are converted into emissive singlet excitons *via* TTA and TADF. The process of TTA (also known triplet fusion, TF) forms singlet excitons by means of a bimolecular annihilation process where at least two triplets are required to interact with each other and then subsequent DF arises from excited singlet state. By way of TTA, the maximum achievable singlet generation is limited to 0.625 (0.25 singlets + 0.75 x 0.5= 0.375 triplets), depending on the relative energy order of the excited singlet and triplet energy levels [12] which also help to determine the possibility of higher excited triplet state (T_N) involvement.

TADF is an alternative photophysical process where one-to-one conversion of triplets into excited singlet states occurs *via* reverse intersystem crossing (rISC). The great benefit of TADF is the possibility of 100% triplet harvesting[17] effectively exceeding the quantum statistic limitation of device efficiencies (above 0.2 EQE now, but presumably much higher in the future with novol structural designs) without using any heavy metal based phosphorescent complexes, and also providing an alternative solution for the deep blue emitter problem. The particular requirement of TADF molecules is having a small

energy gap (ΔE_{ST}) between excited singlet and triplet states of the molecules, which is governed by electron exchange energy. As reported by Baldo and his co-workers,[18] having an intramolecular charge transfer (ICT) state helps to reduce the ΔE_{ST}, where the ICT state appears as an intermediate step prior to (re)population of the excited singlet state in the molecules, or it might be the main emitting state, i.e. an exciplex.[19] The advantage of ICT emitters is to get a certain degree of separation between the highest occupied molecular orbital (HOMO) and the lowest unoccupied molecular orbital (LUMO). Minimum overlap can be satisfied by means of perpendicular orientations of HOMO-LUMO levels,[20] and concomitantly zero exchange energy can be achieved by means of equalizing the excited singlet and triplet states. Recent materials were reported having ~0.1 eV energy gap which have spatially pretwisted ICT geometry resulting from the steric hindrance between donor and acceptor moieties.[21] This particular molecular arrangement gives rise to efficient triplet exciton confinement in active layers of OLEDs and concomitantly it is likely to achieve highly efficient blue- emitting OLEDs.[22] However, at high current density conditions, the OLEDs brush up against the efficiency roll-off which mainly arises from the large energy splitting, ΔE_{ST}, and long excited state lifetime of the molecules.[21] Therefore, for efficient OLEDs, investigations should be focused on structure-property relationship to get more insight into their fundamental photophysics.

1.1 Thesis Motivation

Understanding the electronic processes that govern light emission in conjugated molecules is the key objective of this thesis. The emissive excited states can be either formed by direct absorption of light (primary process) or (as mentioned above) they may be populated following energy transfer or annihilation processes, which are secondary processes for singlet generation and result in (delayed) emission at longer time scales (compared to the primary process). The importance of the latter comes from generating additional singlet excitons, hence overcoming the theoretical spin statistic limitation. In particular, considering the potential applications of conjugated molecules in technology,

development of efficient molecules, with high internal quantum efficiency, is strongly desired. At this point, it seems crucial to understand the relationship between the secondary processes and molecular structures. For this purpose, in this thesis, the investigations are made with particularly chosen molecules, including commercial dye molecules (Rhodamine 6G and ATTO-532), a polymer (Polyspirobifluorene) and series of novel small molecules.

Following on from this introductory chapter, a brief fundamental background theory on conjugated molecules is given in Chapter 2, which includes a basic overview of the formation of excited states, energy transfer mechanisms and bimolecular and thermally activated processes for delayed fluorescence. The experimental section is presented in Chapter 3, which involved in sample preparation procedures and details of spectroscopic techniques used in this thesis.

Chapter 4 is particularly designed as a model chapter for the following ones, which offers the methods for how to distinguish the monomolecular and bimolecular electronic processes that involved in DF. Addressing this point, the chapter includes a brief background theory of possible photophysical mechanisms behind the DF, i.e. TTA, TADF and geminate electron hole pairs recombination (GPR). In addition, the characteristics of DF processes that have been reported in literature are presented, which particularly include exciton decay dynamics, the intensity dependence of DF on excitation energy and temperature dependence of DF. Afterwards, using this knowledge, the presence of electronic states in Rhodamine 6G and its derivative ATTO-532 are picturized and the origin of DF is determined.

Chapter 5 demonstrates the complex excited state nature of the conjugated polymer, polyspirobifluorene (PSBF). The existing electronic states are picturized in variety of solvents with particularly attention paid to the crucial role of solvent viscosity and polarity on the formation of emissive states, which are designated as charge transfer (CT) states and arising from particular spatial geometry of the molecule. Afterwards, the role of the CT state is questioned in depth to understand how this particular excited state can make a significant contribution to the total photoluminescence (PL). Consequentially, the active role of both monomolecular and bimolecular processes behind the formation of DF is

determined. Chapter 6 attempts to further the work of Chapter 5, where the findings are further investigated in PSBF film, by way of using a unique two-pulse-pump spectroscopy technique. This technique yielded important results relating the energy levels of the PSBF molecule, and reinforced the observed data in Chapter 5.

In Chapter 7, the dynamics of triplets are investigated in novel anthracene derivatives using a sensitizer-acceptor based up-conversion technique. The technique is explained in detail and some background theory on the kinetics of triplets is given. It is shown that the latter plays a fundamental role in observing the up-converted delayed fluorescence (UC-DF), which strongly depends on the efficiency of energy transfer and bimolecular process (triplet-triplet annihilation). Therefore, to get a better understanding of how the efficiency of UC-DF is affected by the molecular structure of acceptor unit, a series of anthracene based molecules (including different electron donor, acceptor and neutral side groups) are investigated and the findings are presented.

Finally, Chapter 8 focuses on the question of how ground and excited state configurations affect the charge transfer properties and the origin of DF. For this purpose, a series of novel donor-acceptor-donor (D-A-D) type structured pyridine derivatives are investigated and their ground and excited state configurations are determined both in solutions and films. Actually, the importance of D-A-D type small molecules comes from them being one of the most desired candidates for OLED applications due to the ability to reduce the HOMO-LUMO energy gap by means of changing the relative configurations of the D-A moieties (i.e. perpendicular orientations of D-A), and the highly favourable formation of CT states. Therefore, it seems necessary to understand how molecular geometry is affected by the type of donor unit and its relationship with delayed fluorescence.

1.2 References

1. Kotchen, M. J. & Grant, L. E. Does Daylight Saving Time Save Energy? Evidence from a Natural Experiment in Indiana. *Rev. Econ. Stat.* **93,** 1172–1185 (2011).

2. Garnsey, E, Hill, S & Smart A. The effect on energy usage of extending British Summer Time: oral and written evidence, *Stationery office,* London (2011).

3. Hadley, S. W., Belzer, D. B., Chin, S-M. Impact of extended daylight saving time on national energy consumption report to Congress, *U.S. Dept. of Energy* (2008).

4. Kamstra, M. J., Kramer, L. A. & Levi, M. D. Losing sleep at the market: The daylight saving anomaly. *Am. Econ. Rev.* **90,** 1005–1011 (2000).

5. Janszky, I. & Ljung, R. Shifts to and from daylight saving time and incidence of myocardial infarction. *N. Engl. J. Med.* **359,** 1966–1968 (2008).

6. D'Andrade, B. W. & Forrest, S. R. White organic light-emitting devices for solid-state lighting. *Adv. Mater.* **16,** 1585–1595 (2004).

7. Tang, C. & Vanslyke, S. Organic Electroluminescent Diodes. *Appl. Phys. Lett.* **51,** 913–915 (1987).

8. http://www.samsung.com/uk (2016).

9. http://www.lg.com/uk (2016).

10. Kondakov, D. Y. Role of triplet-triplet annihilation in highly efficient fluorescent devices. *J. Soc. Inf. Disp.* **17,** 137–144 (2009).

11. Kondakov, D. Y. Triplet-triplet annihilation in highly efficient fluorescent organic light-emitting diodes: current state and future outlook. *Philos. Trans. R. Soc. -Math. Phys. Eng. Sci.* **373,** 20140321 (2015).

12. Kondakov, D. Y., Pawlik, T. D., Hatwar, T. K. & Spindler, J. P. Triplet annihilation exceeding spin statistical limit in highly efficient fluorescent organic light-emitting diodes. *J. Appl. Phys.* **106,** 124510 (2009).

13. Lee, S. Y., Yasuda, T., Nomura, H. & Adachi, C. High-efficiency organic light-emitting diodes utilizing thermally activated delayed fluorescence from triazine-based donor-acceptor hybrid molecules. *Appl. Phys. Lett.* **101,** 93306 (2012).

14. Goushi, K., Yoshida, K., Sato, K. & Adachi, C. Organic light-emitting diodes employing efficient reverse intersystem crossing for triplet-to-singlet state conversion. *Nat. Photonics* **6,** 253–258 (2012).

15. Adachi, C., Baldo, M. A., Thompson, M. E. & Forrest, S. R. Nearly 100% internal phosphorescence efficiency in an organic light-emitting device. *J. Appl. Phys.* **90,** 5048–5051 (2001).

16. Sun, Y. & Forrest, S. R. Multiple exciton generation regions in phosphorescent white organic light emitting devices. *Org. Electron.* **9,** 994–1001 (2008).

17. Dias, F. B., Bourdakos, K.N, Jankus, V., Moss, K.C., Kamtekar, K.T., Bhalla, V., Santos, J., Bryce, M. & Monkman, A.P. Triplet Harvesting with 100% Efficiency by Way of Thermally Activated Delayed Fluorescence in Charge Transfer OLED Emitters. *Adv. Mater.* **25,** 3707–3714 (2013).

18. Segal, M., Singh M., Rivoire, K., Difley, S., Van Voorhis, T. & Baldo, M.A. Extrafluorescent electroluminescence in organic light-emitting devices. *Nat. Mater.* **6,** 374–378 (2007).

19. Jankus, V., Data, P., Graves, D., McGuinness, C., Santos, J., Bryce, M.R., Dias, F.B & Monkman, A.P. Highly Efficient TADF OLEDs: How the Emitter-Host Interaction Controls Both the Excited State Species and Electrical Properties of the Devices to Achieve Near 100% Triplet Harvesting and High Efficiency. *Adv. Funct. Mater.* **24,** 6178–6186 (2014).

20. Jankus, V., Aydemir, M., Dias, F. B. & Monkman, A. P. Generating Light from Upper Excited Triplet States: A Contribution to the Indirect Singlet Yield of a Polymer OLED, Helping to Exceed the 25% Singlet Exciton Limit. *Adv. Sci.* **3,** 1500221 (2016).

21. Zhang, Q., Li, J., Shizu, K., Huang, S., Hirata, S., Miyazaki, H & Adachi, C. Design of Efficient Thermally Activated Delayed Fluorescence Materials for Pure Blue Organic Light Emitting Diodes. *J. Am. Chem. Soc.* **134,** 14706–14709 (2012).

22. Zhang, Q. Li, B., Huang, S., Nomura, H., Tanaka, H. & Adachi, C. Efficient blue organic light-emitting diodes employing thermally activated delayed fluorescence. *Nat. Photonics* **8,** 326–332 (2014).

23. Kondakov, D. Y. Role of triplet-triplet annihilation in highly efficient fluorescent devices. *J. Soc. Inf. Disp.* **17,** 137–144 (2009).

CHAPTER 2: THEORETICAL OVERVIEW ON CONJUGATED MOLECULES

"Truth is ever to be found in simplicity, and not in the multiplicity and confusion of things"

Isaac Newton

The purpose of this chapter is to understand the electronic properties of conjugated molecules, e.g. conjugated aromatic hydrocarbons either small molecules or polymers which are particularly used in organic light emitting devices (OLEDs), and their excited-state photophysical behaviours. The chapter is specifically equipped with conceptual theoretical approaches, which shed light on the field of conjugated organic molecules. However, it should be noted that the aim of this chapter is not to present a comprehensive investigation of this field of research, but is rather a background to the theory considered within the context of this thesis, presented in following results chapters (in Chapter 4, 5, 6, 7 and 8).

2.1 The molecular structure of conjugated molecules

The structure of conjugated molecules can be formed as a result of bonding several atoms, i.e. carbon, oxygen, etc. Therefore, the structural diversity of molecules is directly related to the chemical properties of these atoms. For instance, carbon has six electrons, four in the outer shell and is able to make four chemical (covalent) bonds with neighbouring atoms. Chemical bonds can be categorized into strong and weak bonds. The former includes intramolecular forces that hold the atoms together, i.e. covalent, ionic and metallic bonds, where the bonding principle is based upon sharing or exchanging the electrons between the atoms. For the latter, the bonds include intermolecular forces between the molecules, i.e. van der waals, H-bonding or π-π stacking interactions, and usually result from electrostatic interactions between the molecules. As a result of

bonding, carbon-based molecules arise which can be classified into two groups on the basis of their molecular weight; small and polymeric molecules. The term "small molecule" is used for the molecules having lower molecular weight (< 1000 Da) compared with polymeric molecules, for instance, the molecular weight of polyfluorenes ranges between 50.000 -100.000 Da.[1]

A conjugated polymer is a large macromolecule consisting of hundreds of repeating monomer units (see Fig.2.1 as an example of polymer structure) which are chemically bonded into long chains to form the backbone (main chain) and functional side groups. The structure of the backbone consists of alternating single and double covalent bonds where conjugation can occur as a continuous orbital overlap by means of coupling between the conjugation segment and neighbour atom's π-orbitals (the details will be given below). The side chains usually consist of singly bonded carbon atoms and they can be attached to the polymer either linearly or in a branched manner. They are responsible for determining the particular physical properties of the polymer such as solubility, tuning the energy of emission, charge transport, etc.[1] In addition, side chains play an important role in determining the degree of interactions between the polymer chains, i.e. inter-chain interactions.[2] The types of polymers are categorized depending on the arrangement of the repeat units; homopolymers (the repeat units are the same), copolymers (the repeat units are different), main-chain polymers (the repeat units located electronically active backbone part of the polymer) or side-chain polymers (electronically active part of the polymer located in side chains). The polymers typically consist of rings which are connected each other at different particular positions (para (p), meta (m) or ortho (o)) to form a chain.

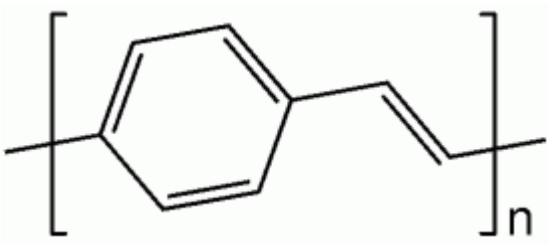

Figure 2.1 Chemical structure of commonly used main-chain homopolymer, poly (p-phenylene vinylene)

The unique electrical and mechanical properties of polymers arise due to the flexibility of the carbon-carbon bonds giving rise to enhanced molecular interactions that result in the formation of complex shapes. In particular, once the polymers are dissolved in solution, the molecular mobility is enhanced and they have many degrees of freedom to form a variety of complex structural shapes, e.g. random coils, rigid rods, etc.[3] For instance, "*random coil"* shapes of polymers are generally formed as a result of random collisions between solvent molecules and the segments of polymer chains (generally 20-50 carbon atoms) which give rise to spheroidal conformations. In reality, the conformational changes occur very slowly in polymers in solution, indeed compared to those for small molecules and the spectra of molecules show the hints of complex excited state behaviours.

2.1.1 Molecular orbitals of organic molecules

In conjugated organic molecules, mainly the types of bonding which occur between the atoms determine electronic properties. According to valence bond theory, bonds are formed between two atoms if bonding conditions are met; these are orbital overlap and the rule of occupying a limited number of electrons in the orbitals. The latter case is explained by Pauli's Exclusion Principle, which states that the orbitals do not hold more than two electrons if the set of quantum numbers are the same, i.e. principle quantum number (n), orbital angular quantum number (l), spin quantum number and magnetic quantum number (m). For the former case, the orbital overlap process occurs by means of approaching atomic orbitals whereby the same atomic orbital space is occupied by both atomic orbitals and the electrons of each atom start moving around the same nuclei. This situation gives rise to an attraction of the electrons by both nuclei of the atoms, resulting in an attractive force between the negative and positive charges, which plays a key role in holding the atoms together. Attractive forces determine the degree of overlap. If the attractive force is great, the degree of overlap is great, which is crucially important to understand the strength of the bonding.

In organic systems, five types of molecular orbitals are of interest which are mainly sigma-bonding (σ), sigma-antibonding, (σ*), pi-bonding (π), pi-antibonding (π*) and

nonbonding (n) orbitals. In order to explain sigma and sigma-anti- bonding molecular orbitals, we can consider the diatomic hydrogen molecule as a well-known example. Each hydrogen atoms has one electron in its 1s orbital. Once the hydrogen atoms approach to each other, their orbitals begin overlapping with each other, resulting in electrostatic attraction between the negatively charged 1s orbital electron of one atom and the positively charged nucleus of the other atom (*or vice versa*). Consequentially, symmetrical 1s-1s orbital overlapping results in formation of a covalent bond with the sharing of electrons between atomic orbitals in the overlapping region. As a result of these processes two types of molecular orbitals are formed with different energies; one of lower energy sigma orbitals (σ, constructive overlap) and one of higher energy anti-sigma orbitals (σ*, deconstructive overlap).

In the case of constructive (in-phase) overlap, a single bonding orbital is formed between the two atoms in a way that orbital overlaps occur by means of a linear or head-to-head arrangement, such as between s-s (H_2), p-p (F_2) or s-p (HF) orbitals. Combining two atomic orbitals constructively gives rise to an increase in inter nuclear electron probability intensity due to a maximum overlapping of the orbital wave functions.[4] Mathematically the molecular orbital formation can be described as a sum of the atomic wave functions ($\psi_{final} = \psi_1 + \psi_2$). For example, in the hydrogen molecule model (see Fig. 2.2), the overlap occurs between 1s atomic orbitals and results in formation of a σ-bonding molecular orbital. In a sigma orbital, the electron density along the nuclear axis is enhanced and cylindrically symmetric and there is a high probability of electron occupation between the two nuclei regions which gives rise to large electron-nucleus electrostatic attractions. For this reason, the electrons in the σ-bonding molecular orbital are strongly bonding and essentially localized, hence, requiring great energy for excitation. This electron localization is also represented mathematically with the square of wave functions (ψ^2) showing high electron probability density in the sigma bond region (see Fig.2.2 b). The energy of the constructive overlap (E_+) is defined by overlap (S), coulomb (α) and exchange (β) integrals, which can be written as,

$$\boldsymbol{E_+ = (\alpha + \beta)/(1 + S)} \qquad \textbf{(2.1)}$$

In the case of deconstructive (out of phase) overlap, an anti-bonding (σ*) orbital is formed between the hydrogen atoms (see Fig. 2.2 c). In the σ* orbital, a nodal plane is formed between the region between two atoms where there is a zero probability of finding an electron and lies perpendicular to the inter nuclear axis, therefore, the electrons reside outside of the bonding region where they are also tightly confined. The interacting atoms behave in a way that positively charged nuclei push each other which consequentially gives rise to an increase to the total energy of the system compared with the initial separate energy of atomic orbitals (see Fig.2.3).[5] The sigma molecular orbital is much more stabilized in comparison to the single atomic orbitals, whereas, the anti-sigma molecular orbital is destabilized. Destructive overlap can be defined mathematically (see Fig. 2.2 d) as the subtraction of the wave functions ($\psi_{final} = \psi_1 - \psi_2$) where the atomic wavefuctions come together in a destructive manner giving rise to reduced charge density between the nuclei. Further, the electron localization is also represented mathematically with the square of wave functions (ψ^2) showing a zero electron probability density in nodal plane zone (see Fig.2.2 d). The energy of the deconstructive overlap can be written as,

$$\boldsymbol{E_- = (\alpha - \beta)/(1 - S)} \qquad \textbf{(2.2)}$$

which shows a qualitative measure of the overlap of two atomic orbitals. Coulomb integral shows a measure for the Coulomb interaction between the electron and the nucleus of the atomic orbitals. And finally, exchange integral shows the interaction between a nucleus and an electron located in partly different atomic orbitals which plays an important role in determining the energy splitting between the atomic orbitals. If the energy of interacting orbitals has identical energy, then the energy splitting (ΔE) between constructive and deconstructive molecular orbitals is equal to ~2β,[1] but, if the energy of the atomic orbitals is different, then ΔE is equal to $(a_2 - a_1) + 2\beta(\beta/(a_2 - a_1))$.[1]

In the hydrogen molecule, the electrons are located in σ molecular orbitals in such a way that the energy of the overall system is reduced whilst no more than two electrons with equal but opposite spin orientations occupy each orbital, as defined by Pauli's

exclusion principle. The electrons are filled in molecular orbitals by starting from the lowest energy level orbitals (most stable conditions), as explained by the Aufbau principle, to higher energy level orbitals only if the lower energy ones are fully occupied. However, if there are several molecular orbitals with equal energies, e.g. $2p_x$, $2p_y$ and $2p_z$, then the orbital filling starts by occupying the same spin oriented electrons in each sub-orbitals until all energetically equal sub-orbitals are half-filled, and then each of them are paired as explained by Hund's principle. Eventually, the highest occupied molecular orbital (HOMO) is formed by means of filling the molecular orbital (in this case a σ-orbital) and the lowest unoccupied molecular orbital (LUMO) is formed by empty molecular orbitals (σ*- orbital).

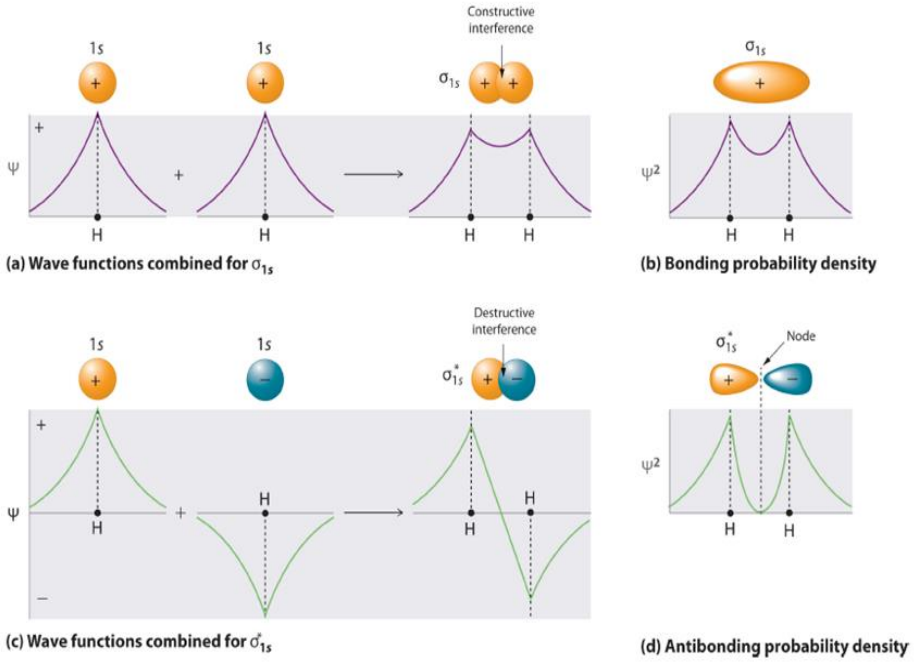

Figure 2.2 a) Constructive overlapping of single hydrogen atoms results in the formation of σ molecular orbital which can be mathematically defined as the sum of each atomic wave function (ψ). **b)** The electron probability density is represented between the two hydrogen nuclei as square of the wave functions (ψ^2). **c)** Deconstructive overlap of single hydrogen atoms results in formation of anti-bonding sigma orbital which can be mathematically defined as the subtraction of the hydrogen atom wave functions. **d)** The electron probability density is represented between the two hydrogen nuclei with square of the wave functions (ψ^2). The formation of nodel plane shows the zero electron density region. Figure adapted for use from Ref.[4]

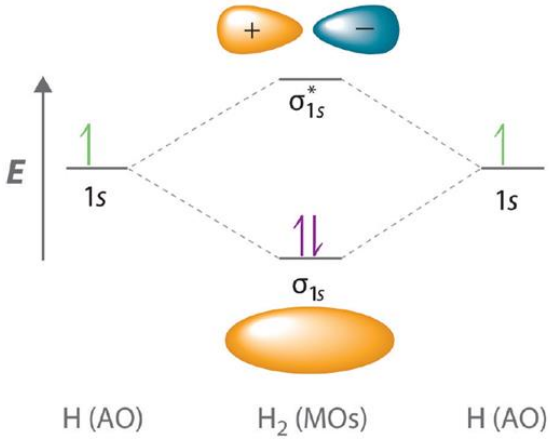

Figure 2.3 Molecular orbital energies of a hydrogen molecule. The electrons of each hydrogen atom fill the σ molecular orbital according to Pauli Exclusion Principle. The σ bonding orbital has lower energy than the individual atomic orbitals and the hydrogen molecule is more stable than high-energy anti-bonding sigma orbital. Figure adapted for use from Ref.[4]

In the case of inhomogeneous molecules, e.g. HF molecule, anti-/sigma bonding orbitals are formed between the 1s orbital of hydrogen and the 2p orbitals of the fluorine. Unbound 2s and the 2p orbitals (e.g. $2p_y$ and $2p_z$) of the fluorine remain as nonbonding orbitals because hydrogen does not have any orbitals except 1s to make further bonds with fluorine. The strength of the interaction between the atomic orbitals is determined by the electronegativity and the amount of overlap. The energy difference between the atomic orbitals is known as electronegativity. In the HF molecule, fluorine shows more electronegativity and the 2p orbitals of fluorine stay lower in energy than the hydrogen 1s orbital, resulting in the molecular orbital formed showing spatially p orbital characteristics. This means the electrons in the bonding orbital pile up in the vicinity of fluorine atom, while, the anti-bonding orbital is spatially very similar to 1s orbital characteristics. This subsequently denotes that, the electronegativity and the comparable size of the atoms play a crucial role in achieving spatial orbital overlap, which determines the strength of the orbital interactions. In particular, once the energy of the orbitals is more or less similar the maximum overlap is achieved.

2.1.2 Hybrid orbitals of organic molecules

The molecular geometry of the organic systems can be explained by hybridisation phenomena, in which atomic orbitals (2s and 2p) come together to form a new set of hybrid orbitals with different energies, orientations and shapes. Addressing this point, the carbon atom is considered as a good example showing the requirement of hybrid orbitals. The ground state electronic configuration of carbon is $1s^2 2s^2 2p^2$ or $1s^2 2s^2 2p_x^1\ 2p_y^1\ 2p_z^0$, in this case, carbon atom can only make two covalent bonds, unless one of the 2s electrons move into the empty $2p_z$ orbital. Then two electrons localize in the inner shell (s orbital) and four are in the outer (valence) shell, in this case, the carbon could make four covalent bonds, such as in methane (CH_4).[6]

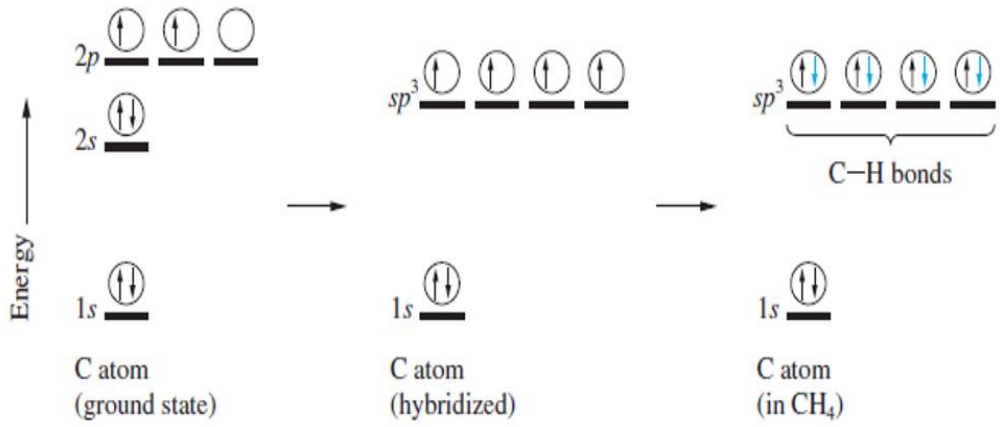

Figure 2.4 The electronic configuration of methane molecule by means of sp^3 hybridization. Figure adapted for use from Ref. [6]

Hybrid orbitals are formed by means of various combinations of atomic orbitals (s and p), which are assumed to be mixed into new degenerate orbitals, i.e. sp, sp^2 and sp^3. For instance, sp^3 hybridization results from mixing of s and p orbitals in the ratio of 0.25 2s and 0.75 2p (all three sub-orbitals $2p_x$ $2p_y$ and $2p_z$ involved), where the orbitals of molecules come together in a way that energy differences between the orbitals are compensated by external forces. Concomitantly four equivalent energy hybridized sp^3

orbitals are formed (see Fig. 2.4) and which accompanied by changes in bond lengths and also the geometry of the molecules to reduce the total energy of the system, e.g. ethane C_2H_6. The C-H bonds are established in ethane by means of overlapping highly directional sp^3 hybrid orbitals of the carbon and the 1s orbitals of the hydrogen atoms giving rise to tetrahedral geometrical orientation with a bond angle of 109.5^0 (see Fig.2.5). All the bonds in ethane are σ-bonds.

Sp^2 hybridization shows mixing characteristics of s and p orbitals in the ratio of 0.33 s and 0.66 p orbitals, and occurs between the 2s orbital and two of the three 2p orbitals ($2p_x$ and $2p_y$) resulting in three *sp*^{2} orbitals such as in ethene (C_2H_4). In this case, three highly directional sp^2 orbitals lie in one plane (xy-plane) and give rise to form three strongly localised σ bonds; one σ bond is formed between the carbon atoms due to the sp^2-sp^2 overlap, and the other two σ bonds are formed between carbon-hydrogen atoms. As a result of s-sp^2 overlap oriented at 120^0 which is a trigonal planar arrangement (see Fig. 2.5).

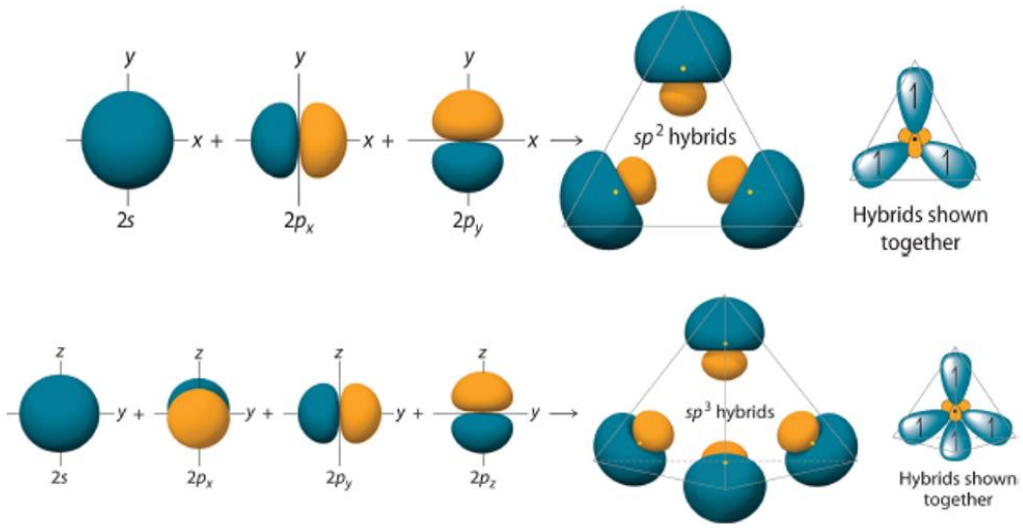

Figure 2.5 The combination of 2s and 2p orbitals results in formation of hybrid orbitals with different orientations. Figure adapted for use from Ref.[4]

Only two of the three 2p orbitals ($2p_x$ and $2p_y$) are involved to form sp^2 orbitals while the remaining $2p_z$ orbital on the carbon atom is positioned perpendicular to the

plane of hybrid orbitals. Each $2p_z$ orbital on the carbon atoms interact with each other and form a second bond (π-bond) resulting from sideways overlap between parallel $2p_z$ orbitals from which two π-orbitals are formed at some distance from the nuclei. In this case, the electrons will have spatial probability density above and below the molecular axis and the attractive force between the nuclei of π-orbitals will be weaker compared to σ-orbitals, therefore, the molecules are held by σ-bonds. The formation of an additional second bond between the carbon atoms is called a double bond, a σ + π bond. The formation of a double bond between carbon atoms makes the bond durable and restricts the possible torsional movements around the bond, therefore, any cleavage of a π orbital will affect the total energy of the system and concomitantly the stability will be decreased. The π orbital is restricted to lie parallel to the plane of the σ bond which gives rise to weak electrostatic interactions,[7] therefore, it is assumed that there are no interactions between σ and π orbitals due to their different symmetry properties. In conjugated polymers, the backbone and the side chains are mainly linked each other with sp^2 bonded carbon atoms and in the case of excitation, all electronic transitions of interest occurs between the π- π* orbitals where the electrons delocalise easily over two or more nuclei due to the weak electrostatic interactions as compared to the σ orbitals (localised orbitals). Therefore the ground and excited states of the molecules are identified by electronic transitions between π- π* orbitals, where the π orbital is assigned as HOMO and π* orbital is LUMO.

2.1.3 Conjugation

Conjugation occurs in organic systems as a result of overlap of $2p_z$-orbitals of the carbon atoms which give rise to a larger, superimposed π–orbital system by means of alternating single (σ) and double bonds (σ + π), e.g. CH_2=CH-CH=CH_2, resulting in a spatially extended π–orbital network. In this network, highly delocalised π electronic states are formed due the resonance interactions between the π bonds, for instance, electron density delocalization region (HOMO) of the conjugated molecule is formed *via* overlap of the π orbitals. The π* orbitals form a region, where the electron density is equal to zero (LUMO). Theoretically, delocalization of electrons along the whole polymer chain (assuming no breaks occur in conjugation) is possible, where continuous

interactions between the π-electrons of the monomers result in extension of the conjugation over the whole chain which affects the fundamental electronic properties of the conjugated system. For instance, if the conjugation length is increased, the energy of the overall system is reduced and the stability of the molecule is increased.

Benzene is a well-known example of a conjugated molecule which has six sp^2 hybridized carbon atoms connected to each other in a single cyclic conjugated system with an alternating series of single and double bonds forming a ring, and its cyclic conjugated structure gives it special stability. Six sigma bonds in benzene ring lie in the common trigonal plane which are oriented to each other with an angle of *ca*. 120^0. Also, each of the six carbon atoms has one unhybridised $2p_z$ orbital which is oriented perpendicular to the trigonal plane and then the conjugated system occurs as a result of overlaps of the six $2p_z$ orbitals in a cyclic manner which gives rise to the theoretical possibility of electron delocalisation over the entire ring.

In macromolecules, e.g. oligomers and polymers, the delocalization of the electrons may occur over part or the entire molecular chains depending on the ratio of overlap between the π–orbitals. The delocalization distance of the electrons (so called "conjugation length") in π–orbital networks defines the value of conjugation length which indicates the size of the π-orbital network. The conjugation length plays a significant role in determining the fundamental electrical and electronic properties, such as the conductivity characteristics[8] and the photophysical features.[3]

In conjugated polymers, there exists at least one backbone consisting of alternating double and single bonds, which makes them conductive. However, the size of the energy gap between the HOMO-LUMO energy levels determines whether the conjugated polymers are either semiconductors or conductors, which is directly related to the extent of delocalization. The situation in metals is different due to having zero energy gap (overlap) between the valence (HOMO) and conduction (LUMO) bands, which results in always having a partially occupied free electron band, therefore the metals are highly conductive. Instead, the energy gap in insulators are too large (up to 3 eV), therefore, it is not that easy for an electron to jump from one electronic state to another, therefore, the valance band is fully occupied by electrons. However, conjugated polymers are

semiconductors and defined by their intermediate energy gap (narrower than insulators, generally in the range of 1.5 eV to 3 eV). If the electrons can be excited to the conduction band (LUMO), then the system becomes conductive, which can be done by exciting the molecule through thermal or photochemical excitation processes. In general, the electrical conductivity arises from polymer backbones through the π-orbital network where the electrons are highly delocalised. However, even if a perfectly linked conjugated network is established, the electrical conductivity still would not be the same as metallic compounds, therefore, they can be doped with oxidising and reducing agents (free charge carriers) to enhance the potential conductivity. Using this process, charge delocalization (or current flow) occurs along the restricted one-dimensional π-π* electronic band (primary electron transition band) as the orbital overlap process in conjugated systems restricts the charge delocalisation direction. Therefore, the delocalisation readily occurs along the one-dimensional direction along the conjugation length, which is very distinctive comparing with the charge delocalisation direction of inorganic conductors and semiconductors (3-D geometry). Instead of π- π* transitions, in some cases, the transitions may occur from non-bonding (n) orbitals to higher energy σ* and π *orbitals which arises usually in heteroatom molecules.

Conjugated polymers are highly disordered semiconductors which consist of domains (or defect points) arising from mainly imperfect arrangements of the contiguous polymer chains or as a result of possible interactions within the close proximity chains (conformational rearrangements), i.e. bending, twisting, etc., resulting in disruption of continuous conjugation with formation of breaks and cleavages. Consequentially, the whole polymer chain is split into various conjugated domains containing different conjugation lengths (typically including 2-5 repeating monomer units) which are the regions responsible for the colour of the molecule and called chromophores (encountered groups of atoms). Considering an average of all the polymer chains, the distribution of chromophores conjugation lengths result in a Gaussian profile. The chromophores are responsible for absorption of light, therefore, they affect the energy of emitted light in the molecule.

2.2 Electronic transitions in organic molecules

The absorption of photons occurs in conjugated molecules when the excitation energy equals to HOMO-LUMO energy gap. In this case, electrons are promoted from occupied orbitals (HOMO) to unoccupied orbitals (LUMO), e.g. $\pi \rightarrow \pi^*$ and $n \rightarrow \pi^*$, etc., resulting in an electronic transition called absorption of a photon. If this excited state decays, then an electronic transition occurs from the LUMO to HOMO which is called the emission of a photon. The light excites an electron from an initially occupied low energy state (Eigen wave function, ψ_i) to previously unoccupied higher energy state (Eigen wave function, ψ_f), this process takes place as a result of interaction between the electric vector component (**E**) of the excitation light and the electric dipole moment (**R**) of the electrons. In other words, the excitation of an electron occurs if the frequency of oscillating light wave function overlaps with the wave function of the electron, then resonance conditions are required for the energy transfer from oscillating light to the electron by absorption. The excitation of an electron can occur from the energy of absorbed light ($E = h\nu$) if two conditions are me: firstly there must be an energetically higher state in the molecule and the absorbed energy of the photon at a particular frequency is to be equal to the difference in energy of the states ($E = \hbar w = E_f - E_i$). Secondly, the interaction between the specific components of the light and the electron results in a significant change in the dipole moment of the molecule, which can be formulated by the transition moment integral (R_{if}),

$$\boldsymbol{R_{if}} = < \boldsymbol{\psi_i} | \mathbf{R} | \boldsymbol{\psi_f} > \qquad \textbf{(2.3)}$$

where the formula indicates the dipole moment change during the electronic transition between the states, the Eigen wave functions show the phase factors of initial and final states of the molecule ($|\psi_i >$ to $|\psi_f >$) which represents that the transition moment integral is a vector quantity and must be non-zero. In addition, the probability of absorption is directly related to the transition moment integral which can be defined as

$|R_{if}|^2$, therefore, the photo-physical transitions can be categorized either as '*allowed*' or '*forbidden*' depending on their absorption probability (more details about allowed/forbidden transitions will be given below).

2.2.1 The transition probability between the states

The probability of transitions are directly related to the interaction of the electric vector component of the excitation light and the dipole moment of electrons which gives rise to a change in the positions and the motions of the electrons from the initial state through to the final state. The rate of transitions is constant in time, and can be defined by Fermi's Golden Rule,

$$\boldsymbol{k_{i,f} = \frac{2\pi}{\hbar} | < \psi_f | H' | \psi_i > |^2 \rho} \qquad \textbf{(2.4)}$$

$$\boldsymbol{H' = e\hat{r}}$$

where $k_{i,f}$ is the transition rate between initial (i) and the final (f) electronic states, ρ is the density of final states, H' represents the perturbation factor between the states and the appropriate operator for the absorption and emission is the electric dipole operator ($e\hat{r}$) which affects only the electronic component of the wavefunction; the vibrational and spin wavefunction are insensitive to the dipole operator. Then Eq.2.4 is re-written considering the electronic (ψ_{el}), vibrational (ψ_{vib}) and the spin (ψ_{spin}) components of the wave function,

$$\boldsymbol{k_{i,f} = \frac{2\pi}{\hbar}\rho | < \psi_{el,f} | e\hat{r} | \psi_{el,i} > |^2 | < \psi_{vib,f} | \psi_{vib,,i} > |^2} \qquad \textbf{(2.5)}$$

$$\boldsymbol{| < \psi_{spin,f} | \psi_{spin,i} > |^2}$$

As seen in Eq.2.5, the transition probabilities of the molecules are characterized by the set of solutions to the wave function. The possibility of changes in orbital (electronic), spin (spin-orbit coupling) and nuclear (vibrational) configurations will appear as prohibition factors during the transition.[9] If any of these factors is zero, then the transition is said to be forbidden. An important approximation is proposed by Born and Oppenheimer, which states that the motions of electrons is faster than the motion of nuclei, therefore the wave function of an energy state can be determined by considering the wave function of electrons and nuclei separately. In the case of fully electronically allowed transitions, these transitions may be restricted due to the possibility of changes in spin or nuclear configurations, thus indicating the key role of structural changes (i.e. stretch of polymer backbone, twist or rotation of the repeat units, etc.). The reason is that, the absorption is so fast and the molecule cannot change shape on this time scale. The transition probability strongly depends on the strength of the coupling between the wave function of the initial and the final states, $< \psi_f | H' | \psi_i >$ is the matrix element, which describes the degree of coupling of the states. That means if the coupling is strong then the transitions occur rapidly. The mean lifetime of the excited states (t) is therefore associated with the transition rate $(k_{i,f})$ or the so-called decay probability and the relation between them is defined as $t = \frac{1}{k_{i,f}}$. For instance, the transition rates between the orbitals that are located on the same part of the molecule, i.e. π-π* transitions, may be higher than the transition rates between orbitals located on different parts of the molecule, i.e. charge transfer transitions. Furthermore, the transition probability depends on the density of final states where the transition may occur through a number of states with the same energy (degenerate states), however, in many cases there is a continuum of final states, e.g. vibrational states.

2.2.2 Selection rules

The transition probability of the electrons can be evaluated more precisely when the geometry or symmetry of the states are considered together with the electronic, nuclear and the spin components of the wave functions. Selection rules describe the

conditions needed to classify the transitions as either allowed or forbidden. Addressing this point, the transitions are classified as "allowed" if the transition moment integral is non-zero, and are called "forbidden" if the transition moment integral is equal to zero. The spin multiplicity (*m*) is one of the selection rules, and can be associated with the electronic state degeneracy in which the change occurs in total angular momentum of the electron. In conjugated molecules, the electronically excited states are formed obeying the *m=2S+1* rule, where *S* is the total spin of the all the electrons in all orbitals. One of the electronically excited states is named as the singlet state (S_1) where the spin of the electrons is opposite (spin-paired), and the overall spin of the state is zero (S=0, see Eq. 2.6), but has the multiplicity of 1. This situation is governed by Pauli's exclusion principle, which states that no more than two electrons in an orbital can contain the same spins. This principle subsequently denotes that the singlet state, the spin number is equal to zero, but, the multiplicity of the state is 1. The ground state of the electrons is also spin-paired and designated as a singlet ground state (S_0).

The second excited state is called the triplet state (T_1) where the spin of the electrons are parallel and the overall spin of the state is non-zero (S=1, see Fig.2.6). The spin number is therefore equal to 1, and the multiplicity of states is 3 ($m_s = 0, \pm 1$, see Eq. 2.7). The triplet excited states are relatively lower energy levels (typically ~1 eV for conjugated polymers)[10] than the singlet excited states in accordance with Hund's rule, which states that the electrons reside in their most stable arrangement when their spin multiplicity is maximum. In the presence of an external magnetic field, the triplet state can be recognized because it splits into three sub-energy levels. However, the same situation is not valid for a spin-paired singlet state. It should also be noted that, the triplet state cannot be populated by direct absorption of light. The reason is that the absorption of a photon occurs on a very short time scale, this time is not sufficient for spin inversion, therefore, the population of triplet states only occurs through indirect photophysical processes (e.g. intersystem crossing) which will be discussed in detail in following section.

The term "*allowed"* is used for the electronic transitions where the multiplicity is conserved between the same multiplicity states, e.g. $S_0 \rightarrow S_1$ or $T_1 \rightarrow T_2$, whereas, the term "*forbidden*" is used for the transitions between the states having different multiplicity,

e.g. $S_0 \rightarrow T_1$. Even though, multiplicity is the most rigid selection rule, it is still highly possible to see the inverse electronic transitions between different multiplicity states, e.g. $T_1 \rightarrow S_0$, however, these states have less transition probability comparing with the spin allowed transitions.[3] In general, the transition between the pure S_1 and T_1 states are strictly forbidden due to the orthogonally positioned spin wave functions give rise to make the probability of transition zero.[11] The difference in energy between excited singlet and triplet states is equal to twice the value of exchange integral ~2β. The exchange interactions strongly depend on the overlap of the respective electron wave functions. If the overlap of the wave functions is significant between HOMO-LUMO, then the exchange energy will be large, whereas, if the overlap is not significant, then the exchange energy will be reduced. The latter typically occurs in the molecules where the HOMO and LUMO occupy different parts of the molecule.

During the electronic transition, angular momentum should be conserved. In general, the magnetic field is generated due to the orbital motions of the electron, which interacts with the spin magnetic moment of the electron and results in a change in direction of spin angular momentum. As a result of this change, the character of singlet and triplet states are exchanged, in which the degree of exchange depends on the distance between the nucleus and the orbital of the electron. Therefore, the transitions between the states are more allowed if high atomic number atoms are involved, e.g. Pt and Ir, which decrease this distance between the electron and the nucleus as well as introduce strong mixing of overlapping orbitals that mix the singlet and triplet character of the state yielding pronounced spin-orbit coupling. In this case, an initially excited triplet state (T_1) may include partial contributions from states with the same or different multiplicity, e.g. S_1, T_2 or even other possible excited states, and form the states with mixed characteristics which depend on spin-orbit enhancing factors, such as the presence of heavy metals, applied exposing magnetic fields or the existence of unpaired electrons.

Symmetry is also one of the important selection rules that determines the allowed/forbidden nature of transition in the molecular system. In order to call the transitions symmetry allowed, the orbital overlaps (in the same region of space) must be maximum between the same symmetry states, e.g. $\pi \rightarrow \pi^*$. On the contrary, the electronic transitions between the different symmetry states are forbidden due to different spatial

arrangement of the orbitals giving rise to small spatial overlap, e.g. n→π* were the orbitals are orthogonal to each other.

$$\begin{aligned} &Singlet\ state\ (S=0) && m_s = 0; && \frac{1}{\sqrt{2}}\left(\,|\uparrow\downarrow\rangle - |\downarrow\uparrow\rangle\right) \\ &Triplet\ state\ (S=1) && m_s = +1; && |\uparrow\uparrow\rangle \\ &&& m_s = 0; && \frac{1}{\sqrt{2}}\left(\,|\uparrow\downarrow\rangle + |\downarrow\uparrow\rangle\right) \\ &&& m_s = -1; && |\downarrow\downarrow\rangle \end{aligned} \qquad \textbf{(2.6)}$$

Figure 2.6 The spin orientations are presented for singlet and triplet states, where the m_s values show the z-component of the spins.

In addition, if the wave functions of electronic states retain their sign (as symmetrical or anti-symmetrical) during the transitions, then they have ungerade (u) or odd symmetry. If the sign of the wave function is altered during the transition process then they have gerade (g) or even symmetry. According to the parity of selection rules, the electronic transitions are called "allowed", once the transitions occur between different parities, e.g. g→u (*or vice versa*). As a good example of allowed transitions can be given the transition from the ground state (S_0) of gerade symmetry to excited state (S_1) of ungerade symmetry of the molecule. Conversely, the transitions between the same parity of wave functions are forbidden, e.g. g→g or u→u, for instance, the transition from S_0 (gerade symmetry) to S_2 (gerade symmetry) is forbidden, which can only occur *via* an intermediate ungrade state.

2.2.3 Franck-Condon Principle

This principle describes the intensity distribution within the vibrational energy levels of the initial and final electronic states. In principle, all electronic transitions including radiative (FC emission), non-radiative or absorption (FC absorption) must

occur vertically as shown in Fig.2.7. The electronic transitions occur in a very short period of time (~10^{-15} s), which is very fast compared with the motion of the nucleus (~10^{-12} s). Therefore, during the electronic transition the relative position and velocity of the nuclei is assumed unchanged due to the massive inertia of the nuclei. After the electronic transition has occurred, vibronic transitions take place and give rise to a change in the equilibrium geometry of the molecule which typically occurs as enhancement of bond lengths resulting in significant change in electron distribution due to the disruption in equilibrium of Coulomb forces of atoms.[12] According to the Born-Oppenheimer approximation,[13] it is possible to predict the electron distribution in diatomic molecules (however for polymers it is really complicated) by means of assuming the nuclei of the molecules are frozen during the electronic transition. Each electronic state in a molecule has its own vibrational energy levels. The shape of their potential energy curves aid in understanding how the molecular energy changes as a function of the molecular bond length.[14]

As seen in Fig.2.7, the electronic transition is represented by simply drawing a vertical line from the lowest vibrational level to the S_1^2, where strong overlap of the wave functions occur. However, it is not always the case that a transition takes place from the lowest vibrational energy level of the ground state, and generally the most probable transitions occur between the states where the position and the momentum of the nuclei remains more or less stable. In addition, if the structure of a molecule does not show displacement during the electronic transition, then, the transition occurs from the lowest vibronic of the ground state to the lowest vibrational excited state of S_1, i.e. $S_0^0 \rightarrow S_1^0$. In this case, the expected absorption spectrum becomes an unstructured sharp band, however, this is a very rare situation. If an electronic transition also results in a shift in the equilibrium position of the molecular structure, then the excited electron from ground state couples with the vibrational energy level of the S_1 where the strong overlap of the wave functions occurs, i.e. $S_0^0 \rightarrow S_1^2$ (Fig. 2.7). In this case, the initially formed excited state geometry seems unstable for its particular electron distribution, and further transition of electrons occur between the same multiplicity states in the range of $10^{-12}s$ where the final states have the most stable geometrical arrangement. The process occurs in a way that the excess energy of the upper excited vibronic states is not conserved in the system

and is released thermally as a result of molecular motions. As a consequence, the Franck-Condon principles states that, during the radiative transitions, the geometry of the nuclei is assumed unchanged, and, during the non-radiative transitions, the motions of the nuclei is assumed unchanged.[7]

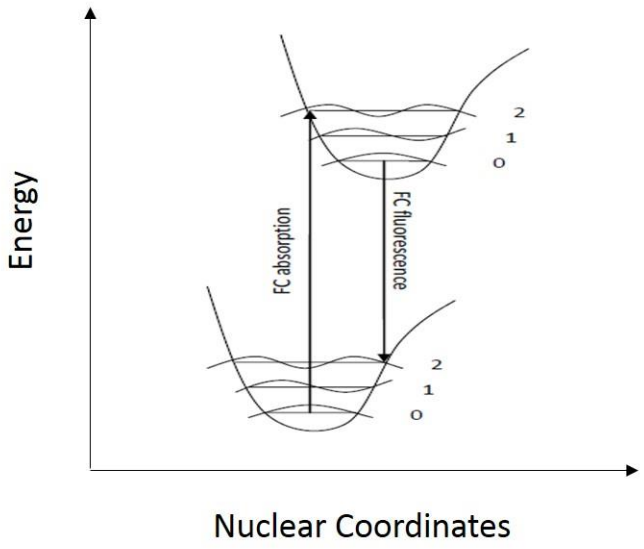

Figure 2.7 The possible transitions are represented as from the lowest ground state to the upper singlet excited state as well as the change in wave functions are schematic in vibrational energy levels of ground and excited states. The figure is adapted from Ref.[15]

2.2.4 Optical decay transitions

After photon absorption, several photo physical processes occur within the electronic states of the molecules which can mainly be categorized as non/-radiative decay processes. The sign of radiative process is "emission" where the excited electrons release their energy through photon emission when returning to the ground state, i.e. fluorescence (FL) or phosphorescence (PH). Fluorescence emission takes place between the lowest excited singlet and ground state ($S_1 \rightarrow S_0$), whereas, phosphorescence emission takes place between the lowest excited triplet and ground state ($T_1 \rightarrow S_0$). As for non-radiative processes, the excited state electron releases its energy by following the internal conversion (IC) or intersystem crossing (ISC) process, as a consequence of these

process no emission appears. For simplicity, these possible non/-radiative processes can be mapped out schematically using a Jablonski diagram as shown in Fig. 2.8.[12]

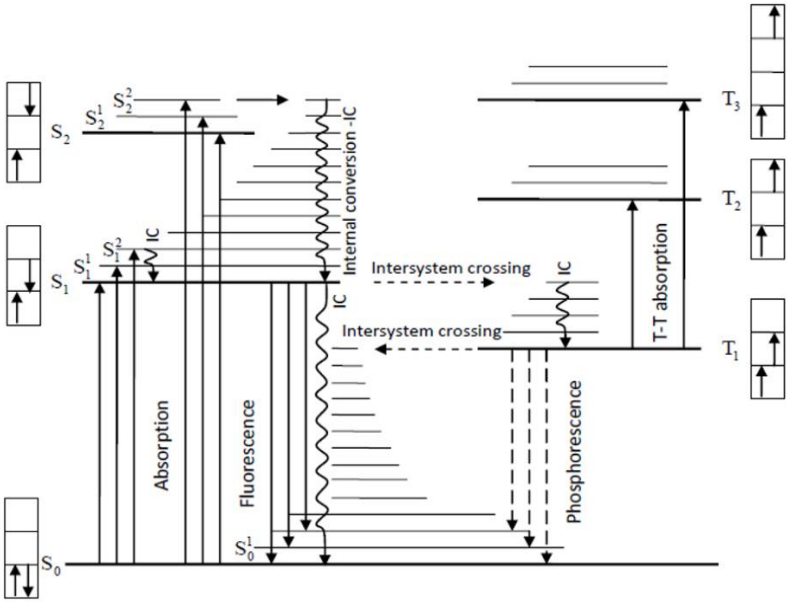

Figure 2.8 A Jablonski diagram showing the possible photo-physical transitions in organic conjugated molecules. The abbreviations are present to make the diagram simply clearer. The figure is adapted from Ref.[8]

One of the possible non-radiative process not represented in the scheme is reverse intersystem crossing (rISC) occurring from an upper excited triplet state to singlet excited state (details will be given in the following section). In the case of high photon exposure, it is possible for triplet-triplet absorption to occur which is assigned as T-T absorption in the diagram. This is a form of energy transfer where a virtual photon is transferred between the two excited states. Furthermore, the singlet states are assigned using S_0 for the ground state, and S_1 and S_2 for the first and higher excited states, respectively. In the same way T_1, T_2 and T_3 are used for denoting the first and higher possible triplet excited states. The spin orientations are assigned in small boxes nearby the corresponding excited state showing the possible spin orientations in the lowest and higher vibrational energy levels of excited states. The excess vibrational energy levels are denoted by using superscripts, e.g. S_1^2 and S_2^1, etc.

In principle, the energy of the absorbed photon is used to excite the electrons from the ground state to higher excited states. In doing so, some portion of the energy is

transferred into electronic ($E_{Electronic}$), vibrational ($E_{Vibrational}$) and rotational ($E_{Rotational}$) energy levels (see Eq. 2.7 for total energy of the ground state) of the molecule. Therefore the energy of emitted light from excited singlet state is relatively less than the energy required for excitation and so the emission usually appears at longer wavelengths comparing with the absorption band as defined by Stoke's law. In essence, rotational energy levels are generally concerned with the gas phase of molecule, therefore, it is out of the scope of this thesis, which concerns itself with organic molecules in the solid state or in solution. Consequently, only electronic and the vibrational energy levels will be considered for interpreting photo-physical processes in this thesis.

$$\boldsymbol{E_{Total} = E_{Electronic} + E_{Vibrational} + E_{Rotational}} \qquad \textbf{(2.7)}$$

In essence, it is possible for the transitions from any vibrational levels of the ground state to any vibrational level of the excited state to occur. As a result of excitation, normally the singlet excited state is formed as the initially excited state. Fluorescence emission occurs as a result of radiative decay of the excited singlet species to a lower ground state (S_o), which is a spin-allowed process between the same multiplicity states. According to Kasha's rule, the fluorescence emission generally arises from the lowest excited singlet to the ground state, the reason why, upper excited states potential energy surfaces cross the S_1, so that, the energy in upper excited states is rapidly lost due to the molecular vibrations which is called "*vibrational cascade"*. Therefore, the upper excited states generally decay non-radiatively to the lowest singlet excited state, as already termed internal conversion (IC). This is a very rapid decay process (~10^{-12} s) and the competition between radiative and non-radiative decay channels is not compatible, except for a couple of examples showing weak emission from upper excited states,[16] hence, the majority of the emission occurs from lowest singlet energy levels.

The lifetime of fluorescence is typically on the order of nanoseconds which can be measured by measuring the decay of fluorescence intensity using some time-resolved techniques (which will be presented in detail in experimental chapter of this thesis). The calculation of the fluorescence lifetime is crucially important to get information about the

sum of the rate constants (including non-/radiative rates) which represents the time that molecules stay in the excited state before returning to the ground state. If the non-radiative processes are ignored, the measured lifetime is called *"intrinsic lifetime"* and shows only radiative decay involvement. Another radiative process that occurs from triplet excited state of the molecule is phosphorescence (PH) which is a spin-forbidden process occurring between the different spin multiplicity states ($T_1 \rightarrow S_0$). The lifetime of the PH is relatively longer (typically in the range of hundreds of microseconds) than the fluorescence lifetime which strongly depends on deactivation process. However, it is not easy to compare directly the lifetimes of both radiative processes due to the different environmental conditions required to measure them. For instance, the lifetimes of fluorescence can be measured either at room or low temperatures, however, the PH measurements are generally only taken in oxygen free environments and at very low temperatures (e.g. at a rigid glass matrix temperature for solutions) due to the fact that the deactivation of triplet states occurs very rapidly at room temperature and the interaction of triplet states with the possible species is a kind of bimolecular processes (that will be discussed below) giving rise to significant reduction in quantum yields and lifetimes of the triplet state. Consequentially, the longer lifetime and lower energy of the triplet excited state compared with the singlet excited state can be associated with the difference in their electron spin arrangements.

In non-radiative processes, the transition of an electron occurs between the excited state and the ground state without photon emission. During these transitions the energy is not conserved, but released thermally. These processes can be classified in two categories in terms of change in their spin multiplicity during the transitions. One of the processes is IC occurring between the same spin multiplicity states, in which the electron in the upper excited states undergoes rapid conversion to the lowest excited state, e.g. $S_1^2 \rightarrow S_1$ or $T_2^2 \rightarrow T_1$, by means of converting the excess energy into kinetic energy. It is also possible to observe IC between the lowest excited singlet state (S_1) to the singlet ground state (S_0), however, there exists a competition with the radiative process (fluorescence). The second process is ISC, which occurs between different spin multiplicity states, e.g. $S_1 \rightarrow T_1$. This is one of the photo-physical mechanisms that populates the triplet state from lowest excited singlet state. In principle, the absorption of a photon gives rise to singlet

state population then the electrons follow intersystem crossing to a triplet state (T_1 or some upper triplet states, T_n) and populate the state before emitting as phosphorescence, therefore, we can call it an *"isoenergetic"* process. In addition, the ISC may happen as a result of direct spin-orbit coupling between the S_1 and the upper vibrational states of T_1 or alternatively $S_1 \rightarrow T_n$. The effective population of the triplet state depends on the intersystem crossing rate (k_{ISC}) which is directly associated with the singlet-triplet energy gap (ΔE), i.e. $k_{ISC} \sim \exp(-\Delta E)$,[17] and the relative electronic configurations of the states. In general, this energy gap is around 1 eV, but, can also depend on the chemical structure of the molecules.[10, 18] So if the energy gap is very small or comparable, efficient transitions are highly likely to occur between the states, whereas, if the energy gap is large and incomparable, the intersystem crossing rate is often slow and inefficient. The same conditions are also valid for the reverse intersystem crossing process (rISC) which occurs between $T_1 \rightarrow S_1$, as the rate of rISC strongly depends on the singlet-triplet energy gap which must be small for effective transitions.

2.2.5 Energy gap between the singlet and triplet excited states

Intersystem crossing is a process occurring between the lowest excited singlet and triplet states ($S_1 \rightarrow T_1$), by means of changing spin orientation. This non-radiative process is more favourable once the vibrational energy levels of excited states overlap greatly. If the spin-orbit coupling interactions are increased in the molecules then a change in spin orientation (flip up and down) becomes easier, therefore, intersystem crossing is most common process in heavy metal complexes. The energy gap between the singlet and triplet states (ΔE_{S-T}) should be considered as one of the important factors for transitions from S_1 state to T_1 which means the smaller energy separation, the more rapid intersystem crossing and more pronounced Franck-Condon overlap. A larger energy separation results in the slower intersystem crossing rate and a poorer Franck-Condon factor. Using this knowledge, the ISC rate (k_{ISC}) can be evaluated depending on mainly two factors; the energy gap (ΔE_{S-T}) and the relative electronic configurations of states. The energy gap is calculated considering Pauli's Exclusion principle, which shows that electron

correlations in a state, reduce electron repulsions, and gives rise to a more stable lower energy triplet state. So, the energy gap is calculated as follows,

$$E_{Singlet} = E_{S_1-S_0} + K + J \quad \textbf{(2.8)}$$

$$E_{Triplet} = E_{S_1-S_0} + K - J \quad \textbf{(2.9)}$$

$$\Delta E_{S-T} = E_{Singlet} - E_{Triplet} = 2J \quad \textbf{(2.10)}$$

where K is the coulomb interaction integral (energy) due to repulsive interaction of electrons and, J is the electron exchange integral (energy) due to repulsive interaction of electrons in the HOMO with those in the LUMO. As an overview of the equations, the coulomb interactions give rise to an increase of the energy of the states, while, the exchange integral plays a crucial role in reducing the energy of the triplet state, but not the singlet state. The reason for this is that, the lowest excited singlet state is populated from the same spin-paired ground state with no need for a spin-flip during the transition, while for the triplet state, a spin-flip is required with the energy of separation is defined by the exchange integral ($2J$). The value of this depends on the degree of overlap between the ground (HOMO) and excited state (LUMO) wave functions. Usually the overlap is significant giving rise to a large exchange value on the order of 0.7-1.0 eV.[10,19]

2.3 The formation of excited states in organic molecules

2.3.1 Excitons

In conjugated molecules, the absorption of a photon promotes an electron from the HOMO to the LUMO resulting in formation of free electron-hole (e-h) pairs. In this case, the delocalisation of an electron does not occur over the entire chain of the molecule, but rather the electron localizes nearby to its correlated hole pair. In this way, a strong

correlation is built up between e-h pairs that attract to each other *via* Coulomb forces ($-e^2/\varepsilon r$). These correlated (couloumbically bound) e-h pairs as well as distortion arising from excitation in organic semiconductors forms a quasi-particle which is called an "exciton". In the Coulomb force formula, r represents the distance between e-h pairs (so-called exciton radius), ε is the dielectric constant associated with the screening effect of the total potential energy, referring to the energy of all atoms and possible free electrons that exist around it. The magnitude of the dielectric constant varies depending on the molecules, and plays an important role in exciton properties. For instance, in inorganic semiconductors, the magnitude of the dielectric constant is typically large, where Coulomb interactions between e-h pairs are reduced by charge screening resulting in large-sized (larger than the typical lattice space) Wannier-Mott type excitons.

An exciton is a neutrally charged state which means the excitons do not play a role in charge-transport properties. Instead, they can move through the system resulting in net energy transportation. The binding energy (E_B) between e-h pairs determines whether the charges will behave as free charges or excitons. If the binding energy is too small < 0.1 eV then the e-h pairs are assumed free (uncorrelated) charges as happens in inorganic semiconductors, whereas, if the binding energy is 0.5 eV or larger, then e-h pairs are assumed strongly localized (correlated) in excited states as excitons. The relative orientations of the electron's spin (multiplicity) designates the origin of the excitons either as a singlet state or triplet state (as explained in section 2.2.2 above). Three types of excitons can be distinguished from each other by their binding energies (E_B) of the electron-hole pairs and also localization units of the conjugated molecules; Frenkel, Wannier-Mott and charge transfer excitons.

Unlike inorganic semiconductors, the dielectric constant in organic semiconductors is small, therefore, the Coulombic interactions between the e-h of an exciton is very strong, i.e. small-sized (usually < 1nm).[20] Frenkel excitons (also termed exciton-polaron), which are tightly bound lowest-energy excited states and the binding energy is around 0.1- 1.5 eV and the charge separation is around 10 Å,[17] therefore, they are small-radius excitons. Frenkel excitons are typically observed in organic materials where the charges are located on the same monomer unit (i.e. on a single conjugated segment) with a

small/zero dipole moment. Frenkel excitons are therefore, also called “intra-chain” excitons in polymer chains. Due to their residence upon the same molecular unit, the singlet-triplet splitting in Frenkel-type excitons are ~1 eV.

Wannier-Mott excitons typically have high dielectric constants where the electron-hole separation is relatively large (~100 Å),[17] resulting in small overlap between their wave functions, and a low binding energy of about ~10 meV. The delocalization of the e-h pairs over different parts of a polymer chain results in Wannier-Mott excitons, generally called “inter-chain” excitons. Furthermore, the binding energies of excitons are affected by the temperature (due to vibrational movements of atoms), therefore, the absorption band experiments are usually taken in the range of room temperature (RT) to low temperature. At RT, the thermal energy of an electron is around 0.025 eV, which is sufficient to dissociate Wannier-Mott excitons as free e-h pairs, however, more energy is required to dissociate Frenkel excitons into free (uncorrelated) charges. The third type of exciton is called a charge transfer exciton where the electron-hole pairs are localized on typically adjacent parts of the molecules and show strong correlations. Generally, these excitons occur as a result of charge transfer between the different molecular species to form the maximum charge density, where large movement of electron density occurs from one part of the molecule to another. Typically, this movement of the charges is driven by a large dipole moment between the electron and the hole giving rise to form a permanent dipole moment in the excited state which is called the intramolecular charge transfer (ICT) state.

2.3.2 Density of states (DOS) and exciton migration

The energy levels of conjugated molecules are characterised by randomly varying length of the conjugated segment (due to kinks, defects, bond angle distortion along the polymer backbone, etc.) resulting in an inhomogeneous distribution (broadening) of electronic transitions which is called density of states (DOS). The broadening is typically more significant in solid states due to an infinite number of possibilities for molecular conformation and enhanced intermolecular interactions (packed nature) resulting in a

broad distribution of the energies for the excitonic transitions. The shape of the DOS is described by a Gaussian distribution,[1]

$$\mathbf{g(\varepsilon)=\frac{1}{\sqrt{2\pi}\sigma}\exp\left(-\frac{(\varepsilon-\varepsilon_0)^2}{2\sigma^2}\right)} \qquad \mathbf{(2.11)}$$

where ε is the energy of charged molecule and ε_0 is the average exciton energy where the Gaussian distribution centred around, and σ is the standard deviation (~50-100 meV in conjugated polymers) representing a measure for the energetic disorder. Within the density of the states, the migration of excitons occurs in a dispersive way between the conjugated segments, which can be understood in terms of energy transfer from higher to lower energy sites (from short to longer chain segments). Due to the highly disordered nature of the films such a migration process takes some time and is considered as a random walk (i.e. diffusion) within the close proximity conjugated segments (see Fig.2.9). However, in solutions, this is a rather rapid process due to the fact that the exciton cannot move between the chain segments.

After excitation, the excitons are created in the high energy tail of the DOS, that is followed by exciton (downhill) migration towards to lower energy sites (see Fig. 2.9), where the migration process shows time-dependent rates. One can consider that there exist many excitonic energy states in high energy tail of DOS. In this case, the downhill migration occurs in short distances and the process is very fast. However, when the mean energy of the distribution is lower, then the available sites become rare and the migration occurs over long distances, hence, the process turns into relatively slow non-dispersive regime. Consequentially, the downhill migration process stops after sometime (~100 ps), when the excitons settle around the energy of the most populated states ($\varepsilon_0 = -\sigma^2/kT$).[1,21]

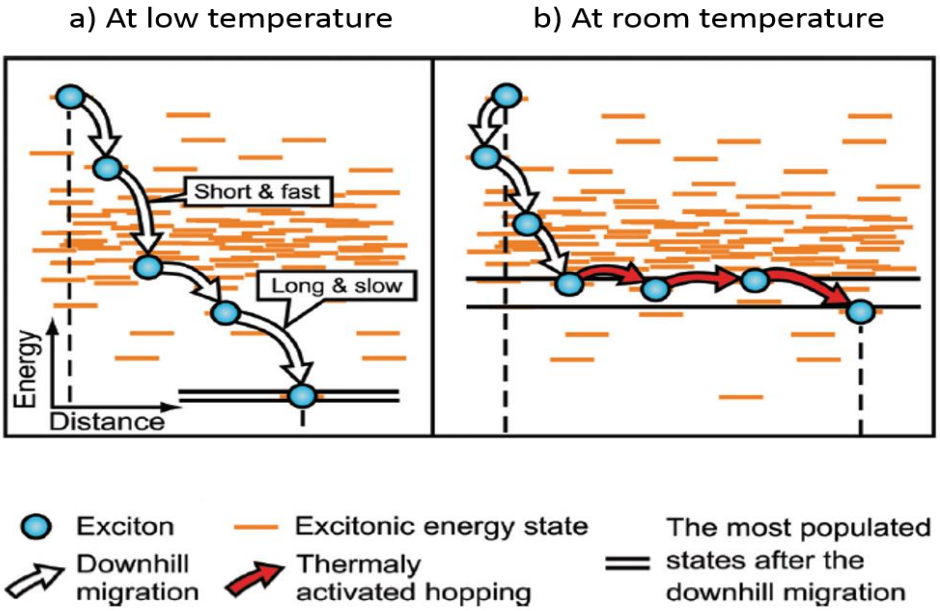

Figure 2.9 Exciton diffusion process and distribution of density of states are picturised a) at low temperature and b) at room temperature. The picture is adapted for use from Ref.[21]

The energy of this state is representative of the peak position of the (0-0) transition and varies with temperature. For instance, at low temperatures, the energy of the state localises around the low energy tail of the DOS, which is due to the fact that there is not sufficient energy to promote the down-hill excitons back to higher energy states, therefore, the excitons are trapped into their low energy sites, and also thermally activated hopping between the close proximity conjugated segments is not a matter of issue (due to weak exciton-phonon coupling). However, at higher temperatures, the energy of the most populated states increases and localisation occurs around the middle of the DOS, the reason is that down-hill excitons are thermally activated by absorption of phonons leading to increase the probability of thermally activated hopping movements between the occupied and close proximity conjugated segments. Therefore, the exciton diffusion distance is relatively longer at high temperatures than at low temperatures. Consequentially, both of the exciton diffusion processes can be explained by either Förster and Dexter type energy mechanisms (will be explained in detail in section 2.4), briefly; the Förster mechanism is usually operative for long-range migrations, i.e. singlet

excitons, however, the Dexter mechanism is appropriate for the short-range migrations, i.e. triplet excitons.

2.3.3 Polarons

In conjugated molecules, the electronic properties are explained with considering the quasi-one-dimensional tight binding model[22] where electron-phonon interactions occur between the electrons and the possible local distortions. Once a charge (either an electron or a hole) is injected into the system, it can move through the conjugated system and perturb the covalent π-bonding molecular structure inducing polarizations and self-localized nonlinear excitations upon the bonds of the molecules due to the strong electron-phonon coupling. Therefore, the presence of charge in the organic semiconductor gives rise to local structural changes (i.e. structural reorganizations to surround the charge by phonons) and particularly local distortions (relaxations) which are the charge trapping regions. This charge, together with associated distortion (phonon) in an organic semiconductor forms a quasiparticle, which is called as "polaron" (P^- for an electron and P^+ for a hole). A polaron is an uncorrelated charge carrier (having $q = \pm e$ and $spin = 1/2$) which can be formed by means of charge injection into the device, doping or by dissociation of an exciton. A polaron is able to move freely, thus, plays an essential role in the conductivity and charge transport properties of a system. For instance, in the case of applying an electric field into the system, the mobility of the polarons is increased (assuming the binding energy is overcome) creating a net electric current, allowing for transportation of charges between the chromophores. In particular, in organic light emitting devices (OLEDs), applying an electric field results in migration of oppositely charged polarons in the active (emissive) layer, where charge recombination occurs for emissive neutral excitons.

Since most organic molecules do not have intrinsic free charge carriers, direct charge generation occurs by following two main processes; either using an external electric field to inject a charge into the system or using a chemical dopant to trigger redox reactions (oxidation or reduction) in the chains. There exist three main types of polaron states in organic semiconductors; free-electron (negative) polarons, free-hole (positive)

polarons and geminate (exciton) polaron pair. The initial two polarons are charge carriers, and there is no correlation between their spin orientations, however, distinctively a geminate-polaron pair is an energy carrier formed by oppositely charged polarons with the same individual event. The geminate polaron pairs are formed when the binding energy of exciton is overcome, then they may decay back to excitonic state and undergo radiative decay, which is thought to be a source of the delayed fluorescence phenomena. Furthermore, If the spin correlation is carried out between the oppositely charged polarons, then, they may recombine and form an intermediate state which is a charge transfer state [23] and can be associated with singlet and triplet characters.[24] Therefore, polaron pairs are usually considered as the intermediate step from excitons to free charges with energy levels of polaron states located between HOMO-LUMO energy level of pristine organic molecules (see Fig.2.10).

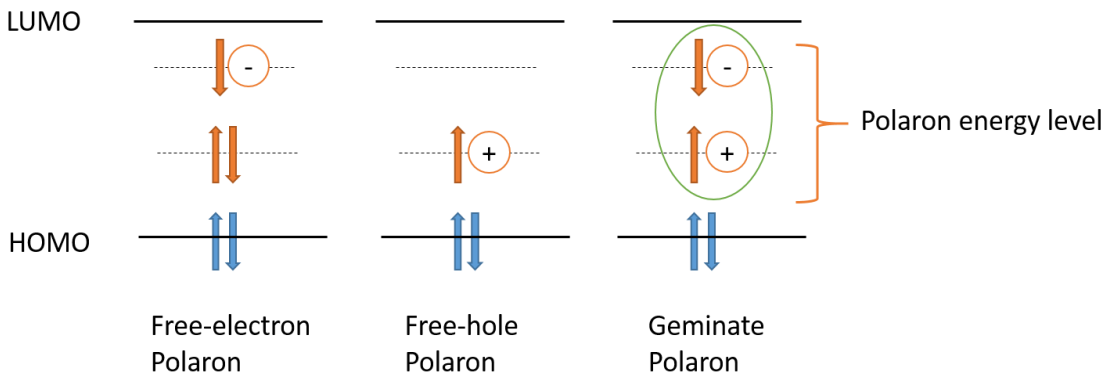

Figure 2.10 Orbital energy level schemes of polaron states from left to right; free-electron polaron, free-hole polaron and geminate polaron states.

2.3.4 Dimers, excimers and exciplexes

Dimers (physical) are formed as a result of weak ground state interactions between two identical molecules where the molecules have special spatial arrangements with respect to each other. Typically, the formation of dimers is favoured depending on relative molecular structure orientations, where the interactions of π-systems are enhanced in particular arrangements, i.e. sandwich and herringbone,[1] however, no chemical bonds are

formed between themselves. The absorption spectrum of dimers or higher aggregates can be obtained due to having ground state interactions, and the obtained emission spectrum is considerably broadened when compared with the monomer spectrum. As a result of the dimerization process, the exciton energy level of dimers show energy splitting, where two energy bands readily exist; one of higher and another of lower energy than the corresponding monomer exciton energy level.[8] The relative orientations of the monomer transition moments decide whether the emission spectrum of a dimer is to be red-shifted or blue-shifted in the energy spectrum. In this case, optically allowed transitions of dimer states are determined by relative orientations of the dipole transition moments of monomer units, which can be written as,[8]

$$\boldsymbol{M_D = \frac{1}{\sqrt{2}}\,(M_1 + M_2)} \qquad \textbf{(2.12)}$$

where M_1 and M_2 denote the dipole transition moments of constituent monomer units. If the dipole moments of monomers are in parallel or antiparallel (head-to-tail) arrangements then one of the excited dimer states (upper or lower lying state) shows a zero transition moment (forbidden), and other one is nonzero (allowed), therefore, the optical transition is only allowed in one state, not both of the dimeric states. However, if the spatial arrangements of dipole moments have different orientations (different from parallel or antiparallel), the transition moments are nonzero, and highly possible to contain optical transitions to both of the dimeric states. In this case, both states become emissive, however, the lower lying dimeric state has a relatively lower oscillator strength than the upper one, that is the reason for why low quantum yield and long-lived emission are observed from energetically lower lying dimeric state.[25]

Excimers can be considered as dimers resulting from the interaction of two identical monomers in which the interactions of pairs are repulsive in the ground state (hence the pairs can easily dissociate), but attractive, once one of the molecules is excited with an intermolecular separation of typically 3-4 Å.[25] Therefore, the excimers only exist in excited states, and are therefore called “excited dimers”. Since the ground state of

excimers are dissociative, the absorption of excimers is not observable (the dimers and higher aggregates are different and have stable ground states giving rise to stronger coupling between the monomers than excimers) and the emission of excimers appears as broadened and unstructured at longer wavelengths of the monomer emission. In particular, the formation of excimer emission shows a concentration dependence. At low concentrations (10^{-5} M or less) emission is concentration independent and only monomer emission is observable, however, at higher concentrations, the monomer emission gradually decreases in intensity, while a new unstructured excimer band is formed and starts emitting at lower energies. During the concentration dependence measurements, it is possible to observe an isoemissive point in the emission spectrum, which is an indication of exclusive involvement of two emitting species (monomer and excimer). Furthermore, the excimers usually do not show significant solvent-polarity dependent shifts as happens in exciplexes. This gives a clue that the charge transfer interactions are much more pronounced in exciplexes, but not significant in excimers, which is due to the more polar environment of exciplexes.[7]

An exciplex (a charge transfer complex or charge transfer state) can be considered as an excimer, stabilised between two non-identical constituents by means of charge transfer resonance interactions. An exciplex is formed from the interaction of two non-identical (i.e. typically in donor-acceptor type molecules) monomers in which the interactions between the monomer units are repulsive in the ground state, however, once one of the molecule is excited, then an attractive force is built up between electronically excited and polarizable ground state monomer units. An exciplex is a totally new electronically excited state and has a totally new emission band showing the unique characteristics of an exciplex, but not its constituents. This band is featureless and red-shifted when compared with the constituent monomer emission which shows strong solvent-polarity dependency, therefore, more polar solvents easily shift the emission to lower energies in the spectrum.

2.4 Energy transfer in conjugated molecules

The migration of excitons (either as singlet or triplet excitons) plays an important role in energy transfer mechanisms between molecules. As a result of optical excitation, the excited electronic states of singlets or triplets can be populated by means of energy transfer from one molecule to another (intermolecular migration, i.e. from donor to acceptor) or as uncoupled parts of a macromolecule. The energy transfer process can be either intermolecular (between different polymer chains) or intramolecular (between different parts of the same chain). One such radiative energy transfer route is termed trivial energy transfer, a self-absorption (or reabsorption) mechanism, and the other non-trivial non-radiative processes are called Förster and Dexter type energy transfers. In trivial energy transfer, the energy of the emitting species, the donor (D*), excites an adjacent molecule the acceptor (*A*) creating a real photon exchange. This is a two-step process, which can be given as,

$$\boldsymbol{D^* \rightarrow D + h\upsilon} \qquad \textbf{(2.13)}$$

$$\boldsymbol{h\upsilon + A \rightarrow A^*} \qquad \textbf{(2.14)}$$

where trivial radiative energy transfer takes place, if the emitting photon frequency from the donor unit is in the range of the absorption band range of the acceptor. This energy transfer does not require any interaction between the D and A units, therefore, it usually appears in dilute solutions.[1] The efficiency of self-absorption strongly depends on the following parameters; the quantum yield of the emitting donor state, the amount of acceptor molecules (concentration) in proximity of emitting photons from D, acceptor extinction coefficient and the portion of spectral overlap between the emission of the donor and the absorption of the acceptor molecules (see Fig. 2.11).[7] For instance, if there exists a good spectral overlap, then the lifetime of the excitation is significantly increased where the trivial mechanism works as a trapping site for radiative decay.

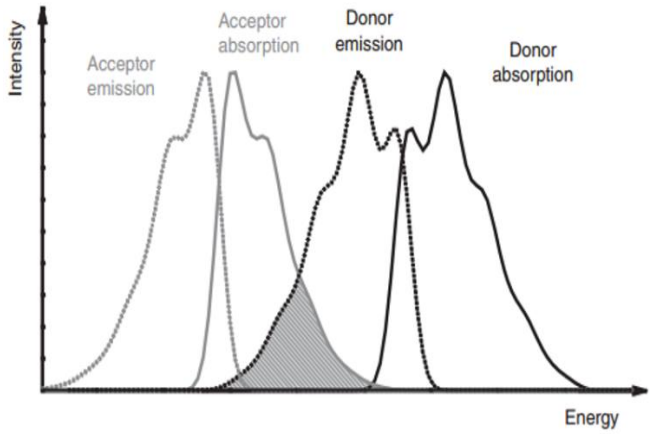

Figure 2.11 The grey area represents the spectral overlap between the emission of donor and the absorption of acceptor. The figure is adapted for use from Ref.[1]

In addition, non-trivial or non-radiative processes occur between the states following Fermi's Golden rule as explained in the previous section (Section 2.2.1). According to this theory the perturbation factor (H') can be considered under two categories; exchange interaction (H'_e) and coulomb interaction (H'_c) which help to determine the energy transfer mechanism as Förster (or resonant) and Dexter type energy transfers.

2.4.1 Förster energy transfer (FRET) mechanism

Förster type energy transfer occurs between the two molecules (e.g. between isolated donor (D) and acceptor (A) units) in a non-radiative way. Unlike the self-absorption mechanism explained above, no intermediate emission is observed from excited donor unit, and the acceptor unit is excited from its ground state by means of a dipole coupling interaction, which is a one-step process and can be summarised as,

$$\boldsymbol{D^* + A \rightarrow D + A^*} \qquad \textbf{(2.15)}$$

the coupling interaction occurs between the electron in donor excited state and the electron in the acceptor ground state which gives rise to excitation by means of coulomb interactions (H_c'). The oscillation of the electron in the donor excited state gives rise to a perturbative effect on the acceptor electron in ground state by means of building a resonant dipole oscillation between the electrons where there is a distance between the D and A units (charge separation) that is usually larger than the molecular sizes. In this case, spectral overlap is required between emission spectrum of donor and the absorption spectrum of the acceptor. Consequentially, the energy transfer may occur to excite the electron of the acceptor from its ground state to excited state by means of dipole-dipole interactions. Therefore, the energy in this system is proportional to the dipole moments of the D-A units (μ_D ,μ_A), and the intermolecular separation (R), with the coulomb interaction energy be defined as,

$$E^C \propto \frac{\mu_D \mu_A}{R^3} \kappa \qquad \textbf{(2.16)}$$

where the κ represents the orientation factor coming from relative orientations of the transition dipole moments of donor and acceptor units (equal to $\cos ø - 3\cos ø_D \cos ø_A$)[1] $ø$ represents the angle between the emission (donor) and absorption (acceptor) transition dipoles, which strongly depends on the relative orientations of transition dipole moments (κ^2, see Fig. 2.12). κ^2 =2/3 is usually the average value of the orientation term, when the dipole moments are identical (Eq. 2.18). In the case of co-linear arrangements the value of κ^2 is 4 and $\kappa^2 = 1$ (for parallel arrangement) and $\kappa^2 = 0$ (for perpendicular arrangement). Considering these parameters, the Förster energy transfer rate can be written considering the measurable value of fluorescence lifetime and the quantum yield of the state,

$$k_{D-A} = \frac{9000\ (\ln 10)}{N_A} \frac{1}{2^7 \pi^5 n^4} \frac{\Phi_D}{\tau_D} \frac{\kappa^2}{R^6} \int_0^\infty I_D\ (\lambda) \varepsilon_A(\lambda) \lambda^4 d\lambda \qquad \textbf{(2.17)}$$

$$\boldsymbol{\kappa^2 = (\cos \phi - 3 \cos \phi_D \cos \phi_A)^2} \qquad \textbf{(2.18)}$$

where N_A is the Avagadro's number (6.02 x10^{23} mol^{-1}), n is the refractive index of the medium, Φ_D is the quantum yield of donor in the absence of acceptor, τ_D is the lifetime of the donor in the absence of acceptor. $I_D(\lambda)$ is the corrected fluorescence intensity in the wavelength range of λ to λ+Δλ with the total area under the emission curve normalized to unity, ε_A is the extinction coefficient of the acceptor ($M^{-1}cm^{-1}$).

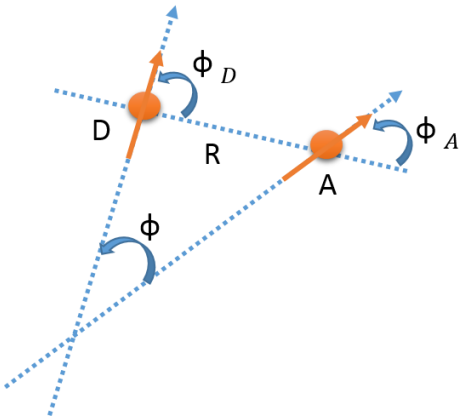

Figure 2.12 The transition dipole moment vectors are represented with the ø angle between the electron dipoles in the D and A units. The distance between the dipoles is assigned with R with their relative angles to the vector joining to the D and A. The figure is adapted for use from Ref.[1]

The transfer rate can be written in a more convenient way, [1,26]

$$\boldsymbol{k_{D-A} = \frac{1}{\tau_D}\left(\frac{R_0}{R}\right)^6} \qquad \textbf{(2.19)}$$

the Förster radius (R_0) is given as,[26]

$$R_0^6 = \frac{9000\,(\ln 10)}{N_A}\,\frac{1}{2^7\pi^5 n^4}\,\Phi_D \kappa^2 \int_0^\infty I_D\,(\lambda)\varepsilon_A(\lambda)\lambda^4 d\lambda \qquad \textbf{(2.20)}$$

where wavelength is given in nanometers and the Förster radius can be calculated from experimental data which is taken from the spectral overlap of emission and absorption. In the case of $R = R_0$, then the transfer rate can be defined as $k_{D-A} = \frac{1}{\tau_D}$ which shows that the Förster energy transfer rate is proportional to the decay rate of donor unit. At R_0 half of the electrons decay radiatively and the remaining half are transferred to the acceptor unit by means of Förster energy transfer mechanism.

The efficiency of the Förster energy transfer between the D-A (Φ_{D-A}) can be determined as,

$$\Phi_{D-A} = \frac{k_{D-A}}{\left(\frac{1}{\tau_D}\right) + k_{D-A}} = \frac{1}{1 + (\frac{R}{R_0})^6} \qquad \textbf{(2.21)}$$

Equation 2.21 describes the fraction of photons absorbed by the donor unit that are transferred to the acceptor unit. Consequentially, the Förster radius is typically around 10-40 Å, therefore, it is called a long range energy transfer mechanism. The Förster energy transfer mechanism preserves spin and so predominantly singlet excited states (donor unit) are transferred to singlet ground states (acceptor unit) (see Fig. 2.13) by the Förster mechanism, however, a triplet exciton that is located on a phosphorescent donor can also undergo FRET.

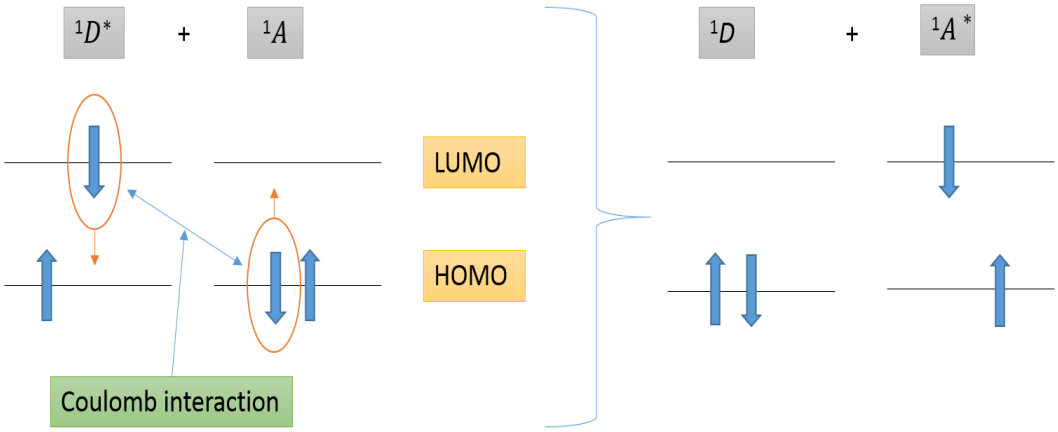

Figure 2.13 The schematic representation of singlet-singlet Förster energy transfer between D-A units. The picture is adapted for use from Ref.[7]

2.4.2 Dexter energy transfer mechanism

Another energy transfer mechanism, Dexter-type energy transfer, appears in organic molecules. The energy transfer mechanism depends on electron exchanges over a small distance which can occur between chromophores on the same or adjacent molecules. According to this mechanism, the energy is transferred non-radiatively by means of exchanging electrons from excited donor unit (e.g. $^1D^*$) to ground state acceptor (e.g. ^1A). This energy transfer mechanism is generally known as "quenching" which is the mechanism that reduces the molecular fluorescence. Typically, Förster energy transfer becomes dominant once the molecular distances are larger than 10 Å, whereas, Dexter energy transfer becomes dominant at smaller molecular distances (< 10 Å), e.g. the molecules in the solid state are packed resulting in pronounced interaction in terms of their wavefunctions. Usually Dexter energy transfer is efficient due to small interaction distances between the molecules. Dexter transfer again preserves spin, but because it is an exchange and only requires wavefunction overlap both singlet and triplet energy can be transferred.

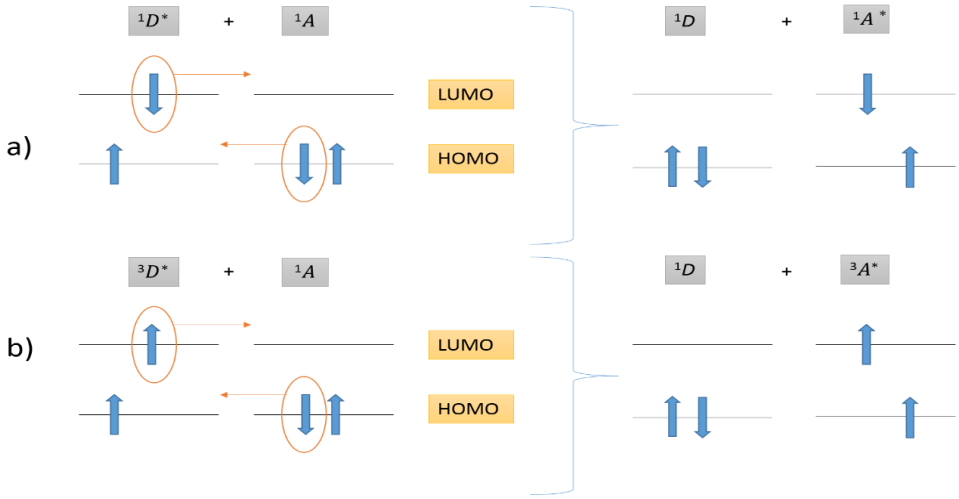

Figure 2.14 The schematic representation of Dexter energy transfer between D-A units **a)** Singlet-singlet Dexter energy transfer **b)** Triplet-triplet Dexter energy transfer**.** The picture is adapted for use from Ref.[7]

The Dexter mechanism for exchanging electrons between the orbital units of D and A, can be represented in Fig.2.14. The overlap of wavefunctions (between excited donor and ground-state acceptor) is required, and for that reason the D and A units must close enough for efficient energy exchange, i.e in solid films. If the D and A units belong to different molecules, then the energy exchange can also occur with collisions, as happens in solutions and gases.

The rate constant of Dexter energy transfer is expressed as,

$$k_{Dexter} = KJexp(\frac{-2R_{D-A}}{L}) \qquad \textbf{(2.22)}$$

According to Eq. 2.22 the rate constant for Dexter energy transfer decreases exponentially, as the distance between the D-A increases, which is due to the exponential decrease in electron cloud density resulting from an increase between the electron and the nuclei distances.

When comparing the Förster and Dexter energy transfer mechanisms, there are some points that need to be highlighted. Firstly, Förster energy transfer is a long-range

energy transfer mechanism by means of transition dipole coupling between the molecules, the efficiency of this transfer is defined by the sixth power of charge separation distance (R^{-6}), therefore, any possible tiny changes in relative distance will affect the overall energy transfer mechanism. However, Dexter is a short range direct electron exchange mechanism which is dependent on the transition dipole moments and the energy transfer rate decreases exponentially ($\exp(-\frac{2R}{L})$. Dexter energy transfer is typically observable in triplets as a triplet-triplet energy (TTE) transfer mechanism, rather than singlets. In singlets, resonance excitation is the dominant energy transfer mechanism compared with the electron exchange mechanism. Secondly, the rate of Förster energy transfer strongly depends on the oscillator strength of the radiative transitions from the excited state to the ground state, however, the rate of Dexter energy transfer is independent of this. Thirdly, the oscillator strength plays key role on the transitions between the ground and the excited state of acceptor which determines the efficiency of energy transfer and can be determined from experimental data, whereas, it is not possible to determine in Dexter energy transfer from such measurements.

2.5 Bimolecular and thermally activated processes for delayed fluorescence

In addition to unimolecular non-radiative decay mechanisms, at high excitation density conditions, radiative bimolecular annihilation processes also play an important role in determining the photophysics of organic molecules. In essence, excitons are highly mobile particles and they may interact with each other in a bimolecular fashion. In the case of unimolecular processes, the rate of reaction depends linearly on the concentration of excitons, whereas, bimolecular processes show a quadratic dependence on the exciton concentration. In a very general form the decay rate of the excited state can be defined as,

$$k_G = k_D[D^*] + k_q[D^*]^2 \quad \textbf{(2.23)}$$

where the $[D^*]$ represents the concentration of excited state excitons, k_D represents the unimolecular decay rate of the excited states and k_q is the rate of bimolecular decay of the excited states. The most common bimolecular processes that occur in organic molecules are singlet-singlet annihilation (SSA), triplet-triplet annihilation (TTA) and singlet-triplet annihilation (STA).[1] However, in this thesis, the SSA and TTA mechanisms are the centre of interest due to nature of the materials used.

2.5.1 Singlet-singlet annihilation (SSA)

The singlet excitons are highly mobile, so they may interact with each other in a bimolecular way and Förster energy transfer may occur between two excited singlet excitons. One of the excitons decays to the ground state and the other one forms a higher energy singlet excited states (e.g. S_N), and then relaxation occurs to the lowest singlet excited state by means of an internal conversion mechanism, which is called singlet-singlet annihilation and results in delayed emission originating from the S_1 state. SSA generally occurs when the singlet exciton concentration is very high giving rise to an increased probability of singlet collision due to the small distance between the excitons (usually smaller than Förster radius). This process can be summarised as,

$$\begin{aligned} S_1 + S_1 &\rightarrow S_N + S_0 \\ S_N &\rightarrow S_1 + heat \end{aligned} \quad \textbf{(2.24)}$$

where one of the singlet state is lost and the rate of singlet excitons decay can be expressed as,[1]

$$\frac{d[S]}{dt} = G_S - \frac{1}{\tau_s}[S] - k_{ss}[S]^2 \quad \textbf{(2.25)}$$

where G_S is the generation rate of singlet excitons, $[S]$ the concentration of singlet excitons, k_{ss} is the bimolecular rate constant, τ_s is the intrinsic lifetime of singlet state. The condition to see the dominant role of bimolecular processes on singlet generation is $k_{ss}[S] > 1/\tau_s$. When this condition is met, the singlet generation can be written as a function of time,

$$[S(t)] = \frac{[S_0]e^{-t/\tau_s}}{1 + k_{ss}[S_0](1 - e^{-\frac{t}{\tau_s}})} \quad \textbf{(2.26)}$$

where the $[S_0]$ represents the singlet concentration at $t = 0$. However, if the $\tau_s > k_{ss}[S_0]$, then the singlet generation as a function of time can be written,

$$[S(t)] = \frac{[S_0]e^{-t/\tau_s}}{1 + k_{ss}[S_0](\frac{t}{\tau_s})} \quad \textbf{(2.27)}$$

where the e^{-t/τ_s} component of Eq. 2.28 is considered $1 - (\frac{t}{\tau_s})$. In practice, the dominant role of SSA upon singlet generation is determined by measuring how the fluorescence intensity depends as a function of excitation light intensity, giving rise to an understanding of the origin of delayed fluorescence. The proportionality can typically be defined as Eq. 2.28.

$$I_{Fluorescene} \propto \sqrt{I_{Excitation}} \quad \textbf{(2.28)}$$

2.5.2 Triplet-triplet annihilation (TTA)

As with SSA, with high excitation density conditions two triplet excitons may collide with each other and annihilate to form either one triplet or one singlet exciton depending on the spin angular momentum conservation law. As a result of these interactions, they can produce a singlet exciton with a probability of 1/9 due to the orientation of triplet states,[1] or triplet excitons or quintuplet states with a total probability ratio of 8/9. This can be summarised as,

$$\boldsymbol{T_1 + T_1 \rightarrow \frac{8}{9}\,(S_0 + T_N)}$$

$$\boldsymbol{T_1 + T_1 \rightarrow \frac{1}{9}\,(S_0 + S_N)} \qquad \textbf{(2.29)}$$

quintuplet interactions cannot participate in TTA, because quintet states are usually energetically untenable and the energy of two triplets is not enough to produce a quintuplet state.[27,28] TTA is a very common triplet depletion mechanism, where higher energy singlet excitons (S_N) are produced a result of a collision of the triplets, which then relax to the lowest energy singlet state resulting in delayed fluorescence (p-type) from the S_1 state. The maximum total singlet generation *via* the TTA mechanism is limited to 62.5%. The spectrum of the delayed emission has the same spectral shape due to emitting from the same excited state as the prompt emission, however, the delayed fluorescence has much longer lifetime compared to the prompt fluorescence.

The rate of triplet exciton decay can expressed as,[1]

$$\boldsymbol{\frac{d[T]}{dt} = G_T - \beta_0[T] - k_{TT}[T]^2} \qquad \textbf{(2.30)}$$

where G_T represents the generation rate of triplets, β_0 is the accumulative rate constant from the radiative (k_r) and non-radiative (k_{nr}) decays, and k_{TT} is the bimolecular annihilation constant. Typically, time dependent phosphorescence and delayed fluorescence is observed depending on low or high excitation conditions. [1] The lifetime of delayed fluorescence is on the order of half of the phosphorescence lifetime.[29] In practice, the dominant role of TTA on singlet exciton generation (by the process of triplet fusion) is determined by measuring the fluorescence intensity as a function of excitation light intensity, which gives rise to an understanding of the origin of delayed fluorescence.

2.5.3 Thermally activated delayed fluorescence (TADF)

Another unimolecular photophysical mechanism behind the formation of singlet states from triplet excitons is thermally activated delayed fluorescence (TADF), or E-type delayed fluorescence. TADF forms the singlet state (S_1) via a reverse intersytem crossing (rISC) mechansim from thermally activated upper vibronic states of T_1, which can be defined as,

$$[\boldsymbol{T_1^*}] = [\boldsymbol{T_1}] \exp\left(-\frac{\boldsymbol{\Delta E_{ST}}}{\boldsymbol{k_{BT}T}}\right) \quad \textbf{(2.31)}$$

where $[T_1^*]$ represents the fraction of triplets, ΔE_{ST} is the singlet-triplet energy gap, k_{BT} is the Boltzman constant and T is the temperature. The reverse intersystem crossing rate constant can be written as,

$$\boldsymbol{k_{rISC} = A\, exp(-\frac{\Delta E_{ST}}{k_{BT}T})} \quad \textbf{(2.32)}$$

where A is the frequency factor. For the efficiency of this mechansim; ΔE_{ST} should be very small (typically $\leq k_{BT}T$ which is ~27 meV at 300 K)[30] and the reverse intersystem crossing rate should be moderately high. A small energy gap means a small overlap between HOMO-LUMO energy levels of molecules. However, the singlet-triplet energy gap is typically large in organic molecules where the excitons strongly localize in their particular energy levels, hence, a high electron exhange energy is required. Therefore, nowadays, an excited metastable state is readily formed by means of using donor-acceptor type molecular designs to make the energy gap smaller, i.e. to form a charge transfer state (CT) or an exciplex, where the high external quantum efficiency is achievable in OLED devices.[31] In this scenerio, the rISC mechanism usually works *via* this existing metastable pathway, i.e. $T_1 \rightarrow$ CT $\rightarrow S_1$ state. The great benefit of TADF is the very real possibility of 100% triplet harvesting effectively exceeding the quantum statistic limitation of OLED device efficiencies.[32] The lifetime of delayed fluorescence is on the order of the phosphorescence lifetime and the intensity of delayed fluorescence is linearly dependent on the excitation intensity, whereas, it is quadratic in bimolecular processes.

2.6 References

1. Köhler, A. & Bässler, H. Electronic processes in organic semiconductors: an introduction. (2015).
2. Aydemir, M., Jankus, V., Dias, F. B. & Monkman, A. P. Inter/Intrachain Interactions Behind the Formation of Charge Transfer States in Polyspirobifluorene: A Case Study for Complex Excited-State Dynamics in Different Polarity Index Solvents. *J. Phys. Chem. C* **119,** 5855–5863 (2015).
3. Guillet. *Polymer Photophysics and Photochemistry*. (Cambridge University Press, 1985).
4. Averill, B. A. & Eldredge, P. *Chemistry: Principles, Patterns and Applications*. (Prentice Hall, 2006).
5. Atkins, P. W. & De Paula, J. *Physical Chemistry*. (Oxford University Press, 2006).
6. Ebbing, D. & Gammon, S. *General Chemistry*.(Houghton Mifflin, 2005).
7. Turro, N. J. *Modern Molecular Photochemistry*. (University Science Books, 1991).
8. Pope, M., Swenberg, C. E. & Pope, M. *Electronic processes in organic crystals and polymers*. (Oxford University Press, 1999).
9. Turro, N. J. *Modern molecular photochemistry*. (Benjamin/Cummings Pub. Co., 1978).
10. Monkman, A. P., Burrows, H.D., Hamblett, I., Navarathnam, S., Svensson, M. & Andersson, M.R. The effect of conjugation length on triplet energies, electron delocalization and electron-electron correlation in soluble polythiophenes. *J. Chem. Phys.* **115,** 9046–9049 (2001).
11. Cowan, D. O. & Drisko, R. L. *Elements of organic photochemistry*. (Plenum Press, 1976).
12. McGlynn, S. P., Azumi, T. & Kinoshita, M. *Molecular spectroscopy of the triplet state*. (Prentice-Hall, 1969).
13. Born, M. & Oppenheimer, R. Quantum theory of molecules. *Ann. Phys.* **84,** 0457–0484 (1927).
14. Ahmed, F. A Good Example of the Franck-Condon Principle. *J. Chem. Educ.* **64,** 427–428 (1987).
15. McGlynn, S. P., Azumi, T. & Kinoshita, M. *Molecular spectroscopy of the triplet state*. (Prentice-Hall, 1969).
16. Birks, J. B. *Photophysics of aromatic molecules*. (Wiley-Interscience, 1970).
17. Pope, M., Swenberg, C. E. & Pope, M. *Electronic processes in organic crystals and polymers*. (Oxford University Press, 1999).
18. Van Dijken, A., Bastiaansen, J., Kiggen, N., Langeveld, B.,Rothe, C., Monkman, A.,Bach, I.,Stössel, P. & Brunner, K. Carbazole compounds as host materials for

triplet emitters in organic light-emitting diodes: Polymer hosts for high-efficiency light-emitting diodes. *J. Am. Chem. Soc.* **126,** 7718–7727 (2004).

19. Kohler, A., Wilson, JS, Friend, R.,Al-Suti, M.,Gerhard, A. & Bassler, H. The singlet-triplet energy gap in organic and Pt-containing phenylene ethynylene polymers and monomers. *J. Chem. Phys.* **116,** 9457–9463 (2002).
20. Sun, S.-S. & Dalton, L. R. Introduction to Organic Electronic and Optoelectronic Materials and Devices. (CRC Press, 2008).
21. Mikhnenko, O. V., Cordella, F.,Sieval, A.B., Hummelen, J.C., Blom, P.W.M. & Loi, M.A. Temperature dependence of exciton diffusion in conjugated polymers. *J. Phys. Chem. B* **112,** 11601–11604 (2008).
22. Su, W., Schrieffer, J. & Heeger, A. Soliton Excitations in Polyacetylene. *Phys. Rev. B* **22,** 2099–2111 (1980).
23. Karabunarliev, S. & Bittner, E. R. Spin-dependent electron-hole capture kinetics in luminescent conjugated polymers. *Phys. Rev. Lett.* **90,** 057402 (2003).
24. Reufer, M., Walter, M.J., Lagoudakis, P.G., Hummel, A.B., Kolb, J.S., Roskos, H.G., Scherf, U. & Lupton, J.M. Spin-conserving carrier recombination in conjugated polymers. *Nat. Mater.* **4,** 340–346 (2005).
25. Sariciftci, N. S. Primary photoexcitations in conjugated polymers molecular exciton versus semiconductor band model. (World Scientific, 1997).
26. Lakowicz, J. R. *Principles of fluorescence spectroscopy*. (Plenum Press, 1983).
27. Kondakov, D. Y. Role of triplet-triplet annihilation in highly efficient fluorescent devices. *J. Soc. Inf. Disp.* **17,** 137–144 (2009).
28. Kondakov, D. Y., Pawlik, T. D., Hatwar, T. K. & Spindler, J. P. Triplet annihilation exceeding spin statistical limit in highly efficient fluorescent organic light-emitting diodes. *J. Appl. Phys.* **106,** 124510 (2009).
29. Aydemir, M., Jankus, V., Dias, F. B. & Monkman, A. The key role of geminate electron–hole pair recombination in the delayed fluorescence in rhodamine 6G and ATTO-532. *Phys. Chem. Chem. Phys.* **16,** 21543–21549 (2014).
30. Graves, D., Jankus, V., Dias, F. B. & Monkman, A. Photophysical Investigation of the Thermally Activated Delayed Emission from Films of m-MTDATA: PBD Exciplex. *Adv. Funct. Mater.* **24,** 2343–2351 (2014).
31. Jankus, V., Data, P., Graves, D., McGuinness, C., Santos, J., Bryce, M.R., Dias, F.B. & Monkman, A.P. Highly Efficient TADF OLEDs: How the Emitter–Host Interaction Controls Both the Excited State Species and Electrical Properties of the Devices to Achieve Near 100% Triplet Harvesting and High Efficiency. *Adv. Funct. Mater.* **24,** 6178–6186 (2014).
32. Dias, F. B., Bourdakos, K.N., Jankus, V., Moss, K.C., Kamtekar, K.T., Bhalla, V., Santos, J., Bryce, M.R. & Monkman, A.P. Triplet Harvesting with 100% Efficiency by Way of Thermally Activated Delayed Fluorescence in Charge Transfer OLED Emitters. *Adv. Mater.* **25,** 3707–3714 (2013).

CHAPTER 3: EXPERIMENTAL METHODS

"*Any physical theory is always provisional, in the sense that it is only a hypothesis: you can never prove it. No matter how many times the results of experiments agree with some theory, you can never be sure that the next time the result will not contradict the theory*"

Stephen Hawking

The aim of this chapter is to give the background information behind the data collection process. This covers sample preparation, and measurement techniques that have been commonly used. The measurements always started with collecting basic information about the samples by measuring steady-state spectra including absorption and fluorescence spectra. Then step by step, the majority of data were collected using time-resolved spectroscopy techniques and the time-correlated single photon counting method.

3.1 Sample preparation

Samples were usually prepared by dissolving each compound in different polarity solvents (generally, methyl cyclohexane, chlorobenzene, 2-methyltetrahydrafuran and ethanol), which were provided by ROMIL and SIGMA-ALDRICH companies. The solvents were excellent for spectroscopy applications requiring high-purity (~99%) and low residue on evaporation. Thin film samples were prepared using three different methods; spin-coating, drop-casting, and thermal deposition.

3.1.1 Solution samples

In order to prepare solution samples, the materials were mainly dissolved in different polarity solvents and left to stir overnight to achieve well-dissolved solutions. Concentrations were prepared as dilute as possible to avoid aggregation (typically in the range of 10^{-5} M -10^{-6} M). The basic absorption and emission measurements were taken both in air-saturated and degassed environments (if necessary) using quartz cuvettes (6Q) with a path length of 1 cm, and a long-necked quartz degassing cuvette with a path length of 1 cm, respectively. Each cuvette was cleaned using nitric acid, whereby, the cuvettes were filled with nitric acid and left for at least two days to remove all possible contaminants.

For degassed solutions, the samples were held in a long-necked cuvette and pump-freezing-thawing cycles were repeated at least five times to remove the dissolved oxygen completely from the environment, which was a really crucial step for triplet based measurements. The cuvette was then properly mounted into a cryostat (Janis Research Co, INC.VNF 100) system where the measurements could be repeated under vacuum either at room temperature or low temperature (at liquid nitrogen temperature ~77 K).

3.1.2 Solid-state samples

Spin coating and drop-casting films

For the fabrication of spin-coated samples, highly concentrated (10 to 15 mg/ml) solutions were prepared using chlorobenzene or toluene solvents. Then, 12 mm diameter sapphire or quartz substrates were cleaned by leaving in nitric acid for 2-3 days followed by UV exposure in a mixture of half nitric acid and half-pure water. The spin-coating technique involves first drop casting an excess amount of sample solution on to the substrates. Then the substrate was accelerated to a tuneable speed level and the fluid material spun off the edge of the substrate in a uniform manner. In this way, the thickness of the samples can be controlled by the spinning speed and timing of the spin-coating

step, and also the concentration and the viscosity of the solution are the key factors to determine the thickness of the films.

For drop casted films, various concentrations of solutions were used, sometimes very concentrated (10 to 15 mg/ml) or very dilute ones (0.1 to 1 mg/ml). In both cases, the solutions were directly drop-cast on top of the substrates and left on the heater (70-80 ^{0}C) for 10-15 minutes. Contrary to the spin-coating method, it is hard to control the thickness and uniformity of films, however, this method is quite simple and the samples can be prepared using a very small amount of material. Typically, it is the preferable method if the measurements do not specifically require a particular film thickness and uniformity. In some measurements, an inert zeonex matrix (cyclo olefin polymer) or PVA (poly-vinyl-alcohol) was used to isolate and confine the molecules, which was commonly the preferred method in weak phosphorescence measurements. These drop-cast films were prepared as a mixture of materials and matrixes (zeonex or PVA) having different weight-to-weight ratios.

Thermally deposited films

Thin film vacuum deposition was made in organic electro active materials (OEM) group's clean room using a commercial Kurt-Lesker Spectros II deposition system (Fig. 3.1) consisting of an 18" x 36" deposition chamber and 6 organic sublimation and 3 metal evaporation sources (Fig. 3.2) where two different materials can be deposited at once. During the deposition process, 12 mm diameter sapphire or quartz substrates were placed in the vacuum chamber with appropriate masks, and the new target material was loaded into one of the ceramic crucibles. Afterwards the chamber was pumped down with rotary and turbo pumps, respectively, until the pressure of the chamber reached ~10^{-7} mbar (the lowest vacuum conditions were required for highly pure films). To achieve this pressure, the chamber needs to be left pumping overnight.

As seen in Fig. 3.2., the 6 organic sublimation source crucibles are separated in space from 3 inorganic evaporation sources and powered by separate thermal source controllers and the evaporation process can be controlled by using Sigma deposition

software, employing the standard deposition procedures. During the evaporation process, the target material was heated continuously and the evaporated molecules condensed on the substrate to produce uniform films.

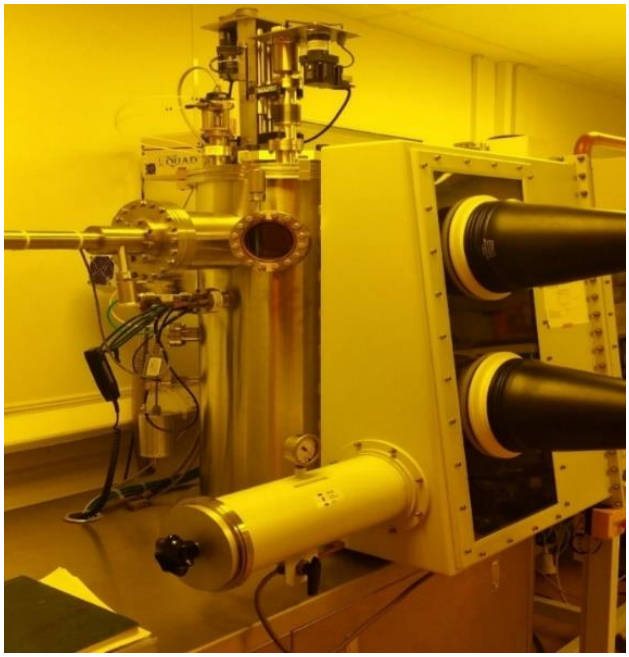

Figure 3.1 Kurt-Lesker Spectros II deposition system in Durham university organic electro active materials (OEM) research group clean room.

The evaporation activity (deposition rate) as well as the thickness of the films were monitored by using separate quartz crystal film thickness sensors (called quartz crystal microbalance system (QCM)) and a software program (called as SAS-242). One of the sensors is used for inorganic sources, which is placed in the middle of three crucibles, and the other ones are for the organic sources. The sensitivity of the sensors is crucial and it is therefore necessary to calibrate them before each deposition, if any of the sensors sensitivity drops below 80%, it should be replaced with a new one for accurate depositions. In essence, the piezoelectric principle is in operation on QCM where an electrical signal is generated in the presence of mechanical stress (addition of mass). There exists a quartz crystal, which is located above the evaporating source in the vacuum chamber and resonates to a frequency generated by an oscillating circuit. During the

deposition process, the materials are deposited on both the substrate and the surface of the crystal and the amount of deposited mass on the crystal surface can be understood by measuring the change in resonating frequency (the difference in initial frequency of crystal and after deposition) as stated by the Sauerbrey equation (Eq. 3.1),[1]

$$\Delta f = \frac{2f_0}{A\sqrt{\rho_q \mu_q}}\Delta m \qquad \textbf{(3.1)}$$

where Δf $(f_0 - f)$ is the measured frequency change, f_0 is the resonant frequency of the crystal prior to the mass change , Δm is the mass change, A is the piezoelectrically active area, ρ_q is the density of quartz (2.648 g cm^{-3}) and μ_q is the shear modulus (2.95 10^{11} $g.cm^{-1}s^{-2}$). Consequentially, a change in the mass per unit area gives rise to a corresponding change in the frequency; for instance, the addition of mass decreases the resonant frequency, that is used to calculate the thickness of deposited films (Eq. 3.2),

$$Thickness_{Observed} = \frac{C_q x \rho_q}{\pi x \rho_m x f}\, x \arctan\{Z\, x \tan\left(\frac{\pi\, x \Delta f}{f_0}\right)\} \qquad \textbf{(3.2)}$$

where C_q is the crystal constant (1.668 x 10^{13} Hz/m^{-10}), ρ_m is the density of the molecule and Z is the Z-factor of the material. So, in order to calculate the thickness of the molecules the density of molecules and the Z-factor should be known. In addition, to determine the true thickness of the films at tooling factor needs to be calculated. A tooling factor corrects the variations arising from relative geometric positions of QCM and the substrate due to the fact that the crystal can show quite different deposition rates than reality, and concomitantly the thickness of the monitored films do not show true values. In practice, when using a new material source in a deposition, an approximate value is usually chosen for the tooling factor, however, this value should be corrected to get the true thickness of the deposited film. Calibration of the thickness monitors is achieved by evaporating the organic materials on silicon dioxide substrates (at least 4 different silicon

dioxide thickness are used) with known silicon dioxide thickness, then the true deposition thicknesses is determined by using a Spectroscopic Ellipsometer VASE (J.A. Woollam Co. Inc.). Consequentially, the actual tooling factor ($T.F._{Actual}$) is determined with the formula (Eq. 3.3.),

$$T.F._{Actual} = T.F_{Appox.} \mathrm{x} \frac{Thickness_{Actual}}{Thickness_{Observed}} \qquad (3.3)$$

where $T.F._{Approx.}$ represents the approximated tooling factor during the deposition, $Thickness_{Actual}$ is the true thickness observed by Elippsometer and $Thickness_{Observed}$ is the thickness that is obtained from thickness monitors. Furthermore, the Z-factor is the ratio of the acoustic impedance of the sensor and deposited molecule (Z-factor = Z_q/Z_m) which is used to match the acoustic properties of the deposited material (Z_m) to the quartz sensor (Z_q=8.83 Pa.s.m^{-1}). The calculation of the Z-factor can be made if the shear moduli of the materials are known. There are reported Z-ratio values for well-known materials, but typically Z-factor and shear moduli are not readily known for the new materials. Therefore, the determination of Z-factors can be made empirically (which was not done in the course of this work).

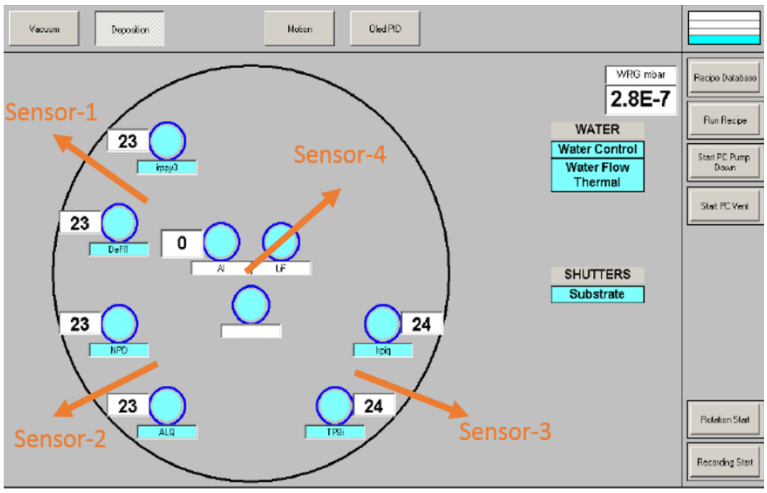

Figure 3.2 The screenshot of the software window representing the sensor positions with crucibles (sky blue circles).

3.2 Steady-state measurements

3.2.1 Absorption

The electronic absorption spectrum of the molecules indicates the probability of absorption of a photon by a molecule and its variation with wavelength. The bulk absorption properties of molecules are governed by the Beer-Lambert law which states that when molecules are illuminated with monochromatic light, the photons of the light pass through the homogenous absorbing sample resulting in interactions with the sample. A portion of these photons are absorbed depending on the distance of transmission, concentration of solution, but not intensity of the light (at low intensities). This process is well-defined by the following equation,

$$\log_{10}\left(\frac{I_0}{I}\right) = A = \varepsilon c d \qquad (3.4)$$

where the intensity of incident and transmitted light are represented with I_0 and I, respectively. d is the transmitted distance (cm) along the sample, c is the molar concentration (moles/litre) and ε is the molar extinction coefficient ($M^{-1}\ cm^{-1}$) showing the measure of transition probability and A is termed the optical density. In the case of highly allowed π→π* transitions, the value of molar extinction coefficient is typically around $10^4 \sim 10^6\ M^{-1}\ cm^{-1}$ which is relatively high value compared to the value of n→π* transitions ($1 \sim 500\ M^{-1}\ cm^{-1}$).[2] This can be determined from the absorption spectra which may include several sharp peaks with different intensities from different optical transitions. The most intense peaks in a spectrum are often associated with π→π* transitions and possibly appear alongside weaker transitions such as, n→π*. The observation of σ → σ* transitions require high energy (typically below 150 nm), therefore, the main transitions in the spectrum in this work are π→π* and n→π* which are readily accessible in the ultraviolet and visible part of the spectrum.

Absorption spectra were taken using a Shimadzu UV-3600 UV/VIS/NIR spectrometer (Fig. 3.3) which has a double beam photometric system ranging from -6 to 6 A. A high sensitivity monochromator makes the stray-light level very low (0.00005% at 340 nm) achieving a maximum resolution of ±0.1 nm. It is also possible to achieve wavelength accuracy of ±0.2 nm, which is more than enough to measure normally broad spectra of the organic materials precisely. To record the absorption spectrum of molecules, the excitation source of the system is split into two parallel beams, one beam passes through the sample and the second one passes through a reference arm. The reference for the solution measurements must be an identical cuvette containing the same solvent used to dissolve the sample. For thin films, the reference must be an identical substrate i.e. quartz or sapphire. The system can be controlled automatically by UVProbe software.

Figure 3.3 Shimadzu UV/VIS/NIR spectrometer in Durham university OEM research laboratory

3.2.2 Photoluminescence

As a result of photo-excitation emission may occur from the sample which is called photoluminescence. If the process is "allowed", e.g. $S_1 \rightarrow S_0$, it is specifically called fluorescence as explained in theory section. The fluorescence spectrum can be approximated as the mirror image of the absorption band. By measuring both absorption

and photoluminescence spectra, it is likely that fundamental information about the conjugated molecules will be obtained.

To measure the steady-state photoluminescence, a Jobin-Yvon Horiba Spex Fluoromax-3 (Fig. 3.4.) or Jobin-Yvon Horiba Fluorolog FL3-22 (Fig. 3.5) spectrofluorimeters waw used. The Fluoromax-3 (Fig.3.4) consists of a xenon arc lamp, housing slits, excitation and emission monochromator, sample compartment (for solution and films), and emission and reference detectors. It also has a fast scanning capability (up to 200 nm/second) and the slits can be adjustable from the computer at the expense of maximum resolution.

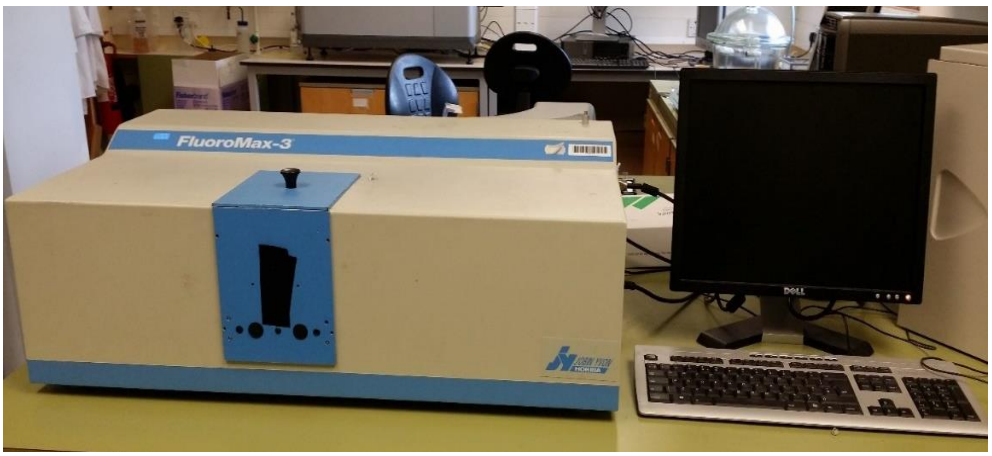

Figure 3.4 Jobin-Yvon Horiba Spex Fluoromax-3 spectrofluorimeter in Durham university OEM research laboratory

Fluorolog FL3-22 spectrometer (Fig. 3.5) consists of a xenon lamp (450 W), double grating monochromator (covers 250 nm to 1000 nm, with the highest spectral resolution of 1 nm) , sample compartments (for solution and films) which incorporates an L-shaped geometry under excitation and the collection of the emission, a photomultiplier tube (PMT) for detection and a reference detector (Si photodiode). The system-slit sizes (both excitation and emission) can be adjusted automatically at the expense of maximum resolution through the software.

Figure 3.5 Jobin-Yvon Horiba Fluorolog FL3-22 spectrofluorimeter in Durham university OEM research laboratory. The blue sphere on top of the spectrofluorimeter is used for PLQY measurements of films.

3.2.3 Quantum yield measurements

The photoluminescence quantum yield (PLQY) is an intrinsic property of organic light emitting materials which can be defined by the ratio of absorbed photons to emitted photons,

$$\Phi_{PLQY} = \frac{Emitted\ photons}{Absorbed\ photons} \qquad (3.5)$$

This equation describes the simplest definition of PLQY measurements, however, various experimental methods were developed to measure PLQYs even for both solution and film samples.

PLQY solution measurements

In general, the measurements were performed using the Fluoromax spectrofluorimeter. The well-known methods for PLQY measurements are single-point

and comparative methods. In this thesis, the comparative method was mainly preferred [3] which involves the use of a reference material with well-known PLQY value. From this point of view, 9, 10-diphenylanthracene (DPA) was chosen as the reference material with known PLQY (actually there are 3 PLQY values of DPA in the literature and the averaged value was taken as 0.74). The PLQY can be calculated using the equation below

$$\Phi_{PLQY}=\Phi_R\left(\frac{m_{sample}}{m_{Reference}}\right)\left(\frac{n^2_{sample}}{n^2_{Reference}}\right) \quad \textbf{(3.6)}$$

where n is the refractive index of sample and m is the slope of integrated intensity versus absorption values for different concentrations of solution (at least 5 different concentrations).

PLQY film measurements

Thin film quantum yield measurements were carried out using an integrating sphere method.[4] With this method, film samples were mounted in a 4.5" integrating sphere (see in Fig. 3.5 blue sphere on top of Fluorolog) and 5 different spectra were taken using a Jobin Yvon Horiba Fluoromax spectrofluorimeter. Then PLQY can be calculated using the equation below

$$\Phi_{PLQY} = \frac{\int I_{sample\ emission} - (1-A)\int I_{secondary\ emission}}{A \int I_{empty\ sphere}} \quad \textbf{(3.7)}$$

$$A = \frac{\int I_{excitation\ beam\ without\ sample} - \int I_{excitation\ beam\ with\ sample}}{\int I_{excitation\ beam\ without\ sample}} \quad \textbf{(3.8)}$$

where A is the absorption of the thin film which can be determined measuring the excitation beam with/out sample, to obtain the intensity difference between excitation spectra, which gives us the absorption of the thin film. The sample emission spectra is collected ($I_{sample\ emission}$) by mounting the sample at 45^0 in sphere, and the secondary emission spectra ($I_{secondary\ emission}$) is collected by putting the sample at the bottom of the sphere.

3.3 Time-resolved nanosecond spectroscopy

The majority of experimental data were taken using a gated time-resolved nanosecond spectroscopy setup (Fig. 3.6.) which provides more detailed information about the molecular behaviour of the fluorophores compared with the steady-state fluorescence measurements. In particular, many sub-atomic events occur on the same time scale as the fluorescence decay, such as radiative/non-radiative transitions between the energy states, resonance-energy transfers or rotational diffusion. Therefore, gated time-resolved nanosecond spectroscopy provides an advantage to investigate the time-dependent nature of photophysical processes thoroughly and is also it allows us to gain much insight into the chemical surroundings of the molecular structures. The set-up consists of two separate excitation sources, one of which is a pulsed Nd:YAG laser (EKSPLA-SL312), the fundamental wavelength (1064 nm) which is frequency doubled and tripled to generate correspondingly two harmonics, 532 nm (2^{nd} harmonic) and 355 nm (3^{rd} harmonic). The specifications of the laser are 150 ± 20 ps pulse duration, tunable energy of each pulse ranging from 100 nJ to mJ (>5 mJ), ±5 % pulse energy stability and the maximum repetition rate is 10 Hz. The second laser source of the setup is a pulsed Nitrogen laser (LTB-MNL 100, Lasertechnik Berlin) which emits 337.1 nm. The main specifications comprise of tunable pulse energy typically up to 120 µJ, tunable repetition rate ranges from 1 to 30 Hz and the pulse energy stability is ≤ 2%. Also, a home-built single pass dye laser system, which can be pumped by both harmonics of the Nd:YAG laser, offering the advantage five further wavelengths as excitation sources over a wide range, i.e. 450, 500, 550, 630, 670 nm.

The emission collection side of the experiments is as follows; the thin film samples are placed in a He Displex cryostat system where the temperature can be tuned in the range of 300 K-14 K, under vacuum conditions (at least 10^{-4} mbar). The samples were mounted on a sample holder plane at a 45^0 angle to the incident laser beam. The sample temperature was controlled precisely (~0.1 K) by LakeShore 321 model temperature controller which features a feedback resistor heater.

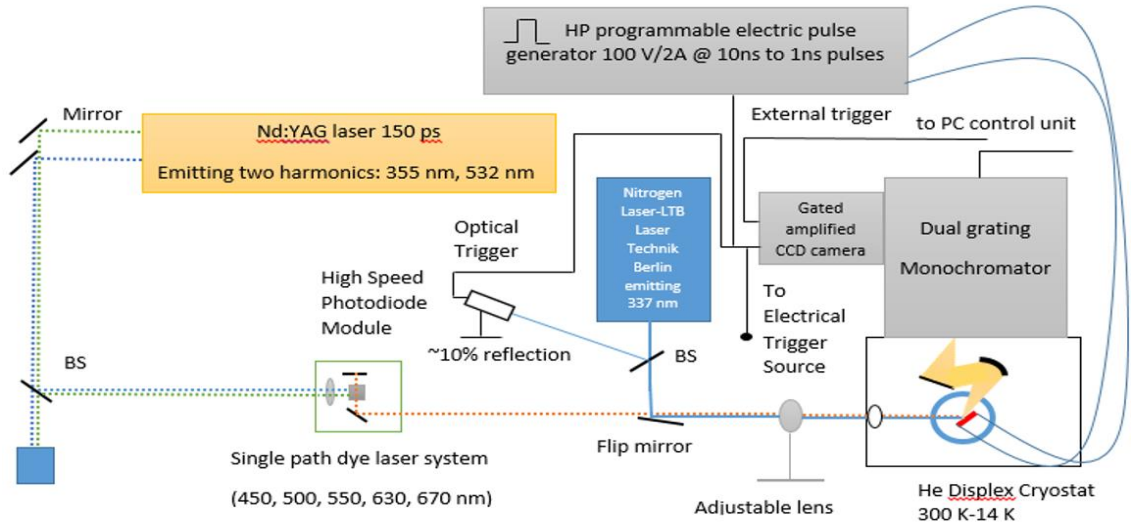

Figure 3.6 Time-resolved gated nanosecond spectroscopy setup. For solid state measurements He displex cryostat system is used in the range of 300 K-14 K, for the solution measurements liquid nitrogen cryostat (Janis Research) is used between 300 K-77 K.

The samples in solution were excited in a liquid nitrogen cryostat system (Janis Research), where precisely a LakeShore 332 model temperature controller controlled the ambient temperature of the cryostat. For the measurements, the cryostat was mounted on a home-built holder. Emission from the samples was passed through a cut-off filter to get rid of the scattered excitation beam and then focused on the entrance slit of a spectrograph (Jobin Yvon, Triax 180) which has a 300 lines/mm gratings blazed at 500 nm (for visible emissions) and a second blazed at 1000 nm (for far-red emissions). The spectrograph gratings and slit width can be automatically controlled by Labview software. The emission was detected using a gated ultrafast iCCD 4 PICOS camera (Stanford Computer

Optics), which consists of a Micro Channel Plate (MCP) image intensifier and CCD array for high sensitivity and sub-nanosecond time resolution (the shortest gating time is 200 ps and the delay time range from 0 to 80 s with min. 10 ps steps). The highest achievable image resolution is ~180 lp/mm, which gives rise to the lowest pixel distortion (<0.1 pixel) and 572 x 736 (VxH) pixel resolution. The horizontal pixel directions were calibrated for certain wavelengths associated with the grating positions using a CAL-2000 mercury-argon calibration light source (Ocean Optics), and, the vertical pixels are particularly related with the integration of the spatially distributed emission for one-dimensional spectra. However, in this thesis, the energetic distribution of the emission in two-dimensions is more important, not the spatial distribution, therefore, vertical calibration has never been done and vertical lines of pixels are integrated.

The camera was synchronized with the laser sources either electrically (for the Nd:YAG laser) or optically (for the nitrogen laser). The Nd:YAG laser is a significant source of jitter (time variation between the pulses), and the data acquisition can be triggered by the laser pulse itself rather than from the external trigger sources. The electrical pulses are directly sent from the Nd:YAG laser control panel to the laser and occur on average ~1 µs before the laser emits. The laser pulse emission then takes some time to arrive at the sample, which is called the zero time. The zero time will be explained more in the next subsection. The Nd:YAG laser synchronization with the iCCD camera was achieved by triggering electrically. The camera can also be synchronized with the Nitrogen laser optically, where triggering of the laser pulse is accomplished by splitting a small percentage (~10%) of the laser beam with a beam-splitter to an external high-speed photodiode module (Becker-Hickl- PHD 400), which sends electrical signals (zero time ~30 ns) to the camera. An electrical pulse generator can also be used to trigger the camera, and in that case, the laser pulse should be delayed long enough to reach the electrical pulse generator, which normally takes 1300 ± 10% ns delay (zero time of Nitrogen laser in the case of using an external trigger) to synchronize with the incoming trigger and for the gate pulse to reach the iCCD camera. In particular, the generator provides great flexibility to change the delay time of the gated pulse that reaches the iCCD, which is a very useful technique especially in a two-pulse-pump experiment.

The intensity of fluorescence can be managed either by tuning the slit size of the spectrograph (from 0.1 to 2 mm with 0.2 µm steps) or by the tuning the iCCD camera gate voltage (500 V to 950 V) at the expense of resolution. If there is no intensity saturation on the iCCD camera, then the time-resolved spectra can be recorded by changing with the delay and integration times (designate the time when the camera shutter remains open and the emission accumulation occurs) *via* 4 Picos camera software. Data collection occurs using logarithmically increasing delay and integration times, whereby the whole desired time region is covered without losing any data at any time frames.

3.3.1 Wavelength calibration and the spectral resolution of the set-up

The energy dispersion of the emission on the iCCD was correlated to the horizontal iCCD camera pixels at the certain wavelength positions using a CAL-2000 Mercury-Argon calibration source (Ocean Optics). Addressing this point, the grating positions of the spectrograph were chosen separately, i.e. 500 nm for the visible region and 1000 nm for the far-red region, and the slit size was minimized (0.4 mm), to observe the known spectral line peaks as sharp as possible, to calibrate wavelength positions to the corresponding iCCD pixels on the overall spectral range. Also, the iCCD camera voltage was chosen such that each line was within the saturation limit. In this way, the iCCD pixel numbers were correlated to the specific wavelength scale with an accuracy of ~1nm, which was an estimated value between the variance of a linear wavelength to pixel relationship. The calibration curves were saved for each fixed grating positions, however, in the case of any positional changes of the iCCD camera, the same calibration procedures must be repeated in the same way.

The spectral resolution can be defined as the ability to resolve the features in the spectrum. In our set-up, the spectral resolution was measured as the full width at half maximum (FWHM) of either the 3rd harmonics of the Nd:YAG laser or using well-known laser dye Rhodamine 6G. Using the 3rd harmonic of the Nd:YAG with very narrow slit size of spectrograph resulted in a value of ~1 nm spectral resolution (FWHM), which was more than the theoretical resolution maximum limit (300nm/736 pixel = ~0.4 nm). The reason for this dispersion might be the angular position of the iCCD camera. If the iCCD

camera is not positioned exactly at the right angle with respect to the spectrograph exit plane, it is possible to experience slight divergences of the resolution. However, the spectra of organic materials are very broad, therefore, ~1 nm spectral resolution is not restrictive to the quality of data collected.

3.3.2 Intensity response calibration of the set-up

In the set-up, the iCCD and spectrograph exhibit different sensitivities to particular energies of light, which prevents the observation of the true emission profile. Therefore, after each experiment, every recorded spectrum should be corrected (*via* multiplication) with a correction curve to get the true emission profile. The way to get this correction curve is to compare the known intensity profile of a tungsten-halogen calibration lamp (LS-1-CAL, Ocean Optics) with the one experimentally obtained. For each grating position and slit size of the spectrograph, the correction curve must be derived.

3.3.3 Time resolution and zero-time calculation of the set-up

Time-resolution is one of the most important aspects of the set-up, which demonstrates the quality of decay measurements, and directly relates to the slowest component of the set-up. The zero-time calculation of the set-up can be made by a fairly simple method. Specifically, the laser beam of the Nd:YAG laser was directed towards the iCCD camera with its voltage and the slit size of the spectrograph chosen to minimise incident intensity, and the triggering was supplied by the electrical signal. The laser pulses arrive at the camera after a time, which is called the zero time of the laser system. Detection occurs during the gated time and can be understood as the time frame between zero time and the opening of the iCCD camera shutter (called integration or detection time). In order to calculate the zero time, the spectra was collected leaving the integration time constant (1 ns) and the delayed time (start point ~970 ns) increased with 1 ns steps. Then each spectra integrated between the particular wavelengths and the calculated intensity values are plotted as function of delayed time as shown in Fig.3.7. As seen from the fitted Gaussian function, the exact zero time of the system is determined by using a

Gaussian equation, which is 976 ± 0.05 ns. One should also note that in the case of changing components of the system, such as changing the length of the connection cable between the laser control panel and the iCCD camera or replacing the ICCD camera, recalculation of the zero-time must be repeated.

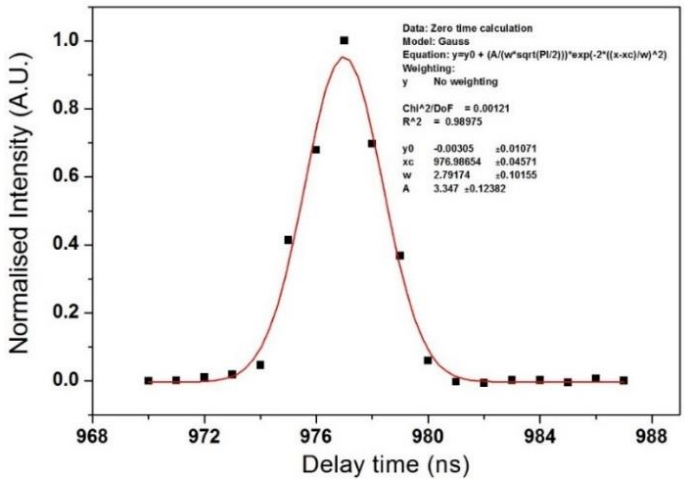

Figure 3.7 The zero-time calculation of the set-up. The normalized integrated points were taken from 970 ns to 987 ns delay times with 1 ns integration time frames. The fitted red-line shows the Gaussian function and the zero time determination can be done from the peak of this Gaussian.

3.3.4 Various integration time width calibration of the iCCD camera

The various integration times of the iCCD camera do not give a linear intensity response in the case of increasing/decreasing detection time conditions. For instance, a 5 ns integration time does not collect 10 times more intensity than (an integration time of) 0.5 ns which is shown in Fig. 3.8. The measurements were taken using a continuous high stability single wavelength LED, and the intensities were measured as a function of integration times of the iCCD camera and divided by the set integration times. As seen, the camera response was not linear below the ~10 ns integration times, and the expected intensity is much higher at small integration times, however, at later times (up to ~12 ns) there were tiny intensity fluctuations, but the intensity is more or less linearly dependent. It should be noted that there is no need to make any correction for this at fixed integration time measurements. However, it is necessary when using dynamically increasing delay

and integration times. In this case, the recorded data should be divided by the appropriately generated iCCD camera correction curves.

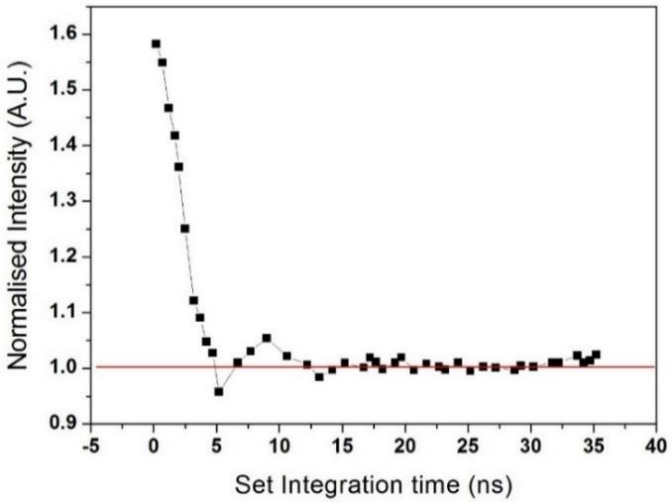

Figure 3.8 The set integration time profile of iCCD camera. The measurements were taken using continuous LED at various integration times. Below the ~10 ns integration time, non-linear regime occurs and after ~12 ns time the camera response more or less linearly dependent.

3.3.5 Measuring the decay dynamics with dynamically increasing delay and integration times

Decay dynamics were measured using the gated iCCD camera, where we can control the delay and integration times logarithmically at increasing time conditions.[5] The reason for using the logarithmic time frames is that at very early times of the decays, the intensity is very strong but decays very quickly, therefore, the detection time window must be chosen on a short time scales so not to lose time resolution. However, at later delay times, the decay is comparatively slower and the intensity is far weaker, therefore, longer detection time windows are required to increase signal to noise ratios, but do not compromise time resolution. To do this, a set of delay times (t_x), that are equally spaced in logarithmic time has been chosen which comprise of whole time region of interest (from nanoseconds to second). The integration time windows have been chosen using a dynamically increasing condition. At this point, one should carefully consider two main

points i) not to lose any covered time region ii) also not to overlap with the following delay time, for instance, if the delay and integration times were chosen as 1000 ns and 100 ns respectively, the next delay time must be 1100 ns, etc. Generally the integration time window has been taken a tenth of the delay time which was found as the ideal time frame between the signal intensity and time resolution. The measured intensity at delay time, t_x, can be formulated as,

$$I_{t_x}^{meas} \sim \int_{t_x - \frac{t_x}{20}}^{t_x + \frac{t_x}{20}} I(t)\, dt \qquad \textbf{(3.9)}$$

where the measured intensity at delay time(t_x) is assigned as $I_{t_x}^{meas}$ and the real intensity is assigned as $I(t)$. If the integration time window is generally a tenth of the delay time, then the true intensity can be expressed by dividing the measured intensity with the delay time as,

$$(t) \sim \frac{I_{t_x}^{meas}}{t_x} \qquad \textbf{(3.10)}$$

In practice, the decay measurements are taken in three basic steps. Firstly, the emission intensities are recorded using a set of logarithmically increasing delay times (t_x) with specifically chosen integration times (tenth of delay times). This step can be automatically achieved by using a self-written program. Secondly, the background is scanned under identical conditions (the same frames, slit size of spectrograph and camera voltage) and then subtracted from the emission. Finally, the recorded spectra are analysed by integrating the emission curves, which gives numerical values for certain delayed times, then divided by the corresponding integration times and multiplied by the correction curves.

Once again, this logarithmically increasing delay times method offers two important advantages to the decay measurements i) it considerably enhances the signal to noise ratio ii) it significantly enlarges the dynamic range of the iCCD camera, which provides up to 12 orders of magnitude (without losing time-resolution) in intensity of one decay measurement. However, it is not possible to achieve the same dynamic range in intensity using the fixed integration time method. In the result chapters of this thesis, two methods were commonly used (dynamically increasing and fixed detection window of the iCCD camera) to record the decay measurements. Decay curves for reference materials are also compared to the results from the single photon counting method (presented below) to give independent verification of each method.

3.3.6 Intensity fluctuations of Nd:YAG Laser

During the decay measurements with the Nd:YAG laser, a major drawback occurs from shot to shot intensity fluctuations. In order to get rid of this instability in intensity, many shots are collected (at least up to 100 frames) and integrated to achieve an acceptable signal to noise ratio. For instance, the intensity fluctuations in 100 shots per curve is on average around 10%, and this increases up to 40% without averaging. Also, mid-term instabilities of the laser also occurs in a time period of roughly ~15 minutes. To overcome these variations the same decay measurements are recorded many times under the same conditions and then averaged, or the nitrogen laser which provides extremely stable shot to shot intensities is used. However, in the case of using the nitrogen laser, an external photodiode is required as a trigger and normally the iCCD camera shows an internal trigger delay of ~30 ns (zero time), which is not useful for measuring very early times of the decays. On the contrary, with the Nd:YAG laser, it is possible to synchronize the iCCD camera with the electrical trigger pulses before the laser pulse is emitted. This offers a great advantage in practice to cover the very early and later time scales of the decay measurements, however of course the intensity fluctuations need to be reduced as much as possible.

3.4 Time-correlated single photon counting

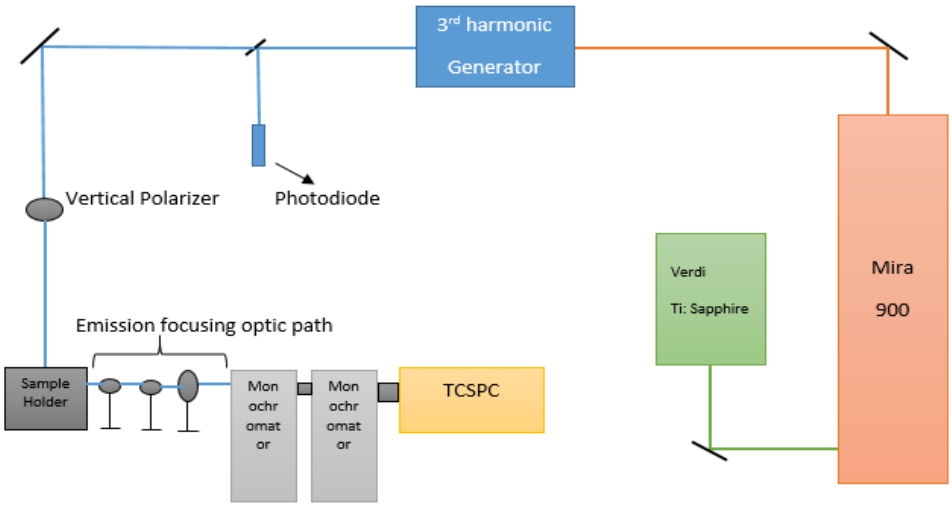

Figure 3.9 Time-correlated single photon counting set up.

Fluorescence life-time measurements were performed using time-correlated single photon counting (TCSPC) spectroscopy (see Fig. 3.9) which helps to clarify the existing excited state lifetimes, i.e. excited singlet or charge transfer state, etc., as well as investigate the transfer rates between them. The technique is widely used and based on counting the individual photons emitted from the sample as a function of time. The system consists of an ultrafast cw-modelocked Ti:Sapphire laser (Mira 900-F, Coherent) which has 2 ps pulse width, < 2% noise level, 76 MHz repetition rate and 0.8 mm beam diameter. The excitation wavelength is adjustable in the range of 710 nm to 1000 nm with ~2W maximum output around 800 nm. The excitation wavelength can be tuned over the typical absorption bands of organic molecules (near UV and green visible region), using a second and third harmonic generator unit (APE, HamoniXX) which was used for frequency doubling and tripling of the laser beam by means of non-linear optical interactions between second and third harmonic crystals. Part of the excitation light was separated by a beam splitter onto a photodiode to generate a sync signal, which was connected to a micro-channel photomultiplier tube (MCP, Hamamatsu R3809U-50) which covered a

total time of 3.33 ns. The detection channel width ranged from 0.815 ps to 3.26 ps depending on the detection channels, either 4096 or 1024, respectively. The majority of the excitation light was passed through, a vertical polarizer, a cut-off filter for low energy residual pump light and a beam collimator which were placed in front of the sample holder. The emitted light was focused using lenses and passed again through a polarizer (at magic angle, 54^0) onto a subtractive double monochromator set to a specific wavelength.

3.4.1 Detection and data acquisition of TCSPC

In the system, the emission from the samples is focused onto a subtractive double monochromator (Acton Research Corporation) which has a ~4 nm spectral resolution and the monochromator gratings and slit sizes can be automatically controlled by Labview software. The emission is detected by a high sensitive MCP including two-dimensional array of channels (4096 channels in total) which are bundled in parallel and placed into a thin disk for high spatial resolution. The role of the each channel is to multiply the electrons independently.

During the data detection process, the system works with "START" and "STOP" signals. When a photon from the sample is detected by the MCP, it generates a "START" signal and the TCSPC starts counting the photons until the "STOP" signal arrives from an external trigger diode. In the system, the sample and the external photo diode is excited with the same excitation source which has 76 MHz repetition rate corresponding to a 13.1 ns pulse. When the "START" signal arrives at the MCP, a capacitor starts charging with a known charging rate, which proceeds charging until the "STOP" signal arrives from the external trigger to the MCP. Consequentially, the voltage on the capacitor is associated with the time gap between the "START"- "STOP" signals, which is called the charging time (t_{charge}) and considering the excitation is a train of pulses having 13.1 ns time difference between each other (t_{pulse}), then the time for detection of a single photon after excitation of a sample can be defined as (t_{photon}) ,

$$t_{photon} = t_{pulse} - t_{charge} \quad \textbf{(3.11)}$$

from which a histogram of an emission decay can be plotted for t_{photon} times. Within the t_{pulse} time, if a successful detection of a photon occurs by the MCP, then the following photons will not be detected in this period of time and the MCP becomes "blind" to detections until the capacitor is fully recharged. In this dead-time period, the sequential exposures do not contribute to histogram of emission decay.

During the data acquisition process, typically two measurements were taken, one for the instrument response function (IRF) and another one for the emission collection. The effective time-resolution of the set-up is characterized by the IRF which shows the temporal dispersion in the optical set-up, the pulse profile of the laser source, the timing jitter in the MCP electronics and transit time spread of the MCP.[6] In order to collect the IRF, the monochromator was positioned at excitation wavelength, then a reference scattering solution (ludox dissolved in water ~10^{-4} M) was perfectly aligned in the sample holder. Afterwards, the scattered light was collected (~10000 counts) which consists of a typically achievable full width at half-maximum (FWHM) value of ~19 ps, corresponding to the temporal response of the system. Then without changing any alignment, the scattering reference solution was replaced with the sample cuvette and the monochromator position was changed to the desired wavelengths depending on the sample emission spectrum. As the materials show wavelength dependent fluorescence decays, a typical set of TCSPC results comprises the IRF decay plus several fluorescence decays, which were taken from different wavelengths. The data collection stop time depends on the emissivity of materials. For instance, if the materials were very emissive, the data collection was continued until ~10000 counts were collected in the peak channel, however, if the emission was weak then the collection was stopped when the peak channel counts were around 6000.

Consequentially, a histogram representing the emission decay was observed which consists of measured data convoluted with the IRF. In order to analyse the measured data, a de-convolution method was used. With this method, it is possible to extract more

information from the experimental data using the re-convolution fitting program which is called “Globals”. With this program it is possible to determine the lifetimes of decays with great certainty. In principle, this program fits the decays by means of using a sum of exponentials convolved with the instrument response function. The output fitting function is the time profile of decays consisting of different fitting parameters such as time constants and amplitudes. The quality of fitting is determined by the value of chi-square (χ^2), in the case of perfect fitting the value approaches to 1.

3.5 References

1. Mecea, V. From Quartz Crystal Microbalance to Fundamental Principles of Mass Measurements. *Anal. Lett.* **38,** 753–767 (2005).
2. Coxon, J. M. & Halton, B. *Organic photochemistry*. (Cambridge University Press, 1974).
3. Williams, A., Winfield, S. & Miller, J. Relative Fluorescence Quantum Yields Using a Computer-Controlled Luminescence Spectrometer. *Analyst* **108,** 1067–1071 (1983).
4. deMello, J. C., Wittmann, H. F. & Friend, R. H. An improved experimental determination of external photoluminescence quantum efficiency. *Adv. Mater.* **9,** 230–& (1997).
5. Rothe, C. & Monkman, A. P. Triplet exciton migration in a conjugated polyfluorene. *Phys. Rev. B* **68,** 075208 (2003).
6. Becker, W. *Advanced time-correlated single photon counting techniques.* (Springer, 2005).

CHAPTER 4: THE PHOTOPHYSICS OF SINGLET, TRIPLET AND COMPLEX STATES IN PHOTO EXCITED RHODAMINE 6G AND ATTO-532

This chapter has been published as:

Murat Aydemir,* Vygintas Jankus, Fernando B. Dias, Andrew P. Monkman, "The key role of geminate electron-hole pair recombination in the delayed fluorescence in Rhodamine 6G and ATTO-532" Phys. Chem. Chem. Phys., **2014**, 16, 21543

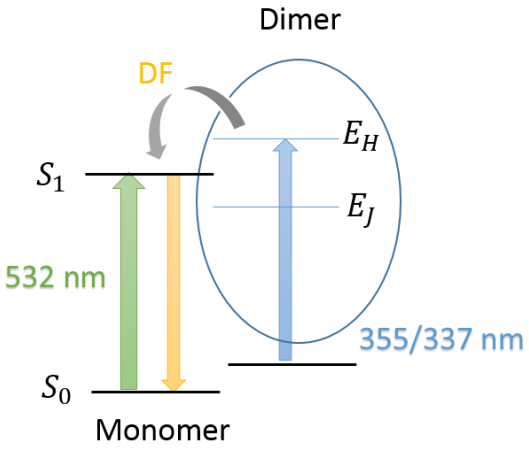

Figure 4.1 The diagram represents the energy levels of monomeric and dimeric states in Rhodamine 6G and ATTO-532. In the case of excitations with high energy lasers (355/337 nm), delayed fluorescence (DF) arises from higher energy dimer state (E_H). However, excitation with 532 nm, only monomer state is excited and no DF is observed.

The purpose of this chapter is to identify the origin of delayed fluorescence (DF) phenomena in widely used laser dyes, Rhodamine 6G and its derivative ATTO-532. Following the sub-headings of the chapter, the origin of the DF is proved through a step by step systematic approach, comparing experimental data to the characteristic features of the possible delayed fluorescence processes such as triplet-triplet annihilation (TTA),

thermally-activated delayed fluorescence (TADF) and geminate electron-hole recombination (GP).

4.1 Introduction

The materials of interest in this chapter can be summarised as, Rhodamine 6G (Rh6G, see Fig. 4.2a), a well-known laser dye[1] and its derivative ATTO-532 (see Fig. 4.2 b). These compounds are purely organic materials that show very high fluorescence yields (≥~95%),[2] which makes them attractive for biological applications, such as in bioassays as fluorescence labels, for example of DNA/RNA molecules,[3] and also in high resolution microscopy methods, such as direct stochastic optical reconstruction microscopy[4] (dSTORM) and stimulated emission depletion microscopy (STED).[5] In addition to common applications, the photo physical and the photochemical properties of these fluorophores have been extensively investigated in the past. For instance, Ringemann *et al*.[6] reported one of the most promising features of Rh6G and ATTO-532, showing single-molecule fluorescence enhancement following reverse intersystem crossing (rISC) when using two excitation sources; one for the $^1(\pi\text{-}\pi)$ transition (high energy laser) and the second one for the T_1 to upper lying triplet states (low energy laser). With this technique, dye dependent fluorescence enhancement were observed (up to a factor of 14) [6] depending on the dye's environment, affording insight into the competing pathways of rISC and photo-bleaching mechanisms.

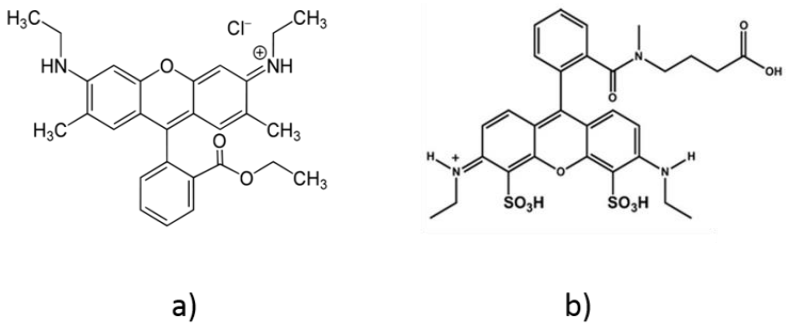

Figure 4.2 Chemical structures of Rh6G (a) and ATTO-532 (b)

Understanding the rISC mechanism (resulting in thermally activated delayed fluorescence, TADF) has become a subject of interest due to its ability to overcome the 25 % limitation of the internal quantum efficiency of OLEDs. In principle, the ratio of emissive singlet and triplet states is limited to 1:3 due to the spin statistics,[7,8] and that gives rise to a serious problem for organic materials and lighting devices. Using the rISC mechanism, dark triplet states can be harvested into emissive singlet species with 100% efficiency.[9] As we have been trying to understand this rISC mechanism in polyspirobifluorene (the subject of Chapter 6), Rh6G and ATTO-532 were predicted to be excellent reference dyes[6] to prove this interesting mechanism. However, the rISC experiments made way for the discovery of an unnoticed phenomenon in the photo-physics of delayed fluorescence (DF) in these materials, which is unmentioned previously in the literature. This then became the subject of interest for this chapter.

In the literature, several studies have addressed the formation of complexes of these dye molecules in solution. It is well-known that Rh6G for example forms dimers[10] and even trimers,[11] which has been confirmed using mass spectroscopy and detailed balance analysis by Toptygin *et al.*[12] and Dare-Doyen *et al.*[13] In dye chemistry, the self-association of dyes is a very common phenomenon in highly concentrated solutions where the weak forces hold the molecules together. In general, the aggregated species in solution can be understood by means of distinct changes in the absorption band, particularly compared with the monomeric species. According to the spectral changes, two types of aggregates commonly exist; bathochromically shifted (through lower energy, positive solvatochromism) J-aggregates and hyposochromically shifted (through higher energy, negative solvatochromism) H-aggregates. These aggregates can be defined in terms of transition moment coupling within the constituents of dye molecules (exciton coupling theory). However, the positive/negative changes in solvatochromic shifts are directly related with the dipole moment of the ground and excited states of the molecules. In general, H and J aggregates are formed as a result of specific arrangements of dye molecules, such as plane-to-plane stacking (H-dimers) and end-to-end stacking (J-dimers) orientations, therefore, the transition moments show either parallel or perpendicular orientations depending on the type of stacking.

Parallel alignment of the molecules (H-aggregate type) results in the formation of two new excitonic bands (which are in accordance with the exciton theory); one of which has higher energy and another which is lower than the monomer energy level. The lower lying energy state shows stabilized characteristics and only the transitions from the ground state to upper exciton states are allowed. Delocalization occurs between the excitonic states very rapidly by means of vanishing the dipole moments and concomitantly non-radiative transitions dominate the overall system. It is found therefore that the fluorescence quantum yield of H-aggregates is very low, and show large Stoke's shift through the lower energies. On the other hand, J-aggregates show very small Stoke's shift and the quantum yields are very high. In the J-aggregates, the order is reversed so it is the lower Davydov band that has very strong oscillator strength and the upper is dark, therefore, J-aggregates have a very high quantum yield.

Rh6G is a well-known material with its dimerization characteristics in solution giving rise to fluorescence quenching once the concentration of the solution is high (~10^{-3} M). Normally, fluorescence from dimer states can only be observed once the fluorescence from the monomer species is quenched, and these characteristic features are signs of H-type aggregation existing in this dye molecule. However, if the relative parallel orientation of the molecules is not perfectly aligned in the dimeric species, then, it is highly possible to observe emission from this species. Additionally, Bryukhanov *et. al.*[14,15] used binary mixtures of polar and non-polar solvents to confirm the formation of complexes and the dependence of delayed fluorescence on solvent polarity. Furthermore, the triplet state of aggregated molecules of Rh6G has also been studied using the flash photolysis technique.[14] From all these studies, it is evident that dimers and even complexes of higher order may play a significant role in the observation of the delayed fluorescence from Rh6G and ATTO-532.

4.2 Overview of possible photophysical mechanisms behind delayed fluorescence

In organic molecules, the excited states can be populated as a result of primary processes of optical or electrical excitation which occur by means of direct light

absorption or through the recombination of charges, or alternatively the excited states can be generated as a result of secondary processes such as energy transfer or exciton-exciton annihilation as explained in Chapter 2. The secondary processes are assigned as "delayed fluorescence" in time-resolved spectroscopy measurements, while, the primary process, resulting from rapid fluorescence decay, is assigned as "prompt fluorescence (PF)" resonating with the excitation pulse. Delayed fluorescence can arise as a result of two main processes: from triplet-triplet annihilation (TTA; also known as triplet fusion) when at least two molecules in the triplet excited state collide and annihilate giving rise to an emissive excited singlet state molecule,[16–18] and thermally assisted delayed fluorescence occurring when a molecule in the triplet excited state undergoes reverse intersystem crossing back to higher energy excited singlet state through use of the thermal energy bath.[7,9,19] For the TADF process to prevail, the energy gap between the S_1 and T_1 is required to be small and also at least a moderately high intersystem crossing rate is required.

A third, but less studied mechanism that involves the recombination of geminate electron-hole pairs (GP) also gives rise to the delayed formation of singlet state excitons and thus results in delayed fluorescence.[20] In general, the electron-hole pairs are bound by coulomb attraction, which are then called "geminate pair" (GP) or "charge transfer" states.[21] The mechanism results from transferring an electron onto a neighbouring intra/intermolecular species (chromophore) and increasing the excited state lifetime. These charges stay separate as long as the distance between the charges is larger than the mutual coulomb attraction radius. In this condition, the charges move freely as unbound mobile charges. Afterwards, the recombination process occurs at a finite rate as a result of encountering diffusive charges and as the corresponding back transfer reaction occurs. In the solid state, optical charge carriers can be produced as a direct result of the photo excitation process in which electron-hole pairs are generated by dissociation of a neutral optical excitation,[22] usually between two molecules, or by dissociation if the photo excitation step gives enough excess energy, which is required to drive charge separation from the molecular excited states.[23] In the latter case, the coulombic capture distance between the separated electrons and holes plays a crucially important role and dictates whether a full dissociation or rapid geminate recombination occurs monomolecularly. In

the literature, the recombination of geminate pairs is reported for the films in two ways,[24] in the first instance, thermally activated hopping drives the charges and concomitantly the recombination occurs due to their mutual Coulombic attraction. Alternatively, the geminate recombination results from following a through-space tunnelling (diffusion) of charges, which happens when the charges do not simply overcome an energy barrier, therefore, long-lived charges result in the observation of a long lifetime in delayed emission. Furthermore, in the case of using highly intense lasers, higher excited singlet states may be populated in a non-linear way, i.e. sequential photon absorption, singlet-singlet annihilation (SSA), indeed the subsequent relaxations occurs very rapidly (~100 fs) through the lowest singlet excited state, but, it has been reported for poly(9,9-dioctylfluorene-co-benzothiadiazole) that a small fraction of higher excited singlets may result in geminate pairs,[25] subsequently the singlet excitons can be formed by GPs as a secondary excitation process. In fact, under high excitation density conditions, it is also likely that the GPs can be formed in a bimolecular fashion (i.e. SSA),[25] which result from the dissociation of vibronically hot singlet excitations (as fusion) on the femtosecond time scale.[24]

Several previous investigations have reported on the dynamics of geminate pair generation and the recombination process within their mutual columbic potentials. The various excited state dynamics involve the kinetics of transitions and Monte-Carlo simulation techniques are commonly used for modelling.[26,27] As a result of these studies, the key role of energetically disordered localised sites was highlighted along with the electron-hole separation of the GP in a film of the conjugated polymer (ladder type methyl substituted poly (p-phenylene) at different temperatures, where the initial energy distribution (at *t=0*) of the carriers is considered to stay far from their equilibrium positions. Subsequently, the relaxation of the charge occurs through the lower energy sites, resulting in a dispersive transport (power law decay) until the quasi-equilibrium is established,[22] which was also confirmed by Ries *et al.*[26] that the recombination rate asymptotically approaches to t^{-1} at low temperatures, where the carriers show long-distance energetic downhill jumps through the lower energy sites, whereas, at higher temperatures, the recombination rate shows turnover from a decay behaviour $I_{DF} \sim t^{-m}$ with the exponent of 1-1.3 to $I_{DF} \sim t^{-2}$. In addition, Hayer *et al.*[28] reported in

polyphenylquinoxalines polymer that the observed delayed fluorescence originates from geminate pair recombination where the decay measurements in dilute frozen solution exhibits a power law part ($I_{DF} \sim t^{-0.3}$) at short time scales then at longer times a turnover to the conventional power law with the approaching exponent of -1 was observed. That was attributed to the recombination of charges at trapped sites, where one of the charges meets with its trapped counterpart (within the mutual Coulombic potential) after following a number of random walk steps. Indeed, the migration of charges at trapping sites is a relatively slow process and follows an exponential decay law (exp (-t/τ)),[29] which has a time-independent rate constant (assuming the mobility of charges is isotropic). Therefore, it has been reported for the one-dimensional systems [28] that the decay of delayed fluorescence may follow an exponential law at short and intermediate time scales. However, modelling the dynamics is not the subject of our investigations in this chapter. Instead, the origin of the delayed fluorescence from these dyes was examined, both in dilute degassed solutions and in molecularly isolated solid film environment.[30]

4.3 Experimental

In the process of sample preparation, ATTO-532 (ATTO-TEC) and Rh6G (Exciton) were dissolved in polar solvents such as ethanol, dimethyl sulfoxide (DMSO) and dichloromethane and left to stir overnight to achieve well-dissolved solutions. The solvents were prepared with similar concentrations, ranging from 4.4 10^{-5} M to 5.5 10^{-6} M for Rh6G and from 4.0 10^{-5} M to 5.0 10^{-6} M for ATTO-532. Degassing was achieved through at least five pump-freezing-thaw cycles with a long necked quartz degassing cuvette. Then, the cuvvette was mounted into a liquid nitrogen cryostat (300 K to 77 K, Janis Research) for temperature dependent fluorescence measurements either for steady-state spectroscopy or time-resolved spectroscopy (the spectroscopy techniques are described in more detail in Chapter 3).

For the solid phase measurements, a polymeric surfactant, poly-vinyl-alcohol (PVA) (M_w 89000-98000 and 99+% hydrolysed) was used, to isolate and confine the

molecules in a rigid matrix. A high temperature was required (around 90 ^{o}C) to completely solvate the PVA in DMSO solvent, then the solvated PVA was mixed with ATTO-532 or Rh6G at the ratio of 9% wt/wt and drop casted onto sapphire discs. Then the film samples were mounted into a helium displax cryostat (300 K to 14 K) for time-resolved decay measurements. The decay measurements were taken with the laser system operating at a repetition rate of 10 Hz until a camera gate time reached an upper limit of 100 ms, after this time frame, a 1 Hz repetition rate was used (see Chapter 3 for details on iCCD measurements). A variable delay time of up to 10 μs was chosen to detect the weak delayed fluorescence after the decay of the intense prompt fluorescence, and, each spectrum has been recorded over 100 laser pulses in order to increase the signal to noise ratio.

4.4 Results and discussion

4.4.1 Investigation of absorption and emission spectra with steady-state spectroscopy

The absorption spectrum of both materials is characterized by a main absorption band (π to π^*) at *ca.* 530 nm and a (relatively) weaker, secondary band at 350 nm (see Fig.4.3.). The significant variations of the shoulder on the blue edge of the main absorption band (*ca.* 490 nm) has been previously reported and attributed to presence of higher aggregated species as dimers, trimers and tetramers.[10,31,32] Bojarski *et.al.* have reported intermolecular aggregations with highly concentrated polar Rh6G solutions (of up to 10^{-2} M), where once the concentration of the dyes is increased, the formation of the dimers and higher aggregates (apart from the monomers of the dyes) is highly favoured.[10,33] The formation of these aggregates shows a strong dependence on the structure of the molecules, polarity and viscosity of solvents and pressure of the environment.[34]

The previous results evidenced that Rh6G consists of two energetically well separated fluorescent species; the energetically well separated monomeric (~ 505 nm) and dimeric (~ 540 nm) states, where the dimeric state consists of energetically separated *H*

and *J* bands.[10] Furthermore, this paper revealed that, as a result of strong spectral overlap between the absorption and the emission bands, back and forth energy transfer occurs between excited monomeric and dimeric states.[10] To possibly observe those energetically separated states, the absorption spectra of Rh6G and ATTO-532 were taken in solutions of differing concentration and solvent polarity (ethanol, EtOH, and dichloromethane, DCM), and show concentration dependent changes on the shoulder of the main absorption spectra. However, due to using dilute ethanol and dichloromethane solutions (~10^{-5} M and 10^{-6} M), such an obvious energy separation between monomer and dimer states has not been observed (see Fig.4.3.). This is in good agreement with previous work that once the concentration was increased, a pronounced half-width of the spectra was observed, confirming the concentration and solvent polarity dependent monomer and (weak) dimer state formation.[10]

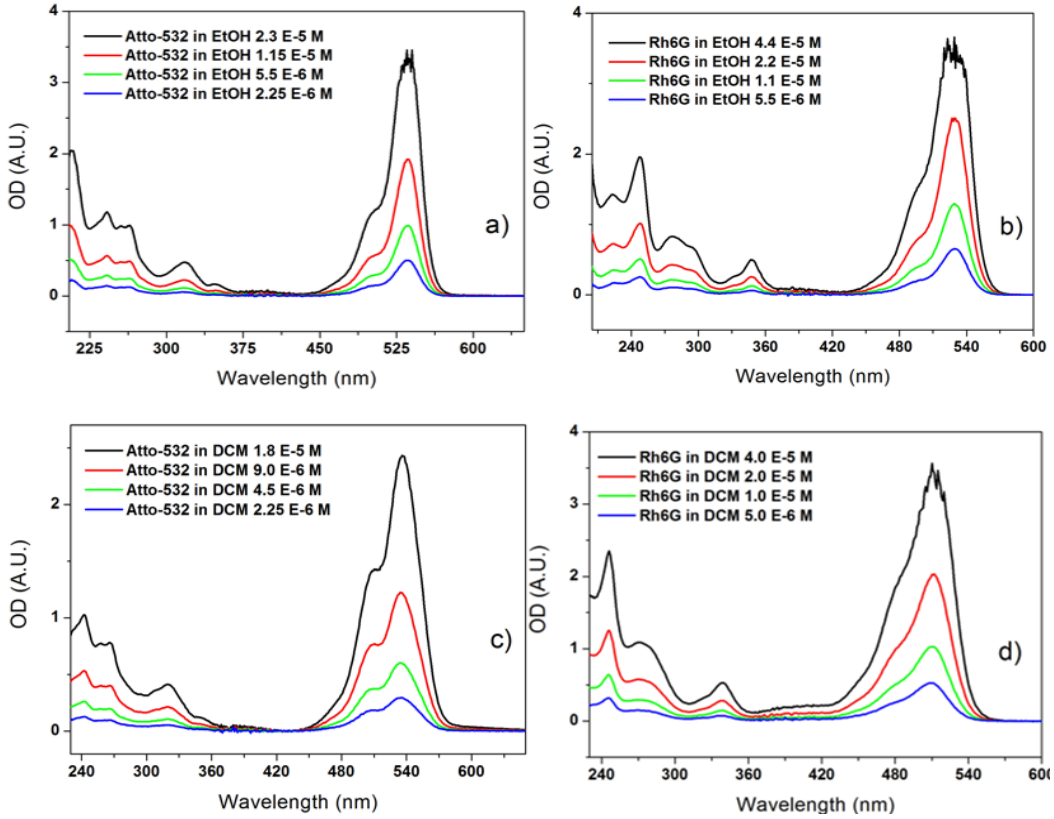

Figure 4.3 The concentration dependence of absorption spectra were taken in air saturated Ethanol solutions **a)** for Atto-532 **b)** for Rh6G, and also in air saturated DCM solutions **c)** for ATTO-532 **d)** for Rh6G

Further investigations were focused on understanding whether the triplet states had any involvement behind the formation of the absorption and emission bands. Addressing this point, the absorption and emission measurements were taken and compared in air-saturated and degassed ethanol solutions (see Fig.4.4 a and b) using the oxygen as the excited triplet state quencher.[35–37] Theoretically, the quenching of triplets in organic molecules is much more rapid than that of excited singlet states. The lifetimes of the triplets are generally long-lived, in the range of hundreds of microsecond to milliseconds, which is due to the spin-forbidden nature of transitions to the ground state. Therefore, it is possible that the diffusion of excited states and quenchers towards to each other may compete favourably with non-radiative and radiative processes, such as intersystem-crossing (ISC) and phosphorescence.

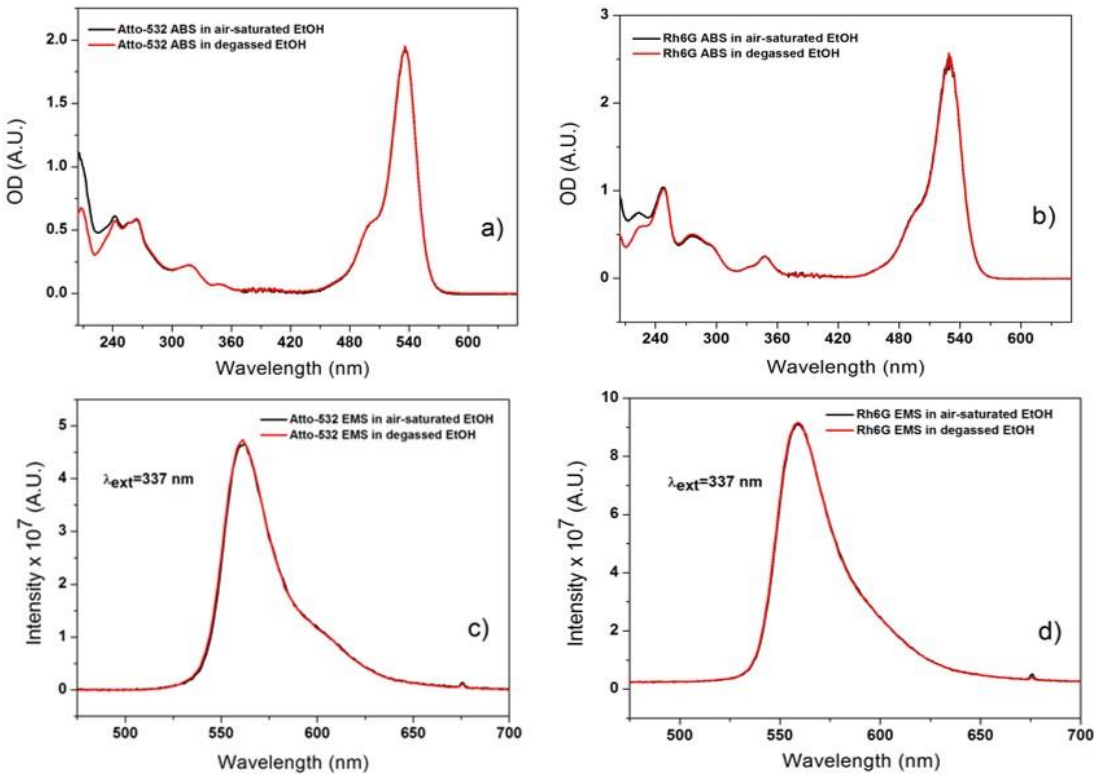

Figure 4.4 The absorption spectra of ethanol solution were taken comparing in air saturated/degassed environment **a)** for ATTO-532 **b)** for Rh6G. The emission spectra of Ethanol (EtOH) solution were taken

with a 337 nm excitation wavelength, and in air saturated/degassed environments **c)** for Atto-532 **d)** for Rh6G.

According to our results, the dimer and monomer states are both responsible for the observed fluorescence and the energy transfer efficiency between the dimer and monomer states, which are strongly dependent on both the solution concentration and the excitation energy. This proposal is strongly supported in the following section using a time-resolved spectroscopy technique, which clearly shows the appearance of delayed fluorescence, particularly, in the case of exciting with high energy wavelengths. It should be emphasized here that triplet states play no role in the formation of any additional absorption band structures (aggregates) and this proposal was confirmed with steady-state photoluminescence measurements, in which the samples were excited at 355 nm and the photoluminescence intensities were found to be identical both within air-saturated and degassed ethanol solutions (see Fig. 4.4 c and d).

4.4.2 Decay dynamics both in solutions and films

Time-resolved and steady-state spectra are presented in one plot for convenience (see Fig. 4.5), which include the absorption, PF, DF and phosphorescence (PH) spectra of ATTO-532 (Fig.4.5 a) and Rh6G (Fig. 4.5 b) in diluted ethanol solution ($2.0\ 10^{-5}$ M for Rh6G and $9.0\ 10^{-6}$ M for ATTO-532). The DF and PH spectra are compared with two different excitation wavelengths (Nd:YAG laser, second and third harmonics, 532 nm and 355 nm). As seen, the emission spectrum at 355 nm excitation wavelength resulted in the observation of DF, peaking at the same wavelength position as the PF emission at 570 nm and 552 nm for ATTO-532 and Rh6G, respectively. Since the emission peak positions and spectral shapes remain unchanged over long time-scales, then it can be concluded that there is no spectral diffusion. However, and also interestingly, once the time-resolved measurements were repeated under exactly the same conditions (at the same delayed, 50 ms, and integration, 1 ms, times) with the excitation source of 532 nm (Nd: YAG laser, 2^{nd} harmonic), only phosphorescence emission was detected around the peak positions of ~670 nm (the PH peak is nicely consistent with a previous report)[14] and no delayed fluorescence was observed (see Fig.4.5). In fact, the steady-state emission spectra peaks

of both materials were identical comparing the three different excitation wavelengths of 337 nm, 355 nm and 532 nm (see Fig. 4.6 a). In addition, moderate solvatochromic shifts as well as broadened fluorescence bands (Fig. 4.6 b) in polar solvents are indicative of the (relatively) strong dye-solvent interactions in more polar solvents (high polarity index ranging 5.2 to 7.2) giving rise to reduced energy differences between excited and ground states.

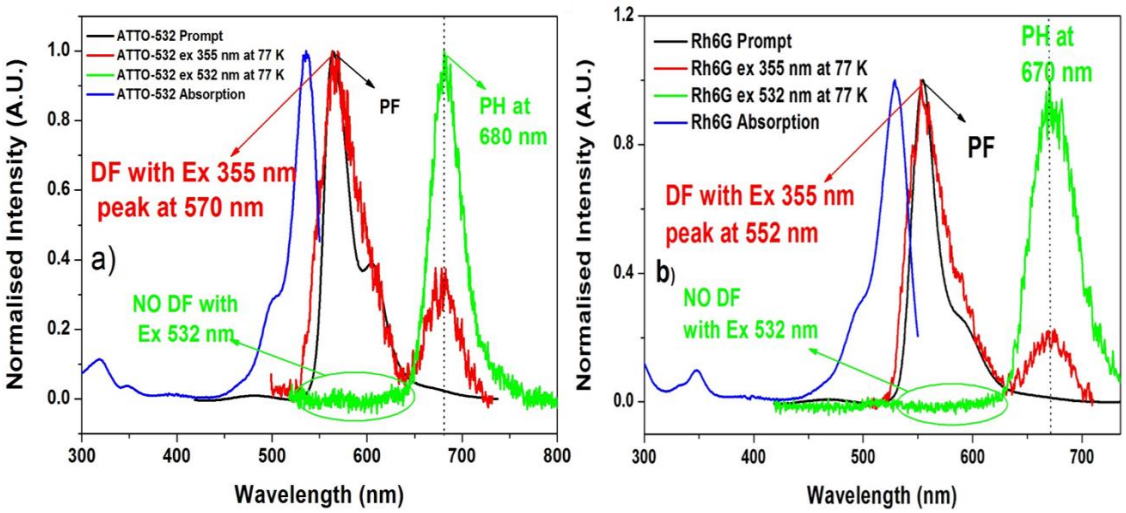

Figure 4.5 **a)** PF, DF and PH spectra of ATTO-532 in degassed ethanol solution at 77 K, the absorption (ABS) spectrum was taken in air-saturated ethanol solution at RT. The red line shows the DF and PH of ATTO-532 appearing simultaneously at 50 ms delay and 1ms integration, where 355 nm excitation energy was used. However, excitation with 532 nm resulted in only PH emission (~680 nm) at 50 ms delay and 1ms integration times **b)** The same colours were used for ABS, PF, DF and PH spectra of Rh6G, which were taken exactly the same experimental conditions with ATTO-532. The peak of PH (~670 nm) is consistent with previous report.[14] Again, excitation with 355 nm resulted in both DF and PH, but, only PH was observed with 532 nm excitation.

Bojarski *et al.*[10] suggested that the total fluorescence appeared as a result of both monomer and dimer contributions, and the dimer bands were energetically separated into two bands, namely E_J and E_H. In that scenario, the E_J band was energetically below, and the E_H band energetically above the monomer band. So, in this case, our observation of the delayed fluorescence with 355 nm excitation wavelength can be linked with previous findings. If these two energetically separate dimer bands exist, excitation of the higher

energy E_H band only can make a contribution to the total fluorescence upon recombination. However, exciting with 532 nm, the E_J band cannot contribute to the DF, because there is not enough energy to repopulate the excited monomer state to yield the DF, hence, the excess energy is such that the E_H band is excited.

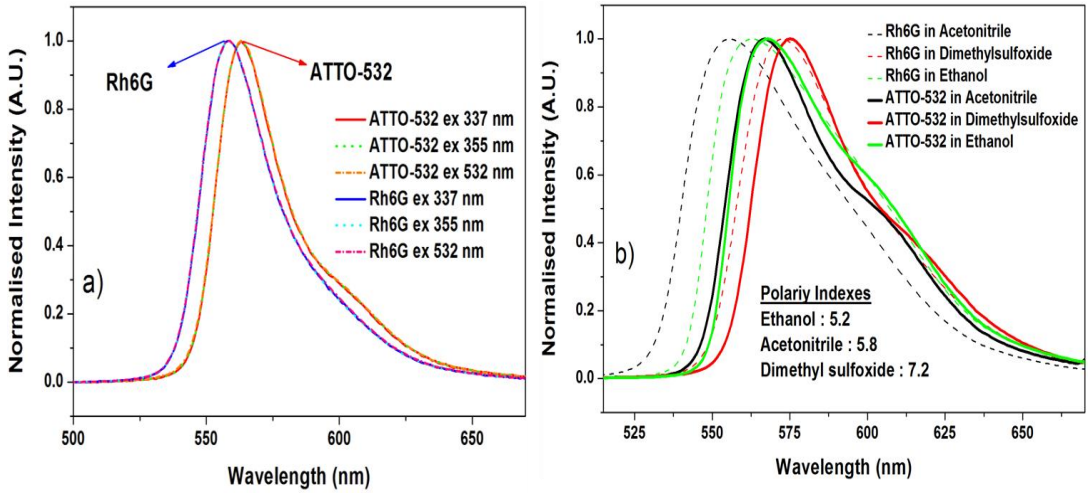

Figure 4.6 a) ATTO-532 and Rh6G steady-state emission in air-saturated ethanol solution with excitation 337 nm, 355 nm and 532 nm at RT, showing the same peak overlap **b)** Steady-state emission spectra of ATTO-532 and Rh6G in air-saturated (different polarity) solvents. Dashed and solid lines were chosen for Rh6G and ATTO-532, respectively.

Fig. 4.7 a depicts the time-resolved decays of prompt and delayed fluorescence of materials in PVA drop cast films at RT and 15 K. In the solid state measurements, the PF lifetime is only weakly temperature dependent. In contrast, the delayed fluorescence, which decays biexponentially, is highly temperature and concentration dependent and the intensity of the DF is dramatically increased on cooling from RT to 15 K (see DF/PF ratios in Table 4.1). Moreover, the impact of concentration upon the intensity of DF is shown in Fig. 4.8, where the intensity of DF increases with increasing concentrations. In Fig. 4.7 b, the solid state (15 K) and the frozen solution (77 K) the lifetime decays are shown in one graph to give better insight into photophysical behaviours in different environments. In solution, the DF decay obeys the power law decay ($I_{DF} \sim t^{-0.25}$), while, in comparison, the DF decays biexponentially in the solid phase. This stabilisation gives

rise to a reduction of the coupling between the excited and ground state, and concomitantly causes long-lived power law lifetime decays of the DF.

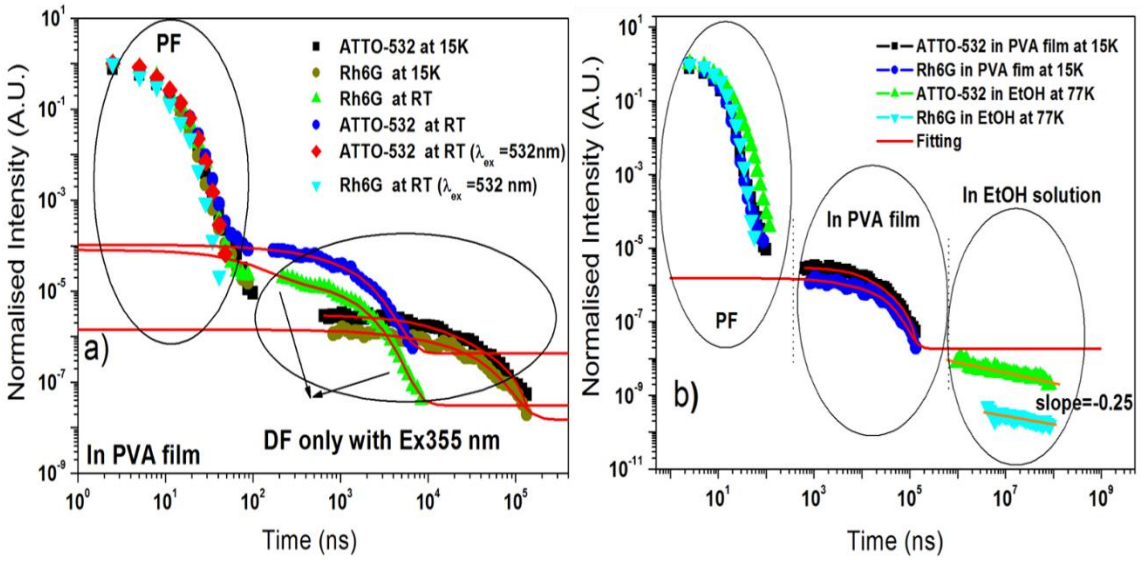

Figure 4.7 **a)** On a Log-log scale, the decay dynamics were recorded in PVA films exciting at 355 nm at 15 K and RT **b)** decays in PVA films and ethanol solution were plotted and compared.

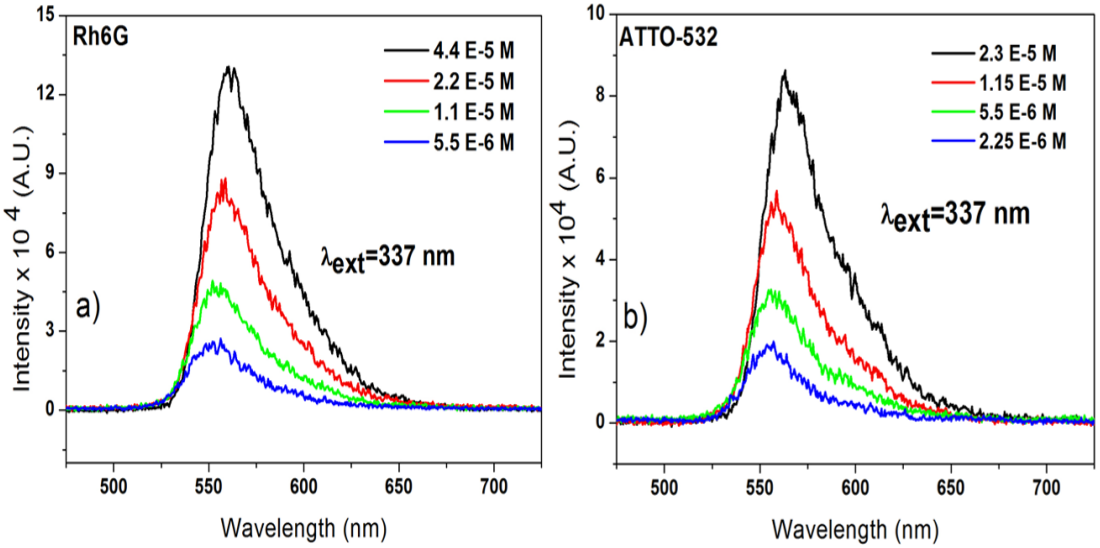

Figure 4.8 At each measurements, the delay time was chosen as 130 ns and the integration time was 1 µs, the DF was measured in variety of concentrations in air saturated ethanol solution **a)** for Rh6G **b)** for ATTO-532. The DF emissions were compared in the same solution either in air saturated and degassed environments.

Table 4.1 Rh6G and ATTO-532 lifetimes of PF and DF in PVA films. The DF/PF ratio is provided and compared with respect to the temperature. PLQY of the materials are provided at two excitation wavelengths, 355 nm and 500 nm

Materials	τ_{PF} at RT/15 K (ns)	τ_{DF} at RT/15 K (μs)	DF/PF ratio at RT/15 K	PLQY Ex 355 nm (%)	PLQY Ex 500 nm (%)
Rh6G	$\tau_1 = 4 \pm 0.2$ $\tau_1 = 3 \pm 0.6$	$\tau_1 = 1 \pm 0.1$ $\tau_2 = 1.2 \pm 0.2$ $\tau_1 = 4 \pm 0.3$ $\tau_2 = 30 \pm 1.2$	0.0028 0.0057	14.3	29.4
ATTO-532	$\tau_1 = 4 \pm 0.1$ $\tau_1 = 3 \pm 0.4$	$\tau_1 = 1.1 \pm 0.2$ $\tau_2 = 1.3 \pm 0.1$ $\tau_1 = 5.3 \pm 0.2$ $\tau_2 = 32 \pm 2.3$	0.0102 0.0132	12.7	26.8

Table 4.2 Rho6G and ATT-532 lifetimes of PF and DF in ethanol solution at RT and 77 K .The DF/PF ratio is also provided and compared with respect to the temperature.

Materials	τ_{PF} at RT/77K (ns)	τ_{DF} at RT (ns)	τ_{DF} at 77 K (ms)	τ_{PH} at 77 K (ms)	DF/PF ratio at RT/77 K
Rh6G	4±0.5	370 ± 10	782 ± 12	763± 18	0.0018-0.0023
ATTO-532	4±1	377 ± 8	785 ± 8	765 ± 9	0.0288-0.0304

4.4.3 Fundamental perspective on the origin of delayed fluorescence

In order to clarify the origin of DF, identification is necessary between the known mechanisms that generate DF emission: triplet-triplet annihilation (TTA), thermally assisted delayed fluorescence (TADF) and geminate pair recombination. The methods to identify the origin of DF are based on time-resolved spectroscopy. One of which is

comparing the lifetimes of DF and PH at the same temperatures (in degassed environments), and second is to measure the intensity dependence of DF and PH on excitation energy, and third, the temperature dependence of DF is measured to determine the thermally activated processes. The second method is commonly used throughout this thesis as one of the most powerful techniques to classify the origin of secondary electronic processes as monomolecular or bimolecular in nature. At this point, it is appropriate to outline briefly the triplet kinetic aspects of DF and PH generated by TTA. Theoretically, assuming that the triplets are formed by intersystem crossing from singlet states, in the case of exciting by a short laser pulses, the decay occurs either monomolecularly or bimolecularly. If DF arises *via* TTA, it should depend on the triplet concentration time evolution given by the equation,[38]

$$\frac{d[T]}{dt} = G - k_m[T] - k_{TT}[T]^2 \qquad \textbf{(4.1)}$$

where k_m represents the sum of nonradiative (k_{nr}) and radiative (k_r) decay constants, k_{TT} refers to the bimolecular decay constants and $[T]$ is the triplet concentration. Under low excitation intensity conditions, the concentration of triplets shows a linear dependence on excitation intensity, however, at high excitation intensity conditions, the last term of the Eq. 4.1 becomes dominant and thus the concentration of triplets shows a quadratic dependence on excitation intensity. The solution of Eq. 4.1. can be written by considering the triplet concentration change in two conditions (Eq. 4.2 and 4.3),

$$[T(t)] = [T_0]\exp[-(k_m)t]; \qquad k_{TT} \ll (k_m)[T] \qquad \textbf{(4.2)}$$

$$[T(t)] = \frac{[T_0]}{(1+k_{TT}[T_0]t)}; \qquad k_{TT} \gg (k_m)[T] \qquad \textbf{(4.3)}$$

From this point, the intensities of phosphorescence and the delayed fluorescence can be defined considering both cases,

in the case of $k_{TT} \ll (k_m)[T]$;

$$\boldsymbol{I_{PH}(t) = k_r[T(t)] = k_r[T_0]\exp[-(k_m)t]} \quad \textbf{(4.4)}$$

$$\boldsymbol{I_{DF}(t) = \frac{1}{2} f k_{TT}[T(t)]^2 = \frac{1}{2} f k_{TT}[T_0]^2 \exp[-2(k_m)t]} \quad \textbf{(4.5)}$$

in the case of $k_{TT} \gg (k_m)[T]$;

$$\boldsymbol{I_{PH}(t) = k_r[T(t)] = \frac{k_r[T_0]}{(1+k_{TT}[T_0]t)}} \quad \textbf{(4.6)}$$

$$\boldsymbol{I_{DF}(t) = \frac{1}{2} f k_{TT}[T(t)]^2 = \frac{1}{2} f k_{TT}[T_0]^2 \frac{1}{(1 + k_{TT}[T_0]t)^2}} \quad \textbf{(4.7)}$$

where f indicates the fraction of encounters between two triplets giving rise to the generation of a singlet state. Eq. 4.5 shows that the DF decays exponentially with time (at low pump fluence conditions) where the rate constant of DF is twice compared with the radiative monomolecular process (phosphorescence). The variation of the delayed fluorescence intensity with excitation shows competition between the rate constants of the radiative monomolecular process (phosphorescence, k_r) and the bimolecular process (the diffusional collisional quenching of triplets, k_{TT}).

In the case of high pump intensity and moderately short time conditions, the relationship between the intensity of DF and the concentration of triplets can be defined as Eq. 4.8,

$$I_{DF} = \frac{1}{2} f k_{TT} [T_0]^2; \qquad k_{TT}[T_0]t \ll 1 \qquad (4.8)$$

where the DF is independent of time. In the case of high pump intensity and long-time conditions, the relationship between the intensity of DF and the concentration of triplets can be defined as Eq.4.9,

$$I_{DF} = \frac{1}{2} f \frac{1}{k_{TT} t^2}; \qquad k_{TT}[T_0]t \gg 1 \qquad (4.9)$$

where the DF is independent of pump intensity and approaches a t^{-2} law asymptotically. As seen from the equations above, once the monomolecular process dominates, the deactivation of triplets occurs more rapidly than the rate of triplet collisional diffusion, so the intensity of DF shows a linear dependence on the excitation intensity. However, if the bimolecular process dominates the system, the intensity dependence of delayed fluorescence upon excitation dose turns to a quadratic regime.

Consequentially, within the TTA framework the delayed fluorescence should decay with a rate twice as fast as the phosphorescence decay. To confirm this, the lifetimes of DF for Rh6G and ATTO-532 were recorded (both in degassed ethanol solution and in PVA films) and compared with their PH lifetimes at 77 K and 15 K (see Table 4.1 and 4.2). No PH emission was observed in drop cast PVA films which was a very surprising observation, because, previously, the phosphorescence emission was reported with water soluble polymer films at RT, where a very good isolation ability of PVA matrix was reported.[30] Furthermore, the integrated intensity of delayed and prompt fluorescence (DF/PF ratios) were also calculated (Table 4.2), showing the average number of cycling steps between the singlet and triplet states, or in another words, the ratio shows the yield of singlet states harvested from triplet states.[39] As seen, the ratios are very low, indicating the negligible triplet contribution to the singlet state. So, the possibility of TTA mechanism behind the DF is very weak. In addition, it can be confirmed that the lifetime

of DF is equal to (within the error) or longer than the lifetime of PH (see Table 4.2) which is again inconsistent with the characteristics of TTA (if the TTA is operative, the lifetime of DF should be half of the lifetime of PH). Clearly, the DF does not arise *via* TTA mechanism in these materials. Last but not least, the intensity dependence of DF on laser fluence (excitation dose, I_{exc}) was plotted at constant temperature (RT) on a log/log graph of I_{DF} versus I_{exc}, where the DF time frame was chosen as 500 ns delay time to 2 μs integration time for both dyes as seen in Fig. 4.9. The DF intensity is linearly dependent (slope 1.02 for ATTO-532 and slope 0.95 for Rh6G) on the excitation dose of over 2 orders of magnitude laser power, at ≤ 100 μJ per pulse per cm^2. If the DF arose from TTA, the power dependence should have a quadratic dependence at low to medium laser intensities; this evidence also supports that TTA cannot be the responsible mechanism behind the DF of ATTO-532 and Rh6G.

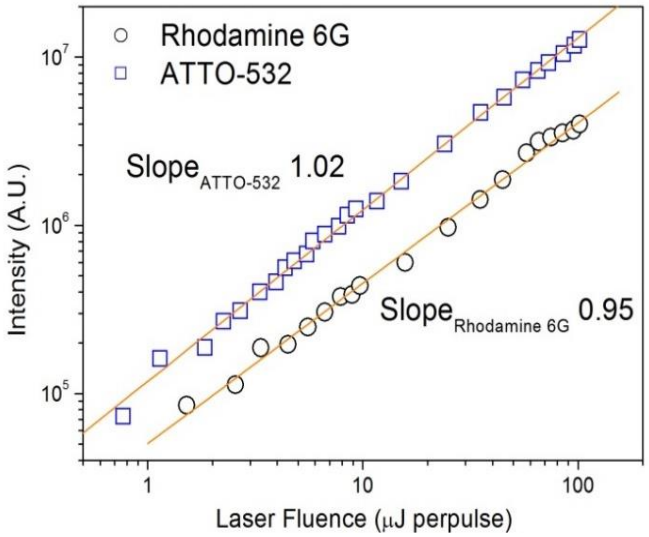

Figure 4.9 The DF intensity dependence of ATTO-532 and Rh6G in solution, laser fluence (I_{exc}) exciting 337 nm in log-log scales at RT. The DF intensity grows linearly with excitation density. 500 ns delay time and 2 μs integration time have been chosen.

The observation of a linear dependence of the DF intensity with excitation energy in both materials would be consistent with E-type delayed fluorescence (or TADF). According to the kinetics of TADF materials, particularly considering the long-time

regime (after the time when the rapid component of prompt emission has decayed), the depopulation of excited singlets and triplets can be written as,[39]

$$\frac{dS_1}{dt} = -k_f S_1 + \quad k_{rISC} T_1 \tag{4.10}$$

$$\frac{dT_1}{dt} = -(k_{rISC} + k_r) T_1 \tag{4.11}$$

where k_f is the rate constant of fluorescence emission from singlet state and the k_{rISC} is the rate constant of reverse intersystem crossing from thermally activated upper lying vibronic states of T_1 to S_1 and the monomolecular decay rate (phosphorescence) from T_1 state is represented with k_r. Once the Eq. 4.10 and 4.11 are solved,

$$T_1(t) = T_0 e^{-Xt} \tag{4.12}$$

$$S_1(t) = \frac{k_{rISC}}{k_f - X} T_0 e^{-Xt} \tag{4.13}$$

where X represents the sum of the rate constans ($k_{rISC} + k_r$) for reverse intersystem crossing (k_{rISC}) and phosphorescence (k_{PH}). Using Eq. 4.12 and 4.13, the steady-state intensity of delayed fluorescence can be written as,

$$I_{TADF} = f_{inst} k_{f0} \int_0^{+\infty} S_1(t)\, dt = f_{inst} k_{f0} \frac{T_0 k_{rISC}}{X(k_f - X)} \tag{4.14}$$

where f_{inst} is the instrumental factor and the natural radiative decay rate is represented with k_{f0}. In the case of $k_f \gg X$, the Eq. 4.14 can be written in a simpler manner,

$$\boldsymbol{I_{TADF} = f_{inst} k_{f0} \frac{T_0 k_{rISC}}{X k_f}} \qquad \textbf{(4.15)}$$

as seen in the equations above, the intensity of delayed fluorescence is linearly dependent on the excitation dose. In the case of plotting the integrated intensity of DF versus the excitation dose on log/log scales, the result must show a slope of 1 indicating a monomolecular process. Another characteristic feature of the TADF materials is the need for a small energy gap between the singlet and triplet states, ΔE_{ST} (electron exchange energy). The calculated value for the energy splitting gap (ΔE_{ST}) was 0.38 ±0.02 eV for Rh6G and 0.36 ± 0.02 eV for ATTO-532 which is a reasonable energy gap for weak TADF emitters.[9] Such a small gap allows for the DF to be caused by TADF. However, clear evidence for the absence of the thermal activation of the delayed fluorescence in these dyes was given by the temperature dependence of DF in Fig. 4.10. The increase in intensity with temperature clearly was not consistent with the materials showing efficient TADF mechanism.

According to Kasha's rule,[40,41] molecules that are excited to the upper singlet states, relax non-radiatively to an emissive singlet state and emit at the same emission wavelength meaning that the emission wavelength is independent of excitation wavelength. Strictly speaking, that gives us strong evidence that TADF is independent of excitation wavelength; hence, DF must appear at all excitations wavelengths (both 355 nm and 532 nm). Here, the DF is completely excitation wavelength dependent which is also inconsistent with TADF phenomena. Hence the only possible origin of the DF is from the coulombically bound geminate pair recombination (GP) process. In general, the optical charge carrier production follows two main steps; i) a photon results in a coulombically bound electron-hole pair as a result of direct charge transfer transition or ii) autoionization of the molecular excited state by means of excess energy.[23] Afterwards,

the formed free charges stay at their initial intra-pair separation , even though this distance is not well defined quantity, as well as the medium is assumed to be homogeneous and owning its dielectric constant. Under these conditions, the charges undergo Brownian motion (random motion of the particles) in a coulombic potential until they either recombine geminately or fully dissociate. This process is called the "infinite sink approximation".[21]

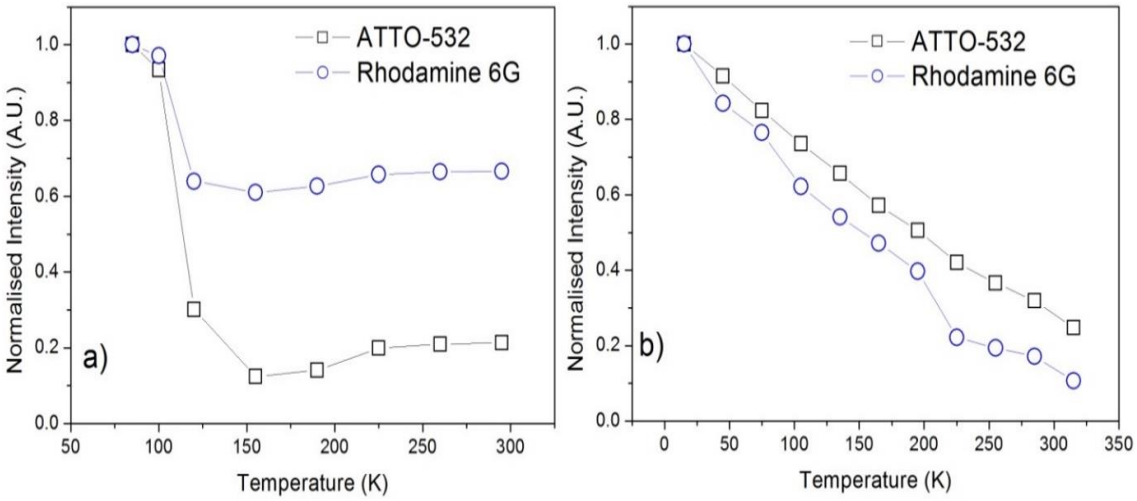

Figure 4.10 a) Temperature dependence of delayed fluorescence of ATTO and Rh6G in ethanol solution **b)** and in solid phase using PVA matrix. Measurements were taken in 200 ns delay time and 3 μs integration time

According to the Onsager theorem, the carriers are found at a distance in which the electrostatic binding energy of two oppositely charged carriers are thermal energetically equal. Therefore, energy must be provided which is considerably larger than the thermal energy, $E_{exc} >> kT$, to separate such pairs. The energy of an individual GP is given by the mean charge separation distance, the coulomb attraction radius ($r_c = e^2/4\pi\varepsilon\varepsilon_0 kT$, ε -dielectric constant of material, k-Boltzmann constant and T-temperature), and recombination rate is also directly proportional to this distance and will reduce at longer time scales. Given that the linear absorption of both materials show the characteristic blue shoulder ascribed to the absorption of the dimer species, it is thus very reasonable to assume that the photo excited charge transfer occurs between the two molecules forming the dimer species, and the electron-hole pairs are generated by means of charge transfer

from a higher excited aggregated state (dimer). As happens in our case, the DF appears at the same energy level with PF emission (see Fig. 4.5). It should also be highlighted here that given the charge separation is across a dimer state, rapid geminate recombination can be avoided. Particularly, in the solution phase, there are more energetically disordered localised sites compared to the solid phase; because of this the recombination time *(t)* takes longer and the DF lifetimes range up to milliseconds at low temperatures (see Table 4.2).

Considering the coulombic attraction distance, the dielectric constant of the environment plays a crucial role in this recombination process. Generally, in organic materials the dielectric constant is low, hence, the coulombic binding energies are relatively large. Typically, the energy of the dimer state exceeds the energy of the singlet excited state by around ~0.2-0.5 eV and intrinsic photoconduction starts only ~ 1 eV above the excitonic absorption edge.[21] However, this energy gap is lowered once the lowest excited state acquires a charge transfer character (that point will be exemplified in more detail in Chapter 5). The binding energy in polar solvents will also be relatively low because of the higher dielectric constants and this results in added stabilisation of the charge separation over longer distances as well as giving more disordered states. This gives rise to a distribution of tunnelling distances for the recombination process which in turn has been shown to lead to a power law decay of the emission [42] which was also observed here. Furthermore, the general solvatochromism of both materials in different concentrations indicate the presence of charge transfer character of the π-π* states (Fig. 4.6 b), especially as the highest dielectric constant belongs to dimethyl sulfoxide and results in a more broadened and more red-shifted emission, and this red shifted emission for the dimer species shifts relatively further than the (π-π*) states.

The effects of different excitation sources were also compared in the case of exciting with 532 nm, only π-π* states are excited and no delayed emission was seen. However, in the case of using 355 nm laser as the excitation source leads to excitation of the higher dimer species (assumed E_H band of dimers) and concomitantly delayed emission was observed as a result of the long lived geminate recombination process. It is clear from our observations of Rh6G and ATTO-532 that the DF is only observed when there is sufficient excess energy to excite the dimer states. The geminate recombination

of well-separated charge pairs on dimer (and higher) species, which eventually undergo monomolecular recombination, have enough energy to populate the π-π* singlet state and emit DF at the same peak position as a ^{1}(π-π*) prompt emission. In addition to the key observation of the cause of the DF, the long lasting lifetime in frozen solution at 77 K (see Table 2), compared with shorter life time in PVA, is consistent with more aggregated species in frozen solvent, where the molecules are stabilised by the polar environment giving a longer time for monomolecular recombination. However, in the polymer matrix, dimerization has less chance to occur in the PVA matrix, which acts to help molecular solubilisation yielding isolated molecules,[30] and recombination occurs at relatively shorter times (see Table 1). The lifetime remains long at low temperatures, as a result of slower recombination process. Consistently, the DF/PF ratios increase at low temperatures, which is also reasonable when compared with the temperature dependence of DF (see Fig.4.10). Given that the dimer species absorption must overlap with the singlet absorption under the main "absorption" band, the observation of DF will be highly dependent on where within the main absorption band excitation occurs. Thus, at 532 nm no DF is observed, but it must be assumed that excitation at higher energies will give rise to dimer excitation and concomitant DF.

4.5 Conclusion

In this chapter, the origins of DF of Rh6G and ATTO-532 were interpreted. It is clearly shown how the origins of DF can be distinguished from the previously suggested DF mechanisms and triplet state involvement. The chapter also proposes that DF results from the geminate pair recombination of optically generated electron-hole pairs on dimer species rather than from triplet-triplet annihilation or TADF. Clearly, if the DF was to arise from triplet-triplet annihilation, the DF would have a decay rate twice as fast as the PH and; its laser fluence dependence would follow a quadratic law initially and later turn to a linear regime at very high triplet densities. However, the laser fluence dependence was found to be linear from low intensities up to high intensities. Furthermore, the temperature dependence of DF in frozen solution and in PVA demonstrates a high intensity increase approaching the lower temperatures, which also confirms that the

source of DF cannot be explained using TADF. Therefore, the conclusion can be made that the origin of DF is from the geminate recombination of dimer (and higher species) electron-hole pairs. They may undergo monomolecular recombination and populate the molecular π^* states as they are higher energy states so that there is enough excess energy in the separated pairs. The power law decay of the DF indicates a distribution of charge separation distances in the disordered manifold of dimer and higher species. With this work, for the first time the origin of DF has been clarified and the photo physical properties shown for Rh6G compared with its derivative, ATTO-532, along with the role played by excess energy necessary for the formation of DF *via* geminate electron-hole pairs.

4.6 References

1. Schäfer, F. P. & Drexhage, K. H. *Dye lasers*. (Springer-Verlag, 1990).
2. Kubin, R. & Fletcher, A. Fluorescence Quantum Yields of Some Rhodamine Dyes. *J. Lumin.* **27,** 455–462 (1982).
3. Mueller, B. K., Reuter, A., Simmel, F. C. & Lamb, D. C. Single-pair FRET characterization of DNA tweezers. *Nano Lett.* **6,** 2814–2820 (2006).
4. Xu, Y., Melia, T. J. & Toomre, D. K. Using light to see and control membrane traffic. *Curr. Opin. Chem. Biol.* **15,** 822–830 (2011).
5. Aquino, D., Schönle, A., Geisler, C., Middendorff, C., Wurm, C.A., Okamura, Y., Lang, T., Hell, S.W. & Egner, A. Two-color nanoscopy of three-dimensional volumes by 4Pi detection of stochastically switched fluorophores. *Nat. Methods* **8,** 353-359 (2011).
6. Ringemann, C., Schönle A., Giske, A., Middendorff, C., Hell, S.W. & Eggeling, C. Enhancing fluorescence brightness: Effect of reverse intersystem crossing studied by fluorescence fluctuation spectroscopy. *Chemphyschem* **9,** 612–624 (2008).
7. Uoyama, H., Goushi, K., Shizu, K., Nomura, H. & Adachi, C. Highly efficient organic light-emitting diodes from delayed fluorescence. *Nature* **492,** 234–+ (2012).
8. Baldo, M. A., O'Brien, D.F., You, Y., Shoustikov, A., Sibley, S.,Thompson, M.E. & Forrest, S.R. Highly efficient phosphorescent emission from organic electroluminescent devices. *Nature* **395,** 151–154 (1998).
9. Dias, F. B., Bourdakos, K., Jankus, V.,Moss, K.C., Kamtekar, K.T., Bhalla, V., Santos, J., Bryce, M.R. & Monkman, A.P. Triplet Harvesting with 100% Efficiency by Way of Thermally Activated Delayed Fluorescence in Charge Transfer OLED Emitters. *Adv. Mater.* **25,** 3707–3714 (2013).
10. Bojarski, P., Matczuk, A., Bojarski, C., Kawski, A., Kuklinski, B., Zurkowska, G. & Diehl, B. Fluorescent dimers of rhodamine 6G in concentrated ethylene glycol solution. *Chem. Phys.* **210,** 485–499 (1996).
11. Arbeloa, F., Ojeda, P. & Arbeloa, I. Dimerization and Trimerization of Rhodamine 6g in Aqueous-Solution - Effect on the Fluorescence Quantum Yield. *J. Chem. Soc.-Faraday Trans. Ii* **84,** 1903–1912 (1988).
12. Toptygin, D., Packard, B. Z. & Brand, L. Resolution of absorption spectra of rhodamine 6G aggregates in aqueous solution using the law of mass action. *Chem. Phys. Lett.* **277,** 430–435 (1997).
13. Dare-Doyen, S., Doizi, D., Guilbaud, Ph., Djedaini-Pilard, F., Perly, B. & Millie, Ph. Dimerization of xanthene dyes in water: Experimental studies and molecular dynamic simulations. *J. Phys. Chem. B* **107,** 13803–13812 (2003).

14. Bryukhanov, V. V., Ketsle, G. A. & Levshin, L. V. Phosphorescence of higher aggregates of rhodamine 6G in mixtures of polar and nonpolar solvents. *J. Appl. Spectrosc.* **28,** 507–509 (1978).

15. Bryukhanov, V. V., Ketsle, G. A. & Levshin, L. V. Delayed fluorescence of simple associates of rhodamine 6G in mixtures of polar and nonpolar solvents. *J Appl Spectrosc J. Appl. Spectrosc.* **28,** 185–189 (1978).

16. Sternlicht, H., Robinson, G. & Nieman, G. Triplet-Triplet Annihilation and Delayed Fluorescence in Molecular Aggregates. *J. Chem. Phys.* **38,** 1326- (1963).

17. Jankus, V., Chiang, C.-J., Dias, F. & Monkman, A. P. Deep Blue Exciplex Organic Light-Emitting Diodes with Enhanced Efficiency; P-type or E-type Triplet Conversion to Singlet Excitons? *Adv. Mater.* **25,** 1455–1459 (2013).

18. Jankus, V., Winscom, C. & Monkman, A. P. Dynamics of triplet migration in films of *N* , *N* ′-diphenyl- *N* , *N* ′-bis(1-naphthyl)-1, 1′-biphenyl-4, 4′′-diamine. *J. Phys. Condens. Matter* **22,** 185802 (2010).

19. Lee, S. Y., Yasuda, T., Nomura, H. & Adachi, C. High-efficiency organic light-emitting diodes utilizing thermally activated delayed fluorescence from triazine-based donor-acceptor hybrid molecules. *Appl. Phys. Lett.* **101,** 93306 (2012).

20. Albrecht, U. & Bässler, H. Efficiency of charge recombination in organic light emitting diodes. *CHEMPH Chem. Phys.* **199,** 207–214 (1995).

21. Köhler, A. & Bässler, H. Electronic processes in organic semiconductors: an introduction. (2015).

22. Nikitenko, V. R., Hertel, D. & Bassler, H. Dispersive geminate recombination in a conjugated polymer. *Chem. Phys. Lett.* **348,** 89–94 (2001).

23. Silinsh, E. & Jurgis, A. Photogenerated geminate charge-pair separation mechanisms in pentacene crystals. *CHEMPH Chem. Phys.* **94,** 77–90 (1985).

24. Gelinas, S., Kirkpatrick, J., Howard, I.A., Johnson, K., Wilson, M.W.B., Pace, G., Friend, R.H. & Silva, C. Recombination Dynamics of Charge Pairs in a Push-Pull Polyfluorene-Derivative. *J. Phys. Chem. B* **117,** 4649–4653 (2013).

25. Stevens, M. A., Silva, C., Russell, D. M. & Friend, R. H. Exciton dissociation mechanisms in the polymeric semiconductors poly(9,9-dioctylfluorene) and poly(9, 9-dioctylfluorene-co-benzothiadiazole). *Phys. Rev. B* **63,** 165213 (2001).

26. Ries, B., Schonherr, G., Bassler, H. & Silver, M. Monte-Carlo Simulations of Geminate-Pair Dissociation in Discrete Anisotropic Lattices. *Philos. Mag. B-Phys. Condens. Matter Stat. Mech. Electron. Opt. Magn. Prop.* **48,** 87–106 (1983).

27. Ries, B. & Bassler, H. Monte-Carlo Study of Dispersive Charge-Carrier Transport in Spatially Random-Systems with and Without Energetic Disorder. *Phys. Rev. B* **35,** 2295–2302 (1987).

28. Hayer, A., Bassler, H., Falk, B. & Schrader, S. Delayed fluorescence and phosphorescence from polyphenylquinoxalines. *J. Phys. Chem. A* **106,** 11045–11053 (2002).

29. Arkhipov, V., Bassler, H., Deussen, E., Gobel, O., Kersting, R., Kurz, H., Lemmer, U. & Mahrt, F. Field-Induced Exciton Breaking in Conjugated Polymers. *Phys. Rev. B* **52,** 4932–4940 (1995).
30. Al-Attar, H. A. & Monkman, A. P. Room-Temperature Phosphorescence From Films of Isolated Water-Soluble Conjugated Polymers in Hydrogen-Bonded Matrices. *Adv. Funct. Mater.* **22,** 3824–3832 (2012).
31. Ghomashchi, E., Ghanadzadeh, A., Mahjani, M., Hasanpour, M. & Niavaran, H. On the Aggregative Properties of Rhodamine 6g in Ethanolic Solutions. *Spectrochim. Acta Part -Mol. Biomol. Spectrosc.* **47,** 211–217 (1991).
32. Selwyn, J. & Steinfel.ji. Aggregation Equilibria of Xanthene Dyes. *J. Phys. Chem.* **76,** 762- (1972).
33. Wyn-Jones, E. & Gormally, J. *Aggregation processes in solution.* (Elsevier Scientific Pub. Co., 1983).
34. Valdesaguilera, O. & Neckers, D. Aggregation Phenomena in Xanthene Dyes. *Acc. Chem. Res.* **22,** 171–177 (1989).
35. Birks, J. B. *Photophysics of aromatic molecules*. (Wiley-Interscience, 1970).
36. Geacinto.ne, Benson, R. & Pomeranz, S. Interaction of Triplets of Aromatic-Hydrocarbons with Oxygen and Nitric-Oxide. *Chem. Phys. Lett.* **17,** 280–282 (1972).
37. Patterson, L. K., Porter, G. & Topp, M. R. Oxygen quenching of singlet and triplet states. *Chem. Phys. Lett.* **7,** 612–614 (1970).
38. Hertel, D., Bassler, H., Guentner, R. & Scherf, U. Triplet-triplet annihilation in a poly(fluorene)-derivative. *J. Chem. Phys.* **115,** 10007–10013 (2001).
39. Dias, F. B. Kinetics of thermal-assisted delayed fluorescence in blue organic emitters with large singlet-triplet energy gap. *Philos. Trans. R. Soc. -Math. Phys. Eng. Sci.* **373,** 20140447 (2015).
40. Klán, P. & Wirz, J. *Photochemistry of organic compounds from concepts to practice*. (Wiley, 2009).
41. Kasha, M. Characterization of Electronic Transitions in Complex Molecules. *Discuss. Faraday Soc.* 14–19 (1950).
42. Huntley, D. J. An explanation of the power-law decay of luminescence. *J. Phys.-Condens. Matter* **18,** 1359–1365 (2006).

CHAPTER 5: INVESTIGATION OF COMPLEX EXCITED STATE DYNAMICS OF POLYSPIROBIFLUORENE IN SOLUTION PHASE: THE INTER/INTRACHAIN INTERACTIONS BEHIND THE FORMATION OF CHARGE TRANSFER STATES

This chapter has been published as:

Murat Aydemir, Vygintas Jankus, Fernando B. Dias, Andrew P. Monkman,* "Inter/Intrachain interactions behind the formation of charge transfer states in polyspirobifluorene: A case study for complex excited-state dynamics in different polarity index solvents" J.Phys.Chem.C, **2015**, 119 (11), 5855-5863

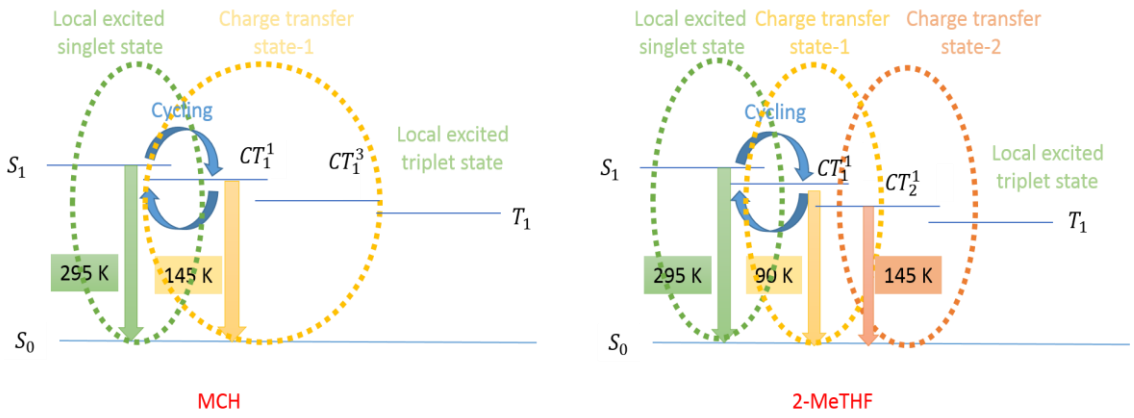

Figure 5.1 The diagram represents the energy levels of ground (S_0) and exited states in two different solvents, methyl cyclohexane (MCH) and 2-methyltetrahydrofuran (2-MeTHF), and the cycling process behind the population of the states. Locally excited singlet $^1(\pi\text{-}\pi^*)$ and triplet $^3(\pi\text{-}\pi^*)$ states are represented as S_1 and T_1, respectively. There also exists a charge transfer (CT_1) state in MCH, where the excited singlet and triplet states are represented as CT_1^1 and CT_1^3, respectively. In addition, in 2-MeTHF, the existing charge transfer states are presented as CT_1 (at 90 K) and CT_2 (at 145 K). In the diagram, the superscripts represent the multiplicity of the states. More detail will be given in the text.

The purpose of this chapter is to understand the complex excited-state nature of the conjugated polymer, polyspirobifluorene (PSBF), in solution phases. The following chapter will explain how formation of charge transfer states in PSBF polymer film play a

crucial role in the up-conversion mechanism. In general, the organic molecules in their film form tend to form more disordered structures compared with inorganic semiconductors. Before exploring the photoluminescence dynamics in the solid-state films, we investigate molecules in dilute solutions, as it might give some insight into the nature of excited states in films. The reason for choosing this particular material is that, previously, a total singlet yield of 0.44 ±0.04 was achieved by fluorene based OLED devices by Rothe *et al*., which was more than the classical spin statistical limit of singlet generation (0.25), therefore, clear understanding was necessary of the photo-physical mechanisms that give rise to "extra" singlet generation. Therefore, in this chapter, measurements were carried out in two different polarity index solvents, in MCH and 2-MeTHF, which allow the resolution of solvent quality and temperature dependent charge transfer state formation arising from 'inter/intra-chain' interaction phenomena.

5.1 Introduction

A great deal of work has focused on highly emissive blue-emitting polyfluorene derivatives in organic light emitting devices (OLEDs) to understand the nature and complex excited-state dynamics of conjugated polymer systems.[1–3] Inherently, conjugated polymers show conformational and energetic disorder which give rise to wave function localization on conjugated segments of different lengths and results in formation of a broad density of states (DOS).[4,5] If a singlet or triplet excitation has initially been generated in a random way within the DOS, then it follows a relaxation process towards the tail of the DOS.[6] As a consequence of this electronic relaxation, the spectal diffusion and dispersion of excitation transports occur. This strongly disordered intramolecular conformation and intermolecular packing nature dominates charge transport properties in conjugated polymers,[7] and many photophysical processes are explained with structural dynamics by means of some degree of electron-phonon coupling. According to the Franck-Condon principle, electronic excitation occurs immediately from the ground state to higher excited states, however, conformational relaxations occur as long as the electronic charge distribution is stabilised, therefore, the overall conformational relaxation takes a finite time and is accompanied by a spectral shift to lower energies.[8] In

particular, if the excited state chromophore and the surrounding solvent is polar, the enhanced solvent-solute interactions give rise to a change in dipole moment of the chromophore and concomitantly a dynamic solvatochromic shift of the spectra is likely towards the lower energies, which can be attributed to formation of new species, i.e. charge transfer states, excimers, etc.[9] Furthermore, conformational relaxation can change the degree of orbital overlap between the backbone and the side chains of the polymer, if the orbital overlap is high, the electron transfer between the backbone and the sidechains is significantly facilitated by the enchanced donor-acceptor effect.[3]

Generally, the chains of a conjugated polymer adopt a "*random coil"* conformation, and changes in spatial arrangements of the chains depend on the environmental conditions. Thermal processing, solvent viscosity and polarity all affect the final conformational relaxation of the polymer chains resulting in new photophysical properties,[2,10] which show dramatic differences when comparing the solution and solid-state phases.[11,12] Several research groups have reported evidence that the energy transfer (migration) process is significantly affected by molecular interactions and polymer chain packing.[13,14] In particular, in dilute solution, chains are considered as isolated and have more conformational degrees of freedom, therefore, intramolecular interactions are highly likely between the different segments of the same chain, and a photoexcitation event may result in an intrachain energy transfer process.[15] The intrachain energy migration requires the motion along the conjugated backbone of a single polymer chain, under the conditions that no more chain-to-chain interactions exist (self-folding is prevented considering a rigid-rodlike structure). In general, rigid-rod type polymers demonstrate more extended conformations compared to the polymers which have more flexible backbones.[16] However, in the solid state, the situation is more complex when there are seveal chromophores in close proximity around the excited chromophore (packing nature of the chains). In this case, intermolecular interactions are highly possible between different polymer chains, and a photoexcitation event may result in interchain energy transfer process.[15] The interchain energy migration is a through-space energy process between close proximity chromophores, where the chromophores belong to different polymer chains or chain folding brings the chromophores together. If the chain

folding process happens, multiple funnels may be formed along the polymer chains which enable excitons to migrate towards quenching or dopant sites.[17] A detailed energy migration process due to inter/intra-chain interactions was reported by Hennebicq *et al.*,[15] where formation of weak complexes between polymer chains was revealed. In addition, intrachain energy migration has been found relatively less effective process compared to interchain migration,[18] which is attributed to the weak dipole coupling of the excitations along the chain direction.

In this chapter, the effects of chain-chain interactions have been investigated in polyspirobifluorene (PSBF) homopolymer (770000 g/mol), which was developed by Merck OLED Materials GmbH. Structurally, the PSBF consists of a polyfluorene backbone with additionally substituted fluorene unit with electron-donating alkoxy side chains by a spiro-linkage at the 9-position (see Fig.5.2). This spiro-linkage means that the fluorene group containing the four branched alkoxy groups is rigidly perpendicular to the backbone which are designed to prevent any possible aggregation and crystalisation of the PSBF. Conjugation is enhanced by means of spatial overlap of π-orbitals between orthogonally positioned fluorene units, that is, spiroconjugation. This gives rise to enhanced charge carrier mobility, photo-chemical stabilization and non-aggregation.[2,3] It should be noted that H-aggregate formation in spiro polymers cannot occur. In general, H- aggregation results from strong intermolecular van der walls type attractive forces between the molecules, which can be determined by distinct changes in the absorption band as compared with the monomeric species. However, the PSBF polymer was designed to prevents any form of crystalization or formation of ordered aggregates through the use of the spiro side groups. This geometry plus the branched nature of all four alkoxy groups prevent any ordering of the backbone or aggregation of the main chain and also prevents co-facial interaction between neighbouring phenyl groups as steric hindrance forces alternated spiro groups to flip 180^0 across the backbone, such that H-aggregates (which need a very high degree of local order, i.e. plane to plane stacking for sandwich type arrangement) cannot form.[19] Furthermore, the attached additional electron donating side groups to the spiro fluorene side group enable solubility of PSBF to increase electron transport properties.[2] The concept of spiro-linkage was offered by Salbeck *et al.*[20] to stabilise the amorphous nature of conjugated molecules, where the presence of

large steric hindrance prevents any kinds of ordering. In addition, the spiro-linkage increases the glass transition temperature of PSBF, which is significantly higher than that of conventional polyfluorene.[21] That enables morphological stability and makes the devices more stable and robust, therefore, the PSBF polymer is considered as one of the most promising blue-emitting materials for PLED applications.[22] Furthermore, the aforementioned donor-acceptor effect can be enchanced remarkably by spiroconjugation, which enables rapid electron delocalisation from the backbone to the sidegroups, and this phenomenon is attributed to formation of a charge transfer (CT) state.[3]

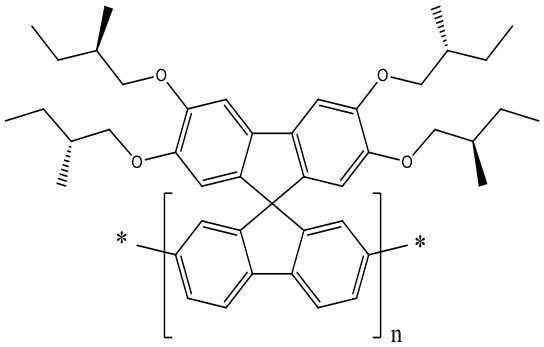

Figure 5.2 The chemical structure of polyspirobifluorene (PSBF) homopolymer

Recently, Monkman and co-workers have reported the investigation of fluorene derivatives to understand the excited-state photophysics,[2,3] and how it affects the high-efficiency of devices.[22] The reports in solution showed that solvent-solute interactions shorten intermolecular distances and tend to favour rotational and translational relaxation.[23] Hintschich *et al.* highlighted the important role of geometrical orientation of the side groups of fluorene derivatives to increase the orbital coupling and enhance spiroconjugation, which facilitates relaxation of the initially excited-state and stabilises the long-lived CT state.[2] In addition, the photoinduced absorption features of PSBF film have reported by King *et al.*,[3] where two excited absorption bands are observed in PSBF: PA1 is due to the singlet excited state absorption, PA2 is assigned to the formation of spiroconjugation enhanced intramolecular CT states. The large lifetime decay differences observed between PA1 (rapid process) and the ground state recovery (slow process)

showed the dominating role of the PA2 band in the recovery of the ground state. However, the literature review reveals that fundamental photo-physical properties of PSBF excited state are still unable to explain the formation of CT state and additional singlet generation mechanism in solution and film. The latter will be the subject of interest in Chapter 6.

5.1.1 Spin-statistics of triplet-triplet annihilation

In the literature, several works showed evidence of additional singlet generation in polyfluorene type polymers resulting from bimolecular processes i.e. triplet-triplet annihilation (TTA) or triplet fusion (TF), in which the basic quantum mechanical spin statistic is broken (the singlets and triplets are formed in the ratio 1:3) by means of interaction within the two uncorrelated triplet excitons to generate secondary production of singlet excitons.[24,25] Theoretically, once two triplets approach close enough to interact in a diffusion controlled environment there are statistically nine equal possible ways for their spins to be combined and form an excited complex which have three different multiplicities: one of which has singlet multiplicity, three of them have triplet multiplicity, and five of them have quintuplet multiplicity.

After the formation of excited complexes, the dissociation process occurs and higher energy singlet and triplet states plus their ground state molecules are formed in the ratio of 1/9 and 3/9 respectively. Then rapid internal conversion occurs and higher energy singlet turns back to emissive singlet excited state where the delayed fluorescence arises as a result of this bimolecular process. In addition, the higher energy triplet state also undergo rapid internal conversion to the initial triplet state and give rise to trigger further annihilation recycles which play an active role in repopulation of the singlet excited state. This process continues until all the triplets are depleted. In other words, the outcome of triplet recycling is formation of an excited triplet state and a singlet ground state molecule. So, in every recycle process, the energy consumption occurs significantly due to deactivation of one annihilating molecule. Consequentially, the maximum emissive singlet yield *via* TTA event can be theoretically predicted as ~11%. However, much experimental evidences show that this theoretically calculated singlet generation value is not totally true and can be overcome.[26,27]

The reason is that the quintet encounter complex cannot undergo an annihilation process and dissociate to initial triplet states with negligible energy loss. In many cases the statistics are different because high energy quintuplets are usually not energetically reachable,[28,29] which means the energy of two annihilating triplets ($2xE_{T_1}$) is not enough to form a high energy quintet encounter. So, the total singlet generation *via* TTA can be determined depending on two conditions;[29,30] i) if the energy of two triplets is higher than the energy of singlet state S_1 ($2xE_{T_1} > S_1$) as well as higher than the energy of one of the higher energy triplet levels E_{T_N} ($2xE_{T_1} > E_{T_N}$), in this scenario the collision between two triplets (TTA) gives rise to form a singlet excited state (S_1) and T_N state where the T_N state rapidly decay back to T_1 state and results in formation of one triplet. Consequentially, five of the triplet excitons are quenched to the ground state and two of them generate one singlet, then, probability to obtain singlet excited state *via* TTA is increased to 2/5. In other words, the fraction of triplets that generate singlets *via* TTA is 20% (0.5 x 2/5). ii) In the most favourable scenario, if the energy of two triplets is higher than the energy of the singlet state S_1 ($2xE_{T_1} > S_1$), however, lower than the energy of E_{T_N} ($2xE_{T_1} < E_{T_N}$), then only singlet states can be formed through TTA, not T_N state. In this case, the fraction of triplet states that generate singlets *via* TTA can be given as 50%.

5.2 Experimental

Dilute solutions of PSBF (~10^{-5} -10^{-6} M or the optical densities <0.8) were prepared in both 2-methyltetrahydrofuran (2-MeTHF) and methylcyclohexane (MCH). After transferring the solutions into the necked cuvette, the oxygen was removed from the solutions by five pump-freezing-thaw-cycles. Then, the cuvette was mounted in a liquid nitrogen cryostat (300 K to 77 K, Janis Research) for temperature dependent fluorescence measurements both for steady-state and time-resolved spectroscopy techniques (the spectroscopy techniques are given in more detail in Chapter 3)

Picosecond time-resolved fluorescence decays were collected using the time-correlated single photon counting technique (impulse response function, IRF: 19.5 ps). A

vertically polarized picosecond Ti:sapphire laser (Coherent) was used as an excitation source, the excitation wavelength was 367 nm, and the power of the laser was 54 MW. Then emission was collected using a polarizer at its magic angle (54^0), which was crucially important to remove any possible polarization effects. For detection of the emission a double monochromator (Acton Research Corporation) which was coupled to a microchannel plate photomultiplier tube (Hamamatsu R3809U-50) were used.

5.3 Results

5.3.1 Steady-state measurements of absorption and emission

Normalised absorption and the emission (exciting with 355 nm) spectra are depicted in Fig. 5.3., which are collected in two solvents with different polarity index, namely in methyl cyclohexane, and 2-methyltetrahydrofuran. When the polarity of the solvent increases the absorption spectra slightly shifts to blue, and the $S_0 \rightarrow S_1$ (0-0) transitions peaks are assigned as *ca.* 400 nm in MCH and *ca.* 395 nm in 2-MeTHF. For the emission, the spectra show structured properties, the peak *ca.* 426 nm in MCH and *ca.* 424 nm in 2-MeTHF are assigned as the π-π* transition peaks. In addition, the π-π* transition peaks almost overlap with each other (~2 nm differences), whereas, once the polarity of solvent increased, the red-shoulder of the emission peak in MCH (*ca*. 447 nm) showed significant enhancement in 2-MeTHF solution and appears *ca.* 450 nm. The slight difference in the peak positions (~3 nm) of the spectra is due to the polarity difference of the solvent. The great enhancement of the half width of the spectral shape arises due to involvement of stabilised states of the singlet-excited state (S_1) in polar solvents, i.e. charge transfer states. The fluorescence enhancement can be calculated from the integrated area of the spectrum, which was ~42%.

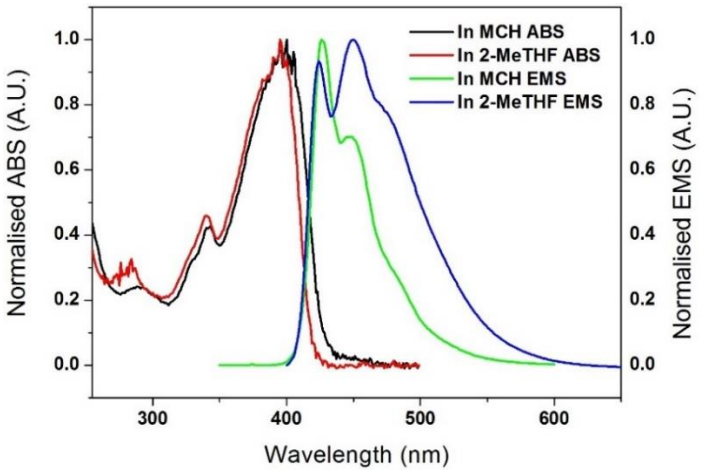

Figure 5.3 Absorption and emission spectrum of PSBF in MCH and 2-MeTHF at RT.

5.3.2 Temperature dependence of photoluminescence in variety of solvents

The steady-state behaviour of PSBF as a function of temperature is observed in the same degassed solutions. Fig. 5.4 a. shows the photoluminescence (PL) behaviour in non-polar degassed MCH solution as a function of temperature. The feature at 426 nm is assigned to a $^1(\pi, \pi^*)$ transition with the 0-0 transition having the highest intensity with vibronic structure at high temperatures. However, on cooling down to 145 K, the spectra gradually loses the structured shape as well as energetically shift to the red by ~0.12 eV and form a red-shifted emission band. The change in the intensity and the shape of structure is depicted as a function of temperature comparing in air-saturated and degassed MCH solutions (see Fig. 5.5). It is worth highlighting that slightly structured emission arises from the new band, not from the S_1 state, and the peak positions are not significantly affected by changes in temperature (145 K to 95K).

The steady-state PL emission behaviour of PSBF in degassed (Fig. 5.4 b) 2-MeTHF solutions are presented as a function of temperature. The feature at 424 nm is assigned to a $^1(\pi, \pi^*)$ transition with the 0-0 transition having the highest intensity with vibronic structure at high temperatures. As a result of cooling, the moderate separation is observed between two emitting species where a clear isoemissive point was observed showing that the two emitting species are kinetically linked to each other. However, on cooling down to 145 K, all the vibronic structure is lost, and a new emission band, with no vibronic

structure is formed. This new emision was strongly red-shifted to *ca.* 500 nm and showed a classic Gaussian line shape, which is a very distinctive emission band and never obtained in MCH solution.

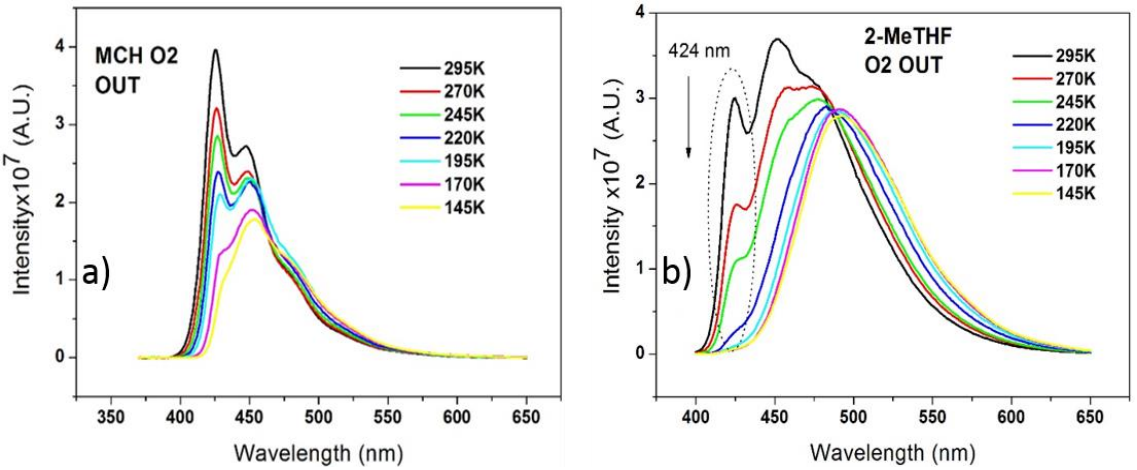

Figure 5.4 Temperature dependence of steady-state emission of PSBF **a)** In degassed MCH solution **b)** In degassed 2-MeTHF solution.

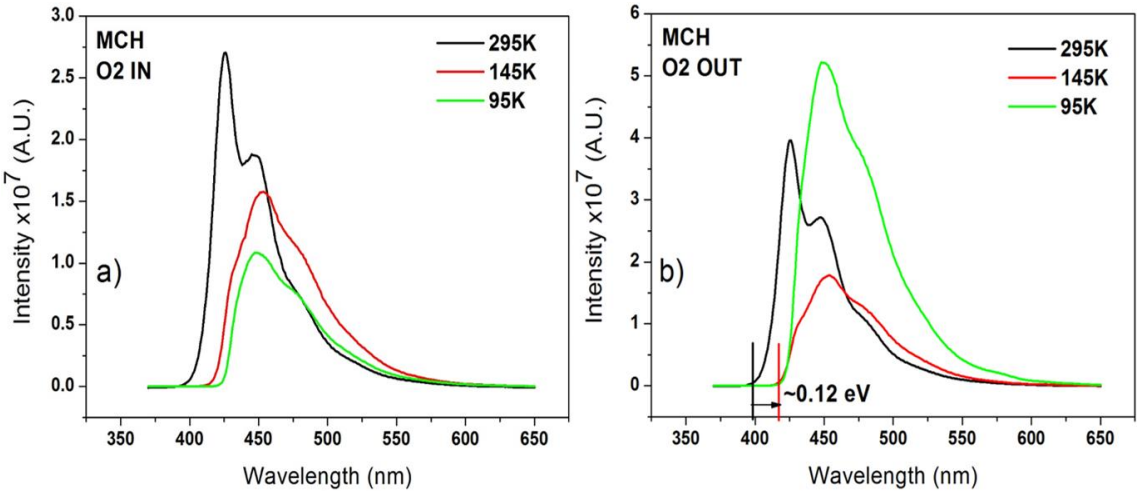

Figure 5.5 Temperature effect upon steady-state spectra of PSBF is represented **a)** in air saturated and degassed spectra at 295 K **b)** in air saturated and degassed spectra at 145K.

It should be noted that during the measurements, very dilute solutions were used so it is highly unlikely that any aggreagations could occur resembling an H-aggregate (that requires a large number of molecules to be highly ordered into an aggreagate to see the effects of Davydov splitting). This can also be compared to poly-3-hexylthiophene where the linear alkyl chains can crsystalize and drive the backbone into a well-ordered rigid rod configuration. These rods then form local ordered regions, which are thought to be large enough to support small H-aggreragate domains.[31] Here, it is attributed to CT state emission which is stabilised by solvent polarity and temperature accompanied by structural changes to adapt the molecular structure to the new emissive species. That is attributed to result from inter-chain interactions, not from intra-chain interactions which is also confirmed by measuring the concentration dependence of emission at 295 K and 145 K in three different optical density values (see. Fig 5.6).

Fig. 5.7 a shows the change in the intensity and the shape of structure as a function of temperature for both air-saturated and degassed 2-MeTHF solutions. The changes in temperature obviously results in the formation of a new unstructured emission band which is energetically lower than $^1(\pi\text{-}\pi^*)$ band (~0.27 eV). However once the solution is frozen, i.e. 90 K, the spectra dramatically shifts to the blue (~0.15 eV) and loses all contribution from the unstructured CT_1 state, in this case, the fluorescence arises from a totally different species which is assigned as an intramolecular charge transfer (ICT) state in which the fluorescence increases dramatically and also phosphorescence emission can be observed even in the steady-state emission spectra (*ca.* 567 nm). The reason for this is that, enhanced ICT character of the lowest singlet excited state gives rise to pronounced intersystem crossing,[32] that proposal is confirmed by obtaining the energy of T_1 state as ~2.20 ± 0.3 eV which is very close value that have been found by Rothe *et al.* in polyfluorene films as 2.22 eV.[22]

In chloroform (see Fig. 5.8) similar CT state formation behaviour is clearly observed. At 220 K the solution is cold enough to form intermolecular CT emission, however, once the temperature is decreased further, i.e. 195 K, red-shifted emission is gradually lost and the transition between the intermolecular CT species (CT_2^1) to intra-molecular CT species (CT_1^1) can be observed by means of spectral overlap between the

peak of 220 K spectra and the red tail of structured 195 K spectra. At low temperatures the spectra completely returns to the intra molecular species (at 95 K), in which the $^1(\pi, \pi^*)$ state and newly formed intra molecular CT state contribute to total fluorescence emission.

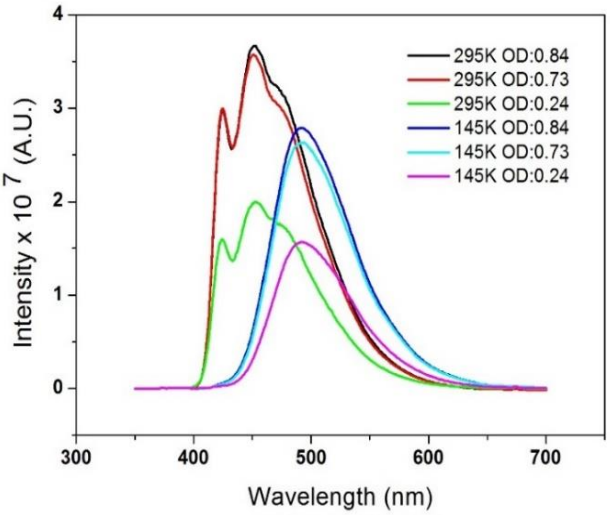

Figure 5.6 Steady-state emission of PSBF at 295 K and 145 K in three different concentrations (optical density values) in 2-MeTHF solution

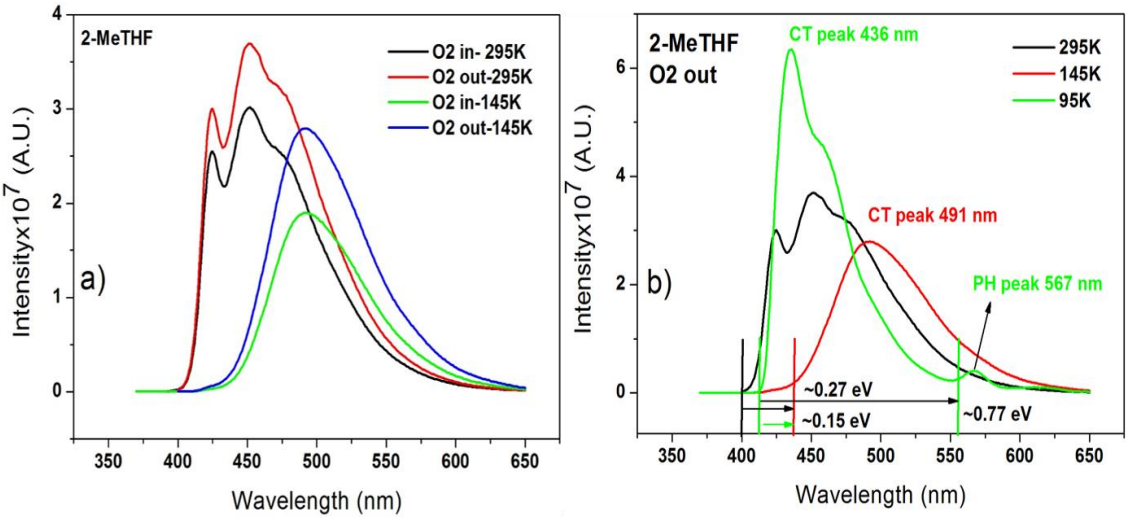

Figure 5.7 Comparison of the effect of temperature on steady-state PL spectra of PSBF in 2-MeTHF **a)** air saturated and degassed spectra at 295 K and 145K **b)** formation of CT states comparing the $^1(\pi\text{-}\pi)$ spectra at various temperatures.

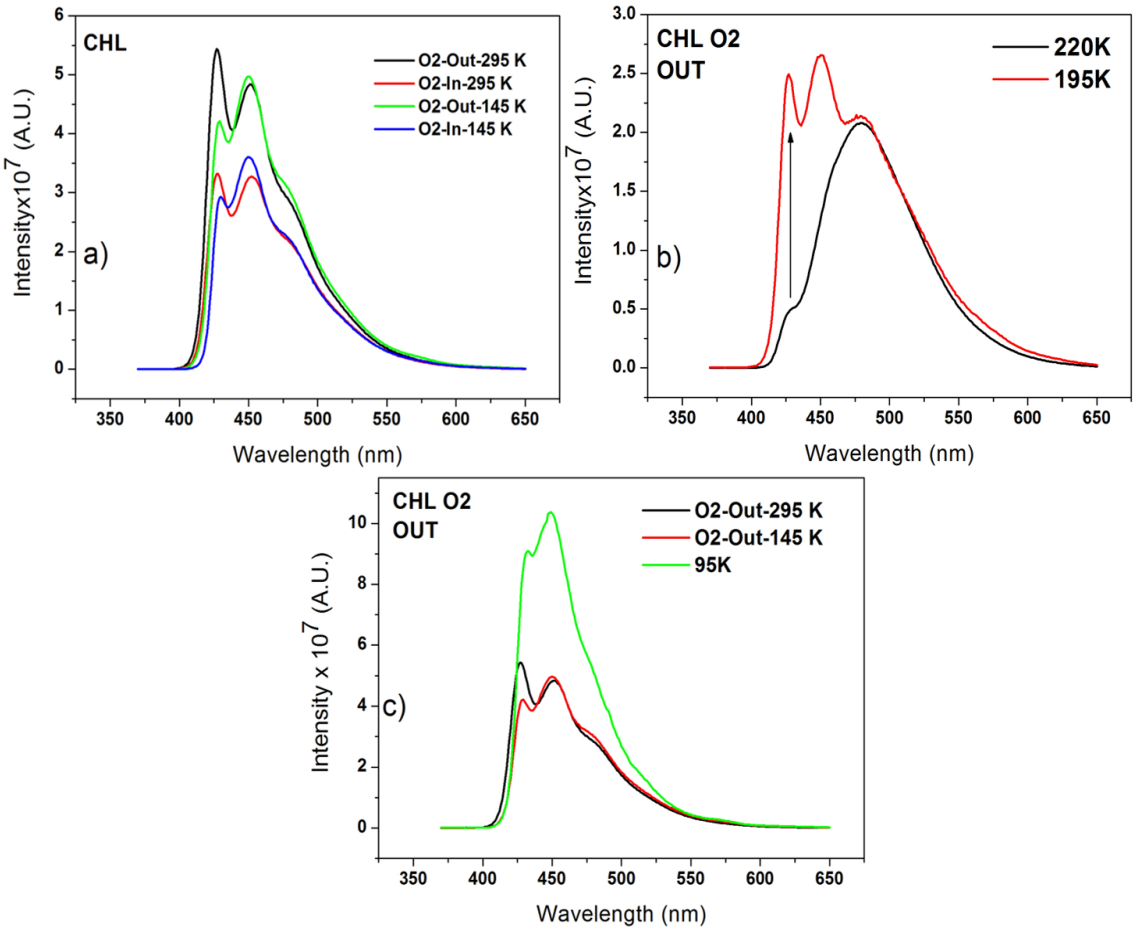

Figure 5.8 Comparison of the effect of temperature on steady-state PL spectra of PSBF in CHL **a)** air saturated and degassed spectra at 295 K and 145 K **b)** degassed spectra shows the clear transitions between the CT states **c)** degassed spectra at 295 K, 145 K and 95 K.

The conclusion can be made that as these new states which form as the temperature is decreased (and solvation becomes progressively worse) are charge transfer in nature through the Gaussian band shape combined with the solvatochromism the new bands exhibit. This spectral shift of the new emission band with increasing solvent polarity shows that the new Gaussian shape band is not just a matter of aggregation and rather involves some degree of charge localization and creation of an excited state dipole moment that is different from the ground state dipole moment, otherwise the "same" aggregate would be present in different solvents, and in particular would not disappear at low temperatures, when below the solvent melting temperature local solvent-solute interactions are no more possible. Further, in our group's previous work on this polymer

^{3} is has been shown that these new states are readily shifted in energy by an applied electric field, again consistent with them possessing a 'permanent' dipole moment. Also, the decrease in the PLQY as a function of temperature is ascribed to the formation of the CT states. As shown previously, the (triplet) CT^3 state can readily recombine to form a local triplet on the polymer backbone, in particular, if the local triplet state is lower in energy, this leads to enhanced (effective) ISC and triplet production.[32] Thus as more CT states form there is a competition set up between CT^1 fluorescence to CT^3 ISC and CT^3 quenching to the local triplet state, which leads to a decrease in PLQY as the temperature decreases.[32,33]

5.3.3 Time resolved decay dynamics with nanosecond gated spectroscopy

In order to clarify our observations in the steady-state measurements, nanosecond gated time resolved spectroscopy was used to measure the decay dynamics in solutions (the methods were given in detail in chapter 3). The key element of the measurement was that more than 12 orders of magnitude in intensity and more than 10 decades of time can be recorded in a single experiment, therefore, it is possible to capture both prompt (PF) and delayed fluorescence (DF) simultaneously (in one curve) as shown in Fig.5.9 using double logarithmic scales.

The initial fast part of the decay is assigned to PF, and the long slower decay component is assigned to DF. Fig. 5.9 a shows the lifetime decay of PSBF in degassed MCH solution at 295K and 145K. The PF follows a biexponential decay with the lifetimes of 3±1 ns and 11±1 ns and at longer delay times a power law regime ($I_{DF} \sim t^{-m}$) occurs with slopes of ~1.29 at 295 K and ~1.31 at 145 K. At 145 K, the solution is not frozen yet, therefore, the decay dynamics follow a similar power law regime. This power law behaviour is in great agreement with previous report on fluorene derivative poly(2,7-(9,9-bis(2-ethylexyl)fluorene)) (PF2/6) in dilute solution,[24] in which the kinetics are attributed to the dispersive triplet excitations. The lifetimes of DF were determined as 252±7 ns at 295 K and 1.1 ±0.2 μs at 145K. The ratio between DF and PF intensities, DF/PF, was calculated as 0.0072 for 295 K and 0.0059 for 145 K. These values are presented on the

plots and will be used to calculate the quantum yield of delayed fluorescence shown below.

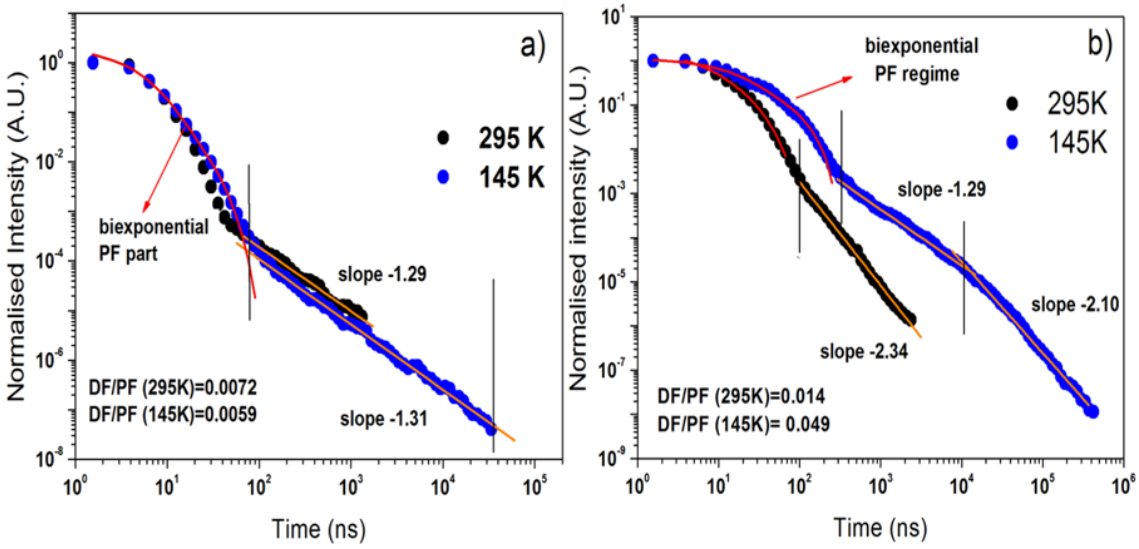

Figure 5.9 Lifetime decays of PSBF in log-log scales **a)** In degassed MCH solution **b)** In degassed 2-MeTHF solution. The molecular structure of PSBF and DF/PF ratios are also inserted into the plots.

The time evolution of spectra at RT shows that the DF emission always appear energetically similar with PF emission from 1.56 ns to 220.21 ns (Fig. 5.10 a), where the thermal background energy keep the aforementioned CT_1^1 and $^1(\pi\text{-}\pi^*)$ states in quasi equilibrium. The mechanism behind the population of this CT_1^1 state might be efficient reversible electron transfer from an on chain exciton state to the CT_1^1 state. Therefore, this thermal background energy ($k_BT \sim$ 27 meV at RT) gives rise to sufficient back and forward (reversible) energy transfer between the states, in this case, the states can be considered as their superposition. Indeed, at 145 K, the excited singlet state relaxed through the lower energy state and the spectra is slightly broadened and red shifted by *ca.* 0.1 eV (Fig. 5.10 b), where the emissive ICT band clearly dominates the overall fluorescence band. This can be attributed to the reduction of the thermal background energy, affecting the reverse transition rate from the CT_1^1 state to $^1(\pi\text{-}\pi^*)$ state, therefore, the energetic separation of the states is highly likely. In this condition, at 145K, the initial time domain of the spectra, i.e. 6 ns to 6.41 ns, originates from the non-relaxed $^1(\pi\text{-}\pi^*)$

state, whereas red-shifted long-live DF emission, i.e. between 20.31 ns and 220.21 ns, originates totally from the new relaxed CT_1^1 state. It should be worth highlighting that this ICT state is only stabilised at low temperatures and has long fluorescence lifetimes.

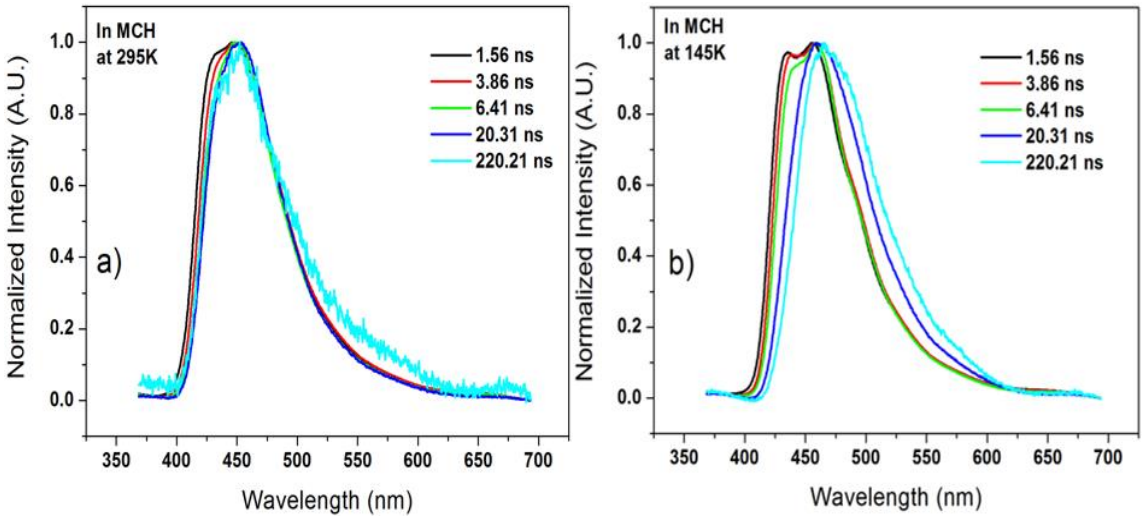

Figure 5.10 Time evolution of PSBF spectra in MCH solution between 1.56 ns to 220.21 ns time scale **a)** at 295K **b)** at 145 K.

However, in 2-MeTHF, stabilisation of the CT state is greatly increased by the polar solvent and so at 295 K the DF contribution on the PL spectra is much higher than that of the MCH case (DF/PF = 0.014). As the temperature is decreased to 145 K, chain collapse increased more rapidly due to poor solvent effect (polymer chains are not well-dissolved) of 2-MeTHF, which enhances the interchain interactions on the same polymer chain to form a CT_2^1 state (this has a different origin from the ICT state formed as a result of electron transfer from on chain exciton state in MCH solution at 145 K), in which there exists higher triplet production and better triplet migration to find each other and annihilate so that the DF from TTA further increases. In fact, the interchain interactions are unexpected in spiro-linked systems, unless the solvent acts as poor solvent for the polymer. In this system, the DF lifetimes were calculated as 284±5 ns at 295 K and 6.2 ± 0.3 μs at 145K. And the ratio of DF/PF intensities were calculated as 0.014 for 295 K and 0.049 for 145 K. The latter confirming the remarkably enhanced triplet migration at 145

K. Fig. 5.11 shows the time evolution of the spectra in 2-MeTHF solution. Fig. 5.11 a shows perfect spectral overlap of PF and DF emission over the time range of 6.41 ns to 514.46 ns at 295 K, where the both PF and DF emission arise from vibronically resolved $^1(\pi, \pi^*)$ state. However, when the temperature is decreased to 145 K, the spectra loses structural shape and turns into an unstructured Gaussian band as well as shifting *ca.* 0.23 eV (Fig. 5.11 c), this CT_2^1 state then dominates the overall fluorescence band over the time range of 2.11 ns to 16 μs (Fig. 5.11 b). The new relaxed excited state, which is assigned as intermolecular CT_2^1 state, shows enhanced charge transfer character in the polar solvent, but the polarity itself does not provide the driving force for the formation of the state, instead temperature plays a significant role in it.

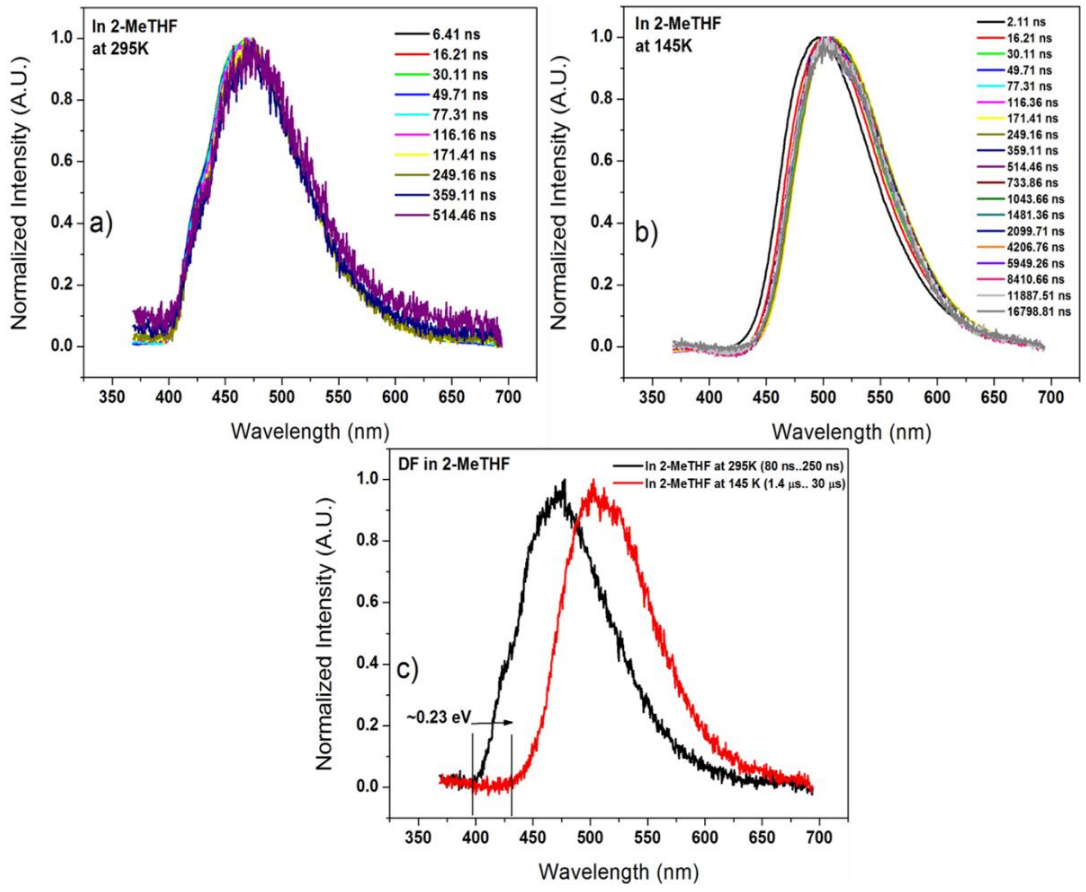

Figure 5.11 Time evolution spectra of PSBF in 2-MeTHF **a)** from 6.41 ns to 514.46 ns at 295K **b)** 2.11 ns to 16798.71 ns at 145 KT **c)** The temperature effect upon the energy shift of DF spectra showing the red shift *ca.* 0.23 eV.

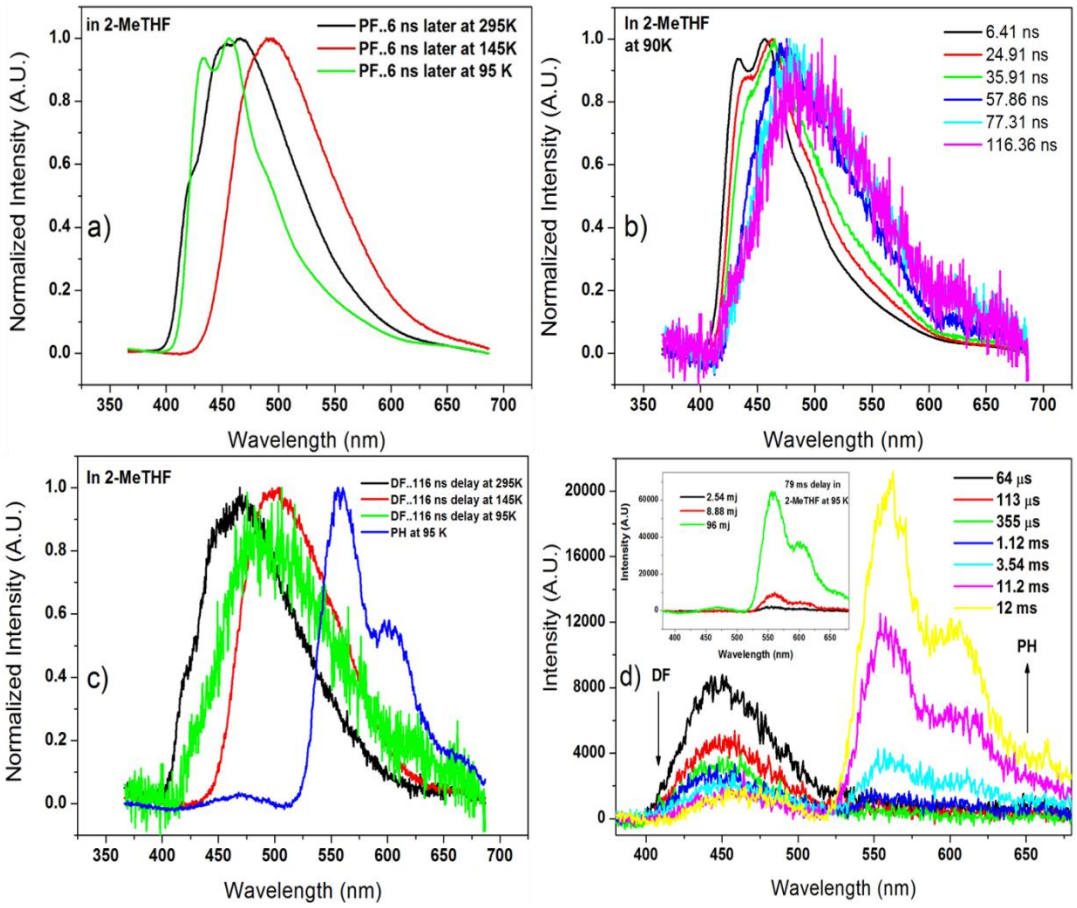

Figure 5.12 The spectra were taken in 2-MeTHF solution **a)** PF spectra were taken after ~6ns delay at 295K, 145K and 95K **b)** time evolution at 90 K from 6.41 ns to 116.36 ns. **c)** DF spectra were taken after ~116 ns delay at 295K, 145K and 95K and the PH spectra were taken 78 ms delay time d**)** time dependent competition of DF and PH at 95 K and inserted graph shows the excitation energy dependence.

However, once the 2-MeTHF solvent is frozen, i.e. at 95 K, the intermolecular CT species loses its Gaussian shape and a remarkable blue shift is observed in PF spectra (Fig. 5.12 a). However, this blue-shifted emission is relaxing through the intramolecular species with time which can be observed with the time evolution of the spectra from 6.41 ns to 116 ns (Fig. 5.12 b). Finally the emissive CT state at 95 K is very distinctive from the intermolecular CT_2^1 state at 145K, because the CT_2^1 was the only emissive species at 145K. In fact, at 90 K, the singlet states decays non-radiatively by ISC through the energetically low lying intramolecular CT_1^1 state, and also to the $^3(\pi\text{-}\pi)$ state which can be represented in Fig. 5.12 c, indicating very complex excited state dynamics of PSBF in 2-

MeTHF at low temperatures. The competition between the radiative decay from the intramolecular CT_1^1 state and $^3(\pi\text{-}\pi^*)$ can be obtained in the microsecond time domain in Fig. 5.12 d, which is very consistent behaviour considering that enhanced CT character of the lowest singlet excited state favours higher intersystem crossing.[32] At early times, only the DF emission was apparent coming from the CT_1^1 state, however, after certain times, the PH becomes dominant and only a small fraction of weak DF emission is observed. After 79 ms delay times, particularly at low excitation conditions, i.e. 2.54 μJ, no DF emission is observed, indeed, weak PH is apparent. However, once the excitation energy is increased up to 96 μJ, a larger triplet reservoir is depleted, therefore, strong PH emission following with the weak DF is obtained (Fig. 5.12 d inserted graph).

5.3.4 Direct investigation of quantum yield of delayed fluorescence

The delayed fluorescence quantum yield (Φ_{DF}) can be determined directly from the DF/PF ratio from Fig. 5.9, where an electron transfer recycle between the CT_1^1 and $^1(\pi\text{-}\pi^*)$ is considered. Addressing this point, the integration of the initial exponential decay give the PF value and the integration of the following long lasting parts give the DF contributions of the total sample emission, hence, the intensity ratio of DF to PF intensity is defined as in Eq. 5.2.[34]

Total fluorescence, that is, PF+DF, of the sample is given by Eq. 5.1 as,

$$\Phi_f + \Phi_f(\Phi_T\Phi_{DF}) + \Phi_f(\Phi_T\Phi_{DF})^2 + \ldots = \Phi_f \sum_{m=0}^{+\infty} (\Phi_T\Phi_{DF})^m \qquad \textbf{(5.1)}$$

where the first term represents the prompt fluorescence (no cycle), and the remaining terms correspond the cycling process between the close energy states for delayed fluorescence. From Eq.5.1 the DF/PF ratio is determined as,

$$\mathbf{R} = \frac{\mathbf{DF}}{\mathbf{PF}} = \frac{\mathbf{F_{inst} N_s \Phi_f (\Phi_T \Phi_{DF} + \Phi_T^2 \Phi_{DF}^2 + \ldots)}}{\mathbf{F_{inst} N_s \Phi_f}} = \frac{\mathbf{\Phi_T \Phi_{DF}}}{\mathbf{1 - \Phi_T \Phi_{DF}}} \qquad \mathbf{(5.2)}$$

where F_{inst} is an instrumental function, N_s is the number of excited states, Φ_f is fluorescence quantum yield, Φ_T is triplet yield, and Φ_{DF} is DF yield from triplet fusion (TF). F_{inst} is the same for PF and DF since they were recorded during the same measurements, likewise for the initial number of excited states after pulsed excitation. All quenching mechanisms including intersystem crossing (ISC), non-radiative decay, and quenching due to exciton migration are accounted for in Φ_f and are identical for both types of emission once again as they come from the same CT state, so Eq. 5.2 is simplified and gives Eq. 5.3 below, from which Φ_{DF} is determined.

$$\Phi_{DF} = \frac{R}{(1 + R)\Phi_T} \qquad \mathbf{(5.3)}$$

In order to determine Φ_{DF}, R is calculated from the data in Fig. 5.9 at each temperature. The starting point for the DF calculation was taken as the inverse time of the intersystem crossing rate of PSBF.[35] The value of Φ_T=0.05 ± 0.01 for solution and Φ_T=0.12 ± 0.02 for films were taken from the previous femtosecond ground state recovery measurements made by King *et al*.[35] Using this information, the various values of Φ_{DF} were found in different solutions at distinct temperatures, such as 0.143 ± 0.002 at 295K and 0.117 ± 0.003 at 145 K in MCH solution and 0.27 ± 0.01 at 295K, 0.93 ± 0.04 at 145K and 0.46 ± 0.02 at 90K in 2-MeTHF solution. The value of 0.93 ± 0.04 at 145 K is a conspicuous point because the quantum yield of PSBF (PLQY) was measured as 0.80 in solution at RT,[3] that shows us that once the temperature is decreased to 145K, the inter molecular CT_2^1 state is stabilised and dominates the system, showing significant DF quantum yield value of 0.93 ± 0.04. At this temperature, the CT_2^1 is the only emissive state lying energetically lower than $^1(\pi,\pi^*)$, ~0.23 eV. Furthermore, for PSBF it is not possible to achieve Φ_{DF}> 0.2 from TTA alone. Clearly, in PSBF $2xE_{T_1} > E_{T_N}$ (E_{T_1} =

2.22 eV, E_{T_N} = 3.77 eV)[22] so that the maximum Φ_{DF} can only be 0.2, considering this point, significant contribution to DF comes from CT_1^1 state at low temperatures.

5.3.5 Excitation dependence of delayed fluorescence at various temperatures

The DF dependence on excitation intensity, measured in degassed solutions, is shown in Fig.5.13. Here a delay time of 0.2 μs and the integration time of 1 μs were chosen. The results for MCH solution in Fig. 5.13 a shows a slope of ~1.5 at low laser dose ($\leq$ 10 μJ), and slope ~1.2 at high excitation doses ($\leq$ 100 μJ). These dependencies indicate that monomolecular (long-lived CT emission) and bimolecular (TTA) processes are both contributing to the observed delayed fluorescence (show a heterogeneity). Approaching the value of slope ~1.5 at low intensity is indicative of nearly equal contributions of the TTA and CT_1^1 emission on delayed fluorescence. In the case of high laser intensity conditions, as shown in Chapter 4, the TTA intensity dependence turns over gradient 1 and this is what gives rise to the observed reduction in slope at high intensity, once again both monomolecular and bimolecular processes contribute to the total DF signal.

In Fig. 5.13 b, the DF intensity dependence on excitation dose in 2-MeTHF. At low laser dose conditions ($\leq$10 μJ), in particular at 145 K, the TTA is the dominant process giving DF showing nearly perfect quadratic dependence with slope approaching the value of ~2. The $^3(\pi, \pi^*)$ triplet state of PSBF with an energy of E_{T_1}=2.22 eV and lifetime of seconds at low temperature decays predominantly *via* TTA with little competition from non-radiative decay. At 145 K, the CT_2^1 state is stabilised in the polar solvent and leads to increased triplet state $^3(\pi, \pi^*)$ generation. This higher triplet density and also higher triplet mobility favour TTA, whereas, at 295 K, the slope was found to be ~1.68 showing relatively less contribution of TTA including with CT_2^1 contribution. Here the non-radiative decay is competing to depopulate the $^3(\pi,\pi^*)$ triplet state, and as there are fewer CT states on the polymer chain the triplet yield is also much lower. At high laser fluence conditions, the observed slopes ~1.52 at 295 K and ~1.3 at 145 K indicate more complex mixed behaviour. At high intensities, the dependence once again turns over to linear

behaviour, indicative of high triplet density and good triplet mobility giving efficient TTA.

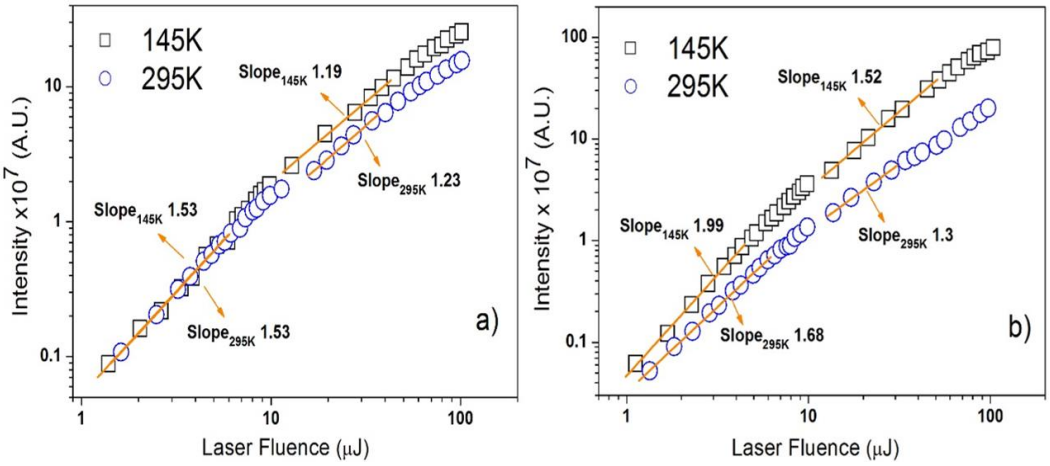

Figure 5.13 Laser fluency dependence of DF **a)** in degassed MCH solution **b)** in degassed 2-MeTHF solution. The excitation wavelength of 337 nm has been used at 0.2 μs delayed and 1 μs integration times.

5.3.6 Temperature dependence of delayed fluorescence

The DF behaviours as a function of temperature is also investigated in the same solutions, where the delay and integration times were chosen as 0.2 μs and 1 μs, respectively. In particular, in MCH, Fig. 5.14 a, the intensity of the integrated area of each spectrum is presented as a function of temperature. Until a certain temperature the DF emission becomes more intense with decreasing temperature, however, once the CT_1^1 contribution becomes slightly apparent the intensity level off is observed, which is due to trapping of excitons in the CT_1^1 state. Concomitantly, the peak position of spectra shows slight red shift (*ca.*19 nm) from a mixed emission to pure 450 nm emission, which is consistent with experimental calculations of the DF/PF ratios above (0.143 ± 0.002 at 295K and 0.117 ± 0.003 at 145 K), where the value is lower at 145K. The inserted graph indicates how the energy peak changes as a function of temperatures, where the energy peaks gradually decrease with decreasing temperature.

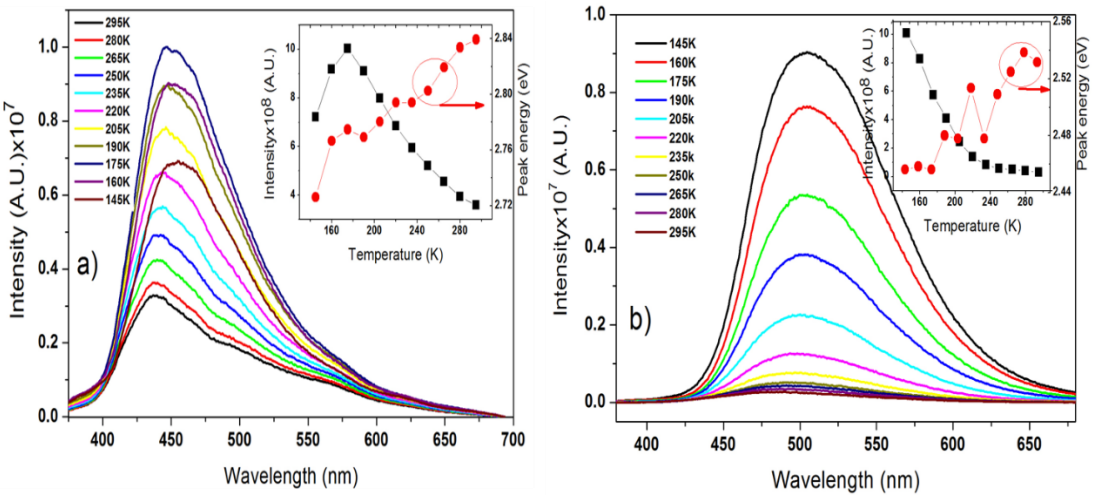

Figure 5.14 Temperature dependence of DF **a)** In degassed MCH solution **b)** In degassed 2-MeTHF solution. The excitation wavelength of 337 nm has been used at 0.2 µs delayed and 1 µs integration times. The inset graphs show how intensity of integrated areas change depending on the temperatures.

Furthermore, in 2-MeTHF (Fig. 5.14 b), the origin of the DF is always inter molecular CT_2^1 state (until the solvent is frozen ~95 K) and results in observing a dominant red-shifted 500 nm Gaussian band all the time with the quantum yield of 0.93 ± 0.04, therefore, temperature changes only affect the relative intensity changes, they do not give rise to any additional quenching pathways, in this scenario, the intensity always increases gradually with decreasing temperatures and no level off is observed in intensity. Again this is consistent with the DF/PF ratio value above.

5.3.7 Decay dynamics of excited state measured by TCSPC

Fig. 5.15 shows the fluorescence decays of PSBF in log-log scales at RT, and the solid lines are triexponential fits to the decays at four different emission wavelengths (425nm, 445nm, 460nm and 500nm) using an excitation wavelength of 376 nm. In the polar 2-MeTHF (Fig. 5.14 a. b.), the dynamics are divided into short (τ_2 and τ_3) and long-lived (τ_1) components. The decay components are determined by fitting the fluorescence decay with three discrete exponential functions with simultaneous deconvolution of the apparatus response function (see Table 5.1).

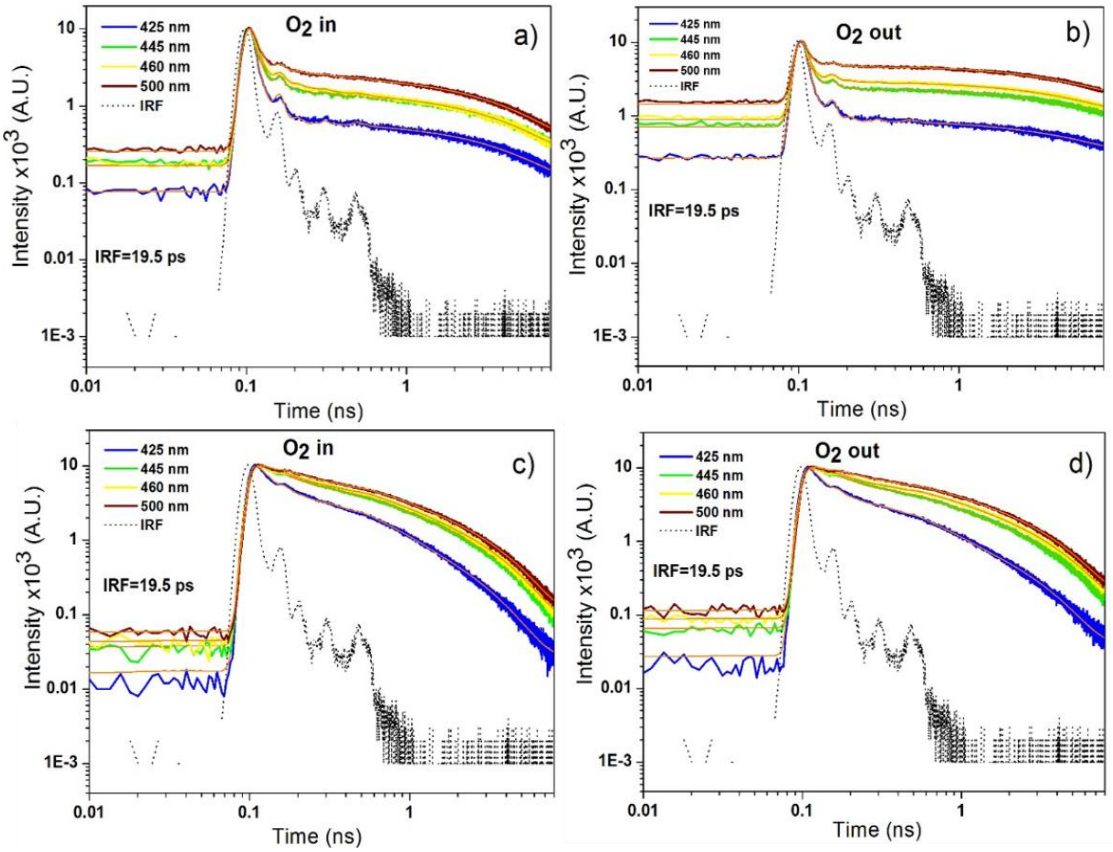

Figure 5.15 Log-Log scaled fluorescence lifetime measurements using time-correlated single photon counting method (TCSPC) at four different wavelengths 425 nm, 445 nm, 460 nm and 500 nm **a)** in air-saturated 2-MeTHF solution **b)** in degassed 2-MeTHF solution **c)** In air-saturated MCH solution **d)** in degassed MCH solution.

The initial fast components have lifetimes on a picosecond time scale, and they show slight variations compared to the longer wavelengths. It is important to note that the short-lived components (τ_2 and τ_3) do not change seriously when comparing them in both air-saturated and degassed solutions. Indeed, the excited state quenching may not be responsible for the rapid quenching components, instead, they may correspond to a rapid relaxation through the highly radiative long-lived state. Because, at RT, both of the CT_1^1 and $^1(\pi, \pi^*)$ states are considered as in quasi-equilibrium above. After that, a pronounced long-lived component dominates the dynamics, there is a clear evidence that the long decay component becomes more important at longer wavelengths, indicating quenching of the $^1(\pi, \pi^*)$ state into a long lived species. Indeed, the lifetime of the τ_1 is longer in

2-MeTHF than in MCH (Fig. 5.15 c.d.), which is again consistent with the stabilisation of the CT_1^1 state in more polar environment, therefore, the DF contribution is more significant than in the MCH case. In all cases degassing generally increases all lifetimes, in 2-MeTHF oxygen quenching is clearly seen on the long-lived species, whereas in MCH there is little effect showing that at these early times no triplet involvement occurs.

Table 5.1 The fluorescence lifetime decays in two different polarity solutions at four various wavelength positions have been calculated. As an excitation wavelength of 376 nm was chosen and the effect of oxygen on the fluorescence lifetime has been revealed.

Material **PSBF**	**Air-saturated Solution** λ_x**= 376 nm**				**Degassed Solution** λ_x**= 376 nm**			
	425 nm	**445 nm**	**460 nm**	**500nm**	**425nm**	**445nm**	**460nm**	**500nm**
In MCH	τ_1**=1.53 ns** τ_2**=0.37 ns** τ_3**=25 ps** χ^2**= 1.05**	τ_1**=1.88 ns** τ_2**=0.38 ns** τ_3**= 39 ps** χ^2**= 1.04**	τ_1**=1.96 ns** τ_2**=0.43 ns** τ_3**= 43 ps** χ^2**= 1.08**	τ_1**=2.01 ns** τ_2**=0.44 ns** τ_3**= 49 ps** χ^2**= 1.03**	τ_1**=1.74 ns** τ_2**=0.36 ns** τ_3**= 24 ps** χ^2**= 1.05**	τ_1**=2.15 ns** τ_2**=0.42 ns** τ_3**= 44 ps** χ^2**= 1.03**	τ_1**=2.27 ns** τ_2**=0.49 ns** τ_3**= 48 ps** χ^2**= 1.05**	τ_1**=2.37 ns** τ_2**=0.51 ns** τ_3**=56 ps** χ^2**=1.08**
In 2-MeTHF	τ_1**=3.80ns** τ_2**= 2 ps** τ_3**= 9.3 ps** χ^2**= 1.06**	τ_1**=3.89ns** τ_2**=7.1 ps** τ_3**= 11 ps** χ^2**= 1.06**	τ_1**= 3.94ns** τ_2**= 8.5 ps** τ_3**=14.7 ps** χ^2**= 1.08**	τ_1**= 4.64ns** τ_2**= 9.3 ps** τ_3**=17.9 ps** χ^2**= 1. 05**	τ_1**= 4.87ns** τ_2**= 1.1 ps** τ_3**= 9.6 ps** χ^2**= 1.06**	τ_1**= 5.24ns** τ_2**= 5.9 ps** τ_3**= 12 ps** χ^2**= 1.06**	τ_1**= 5.32ns** τ_2**= 6 ps** τ_3**=20.1 ps** χ^2**= 1.07**	τ_1**=5.87ns** τ_2**=9.1ps** τ_3**= 30.6ps** χ^2**= 1.04**

In addition, from Fig. 5.14 it can be seen that the long lived species are highly temperature dependent and at room temperature there is little emission from these states so it would not be expected to see much evidence of long lived states at the room temperature TCSPC. Conversely at low temperature these long lived states dominate and TCSPC would show very little in terms of decaying species, thus the measurements were only repeated at room temperature realistically. In MCH, the typical 400 ps decay of the fluorene unit singlet exciton (possibly quenched a little) can be seen and a contribution with ~2 ns lifetime from the CT_1^1 state which itself is rapidly quenched to the CT_1^3 state. Whereas in polar 2-MeTHF, no 400 ps decay is observed, just a very rapidly quenched ~10 ps signal along with the ~4 ns CT_1^1 emission, again quenched to the CT_1^3 state. Thus

the TCSPC confirms that singlet excitons are quenched to charge transfer states and that these are stabilised in polar environment, adding to the general information pool that CT states are important in this polymer.

5.4 Discussion

The observations revealed the complex excited state dynamics, and how these are affected by solvent polarity in a supposed "simple" luminescence polymer, PSBF in solution phases. In particular, the majority of initially excited exciton states do not decay directly to the ground state. Instead, they relax into long-lived states with charge transfer character. In general, a CT state can be populated in a number of ways following an optical excitation; as a result of i) energy transfer from the lowest excited singlet state to the lower lying CT state, ii) direct absorption of the pump photons or iii) charge trapping from the dissociation of the excitons. The findings are in good agreement with the previous reports[2,36] that show the strong interactions between the spiro-linked units of the molecules result in significant orbital overlap, and concomitantly enhanced donor-acceptor effect is reported following by formation of a CT state between the backbone and the side groups, arising from the orthogonally positioned fluorene side group towards the backbone fluorene of the PSBF.

The measurements were taken in dilute solutions, and so inter-chain interactions would be thought to be rather unlikely, especially with the spiro configuration of the alkoxy branched side chains. However, from time-resolved luminescence measurements, that initially photo-created $^1(\pi, \pi^*)$ state gives rise to new lower energy and longer lived states. This process is strongly affected by solvent polarity and temperature, in particular, which is more effective at low temperatures. The relaxed states show clearly a CT state character, as typified by the observation of unstructured Gaussian emission bands and solvent dependent energies. At RT, the fluorescence bands show a mixed character of $^1(\pi, \pi^*)$ and CT_1^1 state due to being in energetic quasi-equilibrium, where there is sufficient thermal background energy hold the states together and back-forward energy transfer is highly likely. However, as the temperature is decreased to 145 K, a red-shifted CT band is separated from $^1(\pi\text{-}\pi)$ band due to insufficient thermal energy between the states and

quenched electrons from $^1(\pi\text{-}\pi)$ state is trapped by CT state, therefore, the CT_1^1 band dominates the overall fluorescence band at low temperatures (Fig. 5.10 b).

Referring first to the emission in MCH, Hintschich *et al.*[2] reported previously that in non-polar solvents the energetic relaxation of the $^1(\pi, \pi^*)$ to CT state is accompanied by the conformational changes of the polymer chain. This explains the important role of the solvent viscosity and the temperature on the observed spectra. TD-DFT calculations also indicate that charge transfer occurs from the polymer backbone into the spiro side groups and form a self-trapped excitonic state having charge transfer character. These intrachain species give rise to emission at 460 nm, as we see in MCH and 2-MeTHF as well. Moreover, it is the emission of this intrachain CT exciton (CT_1^1) that dominates the delayed emission in this polymer, which is indicative of the far longer lifetime of this self-trapped CT exciton species. As discussed by previously,[2] the mechanism for the formation of this new CT species is driven by spiroconjugation between backbone and spiro side groups. As temperature decreases the quality of the solvent decreases and this effects the geometry of the polymer chain and also the side chains,[37] such that formation of the intrachain CT_1^1 state is stabilised. Therefore, even in MCH at low temperatures the emission from this CT_1^1 state dominates, and very little $^1(\pi, \pi^*)$ emission is observed.

In the far more polar 2-MeTHF, a stronger stabilization of this intrachain CT species are observed, such that at room temperature the emission spectra is a mixture of $^1(\pi,\pi^*)$ and CT_1^1 exciton. This is strongly reflected in the time-resolved emission decay as well, where very rapid quenching of the $^1(\pi, \pi^*)$ to the CT_1^1 exciton is observed. As the temperature is decreased, the formation of a wholly new emission band is strongly red-shifted to 500 nm and has a classic Gaussian line shape. The observation of an isoemissive point in temperature dependent of steady-state emission measurements confirm this to be a new emitting species that is kinetically linked with the intrachain states that are quenched to form this new band. However, once the solvent is frozen, it is proposed that the complete loss of this 500 nm feature and a return to pure intrachain CT_1^1 exciton emission. This behaviour is also observed in chloroform. This clearly indicates that chain motion is required to stabilise the formation of the state emitting at 500 nm, and implies that this state has interchain character and can be understood to form as the dilute chains

coil or collapse as the 2-MeTHF becomes a progressively worse solvent as the temperature decreases, in this case, higher triplet production and better triplet migration take place, which enhances the annihilation process so that the DF from TTA increases. Clearly this feature is strongly stabilised by the solvent polarity, where in a collapsed coil structure the triplets have more mobility and can easily find each other.

Returning to the intrachain CT_1^1 exciton state: As previously demonstrated, such intrachain CT states lead to increased formation of triplet states.[32] This can clearly be seen in the measurements as well. For the case of frozen 2-MeTHF, the spectra have lost all contributions from interchain species and emission arises completely from the intrachain CT exciton. In this case phosphorescence at 567 nm can be observed in the steady-state emission spectra. This matches perfectly with the phosphorescence that was previously reported using gated detection measurements,[38] and strongly reinforces the premise that the relaxed intrachain species have charge transfer character and lead to enhanced $^3(\pi, \pi^*)$ triplet exciton formation.

Understanding that the natural intersystem crossing rate in PSBF is enhanced by the presence of CT excited states allows explanation of the oxygen dependencies observed in the emission. From laser fluence measurements, it is clear that the delayed fluorescence from PSBF is a mixture of long-lived geminate CT state recombination and triplet-triplet annihilation giving rise to triplet fusion. Even though the measurements were taken in dilute solution, through the enhanced intrachain triplet generation it is perfectly possible to have multiple triplet excitations on a single chain. The work of Burrows *et al.*[39] on luminescence polymers with pulse radiolysis measurements clearly showed that the creation of more than 30 triplet excitations per chain is possible. Thus, intrachain TTA clearly occurs and contributes to the total luminescence of the sample. However, oxygen will quench these triplet states and removes the TF contribution from the total luminescence.

The mixed contribution of long-lived CT_1^1 emission and TF in the total delayed fluorescence at low temperature is substantiated by the large overall contribution of DF. The value of Φ_{DF} is calculated in different solutions at distinct temperatures: such as 0.143 ± 0.002 at 295K and 0.117 ± 0.003 at 145 K in MCH solution and 0.27 ± 0.01 at

295K, 0.93 ± 0.04 at 145K and 0.46 ± 0.02 at 90K in 2-MeTHF solution. In 2-MeTHF, the stabilization of the charge transfer state is greatly increased by the polar solvent and so at room temperature the DF contribution is much higher than in the MCH case. Moreover, as the temperature is decreased, the chain collapse increases more rapidly in the poor solvent (2-MeTHF) causing interchain CT_2^1 states to form, as aforementioned above which leads to higher triplet production and enhanced triplet migration such that they find each other more easily and annihilate, resulting in enhanced DF from TTA. Whereas in MCH, the interchain CT state is not stabilised and chain collapse does not occur, and hence, triplets can only encounter each other when there is more than one triplet per chain. As the temperature is reduced, the triplet mobility decreases and the rate of TTA also decreases.

The DF/PF ratios are thus controlled by both the temperature dependence of the triplet population and the triplet annihilation rate. So, the greatly enhanced values of Φ_{DF} are obtained at low temperatures where the CT_1^1 and CT_1^3 states are strongly stabilised. In PSBF the maximum DF yield cannot surpass 20% as in this polymer $E_{T_N} < 2xE_{T_1}$ (E_{T_1}=2.22 eV, E_{T_N}=3.77 eV) and given the oxygen effect, DF must include TTA and long-lived CT_1^1 state contributions together. It is therefore clear why all laser fluence dependence of DF measurements showed mixed contributions of monomolecular and bimolecular. Also at low temperatures in 2-MeTHF, the chains have coiled and collapse which will increase the probability of TTA events and contribute to enhance TTA and give the DF intensity dependent behaviour that is observed.

In addition, as aforementioned the photo-induced absorption features of PSBF have shown previously;[3] that two excited state absorption bands are observed in PSBF: PA1 is due to the singlet excited state absorption, and PA2 is assigned to the formation of CT states. The large lifetime decay differences observed between PA1 (rapid process) and the ground state recovery (slow process) showed the dominating role of the PA2 band in the recovery of the ground state. Again, previous observations are in agreement that the CT state is the dominant state in total fluorescence observed at low temperature. Moreover, laser fluence dependence measurements confirmed that both PA1 and PA2 absorption bands show a linear dependence upon the excitation density, ruling out

bimolecular processes giving rise to the decay of these states, that is, singlet-singlet annihilation.

5.5 Conclusion

Measurements of PSBF in two different polarity solvents as a function of temperature revealed the complex excited state behaviour of PSBF. It has been shown that inter/intrachain interactions play a crucial role in forming the additional CT states and they greatly make contribution into the total PL spectra. The results showed that environmental variations, such as quality of solvent, solvent polarity and temperature, had great effects on spatial conformations of the polymer structure and excited state stabilisation. The strength of spiroconjugation was very sensitive to orbital coupling and spatial conformations of backbone and side chains. When the relative conformations were changed by polarity and the temperature, two emissive species are resolved, a fast decaying $^1(\pi\text{-}\pi^*)$ state and long-lived intrachain CT_1^1 state. As the temperature was decreased, the formation of a wholly new emission band was obtained, strongly red shifted to 500 nm (at 145K) with classic Gaussian line shape in 2-MeTHF, which occurred as a result of chain collapse giving an "inter-chain" interaction, as a result of the polymer chain folding on itself due to decreasing the quality of the solvent. The emission had CT character, and was only observed once the polar solvent was able to stabilise it. However, once the solvent was frozen the complete loss of inter-chain emission and a return to pure intrachain CT_1^1 exciton emission was obtained. This clearly indicated that chain motion was required to stabilise the formation of the inter/intrachain state and the observed unstructured PL spectra can be attributed to an increase of vibronic coupling due to changes in temperature and polarity of solvent.

The work in this chapter sheds light on the complex excited-state nature of PSBF and the mixed contribution (heterogeneity) of long-lived CT_1^1 emission and TTA into the total delayed fluorescence is presented by calculating the values of Φ_{DF}. Thus, it has been observed that greatly enhanced values of Φ_{DF} at low temperatures where the CT_1^1 and CT_1^3 states are strongly stabilised and consist of bimolecular (TTA) and monomolecular

(CT) processes together. Consequentially, the understandings from this chapter help to make a good interpretation of up-conversion measurements of PSBF film at low temperatures (which is the subject of interest in Chapter 6).

5.6 References

1. Hintschich, S. I., Rothe, C., Sinha, S., Monkman, A.P., de Freitas, P.S. & Scherf, U. Population and decay of keto states in conjugated polymers. *J. Chem. Phys.* **119,** 12017–12022 (2003).
2. Hintschich, S. I., Rothe, C., King, S. M., Clark, S. J. & Monkman, A. P. The Complex Excited-state Behavior of a Polyspirobifluorene Derivative: The Role of Spiroconjugation and Mixed Charge Transfer Character on Excited-state Stabilization and Radiative Lifetime. *J. Phys. Chem. B* **112,** 16300–16306 (2008).
3. King, S. M., Hintschich, S. I., Dai, D., Rothe, C. & Monkman, A. P. Spiroconjugation-enhanced intramolecular charge-transfer state formation in a polyspirobifluorene homopolymer. *J. Phys. Chem. C* **111,** 18759–18764 (2007).
4. Kersting, R., Lemmer, U., Mahrt, R.F., Leo, K., Kurz, H., Bassler, H. & Gobel, E.O. Femtosecond Energy Relaxation in Pi-Conjugated Polymers. *Phys. Rev. Lett.* **70,** 3820–3823 (1993).
5. Lemmer, U., Mahrt, R.F., Wada, Y., Greiner, A., Bassler, H & Gobel, EO Picosecond Hopping Relaxation in Conjugated Polymers. *Chem. Phys. Lett.* **209,** 243–246 (1993).
6. Köhler, A. & Bässler, H. *Electronic processes in organic semiconductors: an introduction*. (2015).
7. Noriega, R., Salleo, A. & Spakowitz, A. J. Chain conformations dictate multiscale charge transport phenomena in disordered semiconducting polymers. *Proc. Natl. Acad. Sci. U. S. A.* **110,** 16315–16320 (2013).
8. Dias, F. B., Macanita, A.L., de Melo, J.S., Burrows, H.D., Guntner, R., Scherf, U. & Monkman, A.P. Picosecond conformational relaxation of singlet excited polyfluorene in solution. *J. Chem. Phys.* **118,** 7119–7126 (2003).
9. Lakowicz, J. R. *Principles of Fluorescence Spectroscopy*. (Springer US, 1999).
10. Spakowitz, A. J. & Wang, Z. G. Semiflexible polymer solutions. I. Phase behavior and single-chain statistics. *J. Chem. Phys.* **119,** 13113–13128 (2003).
11. Teetsov, J. & Fox, M. A. Photophysical characterization of dilute solutions and ordered thin films of alkyl-substituted polyfluorenes. *J. Mater. Chem.* **9,** 2117–2122 (1999).
12. Cadby, A. J., Lane, P.A., Mellor, H., Martin, S.J., Grell, M., Giebeler, C., Bradley, D.D.C., Wohlgenannt, M, An, C. & Vardeny, Z.V. Film morphology and photophysics of polyfluorene. *Phys. Rev. B* **62,** 15604–15609 (2000).
13. Schwartz, B. J. Conjugated polymers as molecular materials: How Chain Conformation and Film Morphology Influence Energy Transfer and Interchain Interactions. *Annu. Rev. Phys. Chem.* **54,** 141–172 (2003).

14. Simas, E. R., Gehlen, M. H., Pinto, M. F. S., Siqueira, J. & Misoguti, L. Intrachain Energy Migration to Weak Charge-Transfer State in Polyfluorene End-Capped with Naphthalimide Derivative. *J. Phys. Chem. A* **114,** 12384–12390 (2010).

15. Hennebicq, E., Pourtois, G., Scholes, G.D., Herz, L.M., Russell, D.M., Silva, C., Setayesh, S., Grimsdale, A.C., Mullen, K., Bredas, J.L. & Beljonne, D. Exciton migration in rigid-rod conjugated polymers: An improved Forster model. *J. Am. Chem. Soc.* **127,** 4744–4762 (2005).

16. Beljonne, D., Pourtois, G., Silva, C., Hennebicq, E., Herz, l.M., Friend, R.H., Scholes, G.D., Setayesh, S., Mullen, K. & Bredas, J.L. Interchain vs. intrachain energy transfer in acceptor-capped conjugated polymers. *Proc. Natl. Acad. Sci. U. S. A.* **99,** 10982–10987 (2002).

17. Yan, M., Rothberg, L., Kwock, E. & Miller, T. Interchain Excitations in Conjugated Polymers. *Phys. Rev. Lett.* **75,** 1992–1995 (1995).

18. Nguyen, T. Q., Wu, J., Tolbert, S. H. & Schwartz, B. J. Control of energy transport in conjugated polymers using an ordered mesoporous silica matrix. *Adv. Mater.* **13,** 8 (2001).

19. Brown, P.J., Thomas, D.S., Kohler, A., Wilson, J.S., Kim, J.S., Ramsdale, C.M., Sirringhaus, H. & Friend, R.H. Effect of interchain interactions on the absorption and emission of poly(3-hexylthiophene). *Phys. Rev. B* **67,** 64203 (2003).

20. Salbeck, J., Weissortel, F. & Bauer, J. Spiro linked compounds for use as active materials in organic light emitting diodes. *Macromol. Symp.* **125,** 121–132 (1998).

21. Grell, M., Knoll, W., Lupo, D., Meisel, A., Miteva, T., Neher, D., Nothofer, H.G., Scherf, U. & Yasuda, A.Blue polarized electroluminescence from a liquid crystalline polyfluorene. *Adv. Mater.* **11,** 8, 671–675 (1999).

22. Rothe, C., King, S. M. & Monkman, A.P. Direct measurement of the singlet generation yield in polymer light-emitting diodes. *Phys. Rev. Lett.* **97,** 76602 (2006).

23. Reichardt, C., Asharin-Fard, S., Blum, A., Eschner, M., Abdol-Mohammad, M., Milart, P., Niem, T., Schafer, G. & Wilk, M. Solute Solvent Interactions and Their Empirical Determination by Means. *Pure Appl. Chem.* **65,** 2593–2601 (1993).

24. Hertel, D., Bassler, H., Guentner, R. & Scherf, U. Triplet-triplet annihilation in a poly(fluorene)-derivative. *J. Chem. Phys.* **115,** 10007–10013 (2001).

25. Rothe, C. & Monkman, A. Triplet exciton migration in a conjugated polyfluorene. *Phys. Rev. B* **68,** (2003).

26. Monkman, A.P., Rothe, C. & King, S.M. Singlet Generation Yields in Organic Light-Emitting Diodes. *Proc. Ieee* **97,** 1597–1605 (2009).

27. Schulze, T.F. & Schmidt, T.W. Photochemical upconversion: present status and prospects for its application to solar energy conversion. *Energy Environ. Sci.* **8,** 103–125 (2015).

28. Dick, B. & Nickel, B. Accessibility of the Lowest Quintet State of Organic-Molecules Through Triplet Triplet Annihilation - an Indo Ci Study. *Chem. Phys.* **78,** 1–16 (1983).

29. Kondakov, D. Y., Pawlik, T. D., Hatwar, T. K. & Spindler, J. P. Triplet annihilation exceeding spin statistical limit in highly efficient fluorescent organic light-emitting diodes. *J. Appl. Phys.* **106,** 124510 (2009).

30. Kondakov, D. Y. Role of triplet-triplet annihilation in highly efficient fluorescent devices. *J. Soc. Inf. Disp.* **17,** 137–144 (2009).

31. Kline, R. J., McGehee, M.D., Kadnikova, E.N., Liu, J.S., Frechet, J.M.J & Toney, M.F. Dependence of regioregular poly(3-hexylthiophene) film morphology and field-effect mobility on molecular weight. *Macromolecules* **38,** 3312–3319 (2005).

32. King, S. M., Matheson, R., Dias, F. B. & Monkman, A. P. Enhanced triplet formation by twisted intramolecular charge-transfer excited states in conjugated oligomers and polymers. *J. Phys. Chem. B* **112,** 8010–8016 (2008).

33. Martins, L. & Kemp, T. Triplet-State of 2-Nitrothiophen - a Laser Flash-Photolysis Study. *J. Chem. Soc.-Faraday Trans. I* **78,** 519–531 (1982).

34. Baleizao, C. & Berberan-Santos, M. N. Thermally activated delayed fluorescence as a cycling process between excited singlet and triplet states: Application to the fullerenes. *J. Chem. Phys.* **126,** 204510 (2007).

35. King, S. M., Rothe, C., Dai, D. & Monkman, A. P. Femtosecond ground state recovery: Measuring the intersystem crossing yield of polyspirobifluorene. *J. Chem. Phys.* **124,** 234903 (2006).

36. Saragi, T. P. I., Spehr, T., Siebert, A., Fuhrmann-Lieker, T. & Salbeck, J. Spiro compounds for organic optoelectronics. *Chem. Rev.* **107,** 1011–1065 (2007).

37. Goossen, S., Bras, A.R., Pyckhout-Hintzen, W., Wischnewski, A., Richter, D., Rubinstein, M., Roovers, J., Lutz, P.J., Jeong, Y., Chang, T. & Vlassopoulos, D. Influence of the Solvent Quality on Ring Polymer Dimensions. *Macromolecules* **48,** 1598–1605 (2015).

38. Dias, F. B., Maiti, M., Hintschich, S. I. & Monkman, A. P. Intramolecular fluorescence quenching in luminescent copolymers containing fluorenone and fluorene units: A direct measurement of intrachain exciton hopping rate. *J. Chem. Phys.* **122,** 54904 (2005).

39. Burrows, H. D., de Melo, J.S., Serpa, C., Arnaut, L.G. Miguel, M.D., Monkman, A.P., Hamblett, I. & Navaratnam, S. Triplet state dynamics on isolated conjugated polymer chains. *Chem. Phys.* **285,** 3–11 (2002).

CHAPTER 6: INVESTIGATION OF COMPLEX EXCITED STATE DYNAMICS OF POLYSPIROBIFLUORENE FILM: TWO-PULSE-PUMP METHOD TO DETERMINE THE HIGHER EXCITED TRIPLET CONTRIBUTION

This chapter has been published as:

Vygintas Jankus, **Murat Aydemir,** Fernando B. Dias, Andrew P. Monkman,* "Generating light from upper excited triplet states: a contribution to the indirect singlet yield of a polymer OLED, helping to exceed the 25% singlet exciton limit." Adv. Sci., 2016, 3, 1500221

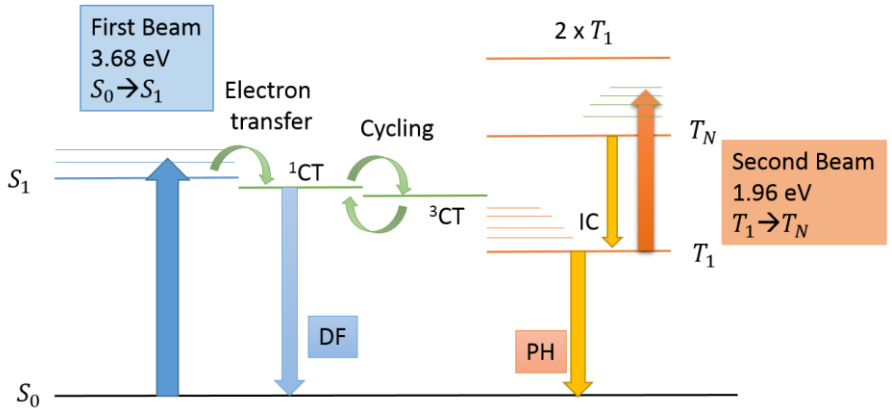

Figure 6.1 Schematic energy level diagram for polyspirobifluorene (PSBF) film constructed from fluorescence (PL), phosphorescence (PH), delayed fluorescence (DF) and photoinduced absorption measurements. From this Jablonski scheme the various decay channels for initial and photoinduced excited states (resulting from a two-pulse-pump excitation) can be seen in PSBF. The S_1 state will be quenched by the ^{1}CT state by electron transfer, which in term is quenched by the ^{3}CT. There is then a competition between TADF and ^{3}CT quenching to the lowest energy state (T_1) of the system. More detail will be given in the text.

According to the findings in Chapter 5, formation of an ICT state was determined in detail which was energetically close to the singlet excited state (~0.1 eV) and the quantum yield of delayed fluorescence was beyond the maximum value of TTA (~20%)

for this particular PSBF polymer. However, on its own the TTA mechanism cannot account for all of this fluorescence enhancement, there should exist another mechanism, i.e. thermally activated pathways, in this particular polymer. To clarify this idea, investigations were made using a two-pulse-pump excitation method, which has been employed by several researchers to understand the reverse intersystem crossing (rISC) mechanism from higher excited triplet state (T_N) to singlet state (S_1) in several small and dye molecules, where additional fluorescence enhancement (or photoinduced fluorescence) was reported resulting from T_N state contributions. Taking inspiration from these reports, this chapter is designed to understand how the T_N state contributes to fluorescence enhancement in PSBF film, and how ICT states play an important role in this particular PSBF polymer case. The two-pulse-pump method has for the first time enabled the rISC mechanism to be studied along with the crucial active role of ICT state at low temperatures.

6.1 Introduction

In general, the first photo-physical investigations of PSBF were made in dilute solutions (see previous chapter) to understand the excited-state behaviours of isolated molecules. However, when investigations are transferred to solid films, the nature and dynamics of excited states do not match completely and sometimes change significantly comparing to the dilute solutions,[1] which is due to electronic interactions between the polymer chains when in close proximity to one another. In solution, the conformation of the polymer chains is easily changed once the polarity, concentration and temperature of the solvent is altered which directly affects the excited state charge distribution. In addition, the conjugated polymer chains show well-dissolved (open conformation) characteristic in "good" solvents in which the chromophores can interact with those on adjacent chains. However, in "poor" solvents, the polymer chains tend to form coiled structure where the chains clump together. In solid films, the close interactions between the polymer chains give rise to enhanced charge transport through the film, which is due to increase in the exciton hopping rate between the neighbouring chains. However, this significantly reduces the overall quantum yield, because defect (impurity) and trap sites

between or on the polymer chains can be reached, and they work as exciton quenching or dopant sites. As is known, many conjugated polymers show very high quantum yields typically up to ~85% in solution, i.e. for PSBF ~80%, however, this value drops remarkably in solid state films, i.e. for PSBF ~25%.

The PSBF polymer is a blue-emitting polyfluorene derivative, which consists of a polyfluorene backbone with additionally substituted fluorene unit with electron-donating alkoxy side chains joined by a spiro-linkage at the 9-position giving rise to chemical stability. This spiro linkage means that the fluorene group containing the four branched alkoxy groups are rigidly perpendicular to the backbone (forms large steric hindrance) and is designed to prevent aggregation and crystalisation of the PSBF film.[2] The role of alkoxy groups is to increase the solubility and electron transport properties as well as making morphologically stable (amorphopous) films. The electronic properties are mainly determined by the polymer backbone (fluorene for PSBF), however, if any π-conjugated side groups are attached to the backbone that will also affect the electronic properties by means of enchancing conjugation (i.e. spiroconjugation for PSBF), between orthogonally positioned fluorene units giving rise to new molecular orbitals. All the above features make the PSBF very unique in terms of polymer stabilization and importantly for OLED performance where the high quantum yield (0.44) was measured by Rothe et al.[3] PSBF was categorized as electron-transporing polymer, therefore, the efficiency of the devices can be enchanced if the PSBF is copolymerized with hole-transporting moiety.[4] In addition, as explained in Chapter 5, triplet-triplet annihilation (TTA) is the operative process behind the formation of delayed fluorescence in PSBF polymer, where the PSBF has the conditions of $2xE_{T_1} > S_1$ and $2xE_{T_1} > E_{T_N}$,[3] and under these conditions the maximum singlet generation via triplet fusion (TF) is ~20%, however, to explain higher values of quantum yield of delayed fluorescence there must be another operative triplet harvesting mechanism.

6.1.1 Triplet migration process

Considering the possible TTA contributions to emissive singlet excited state formation, the key factor behind the rate limiting process for the annihilation mechanism

is the triplet exciton migration process where at least two triplets should come together within the interaction radius. Therefore, understanding the triplet migration process is crucially important to explain experimentally observed delayed fluorescence phenomena in conjugated molecules. After photo-excitation, intersystem crossing occurs from singlet to triplet states (within the lifetime range of singlet state) and results in population of the triplet state. The initial population of the triplet state can be assigned as $[T] = [T_0]$ at time zero (t_0) conditions. Afterwards, the triplet density is depopulated by means of monomolecular (decay either radiatively, k_r, or non-radiatively, k_{nr}) and bimolecular processes (k_{TT}), such as triplet-triplet annihilation.[5] Then the depopulation process can be expressed as,

$$\frac{d[T]}{dt} = G_T - (k_r + k_{nr})[T] - k_{TT}[T]^2 \qquad (6.1)$$

where G_T represents the generation rate of triplets, and $[T]$ is the triplet concentration function. In time-dependent conditions, k_{TT} is directly related with the triplet diffusion coefficient (D) which was expressed by Smoluchowski theory as,[6]

$$k_{TT} = 8\pi f R D \qquad (6.2)$$

where f is fraction of triplets annihilated after an encounter (this value was derived as 0.4 for anthracene),[6] R is the interaction radius of triplets and the calculated values of k_{TT} for conjugated polymers are in the range of 10^{-13}-10^{-14} cm^3s^{-1} at RT. Usually, the lifetime of a triplet state is in the range of hundreds of milliseconds, therefore, the monomolecular term of the Eq. 6.1 can be neglected by considering only the early time frame after photo-excitation (typically < 100 ms) and the non-radiative quenching is not the dominant depopulation mechanism of triplet states. Then only the bimolecular term of the equation is left to determine the triplet decay mechanism. Addressing this point,

the solution of Eq. 6.1 can be written for initially excited triplet state decays (where k_{TT} is time-independent),

$$[T] = \frac{[T_0]}{1 + k_{TT}[T_0]t} \tag{6.3}$$

or in a more general form considering k_{TT} as time dependent,

$$[T] = \frac{[T_0]}{1 + [T_0]\int k_{TT}(t)dt} \tag{6.4}$$

from Eq. 6.3 a differentiated expression can be written for the delayed fluorescence resulting from TTA,

$$DF \sim \frac{d[T]}{dt} = k_{TT}[T_0]^2 \frac{1}{(1 + k_{TT}[T_0]t)^2} \tag{6.5}$$

In general, at t_0, the initially excited sites of conjugated polymers show random distribution within the density of states and the average energy of the excited states (E_A) is higher than k_BT (considering finite temperature conditions), then triplet exciton migration process can be explained by means of incoherent jumps (due to energetic disorder) between the spatially and energetically localized states (hopping sites) which give rise to the density of states with a characteristic Gaussian distribution profile. As shown by theoretical work[7,8] and Monte Carlo simulations,[9–11] the photo-excitation gives rise to triplet exciton migration towards lower lying energy sites (at particular time after t_0, but before so-called critical time, t_s). At $t < t_s$, the triplet excitons show diffusive movement (not thermal hopping) in energy (i.e. percolation) through the lower lying energy sites as long as $E_A > k_BT$. In this condition, triplet excitons stay in a so-called

non-equilibrium dispersive regime and undergo time-dependent energy relaxation (diffusion) from upper to lower sites within the density of states giving rise to spectral dispersion with a Gaussian distribution profile. However, after some time after the excitation, the critical time is reached (t_s), in this time frame E_A is considered to be equal to k_BT, and triplet exciton diffusion occurs *via* both percolation and thermally hopping and both processes become equal. Now, the diffusion coefficient can be expressed as,

$$\boldsymbol{D = \frac{d\langle \Delta R^2(t)\rangle}{dt}} \qquad \textbf{(6.6)}$$

where $\langle \Delta R^2(t)\rangle$ represents the derivative of the mean square displacement. Additionally, triplet exciton migration can be defined with the Miller-Abraham equations where the hopping rate (v_{if}) between the localized sites are expressed in a different way depending on the value of energy difference between initial (i) and final (f) energy sites,[8]

$$\boldsymbol{v_{if} = v_0 e^{-2\propto R_{if}} e^{-(E_f - E_i)/k_BT}}, \qquad \boldsymbol{E_i < E_f}$$

$$\boldsymbol{v_{if} = v_0 e^{-2\propto R_{if}}}, \qquad \boldsymbol{E_i > E_f} \qquad \textbf{(6.7)}$$

where v_0 is the attempt-to-jump frequency, $\propto$ is the inverse localization length of the triplet excitons, R_{if} is the distance between the localized sites, E_i and E_f are the initial and the final energies of the localised states, respectively. T-temperature and k_B is the Boltzmann constant. As seen in Eq. 6.7, the jumps of the triplet excitons through the lower energy sites depend on the distance between the localized sites, therefore, hopping rate is related to the energy difference between the sites involved. In the non-equilibrium regime, Movaghar *et al*.[7] explained the time-dependent average hopping rate (the temperature was approaching zero), hence, the diffusion coefficient ($D\ (t)$) is proportional to the hopping

rate ($v(t)$) and triplet-triplet annihilation constant (k_{TT}) which can also be linked with the number of visited new energy sites ($N_s(t)$) over the time,[9]

$$\boldsymbol{D(t) \sim k_{TT} \sim v(t) \sim \frac{dN_s(t)}{dt} \sim \frac{1}{tln(v_o t)}} \qquad \textbf{(6.8)}$$

At $t > t_s$, a classical diffusion regime appears, the so-called non-dispersive or quasi-equilibrium regime (because the triplet is a transient particle), in which thermal hopping plays a dominant role in triplet migration (no more energy downhill occurs). In this case, $N_s(t)$ is constant, which means the number of visited energy sites increase linearly with time and no more energy relaxation occurs in DOS.

The behaviour of delayed fluorescence in both the dispersive and non-dispersive regimes is defined by many experiments and Monte Carlo simulations which show that the triplet concentration follows a power law decay regime (t^{-m}) with the m exponent close to -1.[11,12] However after a critical time (t_s), when the classical equilibrium non-dispersive regime starts the diffusion coefficient approaches D_∞ and the power law decay regime with the m exponent close to -2 applies. Therefore, the critical time shows strong temperature dependence (activation energy) between the regimes which was calculated analytically by using an effective medium approximation,[13]

$$\boldsymbol{t_s = t_0 e^{(\frac{c\sigma}{k_B T})^2}} \qquad \textbf{(6.9)}$$

where t_0 is the dwell (or jump) time for the triplets migration (which is inversely proportional to the attempt-to-frequency) which can also be expressed as Eq. 6.10, c is a dimensionality dependent migration constant, i.e. the value for 1-D is 0.93 or for 3-D 0.67,[14] and σ is the variance between the DOS sites.

$$t_0 = \frac{1}{6v_0 e^{-(2\propto R_{if})}} \quad \textbf{(6.10)}$$

Consequentially, at low temperature limits ($T \rightarrow 0$), the organic molecules are energetically disordered. This disorder can simply be determined with variance parameter (σ^*=σ/k_BT), showing the variation of energy in density of states. Under this condition, the critical time becomes long-lasting and strongly depends on the temperature, and the type of transition is always described in the dispersive non-equilibrium regime. In other words, once the temperature is decreased the triplet excitons are trapped and the diffusion coefficient shows temperature dependent (activation energy) behaviour as given in Eq. 6.8 by Movaghar *et al*. where the low temperature limits are considered with small variations of density of states, $k_BT < 0.1\sigma$, Furthermore, Richert *et al*. [15] showed that triplet migration in organic glasses (at low temperatures) is usually dispersive and $D(t)$ is time dependent, therefore the final conclusion can be made that at early times, the dispersive regime dominates the overall triplet migration process, however, once thermal equilibrium is reached a turnover time appears and the dispersive regime turns into non-dispersive regime that can be experimentally observed with the change in power law exponent (m) from -1 to -2.

6.1.2 Possibility of rISC from excited triplet states

In general, reverse intersystem crossing phenomena are usually observed with the materials that showing thermally activated delayed fluorescence arising from the back transfer of the triplets from upper vibronic of the T_1 to S_1 state. The strength of the delayed fluorescence (DF) is dependent on temperature and energy gap (between $S_1 - T_1$, ΔE_{S-T}), where the proportionality can be expressed as exp –$\Delta E_{S-T}/k_BT$, where k_B – Boltzmann constant and T –temperature (as explained in Chapter 2). Therefore, at high temperatures and small energy splitting conditions the rISC possibility increases remarkably and the lifetime of DF is proportional to that of T_1 state. However, in conjugated molecules, the singlet-triplet energy gap is quite large (*ca*. 0.7 eV) due to

strong electron-electron correlation which prevents thermally assisted back transfers, therefore, for efficient rISC process a narrower inter-multiplicity gap than $S_1 - T_1$ is required. Nowadays, intramolecular charge transfer emitters have become a centre of interest due to their ability to reduce the singlet-triplet energy gap thus significantly favouring the repopulation of the singlet state from the triplet manifold.[16,17] Furthermore, according to previous reports,[18,19] the rISC process may also occur from higher excited triplet states (T_N) to the singlet manifold competing with the direct internal conversion to the lowest triplet state (T_1). It has been thought that this transition process was very improbable particularly compared to the efficient internal conversion (within the time range of $10^{-11} - 10^{-14} s$) to T_1, whereas, rISC mechanism between $T_n - S_m$ states were reported several times, particularly for Rose Bengal, erythrosine B, tetraphenylporphrin, cyanine dyes and anthracene derivatives.[19–21]

6.1.3 The technique to determine the rISC contribution from upper-lying triplet state

According to literature reviews, the common techniques to measure the rISC mechanism in higher excited triplet states are based on two steps excitation method where typically two excitation sources are used to excite different energy states of the molecules. The experimental set-ups are typically based on time-resolved emission spectroscopy, or transient absorption techniques. The latter will not be the subject of interest in this chapter. In this chapter, the T_N state contribution is detected from intensity changes in the emission spectra. In this technique, two energetically different laser sources are used to excite singlet and triplet states simultaneously; the first high energy laser is chosen in the range of absorption spectrum of the ground state of the molecule for the main $S_0 \rightarrow S_1$ excitation, giving rise to PF and DF. A second low energy laser is chosen which is transparent to the ground state of the molecule, but sensitive to the absorption of the lowest excited triplet state which means the separate excitation event should not result in emission. The main objective of this second source is to excite the lowest triplet state to the higher triplet energy levels in a simultaneous excitation event, i.e. $T_1 \rightarrow T_N$. Usually, two excitation sources are not employed in the same time regimes, the right delayed time

(which is taken as the zero time of second laser pulse) is typically chosen just after the decay time of S_1, where the delayed fluorescence starts emitting, but before the T_1 states decay significantly to the ground state. Then after the zero time of the second excitation, triplets are excited to the higher energy levels (T_N). At this energy level, the triplets tend to decay back to energetically more stable states by means of internal conversion to a lower energy state of the same multiplicity, i.e. T_1 or charge transfer triplet state (as obtained in this chapter), or alternatively following a rISC step to a state of different multiplicity, i.e. S_m. In the latter case the higher excited triplet may follow a decay pathway, i.e. $T_N \rightarrow S_m \rightarrow S_1$,[19] and photo induced fluorescence enhancement can be obtained which strongly depends on the reverse intersystem crossing yield between T_N - S_m states.

6.2 Experimental

The spin-coated films were prepared by embedding the PSBF polymer into zeonex - a cyclo polyolefin, at a concentration of 0.01% PSBF, and mounted into the cold finger of the helium displex cryostat (300K-14K) under a vacuum pressure of 10^{-4} mbar or in a nitrogen cryostat sysytem (Janis Reasearch, 300K -77K). Two series of experiments were performed; firstly, the lifetime decay measurements were taken using typical nanosecond gated spectroscopy method (as explained in detail Chapter 3) using 355 nm excitation wavelength (15 μJ per pulse) at RT and 14K. Secondly, a two-pulse-pump method was used for photo-induced fluorescent measurements at 14 K, where two excitation sources were used at the same time to probe $T_1 \rightarrow T_N$ transitions. The experimental set-up is depicted in Fig. 6.2.

The main objective of using two excitation sources is to excite different excited states of the PSBF molecule; with a high energy (3.68 eV) pulse for $S_0 \rightarrow S_1$ excitation and a lower energy pulse (1.96 eV) for the upper excited triplet excited states (for T_1 to T_N transitions). To get 632.7 nm excitation, a 632. 7 nm emitting dye laser was excited with the second harmonic of Nd:YAG laser (SL312, EKSPLA), 532 nm, where the pulse duration was approximately 150 ps. The output energy of second harmonic was around

80-100 μJ which was used to excite a single pass dye laser system, and the final output energy of dye laser system was reduced to 20-30 μJ. The high energy pulse is provided by nitrogen-laser (LTB Laser Technik, Berlin) where the pulse duration is around ~ 1 ns and the output energy of per pulse was around 80-100 μJ. So, the first pump pulse had an energy of 3.68 eV nm and the second pump pulse had an energy of 1.96 eV.

Synchronisation of both lasers was successfully achieved with using an HP programmable electric pulse generator, the second dye laser pulse delayed by ~177 ns relative to the first nitrogen laser pulse. Then the two pump pulses are combined spatially to excite the sample in the cryostat holder. In addition, a band-pass filter (with the highest transition wavelength of 460nm) was used in front of the dual grating monochromator entrance slit to prevent any undesirable scattered light entering the spectrograph to increase the signal-to-noise ratio. Therefore, the emission spectra which will be represented in the text shows the filtered emission. The emission was detected with a sensitive gated amplified iCCD camera (Standford Optics) having a sub-nanosecond resolution.

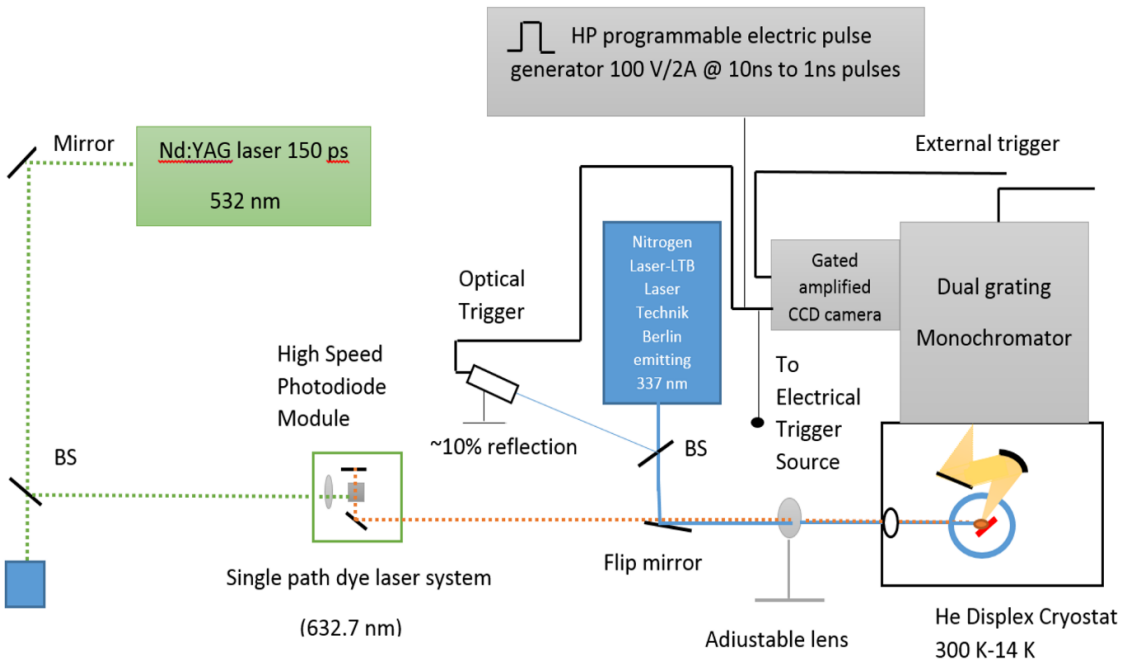

Figure 6.2 Two-pulse-pump set-up, the first 3.68 eV excitation source is shown with a blue line and the second 1.96 eV pulse is depicted with red dots arising from single path dye laser system as a result of

excitation with the second harmonic of Nd:YAG laser, green dots represents the 532 nm excitation wavelength.

Picosecond time-resolved fluorescence decays were collected (from 3 ps to 10 ns, at <1 nJ per pulse excitation) using the time-correlated single photon counting technique (impulse response function, IRF: 19.5 ps). A vertically polarized picosecond Ti:sapphire laser (Coherent) was used as an excitation source, the excitation wavelength was 352 nm, then emission was collected using a polarizer at its magic angle (54^0), which is crucially important to remove polarization effects. For detection of the emission a double monochromator (Acton Research Corporation), coupled to a microchannel plate photomultiplier tube (Hamamatsu R3809U-50) were used.

6.3 Results

6.3.1 Time resolved decay dynamics

To understand the DF contribution in films directly, the nanosecond gated time resolved spectroscopy was used similarly to that which has been previously introduced in detail in Chapter 3. The feature of this spectroscopy technique was the ability to capture both prompt (PF) and delayed (DF) fluorescence simultaneously (in one curve) as shown in Fig.6.3 a and b. The initial fast decaying part was assigned as the PF emission having the biexponential lifetime of τ_1=1.32 ± 0.02 ns and τ_1=15.99 ± 0.31 at 20K. This was confirmed by TCSPC measurements on the same films which showed very good overlap with nanosecond gated spectroscopy decay (see inserted graph highlighting the early part of the decay in Fig 6.3 a.) showing a biexponential decay with ~3 ns average fluorescence lifetime (calculated from Eq.6.11), calculated as,

$$< \tau >= \frac{\sum_i a_i \tau_i^2}{\sum_i a_i \tau_i} = \frac{a_1 \tau_1^2 + a_2 \tau_2^2}{a_1 \tau_1 + a_2 \tau_2} \qquad \textbf{(6.11)}$$

where $< \tau >$ is the intensity average lifetime for biexponential fluorescence decay, a_i is the amplitude fraction for each decay component, τ_i, which shows the average lifetime of a collection of different excited state population. More detailed analysis in solution (in Chapter 5) revealed a triexpontential decay with two major emitting species which were initially a photo-generated local exciton, $^1(\pi\text{-}\pi^*)$ state having the lifetime of ~1 ns, and a slightly lower energy (~0.1 eV) ^{1}CT state having the lifetime of ~5 ns. At 20 K, under low excitation conditions (at 15 μJ per pulse) with the third harmonic of Nd:YAG laser emitting at 355 nm, the decay tail (between ~100 ns to 0.1 s) after the biexponential PF part is assigned to DF part which follows a power law decay (t^{-m}) with the exponent of -0.99 ± 0.003 showing the approaching value to -1 consistent with the exponent of dispersive triplet exciton regime (t^{-1}). However, at RT, the power law part consists of two triplet migration regimes; the initial part of the DF shows dispersive regime with *m* value of -1.47 ± 0.02, then the regime turns into classical non-dispersive regime with the exponent of -1.82. These power law behaviours can be understood in terms of triplet diffusion mechanism, which consists of non-equilibrium and equilibrium dispersive regimes. [22] In the non-equilibrium dispersive regime, at early times, "hot" triplet exciton migration is time dependent (decelerates) towards low-energy sites. As explained in the beginning of this chapter, in this regime the DF intensity is proportional to the variation of the triplet population, d[T]/dt, and the DF decay follows a power law regime ($I_{DF} \sim t^{-m}$) with *m* values approaching -1. Once the triplets have thermalized, the non-dispersive migration dominates and the DF decays with *m* approaching -2 at certain time. Experimentally, the transition time can be calculated by means of plotting the transition time versus the inverse square of the temperature. Then fitting with linear line on a semi-log scale yields the DOS width (σ) parameter in accordance with Eq. 6.9 which has already been calculated by Rothe *et al.* [23] as ~41 meV for PSBF film. The intercept of the curve gives the dwell time value (t_0) which has been calculated from the PSBF film as 70 ns. The value of DOS width suggests exciton relaxation (energy downhill) towards the edge of the DOS due to having higher energy (~41 meV) than k_BT~25 meV (that is almost half width of DOS). Under these conditions, triplet excitons will be in the non-equilibrium regime, hence, at the beginning of transport will follow a power law decay showing a value of close to -1, then the value approaches -2 (equilibrium regime).

In addition, the DF undergoes a rapid intensity roll-off (~ 800 ns) and the DF efficiency decreases substantially. This DF intensity roll-off is due to a change from dispersive to non-dispersive triplet exciton migration and has been observed previously in both small molecules and polymer (polyfluorene) films.[12,24]

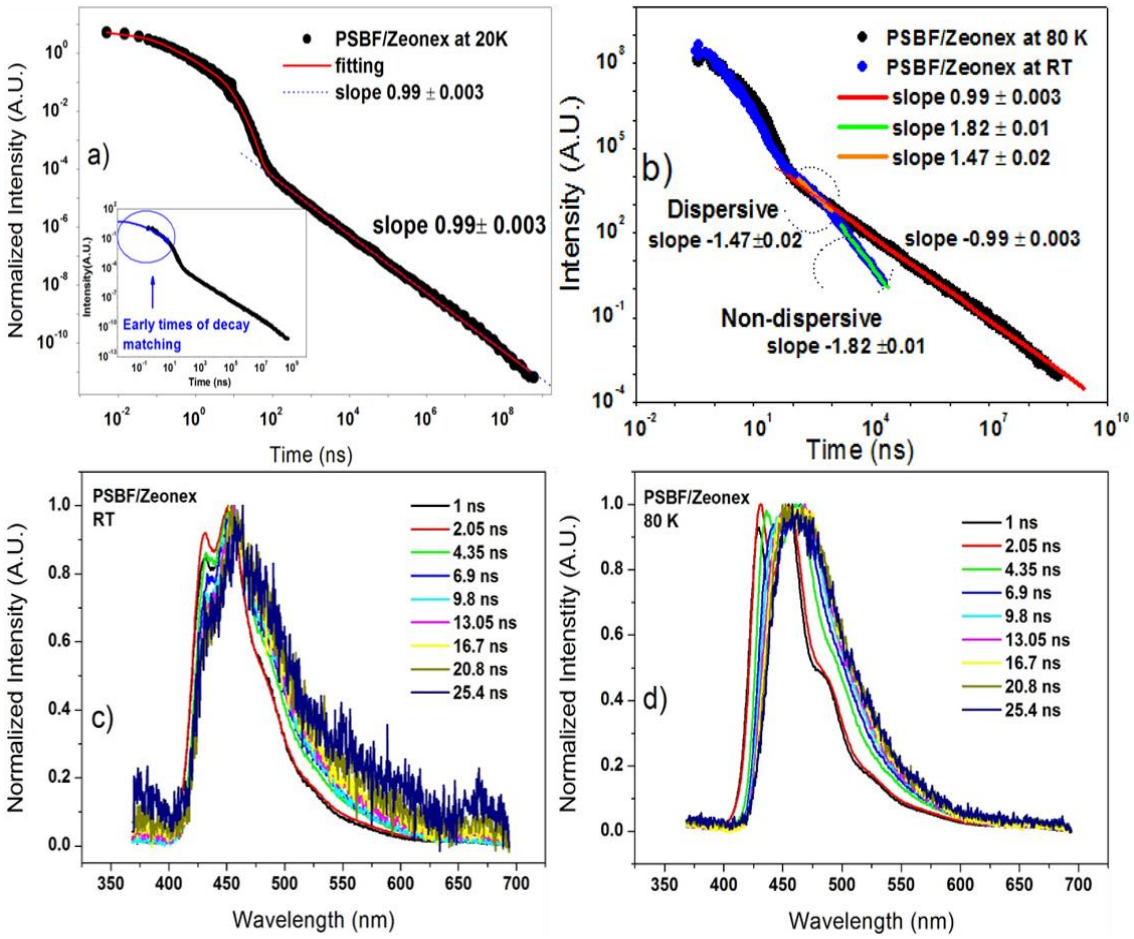

Figure 6.3 a) Emission decay of PSBF/Zeonex mixture (0.001% PSBF) spin coated film recorded at 20 K (black circles).The inserted curve was obtained by combining decays recorded using nanosecond gated time resolved spectroscopy (from 1 ns to 1 s, at 15 μJ per pulse excitation) and singlet photon counting techniques (from 3 ps to 10 ns, at <1 nJ per pulse excitation) **b)** Emission decay of PSBF/Zeonex spin coated film recorded at 80 K and RT **c)** Time evolution spectra of PSBF/Zeonex film at RT between 1ns to 25.4 ns **d)** Time evolution spectra of PSBF/Zeonex film at 80K

At RT, non-radiative decay becomes much stronger (in polymers) and so the quenching of the locally excited triplet states $^3(\pi\text{-}\pi^*)$ competes with triplet fusion (TF) reducing the overall amount of singlets generated by TF and so the overall DF yield reduces. The spectral evolution was obtained through the lower lying CT state, where the initial S_1 $^1(\pi\text{-}\pi^*)$ spectrum loses its vibronically well-resolved shape within 1 ns to 4.35 ns, then spectral diffusion of singlet excitons red shifts the S_1 emission over *ca.* 6 ns (red-shifted trace) and concomitantly unstructured long-lived ICT emission dominates the overall fluorescence at 80K (Fig. 6.3 d.), which again confirms our solution phase observation in the sense that the ICT state is formed at low temperatures. At 80 K, the new emission band shows totally unstructured CT emission which is energetically well-separated below the $^1(\pi\text{-}\pi^*)$ state ~0.1 eV.

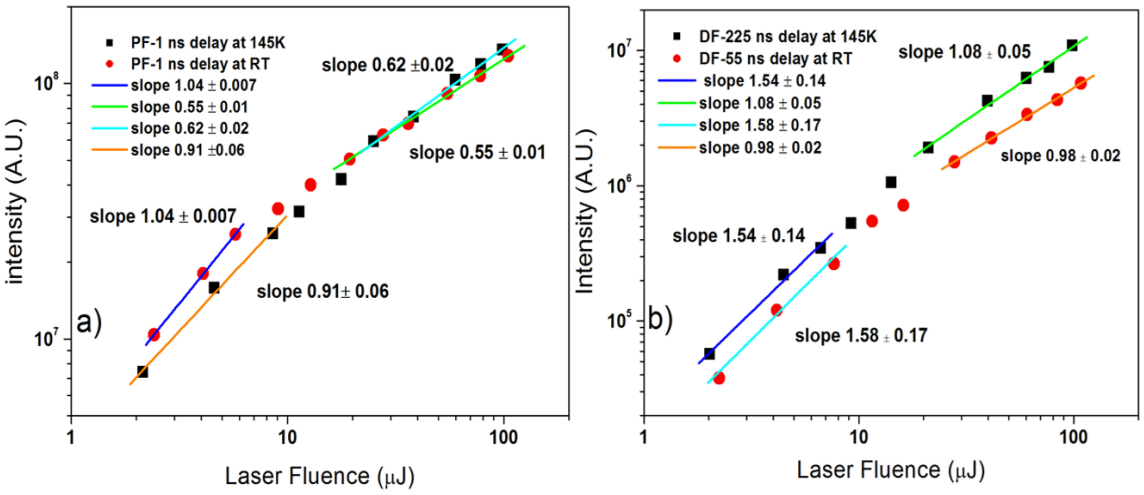

Figure 6.4 a) Excitation intensity dependences of the PF intensity was recorded after 1 ns delay at RT and 145K **b)** Excitation intensity dependence of the DF intensity was recorded after 55 ns delay and 1.5 μs for RT and 225 ns delay and 1.2 ms integration at 145K.

The intensity of prompt (S_1) emission upon laser fluence (after 1 ns delay time), shows a slope of 1.04 ± 0.007 at RT and 0.91 ± 0.06 at 145K under low excitation conditions. These values turn into 0.55 ± 0.01 at RT and 0.62 ± 0.02 at 145K under higher excitation conditions (Fig. 6.4 a). This shows a classic bimolecular behaviour of the PF emission. However, the dependence of the intensity of delayed fluorescence on laser

fluence shows a mixture of behaviours (see Fig. 6.4 b), under low excitation conditions, the slope follows 1.58 ± 0.17 at RT and 1.54 ± 0.14 at 145K, then at high intensities, the slopes turn into 0.98 ± 0.02 at RT and 1.08 ± 0.05 at 145K, where the measurements were recorded after 55 ns delay and 1.5 μs integration time conditions at RT, and 225 ns delay and 1.2 ms integration time at 145K. These measurements are consistent with the solution measurement in Chapter 5, showing almost equal bimolecular (TTA) and monomolecular (CT state) contributions.

6.3.2 Direct investigation of quantum yield of delayed fluorescence in film of PSBF

The investigation of quantum yield of the delayed fluorescence (Φ_{DF}) was repeated for solid-state films of PSBF at RT and 20 K in a similar way that employed in Chapter 5 for the solutions. The equation was already formulated in detail, but here, the final part of the equation is shown in Eq. 6.12, where R is the experimental parameter and can be calculated from the integrated area of each decay curve (Fig. 6.3 a). Addressing this point, the integration of the initial biexponential part of the decay curve gives the PF fraction and in the same way integration of the power law part gives the DF contributions,

$$\Phi_{DF} = \frac{R}{(1+R)\Phi_T} \qquad (6.12)$$

Here Φ_T is the triplet quantum yield. The starting point for the determination of quantum yield of DF was taken as the inverse time of the intersystem crossing rate of PSBF.[25] For the Φ_{DF} calculations, it has been assumed DF starts when 67% of triplets have formed, such that the concentrations are high enough to achieve TTA in films. The value of Φ_T=0.12 ± 0.02 was taken from the previous femtosecond ground state recovery measurements made by King *et al*.[26] So using this information two values of Φ_{DF} were calculated at RT (0.082 ± 0.01) and 20 K (0.344 ± 0.06). As realized from the calculations, the quantum yield at 20 K is significantly higher than the value at RT, which is to be expected, based on our understanding from Chapter 5. Considering the value at 20 K

(~Φ_{DF}= 0.34), the total contribution of DF on the emissive singlet state can be calculated; assuming a spin independent charge recombination triplet yield of 75%, then the contribution of DF to the total singlet yield would be 0.34 x 0.75=0.25 ± 0.06. If then this value (0.25 ± 0.06) is added to the initially created 25% singlet excitons, then the totally generated spin independent singlet state yield can be given as 0.50 ± 0.1 which is within error limits and is in excellent agreement with the measured singlet yield of 0.44 ± 0.04 in PSBF OLED device at 20K.[3] The agreement is particularly good considering that different experimental methods have been used. However, as mentioned several times, for PSBF, it is not possible to achieve Φ_{DF}> 0.2 from TF alone, due to the triplet energy conditions of PSBF, $2xE_{T_1} > E_{T_N}$ (E_{T_1}= 2.22 eV, E_{T_N} = 3.77 eV),[3] which limits the maximum value to Φ_{DF} ~ 0.2. However, according to the quantum yield of DF measurements of PSBF in solution (in Chapter 5) and film, the results show DF values of over 0.2, therefore, there must be another mechanism in addition to TF to explain the high quantum yield of DF. As the decay lifetime measurements above obviously hint at a TADF component, there may exist a rISC mechanism from a higher excited triplet state to the higher excited singlet manifold that results in fluorescence enhancement, i.e. $T_N \rightarrow S_m \rightarrow S_1$. However, this process would be in competition with rapid internal conversion process as most likely the transition will happen as $T_N \rightarrow T_1$.

Also the fact is that, in the literature, such a rISC mechanism has never been reported for conjugated polymers to date, whereas, there exist some reports showing the possibility of rISC processes for only some organic molecules (as mentioned above). Leaving this idea for now (it will be reconsidered below), the CT state formation will be considered at 20 K. Recent findings on CT states show that triplets can be harvested efficiently if the strong coupling occurs between energetically close lying triplet states, resulting in rISC between the triplet manifolds and concomitantly TADF may occur.[17] In particular, in PSBF polymer, the spatial orientations of HOMO-LUMO orbitals are orthogonal giving rise to CT formation across the orthogonal spiro unit by means of enhanced spiroconjugation. This spatial molecular arrangement results in small energy splitting between the singlet and triplet CT states (^{1}CT-^{3}CT) where the orbitals are weakly coupled and gives rise to a small electron exchange energy.[27] Indeed, the ^{1}CT state is positioned energetically below to locally excited singlet state (^{1}LE) ~0.1 eV at low

temperatures, and the emission only arises from the ^{1}CT state after an intermediate delay times (~200 ns). In this case, two active pathways can be considered behind the population of ^{1}CT state; i) electron transfer channel from the ^{1}S state (^{1}LE→^{1}CT) and ii) possibly an active TADF channel, such as following ^{3}LE→ ^{3}CT→ ^{1}CT pathway. However, the back electron transfer rate from ^{3}CT→ ^{3}LE is typically slow (~5 x 10^6 s^{-1})[19] and therefore ^{3}CT harvesting will compete with the rapid process of internal conversion. This results in ^{1}CT emission being observed at intermediate times (~200 ns), but at longer times only TF is operative. Clearly, an increase observed in the intensity of ^{1}CT emission at RT compared to the low temperature in Chapter 5, indicates that an active TADF recycle operates[27] between ^{3}CT and ^{1}CT in this particular polymer.

6.3.3 Study of two-pulse-pump experiment

To get a better insight into fluorescent enhancement from ^{1}CT states, the investigations were performed at 20 K using a two-pulse-pump experimental set-up (see Fig. 6.2) using 0.01% PSBF/Zeonex matrix isolated films where the low polymer concentration prevents interchain TTA and results in a triplet yield of Φ_T=0.12,[26] also under low excitation intensities intrachain TTA should be very low. This set-up was expected to provide additional information on the deactivation mechanism of upper excited triplet states, i.e. T_N. The experimental technique is as explained at the beginning of the chapter where two excitation sources for different excited states were used; 3.68 eV (337 nm) pulsed-laser source was used to excite the local singlet states (from S_0 to S_1), and 1.96 eV (632.7 nm) pulsed-laser source used to excite upper triplet states , i.e. T_1 to T_N, (see Fig. 6.5). Lifetime decays were recorded following excitation with only the 3.68 eV (~80 μJ per pulse) pulse (see in Fig. 6.6 with black dots) and secondly exciting with both lasers (3.68 eV +1.96 eV) together, where the energy per pulse was ~30 μJ for 1.96 eV.

First, the lifetime decay was measured with 3.68 eV excitation pulse (see Fig. 6.5, with black dots) where the initial exponential part of the decay was assigned as the tail of PF, because it is not possible to measure early decay times of PF with the 3.68 eV laser which is due to a ~30 ns zero time. Therefore, the lifetime decay started around 30 ns,

and the long-lasting power law part was assigned as DF. Secondly, the decay was measured using both sources together to induce T_1- T_N transitions (shown in Fig. 6.6 with red-triangles), in this case, the zero time of 1.96 eV was arranged at the time when the PF emission was depleted and DF emission had started. Therefore, the zero time of 3.68 eV was delayed ~177 ns using an electric pulse generator, which was also the zero time of the second pulse (1.96 eV). At this time, a significant intensity increment was observed (~40%, see Fig. 6.6 b), which was not only one single peak of the emission appearing at zero time of the second beam, instead, the induced emission gradually decreased back again to overlap with 3.68 eV decay. And it must also be highlighted here the increase was only detected at 20K not at RT.

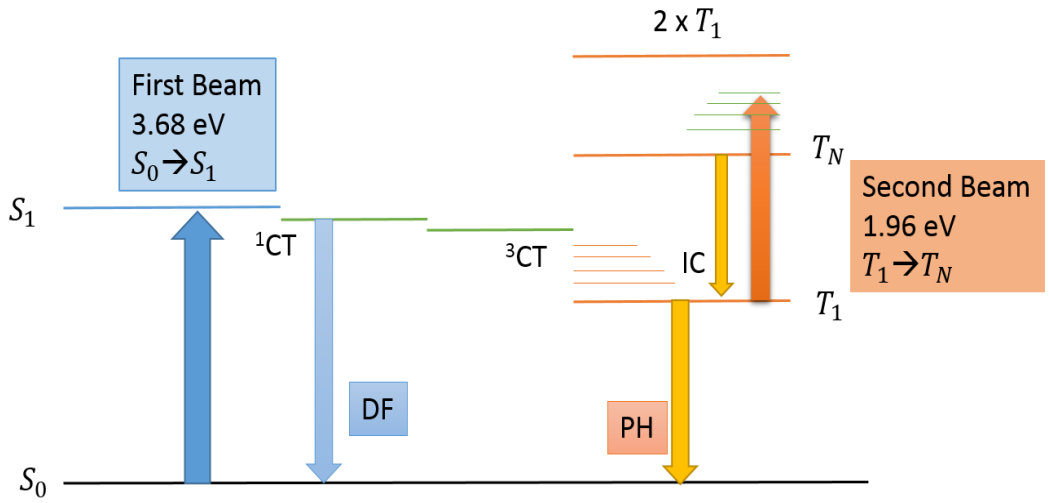

Figure 6.5 The diagram represents the two-pump-pulse method, where the first excitation beam (3.68 eV) excites the local singlet states from ground state to first excited state ($S_0 \rightarrow S_1$) and the second beam excites the triplet states ($T_1 \rightarrow T_N$).

The ground state absorptions were checked for each excitation source, the first 3.68 eV pulse resulted in ^{1}CT emission, but the second 1.96 eV pulse is clearly transparent to the ground state [3] (see Fig. 6.6 b) and S_1 states given that the lifetime of S_1 is 1 ns, [2] but rather excites the long lived existing T_1 excitons to the higher T_N level, through an optically allowed transition.[26] It is evident from the data in Fig. 6.4a that after excitation with the 1.96 eV pulse, the DF intensity increases by as much as 40% compared to the

intensity of the 3.68 eV (see Fig 6.6 b with black line). This intensity enhancement is called "induced emission" from higher excited triplet states and only detectable in the case of using both excitation sources and was not present when the 1.96 eV dye pulse alone was incident on the sample. Comparable results have also been obtained using 1.55 eV pulses which are resonant with the allowed T_1 to T_N transition, onset at 1.35 eV.[26] The lifetime of this induced delayed emission was calculated as, *ca.* 5-10 ns, which was considerably longer than the 1 ns 1.96 eV pump pulse, and orders of magnitude too long to be an upper excited T_N state, therefore, it is hard to believe that the induced delayed fluorescence arises following the rISC mechanism from the $T_n \rightarrow S_1$ state. The clear enhancement was observed on total DF emission, simply by exciting the T_1 states to the T_N states, but the second excitation beam does not increase the total number of excited states, it only perturbs the triplet population (excites them). That means the second pump beam cannot induce extra TF, therefore a new physical decay channel must be accessed from the T_N population, i.e. a further radiative decay channel becomes operative from T_N state.

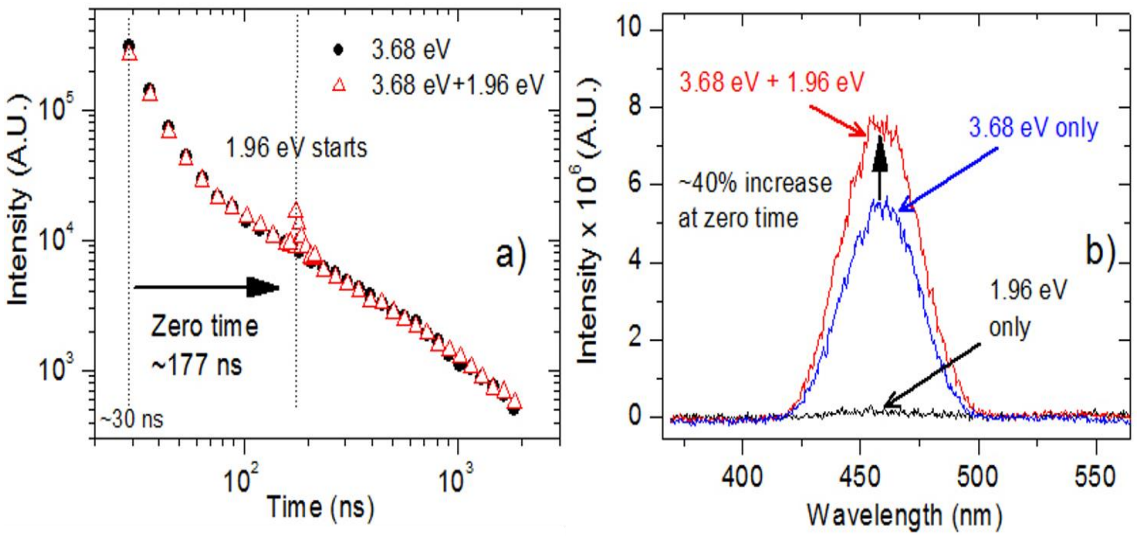

Figure 6.6 a) Black dots shows the decay of PSBF film exciting with 3.68 eV laser source, and the red triangles shows the decay exciting with 3.68 eV and 1.96 eV together, and the zero time of 1.96 eV was arranged ~177 ns where the low energy contribution comes up. **b)** The spectra depicted are those with a ~177 ns delay where the low energy excitation starts showing ~40% increment in intensity.

6.4 Discussion

Given the lifetime and spectral shape of this induced delayed fluorescence, it must arise from the decay of the ^{1}CT state. The investigations with the two-pulse-pump method suggest that the T_N state might predominantly decay to the next lowest triplet state, which is the ^{3}CT triplet state stays energetically very close to T_N state, thus a kinetic competition will take place before finally reaching the lowest lying $^3(\pi,\pi^*)$ level as well as the ^{3}CT state vibronics will be weakly coupled to vibronics of $^3(\pi,\pi^*)$ state, giving it a relatively long phosphorescence lifetime (~1 s). The T_N state is energetically positioned ~1.55 eV above the T_1 state (~2.22 eV) and the lifetime might be considerably long due to the orthogonal arrangements of $T_1 - T_N$ transitions, where usually T_N are highly delocalized sites and delocalization occurs along the polymer chains, however, T_1 is comparatively more localized and electronic distribution occurs perpendicular to the chains.[28] Indeed such a large $T_N - T_1$ energy gap can give rise to T_N, in the case where T_N lies below S_1, showing that upper-excited state lifetimes can be relatively long, at least on a par with S_1 which readily allows $S_1 \rightarrow {}^1$CT electron transfer.

Thus, the T_N states formed by TTA will decay via electron transfer to the ^{3}CT state and TADF recycling between the ^{1}CT $\leftrightarrow$ ^{3}CT will generate the extra DF signal from the ^{1}CT as observed after employing the second pump pulse, where the exchange energy between the CT manifolds, estimated by King *et al.* as 14 meV,[25] plays an important role for efficient TADF. As has recently been shown, the ^{3}CT can couple rather efficiently to the ^{1}CT via TADF when the ^{3}CT lies very close in energy to the ^{1}CT, and can cross back to the ^{1}CT by thermal activation and reverse intersystem crossing.[16] So, smaller exchange energy implies stronger mixing between the singlet and triplet CT manifolds. Consequentially, a new mechanism ($T_N \rightarrow {}^3\text{CT} \rightarrow {}^1$CT) was introduced for generating DF from T_N state which can readily give rise to an extra 0.14 (experimental value of 0.34 – the maximum TTA 0.2 = 0.14) DF contribution via TADF. As TTA generates a T_N (2x $E_{T_1} > T_N$), then the formation of CT states at low temperature resulting in efficient TADF gives efficient DF production by induced TADF mechanism. This is a very unique mechanism (see Fig. 6.7) and is the only way in which photoexcitation of T_N states (from

T_1 states) can give rise to extra DF as observed: if they simply decay back to T_1, no increase would be seen in DF after second pulse. The rISC seems implausible as it would have been seen in many other non-CT containing luminescent polymers so far.

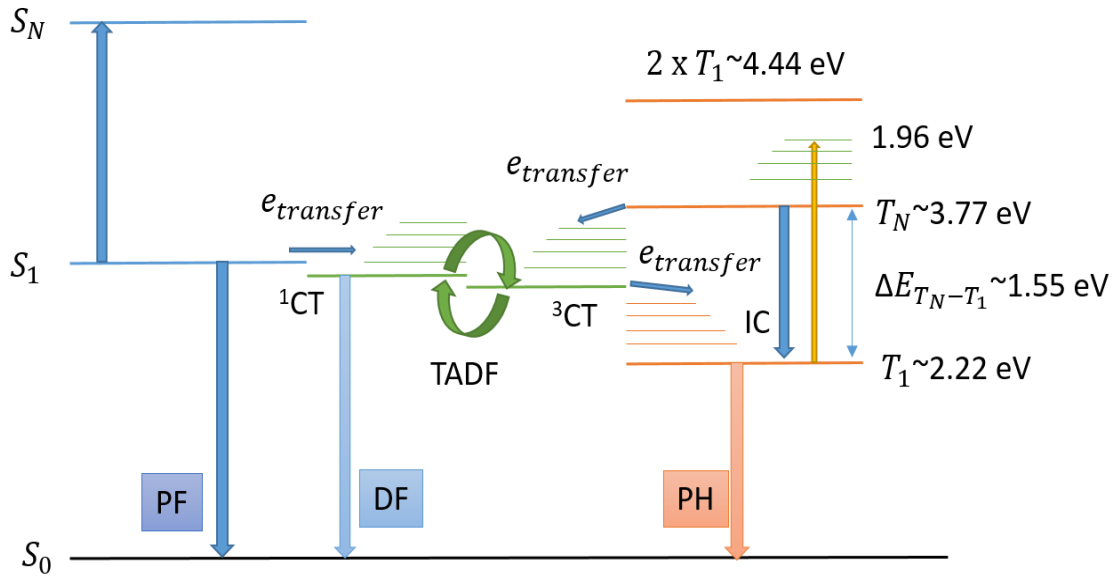

Figure 6.7 Schematic energy level diagram for PSBF constructed from fluorescence, phosphorescence and photoinduced absorption measurements and delayed fluorescence. From this Jablonski scheme the various decay channels for initial and photoinduced excited states can be seen in PSBF. The S_1 state will be quenched by the ^{1}CT state by electron transfer, which in term is quenched by the ^{3}CT. There is then a competition between TADF and ^{3}CT quenching to the lowest energy ^{3}LE state (T_1) of the system.

6.5 Conclusion

In this chapter, the first direct evaluation of the total singlet exciton yield produced from triplet excitons in a luminescent polymer was presented for PSBF. At 20 K, a lower limit of Φ_{DF}=0.34 for the total delayed fluorescence was obtained, which was clearly much greater than the 'classical' TTA singlet TF yield of 0.055 and also above the expected 0.2 yield given that only the quintuplet TTA channel is energetically unattainable. These results indicate that a further process must contribute to the efficiency

of delayed fluorescence, which was identified as induced TADF *via* decay of T_N states to the ^{3}CT state not directly to the $^3(\pi,\pi^*)$ state.

Consequentially, according to these findings, the TTA can generate singlets in two ways, first of all *via* triplet fusion, where the encounter complex gains sufficient singlet wavefunction character that the two triplets become a singlet state, and secondly, through a distinct process requiring an intermediate charge transfer state. The normally unused T_N state formed *via* the TTA triplet channel under conditions of 2x $E_{T_1} > T_N$, then decays by electron transfer to ^{3}CT giving rise to triplets which are harvested *via* the TADF mechanism through the emissive ^{1}CT state. Intensity enhancement of the DF signal is then observed, arising from the ^{1}CT state. To understand the T_N state contribution to the total fluorescence a two-pulse-pump experimental set-up is strongly required.

6.6 References

1. Teetsov, J. & Fox, M. A. Photophysical characterization of dilute solutions and ordered thin films of alkyl-substituted polyfluorenes. *J. Mater. Chem.* **9,** 2117–2122 (1999).
2. Hintschich, S. I., Rothe, C., King, S. M., Clark, S. J. & Monkman, A. P. The Complex Excited-state Behavior of a Polyspirobifluorene Derivative: The Role of Spiroconjugation and Mixed Charge Transfer Character on Excited-state Stabilization and Radiative Lifetime. *J. Phys. Chem. B* **112,** 16300–16306 (2008).
3. Rothe, C., King, S. M. & Monkman, A. P. Direct measurement of the singlet generation yield in polymer light-emitting diodes. *Phys. Rev. Lett.* **97,** 76602 (2006).
4. Laquai, F., Wegner, G., Im, C., Bassler, H. & Heun, S. Nondispersive hole transport in carbazole- and anthracene-containing polyspirobifluorene copolymers studied by the charge-generation layer time-of-flight technique. *J. Appl. Phys.* **99,** 33710 (2006).
5. Pope, M., Swenberg, C. E. & Pope, M. *Electronic processes in organic crystals and polymers*. (Oxford University Press, 1999).
6. Köhler, A. & Bässler, H. *Electronic processes in organic semiconductors: an introduction*. (2015).
7. Movaghar, B., Ries, B. & Grunewald, M. Diffusion and Relaxation of Energy in Disordered-Systems - Departure from Mean-Field Theories. *Phys. Rev. B* **34,** 5574–5582 (1986).
8. Movaghar, B., Grunewald, M., Ries, B., Bassler, H. & Wurtz, D. Diffusion and Relaxation of Energy in Disordered Organic and Inorganic Materials. *Phys. Rev. B* **33,** 5545–5554 (1986).
9. Ries, B., Bassler, H., Grunewald, M. & Movaghar, B. Monte-Carlo Study of Relaxation and Diffusion in Glassy Systems. *Phys. Rev. B* **37,** 5508–5517 (1988).
10. Ries, B. & Bassler, H. Monte-Carlo Study of Dispersive Charge-Carrier Transport in Spatially Random-Systems with and Without Energetic Disorder. *Phys. Rev. B* **35,** 2295–2302 (1987).
11. Scheidler, M., Cleve, B., Baessler, H. & Thomas, P. Monte Carlo simulation of bimolecular exciton annihilation in an energetically random hopping system. *Chem. Phys. Lett.* **225,** 431 (1994).
12. Hertel, D., Bassler, H., Guentner, R. & Scherf, U. Triplet-triplet annihilation in a poly(fluorene)-derivative. *J. Chem. Phys.* **115,** 10007–10013 (2001).
13. Grunewald, M., Pohlmann, B., Movaghar, B. & Wurtz, D. Theory of non-equilibrium diffusive transport in disordered materials. *Philos. Mag. Part B Philos. Mag. Part B* **49,** 341–356 (1984).

14. Cordes, H., Baranovsli, S.D., Kohary, K., Thomas, P., Yamasaki, S., Hensel, F. & Wendorff, J.H. One-dimensional hopping transport in disordered organic solids. I. Analytic calculations. *Phys. Rev. B* **63,** 94201 (2001).

15. Richert, R. & Bassler, H. Dispersive Triplet Excitation Transport in Organic Glasses. *J. Chem. Phys.* **84,** 3567–3572 (1986).

16. Dias, F. B., Bourdakos, K.N, Jankus, V., Moss, K.C., Kamtekar, K.T., Bhalla, V., Santos, J., Bryce, M. & Monkman, A.P. Triplet Harvesting with 100% Efficiency by Way of Thermally Activated Delayed Fluorescence in Charge Transfer OLED Emitters. *Adv. Mater.* **25,** 3707–3714 (2013).

17. Jankus, V., Data, P., Graves, D., McGuinness, C., Santos, J., Bryce, M.R., Dias, F.B & Monkman, A.P. Highly Efficient TADF OLEDs: How the Emitter-Host Interaction Controls Both the Excited State Species and Electrical Properties of the Devices to Achieve Near 100% Triplet Harvesting and High Efficiency. *Adv. Funct. Mater.* **24,** 6178–6186 (2014).

18. Larkin, J. M., Donaldson, W. R., Foster, T. H. & Knox, R. S. Reverse intersystem crossing from a triplet state of rose bengal populated by sequential 532-+1064-nm laser excitation. *Chem. Phys.* **244,** 319–330 (1999).

19. Reindl, S. & Penzkofer, A. Higher excited-state triplet-singlet intersystem crossing of some organic dyes. *Chem. Phys.* **211,** 431–439 (1996).

20. Ringemann, C., Schönle A., Giske, A., Middendorff, C., Hell, S.W. & Eggeling, C. Enhancing fluorescence brightness: Effect of reverse intersystem crossing studied by fluorescence fluctuation spectroscopy. *Chemphyschem* **9,** 612–624 (2008).

21. Mcgimpsey, W. & Scaiano, J. Photochemistry and Photophysics from Upper Triplet Levels of 9,10-Dibromoanthracene. *J. Am. Chem. Soc.* **111,** 335–340 (1989).

22. Jankus, V., Winscom, C. & Monkman, A. P. Dynamics of triplet migration in films of *N* , *N* ′-diphenyl- *N* , *N* ′-bis(1-naphthyl)-1, 1′-biphenyl-4, 4″-diamine. *J. Phys. Condens. Matter* **22,** 185802 (2010).

23. Rothe, C. & Monkman, A. P. Triplet exciton migration in a conjugated polyfluorene. *Phys. Rev. B* **68,** 75208 (2003).

24. Rothe, C. & Monkman, A. P. Triplet exciton migration in a conjugated polyfluorene. *Phys. Rev. B* **68,** 75208 (2003).

25. King, S. M., Hintschich, S. I., Dai, D., Rothe, C. & Monkman, A. P. Spiroconjugation-enhanced intramolecular charge-transfer state formation in a polyspirobifluorene homopolymer. *J. Phys. Chem. C* **111,** 18759–18764 (2007).

26. King, S. M., Rothe, C., Dai, D. & Monkman, A. P. Femtosecond ground state recovery: Measuring the intersystem crossing yield of polyspirobifluorene. *J. Chem. Phys.* **124,** 234903 (2006).

27. Mehes, G., Nomura, H., Zhang, Q., Nakagawa, T. & Adachi, C. Enhanced Electroluminescence Efficiency in a Spiro-Acridine Derivative through Thermally Activated Delayed Fluorescence. *Angew. Chem.-Int. Ed.* **51,** 11311–11315 (2012).

28. King, S. M., Vaughan, H. L. & Monkman, A. P. Orientation of triplet and singlet transition dipole moments in polyfluorene, studied by polarised spectroscopies. *Chem. Phys. Lett.* **440,** 268–272 (2007).

CHAPTER 7: STUDY OF UP-CONVERTED DELAYED FLUORESCENCE PHENOMENA IN SENSITIZER-ACCEPTOR SYSTEMS USING ANTHRACENE BASED NOVEL SMALL MOLECULES AS AN ACCEPTOR

This chapter has been published as:

Murat Aydemir, Gulcin Haykir, Ahmet Battal, Vygintas Jankus, Sunish K. Sugunan, Fernando B. Dias, Hameed Al-Attar, Figen Turksoy, Mustafa Tavasli, Andrew P. Monkman, "High efficiency OLEDs based on anthracene derivatives: The impact of electron donating and withdrawing groups on the performance of OLEDs" Organic Electronics, 30, **2016**, 149-157.

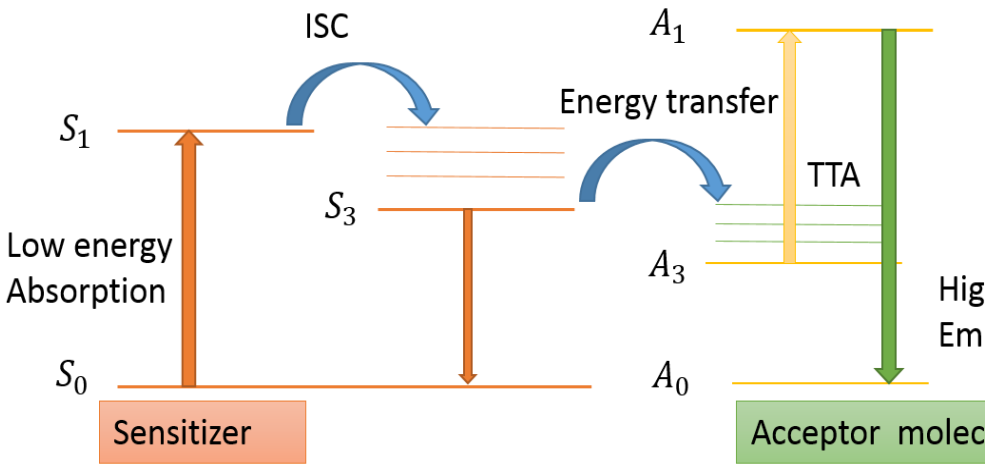

Figure 7.1 Schematic representation of general Jablonski diagram of the up-conversion process between sensitizer and acceptor molecule, which represents how up-converted delayed fluorescence process occurs.

In this chapter, up-converted delayed fluorescence phenomena are investigated in sensitizer-acceptor systems using platinium-octaethylporphyrin (PtOEP) as a sensitizer and anthracene based novel small molecules as an acceptor. In this system, low energy light is converted into high energy form by means of the following two steps energy processes; i) "triplet-triplet energy transfer" from the triplet state of the sensitizer to the

triplet state of the acceptor molecule, ii) "triplet-triplet annihilation (TTA)" process for up-converted delayed fluorescence. In general, the anthracene derivatives are known to have low intersystem crossing rates, therefore, the population of the triplet states is low and usually the phosphorescence is hard to detect, which make the conventional delayed fluorescence (arising from TTA) inefficient. To overcome this low delayed fluorescence efficiency as well as to understand how molecular structure affects the efficiency of the energy transfer process, this sensitizer based up-conversion experiment was performed. Additionally, at the end of the chapter, the time-resolved dynamics of a neat film (8d molecule) are included. This was the only molecule that helped us to make a good estimation of the T_1 energy levels. The particular findings on one of the material revealed the presence of mixed triplet harvesting mechanisms, which was further confirmed in OLED applications with this particular molecule. However, the latter is beyond the scope of this chapter, and more details can be found in the original publication as detailed above.

7.1 Introduction

7.1.1 Overview of the up-conversion mechanism

Incoherent up-conversion (UC) phenomena were first introduced by Parker *et al.*[1] who stated that the photons of low energy are converted to a higher energy form by means of a sensitized triplet-triplet annihilation (TTA) process, which has potential applications in organic-light emitting devices (OLEDs),[2] bio-imaging[3] and particularly photovoltaic solar cells (as energy conversion).[4] The efficiency of solar cells are determined by the energy gap of the molecules and usually absorption does not occur if the energy of photons is lower than the electronic band, and also, the photons which have higher energy than the band gap are wasted due to thermalisation (more information can be found about this for solar cells elsewhere[5]). Therefore, the up-conversion process is a promising method to use low energy photons to produce higher energy photons. In essence, the working mechanism of energy up-conversion process is based on a bimolecular system consisting of a sensitizer (S) and an emitter (acceptor, A) molecule. The process can be outlined as, first of all, the low energy photon is absorbed by the ground state of the

sensitizer and form the excited singlet state ($S_0 \rightarrow S_1$), then rapid intersystem crossing (ISC) occurs to the lowest excited triplet state of sensitizer ($S_1 \rightarrow S_3$). For the efficiency of the system, the sensitizers should facilitate efficient ISC and have high triplet yields approaching ~100%. Secondly, Dexter type electron energy transfer occurs[6] (requires orbital overlap and short interaction distance) from the triplet state of the sensitizer towards the energetically lower lying triplet state of the acceptor, this process yields optically dark long-lived triplets and regenerates the ground state sensitizer ($S_3 + A_0 \rightarrow S_0 + A_3$) which continues until the sensitizer triplets are exhausted. The transmitted energy is stored due to long lifetime of the acceptor triplet states where there is less probability of ISC of the acceptor molecules (~0.02-0.09 for anthracene derivatives)[7], preventing radiative decay of the triplets, i.e. phosphorescence, hence, the transferred triplets are ideal for the TTA process.

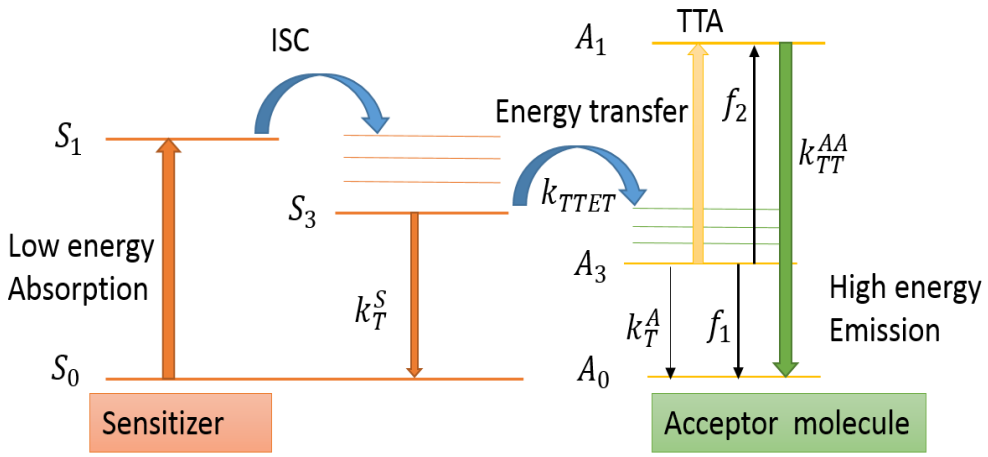

Figure 7.2 Schematic representation of general Jablonski diagram of the up-conversion process between sensitizer and acceptor molecule, which includes the rate constants.

As a result of this weak ISC probability of the acceptor triplets, the triplet population becomes very high, so that the probability of TTA is greatly enhanced due to increased probability of diffusive collisions between triplet states of the acceptor, which pave the way for homogenous-TTA (homo-TTA) process to form an excited singlet state (A_1), from which the up-converted higher energy (than the photon energy of excitation

source) delayed fluorescence is emitted, and a ground state of acceptor is formed ($A_3 + A_3 \rightarrow A_1 + A_0$). It should be highlighted that it is also possible to observe heterogeneous-TTA (hetero-TTA) process between the triplets of sensitizer and acceptor, but this becomes negligible if there exists a large concentration difference between the sensitizer and acceptor molecules.[8] Then only the homo-TTA channel becomes active for TTA process whereby the collision of two triplets results in encounter complexes from which an excited singlet state is formed and the delayed fluorescence arises ($A_1 \rightarrow A_0$+hν, see Fig. 7.2.). So, the maximum theoretical quantum efficiency of this up-conversion mechanism could be 50% due to a two to one photon conversion process, however, the achievable efficiency values are in the range of 11-30% so far.[9–11]

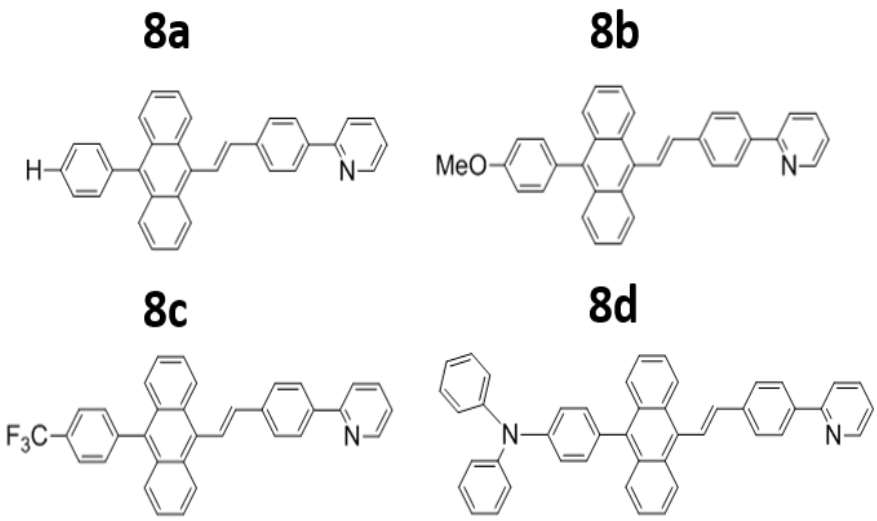

Figure 7.3 Molecular structures of anthracene derivatives as acceptors

For this particular energy transfer mechanism to work well, there are some specific requirements, for instance, sensitizers are chosen depending on their low energy absorption ability (typically in the range of visible to near infrared),[5] long-lived triplet state (typically should be on the order of microseconds or milliseconds serving as energy reservoirs for the acceptor), and strong intersystem crossing rate (typically obtained with heavy metal atoms due to strong spin-orbit coupling with approaching value of 1). In this

chapter, platinium-octaethylporphyrin (PtOEP) heavy metal complex is selected as a triplet sensitizer which possesses a relatively long triplet lifetime (~80 μs) and the quantum yield of luminescence is around 50%.[12] For the emitters, high fluorescence quantum yield is desirable, the lifetime of the triplet state should be long and the energy of the triplet state should be lower than the triplet energy of the sensitizer (the large energy gap becomes a driving factor for more efficient energy transfer),[13] additionally, the singlet energy level of sensitizer should be below the singlet energy level of the emitter molecule. For efficient TTA, the energy of two triplets should be comparable or higher than the energy of singlet state. In these cases, the observed up-converted delayed emission has the same spectral profile comparing with the emission spectra of the emitter molecules and shows a quadratic power dependence as a function of the intensity of excitation light, which is the one of the typical behaviours of bimolecular processes. In this chapter, anthracene based small molecules have been selected as acceptor molecules which structurally consist of an anthracene as the central core attaching 2-(4-(2-pyridinyl)-phenyl)vinyl and 4-R-phenyl unit, then the radicals are changed as H (**8a**), OMe (**8b**) and CF_3 (**8c**), $N(Ph)_2$ (**8d**)] groups at 9- and 10- positions. These different radical groups serve as electon donor (OMe, methoxy group, 8b, and amine group, 8d), electron acceptor (CF_3, trifluoromethyl, 8c) and neutral (H, 8a) side groups (see Fig.7.3.). More details on synthesis procedure can be found elsewhere.[14]

7.1.2 Kinetics of the triplets in both sensitizer and acceptor

In an up-conversion mechanism, the overall efficiency of the system is determined with electron transfer and TTA steps, which are kinetically linked to each other. For the latter step to occur, two electron transfer must occur significantly from the triplet state of sensitizer molecule to the triplet state of the acceptor molecule, then, the first and second order kinetics of the acceptor triplet state determine the TTA efficiency. Considering the non-/radiative rate equations for the triplet manifolds of sensitizer and acceptor, the build-up and decay kinetics can be written in a very general form as,[5,11]

$$\frac{\mathbf{d[S_3]}}{\mathbf{dt}} = \mathbf{k_\phi[S_1] - k_T^s[S_3] - k_{TTET}[S_3][A_1] - k_2^{SA}[S_3][A_3] - k_{TT}^{SS}[S_3]^2 = -\frac{d[S_1]}{dt}} \quad \textbf{(7.1)}$$

and for the acceptor,

$$\frac{\mathbf{d[A_3]}}{\mathbf{dt}} = \mathbf{k_{TTET}[S_3][A_1] - k_T^A[A_3] - k_2^{SA}[S_3][A_3] - k_{TT}^{AA}[A_3]^2 = -\frac{d[A_1]}{dt}} \quad \textbf{(7.2)}$$

where abbreviations of S and A are used for sensitizer and acceptor molecule, respectively. And the subscripts represent the excited singlet (1) and triplet (3) states, and (0) is used for the ground states. The equations show that the concentration changes of triplets with time depend on various parameters and the population of triplet states kinetically equalized with the ground state depletions. According to Eq. 7.1., the triplet state of the sensitizer is populated with excitation of $S_0 \rightarrow S_1$, which triggers all the upconversion mechanisms, and k_ϕ represents the rate of excitation depending on the absorption cross section of the sensitizer. Then very rapid ISC occurs to triplet state of the sensitizer, it is assumed to be unity due to the inclusion of a heavy metal complex. Then the first order rates are represented with k_T^S and k_T^A showing the sum of non-/radiative triplet decays of sensitizer and acceptor, respectively. k_{TTET} is the triplet energy transfer rate between $S_3 \rightarrow A_3$, which is one of the depopulation rates for the sensitizer, whereas, that populates the triplet state of acceptor. k_2^{SA} is the possible hetero-TTA rate between the triplet manifolds. The second order rates are represented with k_{TT}^{SS} and k_{TT}^{AA} which are the homo-TTA rates that occur between the same triplet states of the sensitizer and acceptor, respectively.

7.1.3 Triplet-triplet energy transfer (TTET)

In an ideal up-conversion mechanism, the energy consumption must be minimum during the triplet-triplet energy transfer (TTET) process which is a strong requirement to get high efficiency from the system. As mentioned above, using the heavy metal complexes as sensitizers can strongly enhance the spin-orbit coupling, therefore, ISC rate between the $^1S^* \rightarrow {}^3S^*$ is near unity as well as having long triplet lifetimes which appears as a driving force for the triplets to diffuse further distances, resulting in an increase in collision probability between the triplets of the sensitizer and the acceptor during the TTET process. Actually, the TTET is a Dexter-type energy transfer which requires close proximity between the encounters.[15] Therefore, the working mechanism of this particular system depends on physical interactions (collisons) of the triplets of the sensitizer and the acceptor, for that, the triplets from both of the states must potentially exist in the solution at the same time. In this case, exchange interactions occur as a result of spatial overlaps between the wavefunctions of the resonating sensitizer and the acceptor triplet states. The up-conversion process can quantitatively be explained with the efficiency of the TTET quenching, where bimolecular triplet energy rate (k_{TTET}) can be determined using with the Stern-Volmer equations (see eq. 7.3), which can be written in a general form,

$$\frac{\mathbf{I_0}}{\mathbf{I}} = \mathbf{1} + \mathbf{k_{TTET}\tau_0[A]}$$
$$\frac{\boldsymbol{\tau_0}}{\boldsymbol{\tau}} = \mathbf{1} + \mathbf{k_{TTET}\tau_0[A]} \qquad \textbf{(7.3)}$$

where I_0 and I are photoluminescence intensities of sensitizer in the absence and presence of the acceptor, respectively. In the same manner, τ_0 and τ are the lifetimes of phosphorescence in the absence and presence of acceptor, respectively. [A] is the concentration of the acceptor. Afterwards, the triplet-triplet energy transfer efficiency (Φ_{TTET}) can be defined by considering the triplet energy transfer rate and the radiative

triplet decay rate of the sensitizer in the absence of acceptor, which can be written in a general form as,[16]

$$\Phi_{TTET} = k_{TTET} / k_{TTET} + k_q + k_T^S \quad (7.4)$$

where k_q is the concentration quenching, in the case of using different concentrations of sensitizer and the acceptor molecule.

7.1.4 Triplet-triplet annihilation process for up-converted delayed fluorescence

After triplets are sensitized through the triplet state of the acceptor, there occurs a great potential for the triplet-triplet annihilation process which is the origin of the up-converted delayed fluorescence. When two triplets encounter in their respective triplet states (A_3), they collide and form an encounter complex having three different multiplicities due to the degeneracies of the spin states; 1/9 singlet $(AA)_1$, 3/9 triplet $(AA)_3$ and 5/9 quintet $(AA)_5$. According to spin statistics, only 1/9 of all TTA events result in an emissive singlet state (A_1), however, in most cases the statistics are different because quintuplets are usually energetically inaccessible. In this case, the quintet channel will not open, therefore, no energy loss occur and the formed quintet complex will dissociate back to initial two encounter triplets. Consequentially, the singlet to triplet yield depends on this or the possible participation of higher excited triplet channel as aforementioned in Chapter 5. As a reminder, if the energy of two triplets is larger than the S_1 (A_1) energy and larger than the energy of one of the higher triplet levels (T_N), i.e. $2xE_{T_1} > E_{S_1}; E_{T_N}$, the collision between two triplets can only generate 1 singlet and 3 triplets. In this case the fraction of triplet states that originate singlets through TTA is 20%. In the most favourable situation where the energy of two triplets is larger than the S_1 (A_1) energy ($2xE_{T_1} > E_{S_1}$) but smaller than the energy of T_N ($2xE_{T_1} < E_{T_N}$), only singlet states can be formed through TTA, and the fraction of triplet states that originate singlets through TTA goes up to 50%. Therefore, theoretically, it is possible to achieve

50% total efficiency (Φ_{UC}) from the up-conversion mechanism. As a result of the TTA process, the long-lived delayed fluorescence (DF) originates from the singlet excited states, which has similar spectral shape with prompt emission due to arising from the excited singlet state of the molecule.

The first and second order kinetics result in depopulation of acceptor triplet states by means of quenching (non-/radiatively) monomolecularly (k_T^A), i.e. phosphorescence, and by bimolecularly (k_{TT}^{AA}), i.e. the DF fluorescence originating from TTA, where the time evolution of the triplet concentration can be written as,[11,17]

$$\frac{\mathbf{d[A_3]_t}}{\mathbf{dt}} = -\mathbf{k_T^A[A_3]} - \mathbf{k_{TT}^{AA}[A_3]^2} \qquad \mathbf{(7.5)}$$

where k_T^A is the first order decay rate, k_{TT}^{AA} is the bimolecular decay rate (second order rate), and $[A_3]$ is the acceptor triplet concentration. The analytic solution of eq. 7.5. can be written as,[11,17]

$$\mathbf{[A_3]} = \mathbf{[A_3]_0}\frac{\mathbf{1-\beta}}{\mathbf{exp(k_T^A\, t)-\beta}} \qquad \mathbf{(7.6)}$$

where $[^3A]_0$ is the triplet concentration of acceptor at time 0, β can be defined as the initial fraction of decay arising from the TTA process which is equal to a ratio consisting of first and second order rates as well as the initial concentration of the acceptor triplets, which can be written as,

$$\boldsymbol{\beta} = \frac{\mathbf{a}}{\mathbf{k_T^A + a}};\ \ \mathbf{where}\quad \mathbf{a = k_{TT}^{AA}\,[A_3]_0} \qquad \mathbf{(7.7)}$$

experimentally, fitting Eq. 7.7 to the square root of the normalized DF intensity helps to determine the values of a and k_T^A . The importance of determining the value of a is that the proportions of the triplets which decay with first (f_1) and second order rates (f_2) can be identified as,

$$\boldsymbol{f_1 = -[A_3]_0^{-1} \int_0^{\infty} k_T^A [A_3]\, dt = \frac{\beta - 1}{\beta} \ln(1-\beta)} \quad \textbf{(7.8)}$$

$$\boldsymbol{f_2 = -[A_3]_0^{-1} \int_0^{\infty} k_{TT}^{AA} [A_3]^2\, dt = 1 - \frac{\beta - 1}{\beta} \ln(1-\beta)} \quad \textbf{(7.9)}$$

Considering the DF arises as a result of TTA process, then, the intensity of DF should depend on triplet concentration time evolution and the second-order component which is governed by,

$$\boldsymbol{I_{DF} \sim \int_0^{\infty} \Phi_f k_{TT}^{AA} [A_3]^2 dt} \quad \textbf{(7.10)}$$

where Φ_f is the fluorescence quantum yield of the emitter. If the monomolecular decay rate is higher then the bimolecular rate ($k_T^A > k_{TT}^{AA}[A_3]$) then the Eq. 7.6. can be re-written neglecting the second order decay part, which allows the triplet concentration to be written as,

$$\boldsymbol{[A_3] = [A_3]_0 \exp(-k_T^A t)} \quad \textbf{(7.11)}$$

then the proportinality of intensity of DF can be written as,

$$\mathbf{I_{DF}} \sim \int_0^\infty \mathbf{\Phi_f}\, \mathbf{k_{TT}^{AA}}\, [\mathbf{A_3}]^2 \mathbf{dt} = \int_0^\infty \mathbf{\Phi_f}\, \mathbf{k_{TT}^{AA}} ([\mathbf{A_3}]_0\, \mathbf{exp}(-\mathbf{k_T^A t})^2 \mathbf{dt}$$
$$= \frac{\mathbf{\Phi_f k_{TT}^{AA}} [\mathbf{A_3}]_0{}^2}{\mathbf{2k_T^A}} \qquad \textbf{(7.12)}$$

According to the eq. 7.12 the DF signal should follow a quadratic dependence on laser fluence (at low excitation conditions) and show a quadratic dependence on the initial triplet concentration, $[A_3]_0{}^2$. However, in the case of high triplet concentrations, where the annihilation rate is dominant ($k_T^A < k_{TT}^{AA}[A_3]$), then Eq. 7.6. can be re-written, particularly neglecting the first order decay part as,

$$[\mathbf{A_3}] = \frac{[\mathbf{A_3}]_0}{(\mathbf{1} + \mathbf{k_{TT}^{AA}} [\mathbf{A_3}]_0 \mathbf{t})} \qquad \textbf{(7.13)}$$

where the triplet concentration is linearly proportional to the time and the proportinality of intensity of DF can be written as,

$$\mathbf{I_{DF}} \sim \int_0^\infty \mathbf{\Phi_f}\, \mathbf{k_{TT}^{AA}}\, [\mathbf{A_3}]^{2^2} \mathbf{dt} = \int_0^\infty \mathbf{\Phi_f}\, \mathbf{k_{TT}^{AA}} \frac{[\mathbf{A_3}]_0{}^2}{(\mathbf{1} + \mathbf{k_{TT}^{AA}} [\mathbf{A_3}]_0 \mathbf{t})^2} \mathbf{dt}$$
$$= \frac{\mathbf{\Phi_f} [\mathbf{A_3}]_0{}^2 \mathbf{k_{TT}^{AA}}}{\mathbf{k_{TT}^{AA}} [\mathbf{A_3}]_0} = \mathbf{\Phi_f} [\mathbf{A_3}]_0 \qquad \textbf{(7.14)}$$

In the high triplet concentration conditions, the intensity of DF follows a linear dependence on the laser fluence (at high excitation densities) and also linearly dependent on the initial triplet concentration. Consequentially, it was observed that DF arising due to TTA via the sensitization of a metal complex obeys a quadratic dependence at low laser fluence, but at high intensities, it turns over and follows a linear laser dependence.

7.2 Experimental

Absorption and emission spectra were collected using UV-3600 double beam spectrometer (Shimadzu), and Fluoromax and Fluorolog fluorescence spectrometers (Jobin Yvon). All solvatochromic measurements were taken in air saturated solutions (ranging 10^{-5} M to 10^{-6} M) using with 1cm depth quartz cuvettes, and 3 pump-freeze-thaw cycles were repeated with a long necked quartz degassing cuvette to achieve totally degassed solutions and the liquid nitrogen cryostat (Janis Research) was used for measurements. Quantum yields were determined in chlorobenzene in comparison with a standard diphenylanthracene (DPA). For up-conversion measurements, PtOEP (~$7.3 \cdot 10^{-4}$ M) and anthracene derivatives (~$7.5 \cdot 10^{-3}$ M) were dissolved in chlorobenzene and doped with 2% (w/w). Thermally deposited films of anthracene derivative (for only 8d material) was prepared at *ca.* 40 nm thickness at a rate of <1 Å/s, at this time, the vacuum pressure of Lesker system was *ca.* 10^{-6} Torr. Time-resolved nanosecond gated luminescence measurements were performed with the same method as explained in detail in Chapter 3. The selective wavelength of 532 nm was chosen where the energy per pulse was chosen in the range of 30 μJ. All solid film measurements were performed under a dynamical vacuum of $<10^{-4}$ Torr using a displex helium cryostat.

The fluorescence decays were collected in hexane, chlorobenzene and dichloromethane solutions using the time-correlated single photon counting technique (TCSPC, impulse response function, IRF: 21 ps). A vertically polarized picosecond Ti:sapphire laser (Coherent) was used as an excitation source, where the excitation wavelength was 380 nm. Then emission was collected using a polarizer at the magic angle (54^0) to prevent any possible polarization effects. For detection of the emission a double monochromator (Acton Research Corporation) was coupled with a microchannel plate photomultiplier tube (Hamamatsu R3809U-50).

7.3 Results and Discussion

7.3.1 Steady state and Lifetime measurements

The absorption and emission spectra of compounds 8a-8d in hexane and ethanol solutions are shown in Fig. 7.4. Both the absorption and emission spectra of the materials appear broad and featureless, in clear contrast with the well resolved absorption and emission spectrum of anthracene. [18] The π-π* transition band of the materials is assigned *ca.* 395 nm and does not change with increasing solvent polarity. Photoluminescence (PL) spectra of 8a to 8d in hexane solution is almost similar, ranging 490 nm to 495 nm. However, in ethanol solution, the PL spectra of **8a** to **8c** show moderate solvatochromic shifts ranging from 505 nm to 508 nm, whereas that of **8d** redshifts substantially to 520 nm.

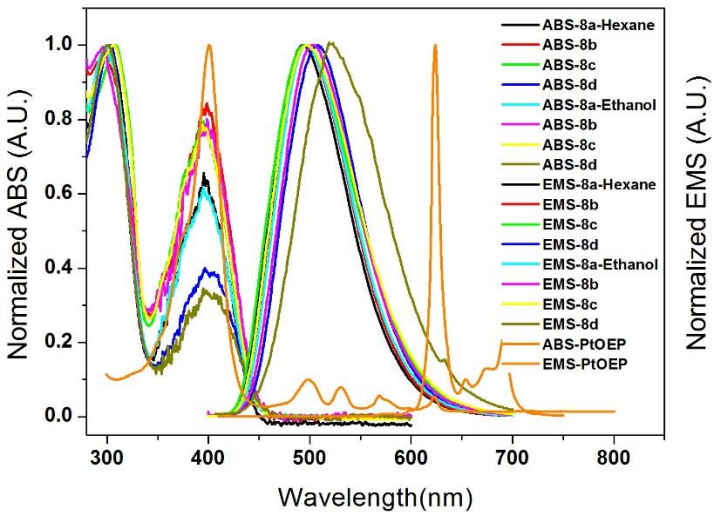

Figure 7.4 ABS ans EMS spectra of materials 8a-8d in hexane and ethanol solutions. Also, ABS and EMS of PtOEP are added for convenience which was taken in toluene solution.

That shows that introduction of extra groups attached to the anthracene core increases the conjugation and red-shifts the emission, relative to pure anthracene (0-0 transition is *ca.* 425 nm and well-resolved). This red-shifted emission of 8d arises due to

the stabilization of an excited charge transfer state, especially strong in the case of the addition of the amine group in the anthracene core. This also explains the decreased of the PLQY of 8d in chlorobenzene, relative to the other materials, and also the possible charge transfer state formation is confirmed by measuring the fluorescence lifetimes with TCSPC in different polarity solvents (from hexane to dichloromethane) (Table 7.1), where the fluorescence lifetimes decreased with increasing solvent polarity for only 8b and 8d.

Table 7.1 Fluorescence quantum yields of materials were measured in air-saturated chlorobenzene solutions. The fluorescence lifetimes were measured using TCSPC in hexane, chlorobenzene and dichloromethane solutions. All decays were well fitted by a single exponential function.

Materials	**Fluorescence quantum yield air-saturated / degassed (%)**	**Fluorescence Lifetime (ns) Hexane/Chlorobenzene/Dichloromethane**
8a	**75 ± 9 / 90 ± 7**	**2.43/2.51/2.83**
8b	**49 ± 5 / 57 ± 4**	**2.24/1.79/1.58**
8c	**67 ± 5 / 74 ± 3**	**2.68/2.72/2.91**
8d **8d thin film**	**17 ± 8 / 22 ± 3** **18. 5± 0.2 / 25.4 ± 0.5**	**0.84/0.55/0.44**

7.3.2 Up-converted delayed fluorescence in PtOEP-anthracene system

The up-converted delayed fluorescence was investigated using anthracene derivatives (8a-8d) doped with PtOEP (2% w/w). The PtOEP sensitizer was excited with the 2nd harmonic of a Nd:YAG laser 532 nm for $S_0 \rightarrow S_1$ transition. As shown in Fig. 7.4, the absorption and emission spectra of PtOEP consists of a Soret (*ca.* 400 nm) and a Q bands (*ca.* 500-575 nm). Upon excitation in the Q-band of PtOEP (Ex 532 nm), 8a-8d do not absorb at this wavelength, an excited PtOEP singlet states are formed (S_1), which then rapidly convert to triplets by ISC in unity due to presence of heavy atom resulting in

strong spin-orbit coupling, and the emission of PtOEP arises only from triplet energy level as long-lived phosphorescence (ca. 1.9 eV or ca. 650 nm).

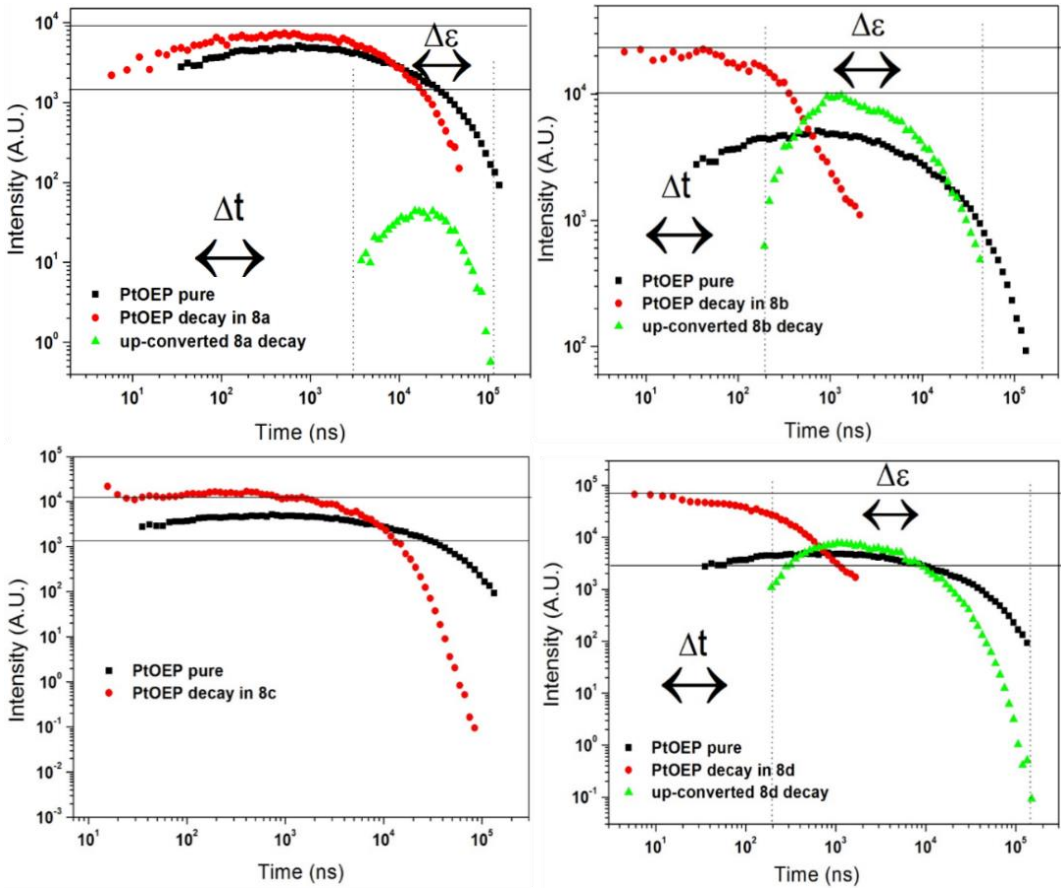

Figure 7.5 The lifetime decays of pure PtOEP (black dots), PtOEP in anhrachene derivatives (red dots) and up-converted delayed fluorescence (green dots) are represented. The measurements were taken exciting with 532 nm laser source in degassed chlorobenzene solution at RT.

As a result of excitation of the doped system, the energy transfer occurred from the triplet state of the sensitizer the triplet state of the acceptor molecules *via* Dexter-type energy process. The efficiency of this process depends on significant overlaps between the orbitals of the sensitizer and the π-orbitals of the anthracene acceptor, and the efficiency can be determined with triplet-triplet energy transfer rate (k_{TTET}). Then TTA process occurs and up-converted delayed fluorescence is observed from the materials in the range of 450-650 nm. The lifetime decays were recorded for each materials at RT (see

Fig. 7.5 and for the decay times see Table 7.2 and 7.3). Each graphs in Fig. 7.5 contains three lifetime decays where the pure PtOEP (without material) decay is represented with black dots, and red dots show the lifetime decay of PtOEP in materials and finally the green dots show the lifetime of the up-converted delayed fluorescence (UC-DF). The UC-DF of each molecules (except 8c) has a rise time (Δt), which represents the time required for the transfer of triplet population from the triplet manifold of the sensitizer to the triplet manifold of the acceptor molecules, therefore, UC-DF arises after sometime before the decay of the sensitizer ends (in the range of 200-4000 ns for the materials here). Then again it takes sometimes to reach a maximum intensity value and subsequently decay exponentially, this time-frame is labelled with Δε on the graphs. One of the distinctive feature of the graphs is that the PtOEP decay in the solutions start decaying at comparatively higher intensity values than the pure PtOEP decay and show shorter lifetimes.

One of the requirements for the triplet energy transfer from sensitizer to acceptor is that the triplet level of the acceptor should be lower than that of PtOEP (ca. 1.91 eV),[19] it was a great challenge to determine the triplet energy level of anthracene derivatives. Initial attempts were taken to find the triplet energy levels of anthracene derivatives in degassed solutions at 77K, however, the phosphorescence (PH) is quenched and no PH could be observed. Secondly, it was attempted to record their phosphorescence by isolating them in zeonex (polyolefin) at low temperature to reduce triplet migration, however, no PH could be detected. However, only using a neat film of 8d at 77 K, very weak but reproducible phosphorescence was detected (Fig. 7.6, after 31μs delay), from where, a good estimate of the triplet energy of 8d as 1.7 ± 0.2 eV can be made which is in very good agreement within the errors comparing with the previous reports in anthracene as 1.76 eV,[20,21] but for the molecules 8a-8c, the energy of the triplet states should be more or less in the same energy range due to similarity of molecular structures. The reduction of the triplet state energy of the anthracene derivative, 8d, is fully in line with the anthracene measurement and clearly reflects the conjugated substituents on the anthracene in 8d forming a more delocalised triplet state.

A general diagram of energy up-conversion *via* triplet-triplet annihilation is depicted in Fig. 7.7, consisting of the excited singlet and triplet energy levels of sensitizer

and anthracene molecules. As a result of this process, two fluorescence signals were observed from these solutions at different delay times; one, arising due to the emission of the PtOEP sensitizer, and another one arising from the up-converted delayed fluorescence originating from TTA process. Fig. 7.8 a presents the emission spectra of sensitizer and the acceptor (only 8d material is presented) where the time evolution of the spectra between 12.6 ns and 422 μs show how depopulation occurs within kinetically linked emissive species. In the beginning (i.e. 12.6 ns delay time) only PtOEP emission exists from its triplet state, however, after some time (i.e. 456.6 ns delay), the energy transfer has taken place and both peaks arise simultaneously, which means a portion of sensitizer triplets transferred to the triplet manifold of the acceptor. Then, the population of triplets becomes sufficient to trigger TTA process resulting in UC-DF. Afterwards, initially the triplet reservoir of sensitizer vanished, then only DF emission was present for a while (i.e. 7494.2 ns delay in Fig.7.8. a). Finally, the DF emission started rolling off and the system became non-emissive.

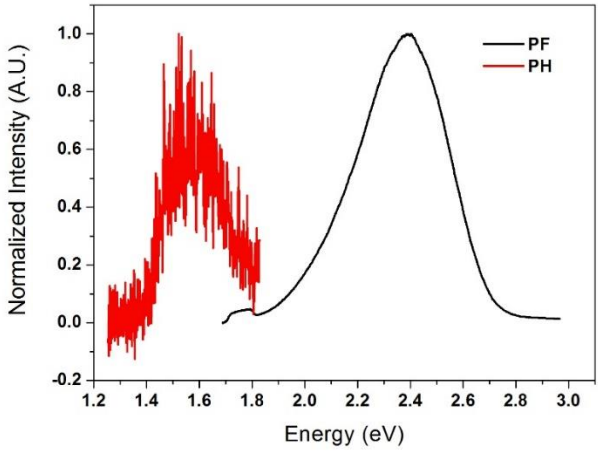

Figure 7.6 The prompt (PF, after 2 ns delay) and phosphorescence (PH, 31μs delay) spectra of 8d neat film at 77K.

During the this up-conversion experiment a cut off filter was used to increase the signal-to-noise ratio due to using 532 nm excitation laser source overlapping the emission spectra, therefore, the UC-DF spectra that was observed from the acceptor was slightly

red-shifted and almost half of the steady-state emission was cut off (Fig. 7.8 b), otherwise it was confirmed that the UC-DF emission peak was observed at similar wavelength seen in the steady state emission of materials.

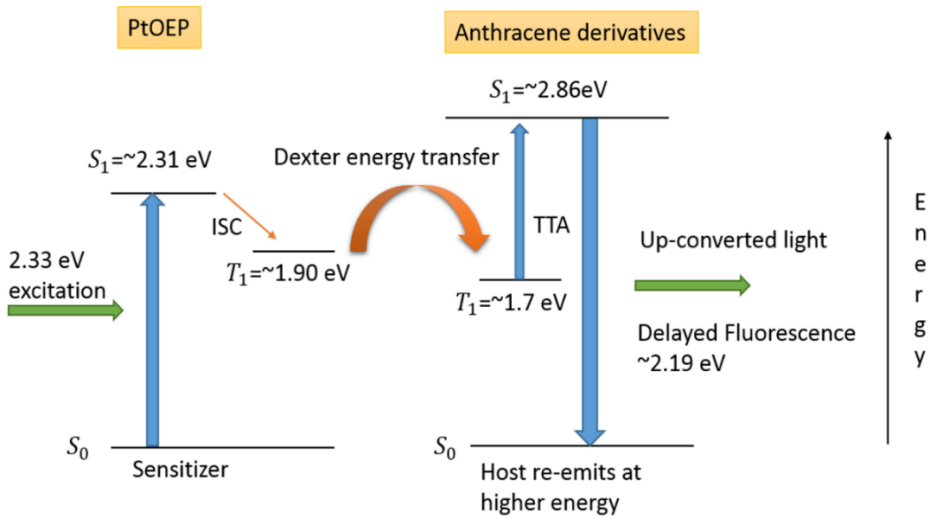

Figure 7.7 Jablonski diagram of up-conversion (UC) *via* triplet fusion. The system consists of acceptor (anthracene derivatives) and sensitizer (PtOEP). The triplet state of each investigated material is harvested *via* the PtOEP triplet, which is populated *via* very efficient intersystem crossing after 532 nm laser absorption. In this way triplet annihilation and delayed fluorescence emission properties of anthracene derivatives can be explored.

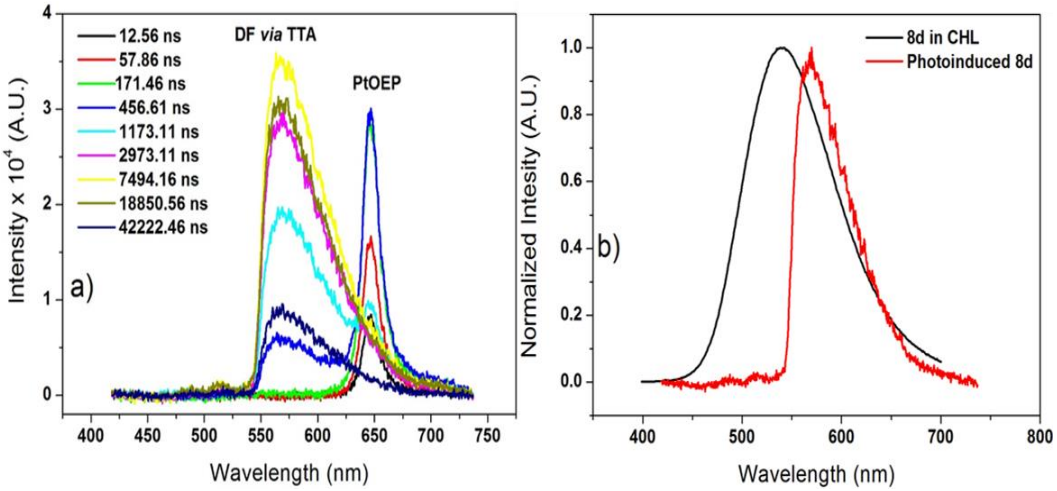

Figure 7.8 a) The Dexter energy transfer of 8d material is represented by time evolution of PtOEP and delayed fluorescence spectra in time range of 12.56 ns to 42222.46 ns. **b)** Steady-state emission of pure 8d

in CHL is compared with photoinduced delayed fluorescence which was taken from mixture of PtOEP+8d after 2973.11 ns delay.

From the decay of the PtOEP signal, triplet energy transfer from PtOEP to the anthracene derivative can be determined. The decay lifetime of unquenched PtOEP (τ_{uq}) can be expressed as follows,

$$\frac{\mathbf{1}}{\boldsymbol{\tau}_{\mathbf{uq}}} = \mathbf{k_r} + \mathbf{k_{nr}} + \mathbf{k_q} \qquad \textbf{(7.15)}$$

where k_r is the radiative decay rate, k_{nr} - non-radiative decay rate, k_q - concentration quenching. The concentration is kept the same for all measurements to keep this rate constant. Experimentally τ_{uq} can be determined by measuring lifetime of the PtOEP in the solution without an acceptor. When the acceptor molecule is added to the solution and its lifetime τ_t is measured, another rate must be included in the equation i.e. triplet transfer from PtOEP to the acceptor rate, k_{TTET},

$$\frac{\mathbf{1}}{\boldsymbol{\tau}_{\mathbf{t}}} = \mathbf{k_r} + \mathbf{k_{nr}} + \mathbf{k_q} + \mathbf{k_{TTET}} \qquad \textbf{(7.16)}$$

Normally, k_{TTET} can then be determined from Eq.7.3, but if the concentration of emitters is kept the same for all the measurements then the equation can be defined,

$$\mathbf{k_{TTET}} = \frac{\mathbf{1}}{\boldsymbol{\tau}_{\mathbf{t}}} - \frac{\mathbf{1}}{\boldsymbol{\tau}_{\mathbf{uq}}} \qquad \textbf{(7.17)}$$

then, the triplet transfer efficiency (TTTE) can be evaluated using the equation,

$$\Phi_{TTET} = \frac{k_{TTET}}{(k_r + k_{nr} + k_q + k_{TTET})} = k_{TTET}\tau_{uq} \qquad (7.18)$$

Table 7.2 The decay lifetime of PTOEP sensitizer mixed with investigated acceptors at the same conditions. The same concentrations of acceptor was ($7.5 \cdot 10^{-3}$ M) with PTOEP ($7.3 \cdot 10^{-4}$ M) in chlorobenzene solution and measured at room temperature in oxygen free environment. PtOEP without acceptor in chlorobenzene ($7{,}3 \times 10^{-4}$ M) is measured as well and used to evaluate transfer efficiencies.

Materials	**Lifetimes, ns**	**$1/\tau_t = k_r + k_{nr} + k_q + k_{TTET}$, ns^{-1} 10^{-5}**	**$k_{TTET} = 1/\tau_t - 1/\tau_{uq}$, ns^{-1}**	**Transfer efficiency, $k_{TTET}/(k_r + k_{nr} + k_q + k_{TTET})$**
PTOEP in 8a	**11156±3**	**8.96**	**5.50**	**0.61**
PTOEP in 8b	**370±5**	**270**	**267**	**0.99**
PTOEP in 8c	**4501±1**	**22.22**	**18.76**	**0.84**
PTOEP in 8d	**320±2**	**313**	**310**	**0.99**
PTOEP in DPA	**2582±5**	**38.73**	**35.27**	**0.91**
PTOEP in pure Anthracene	**223±2**	**448** $1/\tau_q = k_r + k_{nr} + k_q + k_{TTET}$, ns^{-1} 10^{-5}	**445**	**0.99**
Pure PTOEP	**28895±2**	**3.46**	**-----**	**------**

All measurement data for 8a-8d are shown in Table 7.2. The best triplet transfer efficiency was observed for derivatives with electron donating groups (8b and 8d), whereas the worst for the parent compound consisting of neutral side group (8a), the derivative with the electron accepting group falling in between (8c). This demonstrates that neutral molecules are not good candidates for the triplet exciton transfer, the reason may be too high a triplet energy level (which could not be determined empirically). The lifetime of DF arising from the anthracene derivative was dependent on the substitution group. For 8c with the CF_3 electron withdrawing group no delayed fluorescence was observed (see Fig. 7.5), indicating the lack of triplet annihilation or quenching. The DF of the parent compound 8a decays with ~16 μs lifetimes, whereas 8b substituted with MeO electron donating group, the DF lifetime decreased to ~11 μs. And the shortest DF

lifetime ~9 μs was obtained with 8d material consisting of amine side group. According to findings, it can be considered that relatively more triplet-triplet annihilation and subsequent DF efficiency can be obtained from the material having electron donating side groups. The results were compared with the diphenylanthracene (DPA) and pure anthracene in Table 7.3.

Table 7.3 The same concentrations of materials are prepared ($7.49 \cdot 10^{-4}$ M) with PTOEP in chlorobenzene ($7.32 \cdot 10^{-4}$ M) solution and measured at room temperature in oxygen free environment showing the decay of PTOEP in each materials and with pure DPA and anthracene molecules.

Molecules	**Lifetimes, ns**	k_T^A, (10^3 s^{-1})	a, (10^3 s^{-1})	**β**	f_1	f_2	$\Phi_{TTA} = \eta f_2$
8a with PTOEP	**16259±5**	**----**	**----**	**---**	**---**	**---**	**----**
8b with PTOEP	**11004±3**	**2.156**	**2.605**	**0.45**	**0.73**	**0.27**	**0.135**
8c with PTOEP	**----**	**----**	**-----**	**----**	**----**	**----**	**----**
8d with PTOEP	**9086.5±5**	**1.849**	**3.929**	**0.35**	**0.80**	**0.20**	**0.10**
DPA with PTOEP	**13245±3**	**----**	**---**	**----**	**----**	**----**	**----**
Anthracene with PTOEP	**1888±5**	**----**	**---**	**---**	**----**	**----**	**----**

Figure 7.9 shows the intensity dependence of up-converted fluorescence, at low excitation conditions (≤ 10 μJ), the delayed emission of anthracene derivatives showed a quadratic dependence on laser fluence (only result for 8d is presented) which is fully consistent with Eq. 7.12. This indicates that delayed emission arises via triplet-triplet annihilation and subsequent triplet fusion (TF).[22]According to quasi-steady state photoinduced absorption measurements on this 8d material,[14] it has been found that the T_N state as ~4.04 eV and the T_1 state is ~1.7 eV, therefore, the condition of $E_{T_N} > 2xE_{T_1}$; E_{S_1} is satisfied where both quintuplet and excited triplet states are energetically unreachable with the energy of two fusing triplet excitons. Therefore, the only triplet fusion product channel to form the S_1 state is operative yielding a maximum efficiency of 50% (η_{max}) under saturation conditions.

It must be noted that only second-order processes give rise to UC-DF, which is the proportion of triplets (f_2) decaying *via* TF. According to Eq. 7.8 and 7.9, the proportions of the triplets can be determined as first (f_1) and second (f_2) order by means of fitting Eq. 7.7 to the square-root of the normalized intensity of UC-DF, which is the method introduced by Bachilo and Weisman before,[17] then k_T^A and a parameters can be calculated. Using these parameters the unit-less β, showing the initial fraction of decay arising from the second order channel of (A_3), see Fig. 7.2., and f_1 and f_2 values were determined (see table 7.3). However, the fits were only satisfactory for two of the materials (8b and 8d), for the molecules (even considering DPA and pure anthracene) the fits were not perfect and k_T^A and a values could not be determined precisely. From the Table 7.3, significant proportions of the triplets decay with first order (0.73 for 8b and 0.80 for 8d) and the small proportion of triplets decay with second order (0.27 for 8a and 0.20 for 8b) resulting in UC-DF. Considering the maximum triplet conversion probability for emissive S_1 state in these materials ($\eta_{max} \sim 0.5$), then the quantum yield of TTA is to be proportional to f_2, which can be estimated as $\Phi_{TTA} = \eta f_2$.[11] So the estimated values are represented as 0.135 for 8b and 0.10 for the 8d.

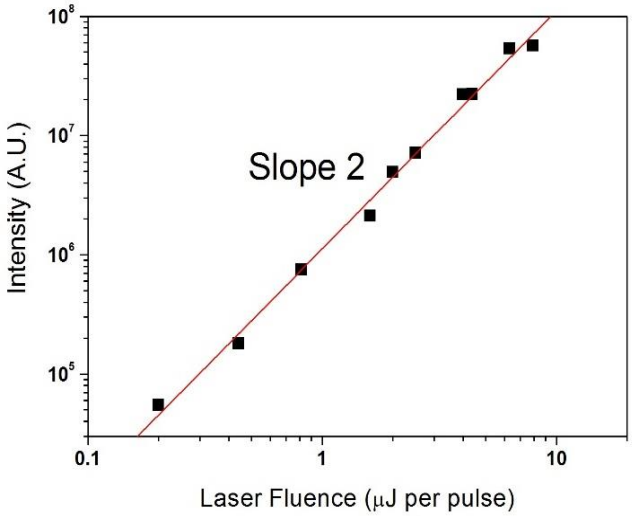

Figure 7.9 Intensity dependence of 8d DF emission (recorded 1.5 μs after excitation) on excitation laser fluence. Quadratic dependence indicates that this emission arises due to triplet-triplet annihilation.

7.3.3 Time-resolved features of 8d neat film

Given the weak emission from long lived species in these new series of materials, only 8d was studied as a neat film at both room temperature and 80K. In Fig. 7.10, the delayed emission from an 8d film shows clearly the presence of a weak red shift emission co-existing with the prompt emission. The two emission bands, one prompt centred at 525 nm (2.36 eV) the other weak and delayed at 575 nm (2.16 eV) are compared to the steady state emission as a function of solvent polarity (see Fig.7.11). The prompt emission is very similar to that seen in non-polar solvents whereas the weak delayed emission compares very well with that in highly polar solvent. From this the conclusion can be made that as in film there is a dispersion of molecular environments, most which have restricted molecular motion and favour only weak (or no) charge transfer character to the excited state, and some which either allow geometric relaxation in the solid state or pin the molecule in a distorted configuration which stabilises a charge transfer excited state.[23] It is clear from this that in the solid state, especially in devices it is expected to see rather complex characteristics associated with this sample heterogeneity.

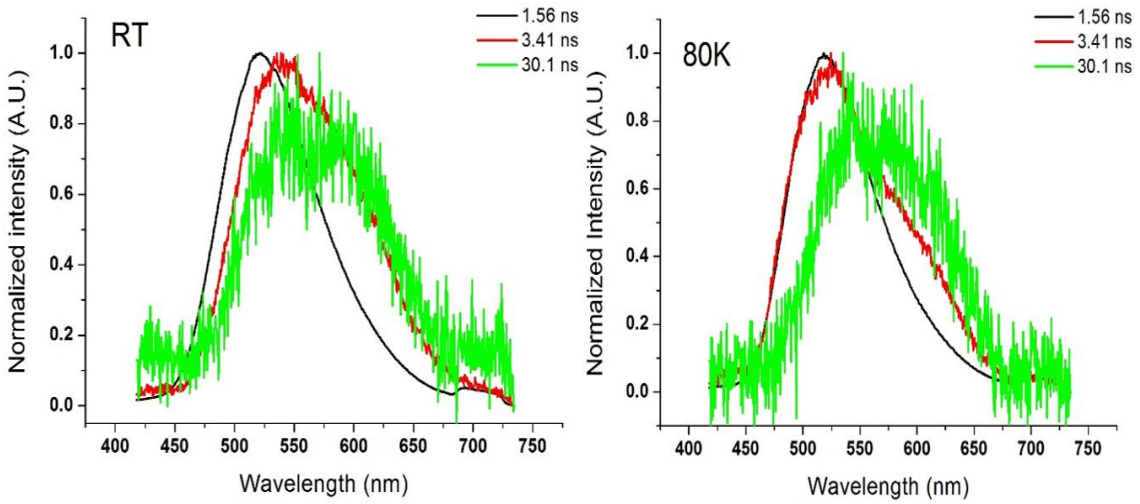

Figure 7.10 The spectra of 8d neat film were taken at variety of delayed times, between 1.56 ns and 30.1 ns at RT and 80K.

To further characterise this, power dependencies were measured from the emission features observed in the neat film of 8d (see Fig. 7.12). The weak CT like delayed fluorescence clearly shows complex behaviour, characteristic of mixed emission. For DF, the slope of 1.6 at low intensity turning over to 0.8 at high intensity is characteristic of a TTA dominated process mixed with a weak monomolecular emission. It has previously been observed such mixed behaviour in heterogeneous systems (in Chapter 6). This is further supported by a weakly oxygen dependent PLQY (see Table 7.1), where it is found that the total emission only changes by some ~20%, indicating a small triplet harvesting contribution to the total photoluminescence concomitant with a weak TADF component. This strong heterogeneity as well as moderate to strong CT character may have two fold effects on device applications; i) charge injection onto the emitter molecule may favour direct CT excited state formation,[24] ii) these CT states could greatly alter the triplet harvesting efficiency of the emitter in the device, generating singlet states *via* the TADF mechanism. It is thus highly likely that both a dominant TTA and a weaker TADF both contribute to the overall singlet yield of the devices, particularly at low current conditions, the efficiency of the devices will be relatively high.[14]

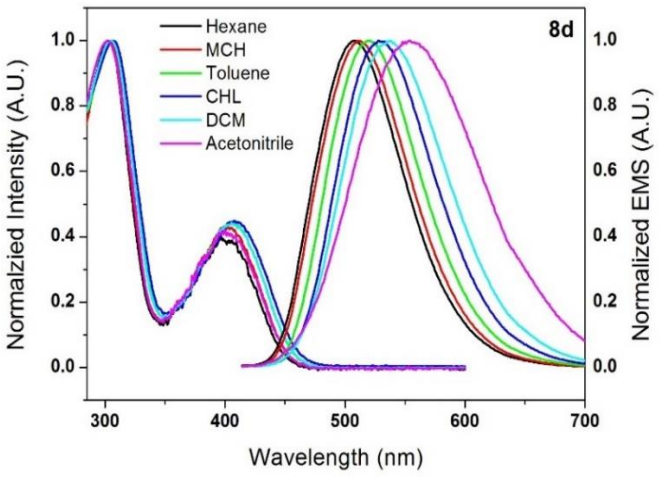

Figure 7.11 Absorption and emission spectra of 8d in solvents of different polarity

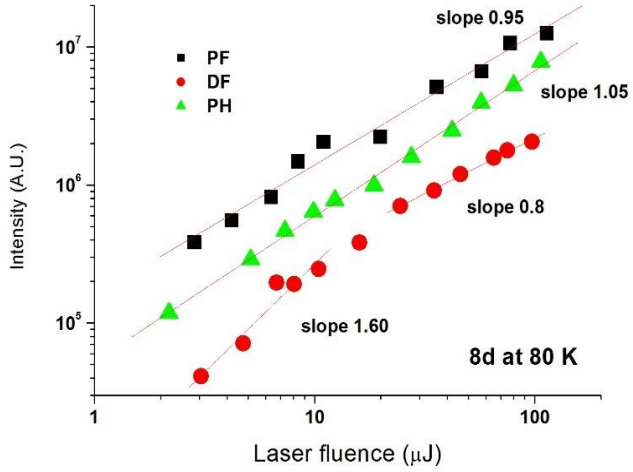

Figure 7.12 Power dependence of PF, DF and PH of 8d neat film at 80 K.

7.4 Conclusion

In this chapter, triplet properties of novel anthracene derivatives were investigated using a sensitizer-acceptor based up-conversion mechanism where PtOEP was chosen as a sensitizer and anthracene small molecules as a host (acceptor). Using a selective excitation wavelength of 532 nm, the low energy photons were up-converted to relatively higher energy photons as observed by the presence of UC-DF. According to the results, the understanding was developed on the molecular structures of anthracene based novel acceptor molecules where structural modifications can be made to improve the efficiency of the next generation up-conversion applications, also with these results the question of how the side groups having different electron donating, withdrawing or neutral units affect the triplet-triplet annihilation efficiency and triplet energy transfer efficiency were clarified. Comparing the results the best triplet transfer efficiency was observed with the molecules including electron donating groups (8b and 8d) which suggest that the molecules having electron donating groups might be suitable alternative molecules to get high quantum efficiency from the up-conversion applications. However, here, the first-order process was the dominant efficiency quenching channel, which limited the proportion of triplets that were involved in second-order annihilation process. From which, Φ_{TTA} values were estimated for 8a and 8b using the proportions of the triplets which decay with second order rates (f_2). Additionally, the time-resolved dynamics of a

neat film (8d molecule) were attached, which was the only molecule that helped us to make a good estimate of the T_1 energy levels. The particular findings of 8d neat film revealed the presence of mixed triplet harvesting mechanisms, which was further confirmed by the results in OLED applications using the 8d molecule.[14] Consequentially, a weak CT like delayed fluorescence was observed which was energetically close to the singlet state and power dependence measurements clearly confirmed a complex DF behaviour (bimolecular + monomolecular) showing there is another weak triplet harvesting mechanism in operation, TADF, rather than TTA. This mixed contribution of TTA and TADF is one of the desired alternative systems to obtain high efficiencies in potential device applications (as seen in polyspirobifluorene polymer in Chapter 6).

7.5 References

1. Parker, C., Hatchard, C. & Joyce, T. Selective and Mutual Sensitization of Delayed Fluorescence. *Nature* **205,** 1282- (1965).
2. Kim, D. Y., Song, D. W., Chopra, N., De Somer, P. & So, F. Organic Infrared Upconversion Device. *Adv. Mater.* **22,** 2260–+ (2010).
3. Liu, Q., Yang, T., Feng, W. & Li, F. Blue-Emissive Upconversion Nanoparticles for Low-Power-Excited Bioimaging in Vivo. *J. Am. Chem. Soc.* **134,** 5390–5397 (2012).
4. Baluschev, S., Miteva, T., Yakutkin, V., Nelles, G., Yasuda, A. & Wegner, G. Up-conversion fluorescence: Noncoherent excitation by sunlight. *Phys. Rev. Lett.* **97,** 143903 (2006).
5. Schulze, T. F. & Schmidt, T. W. Photochemical upconversion: present status and prospects for its application to solar energy conversion. *Energy Environ. Sci.* **8,** 103–125 (2015).
6. Aulin, Y. V., van Sebille, M., Moes, M. & Grozema, F. C. Photochemical upconversion in metal-based octaethyl porphyrin-diphenylanthracene systems. *Rsc Adv.* **5,** 107896–107903 (2015).
7. Armstrong, N. R., Wightman, R. M. & Gross, E. M. Light-emitting electrochemical processes. *Annu. Rev. Phys. Chem.* **52,** 391–422 (2001).
8. Cao, X., Hu, B. & Zhang, P. High Upconversion Efficiency from Hetero Triplet-Triplet Annihilation in Multiacceptor Systems. *J. Phys. Chem. Lett.* **4,** 2334–2338 (2013).
9. Ogawa, T., Yanai, N., Monguzzi, A. & Kimizuka, N. Highly Efficient Photon Upconversion in Self-Assembled Light-Harvesting Molecular Systems. *Sci. Rep.* **5,** 10882 (2015).
10. Monguzzi, A., Tubino, R., Hoseinkhani, S., Campione, M. & Meinardi, F. Low power, non-coherent sensitized photon up-conversion: modelling and perspectives. *Phys. Chem. Chem. Phys.* **14,** 4322–4332 (2012).
11. Cheng, Y. Y., Guckel, B., Khoury, T., Clady, R.G.C.R., Tayebjee, M.J.Y., Ekins-Daukes, N.J., Crossley, M.J. & Schmidth, T.W. Kinetic Analysis of Photochemical Upconversion by Triplet-Triplet Annihilation: Beyond Any Spin Statistical Limit. *J. Phys. Chem. Lett.* **1,** 1795–1799 (2010).
12. Yersin, H. Highly efficient OLEDs with phosphorescent materials. (Wiley-VCH, 2008).
13. Singh-Rachford, T. N. & Castellano, F. N. Photon upconversion based on sensitized triplet-triplet annihilation. *Coord. Chem. Rev.* **254,** 2560–2573 (2010).
14. Aydemir, M., Haykir, G., Battal, A., Jankus, V., Sugunan, S.K., Dias, F.B., Al-Attar, H., Turksoy, F., Tavasli, M. & Monkman, A.P. High efficiency OLEDs based on

anthracene derivatives: The impact of electron donating and withdrawing group on the performance of OLED. *ORGELE Org. Electron.* **30,** 149–157 (2016).

15. Monguzzi, A., Tubino, R. & Meinardi, F. Diffusion enhanced upconversion in organic systems. *Int. J. Photoenergy* 684196 (2008). doi:10.1155/2008/684196
16. Schmidt, T. W. & Castellano, F. N. Photochemical Upconversion: The Primacy of Kinetics. *J. Phys. Chem. Lett.* **5,** 4062–4072 (2014).
17. Bachilo, S. M. & Weisman, R. B. Determination of triplet quantum yields from triplet-triplet annihilation fluorescence. *J. Phys. Chem. A* **104,** 7711–7714 (2000).
18. Chandross, E. A. Absorption and Emission Spectra of Anthracene Dimers. *J Chem Phys J. Chem. Phys.* **45,** 3546 (1966).
19. Tsuboi, T. & Tanigawa, M. Optical characteristics of PtOEP and Ir(ppy)(3) triplet-exciton materials for organic electroluminescence devices. *Thin Solid Films* **438,** 301–307 (2003).
20. Pope, M., Swenberg, C. E. & Pope, M. *Electronic processes in organic crystals and polymers*. (Oxford University Press, 1999).
21. Kepler, R., Avakian, P., Caris, J. & Abramson, E. Triplet Excitons and Delayed Fluorescence in Anthracene Crystals. *Phys. Rev. Lett.* **10,** 400 (1963).
22. Jankus, V., Winscom, C. & Monkman, A. P. Dynamics of triplet migration in films of N, N ’-diphenyl-N, N ’-bis(1-naphthyl)-1,1 ’-biphenyl-4,4 -diamine. *J. Phys.-Condens. Matter* **22,** 185802 (2010).
23. Jankus, V., Data, P., Graves, D., McGuinness, C., Santos, J., Bryce, M.R., Dias, F.B & Monkman, A.P. Highly Efficient TADF OLEDs: How the Emitter-Host Interaction Controls Both the Excited State Species and Electrical Properties of the Devices to Achieve Near 100% Triplet Harvesting and High Efficiency. *Adv. Funct. Mater.* **24,** 6178–6186 (2014).
24. Huang, Y. S., Westenhoff, S., Avilov, I., Sreearunothai, P., Hodgkiss, J.M., Deleener, C., Friend, R.H. & Beljonne, D. Electronic structures of interfacial states formed at polymeric semiconductor heterojunctions. *Nat. Mater.* **7,** 483–489 (2008).

CHAPTER 8: STUDY OF INTRAMOLECULAR CHARGE TRANSFER STATE PROPERTIES OF NOVEL D-A-D PYRIDINE DERIVATIVES: THE EFFECTS OF TEMPERATURE AND ENVIRONMENT UPON MOLECULAR CONFIGURATION AND THE ORIGIN OF DELAYED FLUORESCENCE

This chapter has been published as:

Murat Aydemir,* Gulcin Haykir, Figen Turksoy, Selcuk Gumus, Fernando B. Dias, Andrew P. Monkman, "Synthesis and investigation of intra-molecular charge transfer state properties of novel donor-acceptor-donor pyridine derivatives: The effects of temperature and environment upon molecular configurations and the origin of delayed fluorescence" Phys. Chem. Chem. Phys., **2015**, 17, 25572

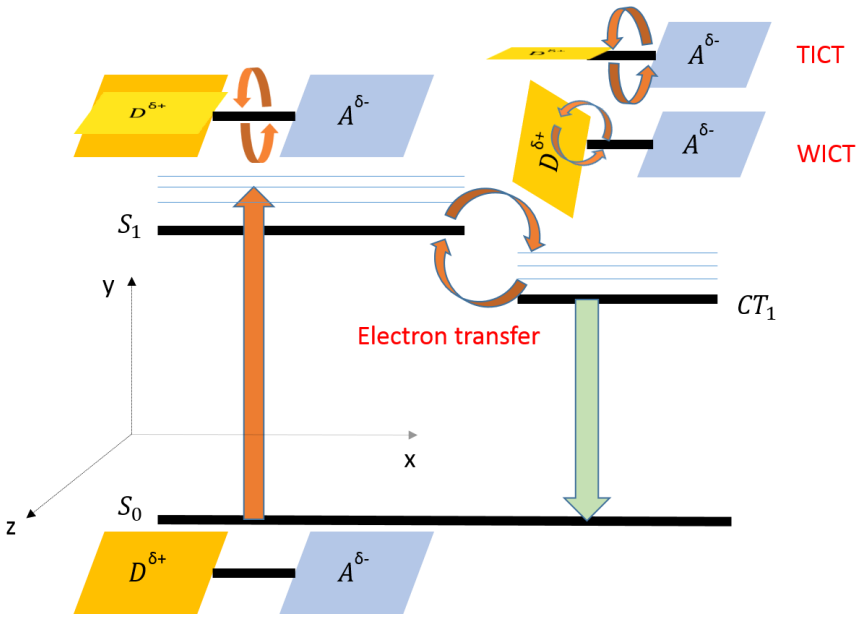

Figure 8.1 The diagram represents the relative configurations of donor ($D^{\delta+}$) and acceptor ($A^{\delta-}$) moieties of molecules both in ground and excited states. The molecular configurations behind the formation of twisted intramolecular charge transfer (TICT) state is represented as perpendicular orientation (yz-axis) of $D^{\delta+}$ moiety relative to the $A^{\delta-}$ moiety. In addition, the molecular configurations behind the formation of wagged intramolecular charge transfer (WICT) state are represented as a folding of the $D^{\delta+}$ moiety (xy-

axis) relative to the $A^{\delta-}$ moiety. As a result of final configuration of the molecules, the photoluminescence is emitted from newly formed charge transfer states. More details will be given in the text.

The focus of this chapter is mainly concerned with an investigation of photo-physical properties of donor-acceptor-donor type novel pyridine derivatives. The purpose of choosing these molecules is to understand the charge transfer properties in different donor-acceptor systems in which the formation of intramolecular charge transfer (ICT) states are highly favoured. The formation of ICT states is one of the desirable features from newly engineered molecular structures due to their potential roles in high efficiency OLEDs. The chapter is designed around two of the novel ICT emitters and the results are discussed considering their particular excited state molecular configurations in solutions and solid-films.

8.1 Introduction

8.1.1 An overview on general and specific solvent effects on fluorescence

In general, the emission spectra of polar fluorophores is strongly affected by solvent polarity, typically more polar solvents shift the spectra to longer wavelengths as well as the shape of the spectra becomes broadened and unstructured. However, the interpretation of spectral shifts is quite complicated which may arise from; i) a general effect of solvent polarity ii) specific solvent-solute interactions or iii) charge distribution in the excited state.[1] In the first case, upon excitation, the fluorophores are excited to Franck Condon state and the solvent dipoles relax and reorient themselves in the vicinity of the excited state dipoles of the polar fluorophores (not in non-polar fluorophores), which can be understood as the solvation giving rise to change in dipole moments of the ground (μ_g) and excited (μ_e) states (typically $\mu_e > \mu_g$). The degree of change in dipole moments depend on the nature of the solvent, and the outcome is a red-shifted emission spectra due to this solvent reorientation. This effect can be understood as the stabilization of excited states by the solvent molecules. As the solvent polarity is increased, the energy of the excited state is decreased, and the spectra shifts remarkably. These solvent-dependent

effects on the emission spectra can quantitatively be interpreted using with well-known Lippert equation (see Eq. 8.1)[1] which shows how the Stokes shift changes as a function of solvent (dielectric constant, ε, and refractive index, n) and solute parameters (μ_E, μ_G, and a is the radius of cavity in which the fluorophore resides in a sphere or ellipse). This formula is valid to interpret the general solvent polarity effects in terms of dipole moment changes and does not account for specific solvent effects, i.e. hydrogen bonding, charge transfer interactions or conformational changes, therefore, importantly solvent cavity radius is usually assumed unchanged during the excitation, whereas, any specific solvent effects can easily change the spherical shape as well as the radius.

$$\boldsymbol{v_A - v_F = \frac{2(\mu_e - \mu_g)^2}{hca^3}\left(\frac{\varepsilon - 1}{2\varepsilon + 1} - \frac{n^2 - 1}{2n^2 + 1}\right) + constant} \qquad \textbf{(8.1)}$$

here v_A and v_F are the wavenumbers (cm^{-1}) of the absorption and emission band maxima, respectively. The difference between the peak positions of absorption and the emission spectra represent the magnitude of Stokes shift. h is the Planck constant and the speed of light is represented with c, where the values are considered in vacuum. According to Eq. 8.1, the difference between the absorption and the emission maximum in wavenumbers is correlated with the solvent parameters, which is referred to as the orientation polarizability (Δf) of the solvent,

$$\boldsymbol{\Delta f = f(\varepsilon) - f(n) = \frac{\varepsilon - 1}{2\varepsilon + 1} - \frac{n^2 - 1}{2n^2 + 1}} \qquad \textbf{(8.2)}$$

in Eq. 8.2, the first term is assigned as the low frequency polarizability, which is a function of dielectric constant (ε) of the solvent indicating a slow process of the orientational motion of the solvent dipoles around the excited state[2] and also an instantaneous process of electron redistribution in the solvent molecules. However, the second term of the Eq. 8.2. is the high frequency polarizability term of solvent which is a

function of refractive index (n) indicating an instantaneous process of electron distribution. The constant in Eq. 8.1 is used due to the possibility of $\Delta f \sim 0$, in this case, weakly coinciding absorption and the emission spectra giving rise to a very small Stokes shift. Consequentially, general solvent effects can be estimated using a Lippert plot where the Stoke shift (cm^{-1}) is plotted against Δf, from which the difference in dipole moments can be calculated from the slope of the plot showing an estimated value for the solvent sensitivity of fluorophores. High values mean large dipole moment separation between the ground and excited states. Furthermore, a linear slope shows evidence that general solvent effects are the main reason for spectral shifts, and the deviations from linearity show that specific solvent effects can make contribution upon spectral shifts.[1,3] Usually, the specific solvent interaction arises due to structural interactions between the solvent and the fluorophore, i.e. formation of hydrogen bonding, in this case the percentage of polar solvent in a polar/ non-polar solvent mixture helps to determine the specific solvent effects. In such a system, the trend is that once the percentage of polar solvent increases, the spectra shows a proportional shift (even for very low polar solvent concentrations) to longer wavelengths and when the solvent becomes totally polar then a wholly new red-shifted spectra dominates the system. From which it can be assumed that specific solvent interactions are involved and can be determined from the Lippert plot where large Stokes shifts occur in some particular protic solvents (water, ethanol, etc.).[1]

It is known that specific solvent interactions may also occur in ground state of the fluorophore (i.e. formation of H-bonding), in this case, the absorption spectra includes evidence such as spectral red-shift and loss of structural shape. Furthermore, strong Stokes shift in polar solvents may also arise from charge transition and the high magnitudes of the Stoke shift suggests that the geometry of the excited state may be different from that of the ground state indicating the formation of intramolecular charge transfer (ICT) state or twisted intramolecular charge transfer [4] state favourably arises in donor-acceptor type structured fluorophores (probes). The formation of CT states depends on the fluorophore structure and orientation of the solvent molecules resulting from significant charge transfer from donor to acceptor moieties that give rise to a higher excited state dipole moment than the ground state.

8.1.2 Temperature effect on solvent

The significant effect of temperature on solvents is viscosity change which is directly associated with the solvent reorientation time. In general, the viscosity of solvent increases with decreasing temperatures which decelerates the solvent reorientation and increases the required time for full reorganization. Considering this temperature effect on solvent, the origin of emission can easily be determined as from relaxed or unrelaxed excited states.

8.1.3 TICT state and dual fluorescence phenomena

One of the unique properties of TICT molecules is to observe dual fluorescence bands arising from relaxed (long-wavelength band) and unrelaxed (short–wavelength band) states which were attributed to TICT and locally excited (LE) states, respectively.[2] The very first findings on dual fluorescence bands were introduced with a simple donor-acceptor molecule (4,N,N-dimethylaminobenzonitrile, DMABN) by Lippert e*t al*.[5] then Grabowski *et al.*[6] accounted for formation of TICT state in polar solvents by means of photoinduced electron transfer from the donor (D) through the acceptor (A) fragments where the interaction of the donor and acceptor molecules is required for efficient electron transfer, i.e. as happens in adiabatic photoinduced electron transfer reactions, which then are often accompanied by structural reorganizations to form a new stabilized dipolar state showing sensitivity to environmental factors including solvent polarity, viscosity and specific solvent interactions, i.e. H-bonding.[7] By this structural reorganization, the HOMO-LUMO are spatially separated from each other by means of relative foldings of the $D^{\delta+}$ and $A^{\delta-}$ moieties at a twist angle of 90^0 giving rise to nearly full induced charge transfer from D (HOMO) to A (LUMO) moieties.[8] In addition, orthogonally positioned π-orbitals result in decoupling (zero overlapping) of the conjugated system that localizes the charge separation and increase the lifetime of the TICT state where the dipole moment of the excited state shows the highest value, whereas, the ground state becomes minimum.

The TICT state has a totally new electronic structure and molecular geometry comparing with the parent ground states. In principle, oppositely charged radical ions can inherently come close together (as a result of coulomb attractions), termed the '*harpooning effect'* which particularly happens between flexibly single bonded donor-acceptor moieties,[9,10] and is accompanied by conformational changes to form a dipolar ICT state, as reported previously either in high-polarity solvents and rigid environments.[11,12] If the D-A fragments are bound by only one C-C single bond, the relative conformational folding between $D^{\delta+}$ and $A^{\delta-}$ units is precluded because of the limited degree of vibrational movement in space giving rise to a torque and internal rotational relaxation around the central C-C bond and concomitantly the relaxed excited (intramolecular charge transfer, ICT) state molecular geometry is shaped by relative orientation of the $D^{\delta+}$ fragment around the $A^{\delta-}$, i.e. twisting, pyramidisation (wagging), bending or planarization.[13] The precursor of the TICT state is observed by dual fluorescence where the molecules emit from two species (typically LE and TICT states) possessing a mother-daugher relationship. The existence of TICT states can be distinguished from the LE state in the emission spectra by repeating the measurements in variety of solvents with different polarities and viscosities. Typically, at room temperature (RT), the emission spectra of the LE state is vibronically structured at shorter wavelengths in non-polar solvents, however, once the solvent temperature is decreased (so the viscosity of the solvent is increased), the spectra of LE state loses the structured shape and shiftes to longer wavelengths. During this period of time it is likely to observe dual fluorescence at different viscosities which can be in thermal equilibrium. Dual emission is not always observed in TICT singlet state and is dependent on the competition between all the rates involved in different solvents.[14] However, in polar solvents, the formation of TICT state is strongly favoured, however the nature of emitting species and their viscosity dependences are quite complex, for instance, the specific solvent-solute interactions may affect the nature of excited-state charge distribution.[15] In the ground state of TICT molecules may exhibit particular structural reorganizations (twisted, wagged, etc.), in this case, the emission spectra of the excited state becomes red-shifted and unstructured and any changes in viscosity of solvent may also result in viscocity-dependent spectral shifts. If the ground state is planar, then the appearance of

unstructured excited state emission spectra takes some time due to structural reorganization of the molecule and grows in relative intensity, while the intensity of the LE band decreases with increasing solvent polarity and viscosity.

8.1.4 The molecular structures of pyridine derivatives

Here, engineered donor-acceptor-donor (D-A-D) type novel pyridine derivatives were designed geometrically with the same bent structures and having the same electron acceptor core at central position, with two cyanine groups on the opposite sides of pyridine unit, and two arms built of different electron-donating groups (see Fig. 8.2.) such as anthracene (5a, 685.81 g/mol) and triphenylamine (5b, 819.99 g/mol). More details on synthesis part of the molecules can be found elsewhere.[16]

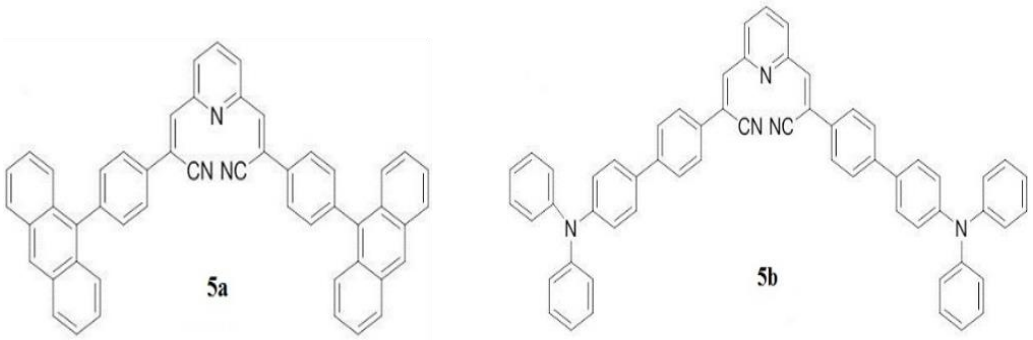

Figure 8.2 Molecular structures of pyridine derivatives

8.2 Experimental

Absorption and emission spectra were collected using UV-3600 double beam spectrometer (Shimadzu), and Fluoromax amd Fluorolog fluorescence spectrometers (Jobin Yvon). All solvatochromic measurements were taken in air saturated solutions (ranging 10^{-5} M to 10^{-6} M) using 1cm depth quartz cuvettes, and degassed solutions using

3 pump-freeze-thaw cycles in a long necked quartz degassing cuvette and a liquid nitrogen cryostat (Janis Research) were used. Quantum yields were determined in chlorobenzene in comparison with a standard diphenylanthracene (DPA). Solid film measurements were done by means of preparing spin-coated films from 15 mg/ml stock solutions (500 rpm for 30 sec conditions). Time-resolved nanosecond gated luminescence measurements were performed by the same method as explained in detail in Chapter 3. The energy per pulse was chosen in the range of 80-100 μJ. All solid film measurements were performed under a dynamical vacuum of $<10^{-4}$ Torr using a displex helium cryostat.

Picosecond time-resolved fluorescence decays (TCSPC) were collected using the time-correlated single photon counting technique (impulse response function, IRF: 21 and 26 ps due to taken the experiments in different times). Vertically polarized picosecond Ti:sapphire laser (Coherent) was used as an excitation source and the excitation wavelength was 402 nm, and the emission was collected using a polarizer at magic angle (54^0), and the detection was made by a double monochromator (Acton Research Corporation) which was coupled with micro channel plate photomultiplier tube (Hamamatsu R3809U-50).

8.3 Results and Discussion

8.3.1 Lippert plots of pyridine derivatives in variety of solvents

The solvent sensitivity of each materials is estimated from the Lippert plots which are plots of Stokes shifts ($\upsilon_A - \upsilon_F$) versus orientation polarizability (Δf). Then difference in dipole moments of ground and excited states ($\mu_e - \mu_g$) can be estimated using the slope of the plots which is equal to,

$$\frac{\mathbf{2}(\mu_\mathbf{e} - \mu_\mathbf{g})^\mathbf{2}}{\mathbf{hca^3}} \qquad \textbf{(8.3)}$$

where μ_e , μ_g are the dipole moments of the excited and ground state, respectively. h is the Planck constant and c is the speed of light in vacuum, considering the difference of absorption and emission maxima in cm^{-1}, then h and c values are considered as 6.626 x 10^{-27} erg.s and 2.9979 x 10^{10} cm s^{-1}, respectively. Different values of dipole moments may result from different assumptions regarding to the cavity radius (a) which was calculated in here using mass-density equation (Eq. 8.4)[17] to give more insight into the dipole moment differences,

$$\mathbf{a} = \sqrt[3]{\frac{\mathbf{3M}}{\mathbf{4\pi\rho N_A}}} \qquad \mathbf{(8.4)}$$

where M is the molecular weight of the molecules, ρ (g/cm^3) is the number of density of solute molecules and N_A is the Avogadro number. The Lippert plots are represented in Fig. 8.3 for each molecules (5a and 5b), plotting the Stokes shift values against the orientation polarizability values and the results are given in Table 8.1-2.

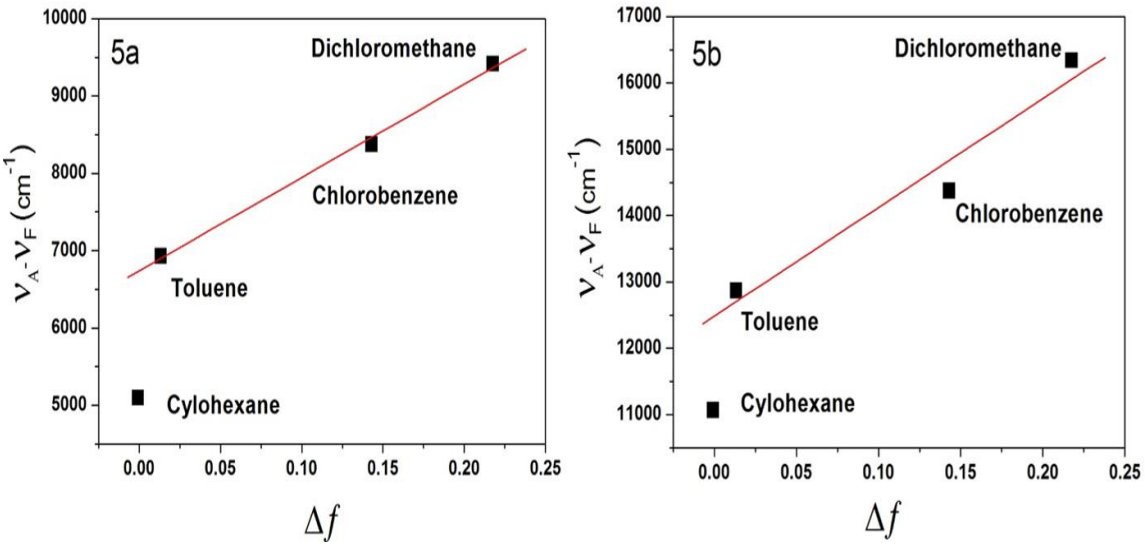

Figure 8.3 Lippert plots of the molecules in variety of solvents.

The orientation polarizability values were calculated using Eq.8.2 as -0.0008 for cyclohexane, 0.0133 for toluene, 0.0143 for chlorobenzene and 0.2175 for dichloromethane. The small negative values of orientational values can safely be ignored,[1] i.e. -0.0008 for cyclohexane. It is important to say that all these measurements were taken at RT. In Table 8.1, the absorption and emission maxima along with the Stokes shifts of 5a are represented in the range of solvents with varying polarity. These solvents are cyclohexane, toluene, chlorobenzene and dichloromethane which have different refractive indexes and dielectric constants. In these solvents, very little (ignorable) solvatochromism is observed in absorption spectra, implying that the ground state energy distribution is not significantly affected which is probably due to less polar nature of the 5a molecule in its ground state rather than excited state, whereas, the emission spectra is considerably red-shifted upon increasing polarity (the Stokes shift *ca*. 9420 cm^{-1} in dichloromethane) and broadened (see Fig. 8.4) suggesting the excited state geometry could be different from that of the ground state.

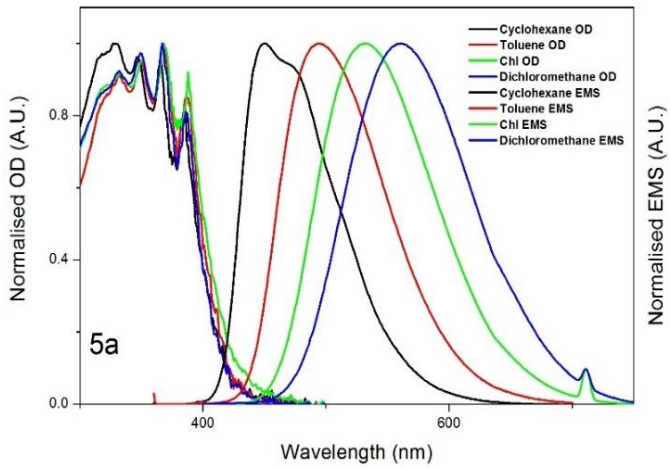

Figure 8.4 The absorption and emission spectra of 5a in different polarity of solvents, i.e. cyclohexane, toluene, chlorobenzene and dichloromethane. The concentrations were in the range of 1.0-5.0 E-6 M.

The pronounced shift in the emission spectra clearly indicates that the dipole moment of the excited state is larger than the ground state. Also, the large values of Stokes shift is an indication of the charge transfer transitions. The general concluding remark is

that there is a trend where the Stokes shift increases with increasing polarity suggesting an increase in the dipole moment on excitation which was estimated from Lippert plot. The regression coefficient (χ^2) was found to be ~1 showing satisfactory correlation among the data points which means the experimental observations are reliable. From the slope of Lippert plot (11321.5 ± 730) cm^{-1}) the difference in excited and ground state dipole moments were estimated as 7.36 D and the assumption made on cavity radius as 3.56 Å (see Table 8.1).

Table 8.1 The refractive index, the dielectric constants of cyclohexane, toluene, chlorobenzene and dichloromethane. From which the orientation polarizability values were determined for each solvents. From the Lippert plot of 5a molecule, the value of slope and correlation coefficient (χ^2) were determined which help to estimate the difference in excited and ground state dipole moments. The cavity radius ($\boldsymbol{a}$) is theoretically estimated from Eq. 8.4.

5a	$\boldsymbol{n}$	**ε**	$\boldsymbol{\nu_A}$ **(cm^{-1})**	$\boldsymbol{\nu_A - \nu_F}$ **(cm^{-1})**	$\Delta \boldsymbol{f}$	$\boldsymbol{a}$ **(Å)**	**Slope (cm^{-1})**	$\boldsymbol{\chi^2}$	$\mu_e - \mu_g$ **(D)**
Cyclohexane	**1.4262**	**2.02**	**27322**	**5100**	**-0.0008**	**3.56 ± 0.28**	**11321.5 ± 730**	**0.99**	**7.36**
Toluene	**1.4969**	**2.38**	**27173**	**6931**	**0.013**				
Chlorobenzene	**1.5248**	**5.62**	**27173**	**8376**	**0.143**				
Dichloromethane	**1.4242**	**8.93**	**27242**	**9417**	**0.218**				

Table 8.2 The refractive index, the dielectric constants of cyclohexane, toluene, chlorobenzene and dichloromethane. From which the orientation polarizability values were determined for each solvents. From the Lippert plot of 5b molecule, the value of slope and correlation coefficient (χ^2) were determined which help to estimate the difference in excited and ground state dipole moments. The cavity radius ($\boldsymbol{a}$) is theoretically estimated from Eq. 8.4

5b	$\boldsymbol{n}$	**ε**	$\boldsymbol{\nu_A}$ **(cm^{-1})**	$\boldsymbol{\nu_A - \nu_F}$ **(cm^{-1})**	$\Delta \boldsymbol{f}$	$\boldsymbol{a}$ **(Å)**	**Slope (cm^{-1})**	$\boldsymbol{\chi^2}$	$\mu_e - \mu_g$ **(D)**
Cyclohexane	**1.4262**	**2.02**	**32573**	**11067**	**-0.0008**	**3.78 ± 0.3**	**14390.4± 3850**	**0.97**	**9.39**
Toluene	**1.4969**	**2.38**	**32362**	**12869**	**0.013**				
Chlorobenzene	**1.5248**	**5.62**	**31948**	**14374**	**0.143**				
Dichloromethane	**1.4242**	**8.93**	**32679**	**16339**	**0.218**				

In Table 8.2, the absorption and emission maxima along with the Stokes shifts of molecule 5b are represented in the range of solvents with varying polarity which are cyclohexane, toluene, chlorobenzene and dichloromethane. In these solvents, very little (ignorable) solvatochromism is observed in absorption spectra, whereas, the emission spectra is considerably red-shifted (the Stokes shift *ca*. 16340 cm^{-1} in dichloromethane) and broadened (see Fig. 8.5), the larger Stokes shift values of 5b indicates there is a larger charge separation than 5a along the molecular long axis in the excited state and suggesting the excited state geometry could be different from that of the ground state and formation of and an ICT state is much favoured rather than only being the general solvent polarity effect on spectra. The effects of formation of TICT or pyramidal distortion (WICT) state are not accounted for in the theory of general solvent effects described by the Lippert

equation (Eq. 8.1). The regression coefficient (χ^2) was found to be ~1 showing satisfactory correlation among the data points, which show evidence of the dominating role of general solvent effects, however, it does not include the viscosity effects on excited state geometry. From the slope of Lippert plot (14390.4 ± 3850 cm^{-1}) the difference in excited and ground state dipole moments were estimated as 9.39 D and the assumption made on cavity radius as 3.78 Å.

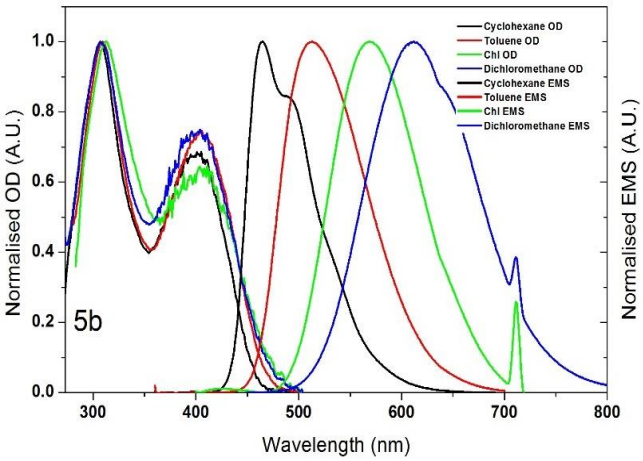

Figure 8.5 The absorption and emission spectra of 5b in different polarity of solvents, i.e. cyclohexane, toluene, chlorobenzene and dichloromethane. The concentrations were in the range of 1.0-5.0 10^{-6} M.

Comparing with the 5a material, the substitution of triphenylamine group by anthracene group further red-shifts the emission spectra and the strong electron donating effect of the triphenylamine groups results in a larger difference between the dipole moments of the ground and excited states at RT. The negligible Stokes shift in absorption spectra with increasing solvent polarities (non-polar cyclohexane to polar dichloromethane) is consistent with a small difference between the dipole moments of the Franck-Condon excited and ground states. Therefore, it can be surmised that the absorption spectra of each molecules arises totally within the cyano acceptor group (A), whereas, the emission spectra arises from the charge separated species ($D^{\delta+}$ and $A^{\delta-}$) showing the solvent polarity dependent behaviour clearly indicate that solvent-solute interactions stabilise the intramolecular charge transfer (ICT) excited-state, yielding a dipole moment, in the ICT excited-state, that is larger than that in the ground state. And

larger value of $(\mu_e - \mu_g)$ in 5b materials indicates that triphenylamine donor group has stronger charge transfer abilities, and also the largest positive solvatochromic shift is typically associated with the material that has the strongest ICT character.

8.3.2 Temperature dependence (thermochromism) of emission in MCH

The steady-state fluorescence spectra of 5a and 5b were collected as a function of temperature (see in Fig 8.6) in non-polar (MCH) solvent in the range from 295- 90 K. In MCH, at RT, a clear well-structured emission characteristic of an excitonic locally excited (LE) state emission was observed where the onset was *ca.* 412 nm; as the temperature was lowered from 295 K to 90 K, a gradually loss of the resolved fluorescence band was observed and the emission onset shifted to *ca.* 440 nm at the same time an unstructured and red-shifted emission band arose originating from a newly formed state (not originating from possible aggregations)[16] indicative of '*charge transfer'* characteristics. With the clear appearance of dual fluorescence at lower temperatures (~170 K) a considerable intensity roll-off of the LE emission (comparing with the intensity of LE emission at ~195 K) and the appearance of a kinetically linked the second CT-type emission band. This effect was ascribed to be caused primarily by a decreasing vibrational excitation of the molecule which otherwise destabilises the twisted geometry between donor and acceptor units preventing ICT formation.

In MCH, the ground state conformation of the molecules is 'twisted', i.e. twisted molecular configuration of the anthracene moiety (5a) and pyramidal distortion ('*wagged'*) molecular configuration of triphenylamine moiety (5b) with respect to the neighbouring phenyl ring as obviously seen from the charge distribution graphs (see Fig. 8.7).[16] At 295 K, the solvent viscosity and polarity are not sufficient to stabilise this twisted configuration, therefore, the thermal fluctuations about the centre of the C-C single bond give rise to a planar molecule configuration in the excited state causing the fluorescence to be emitted only from the (planar) locally excited state (LE). However, as the temperature of the solvent decreases, the ground state molecular structure is stabilised by increasing solvent viscosity and decreasing temperature, and the conformation is stabilised due to the stiffening of the active intramolecular rotations and vibrations around

the centre of the C-C single-bond of the $D^{\delta+}$ groups (anthracene and triphenylamine) to retain the twisted/wagged geometry. It can be seen in the emission spectra (Fig 8.6), that the ICT band does not further relax (to lower energy) with decreasing temperature, the peak positions are energetically stabilized after certain temperatures and show peak-to-peak red-shift from 295 K to 95K which are ca. 0.20 eV for 5a and 0.48 eV for 5b. This is a very important observation which is ascribed to the fact that the solvent is non-polar such that even as the temperature is decreased no significant increase in polarity is achieved, and so, no solvent induced relaxation of the ICT state occurred, thus the ICT in the initial ground state geometry of the molecules. This reveals the subtle role played by the solvent environment in conjugation *versus* a twisted broken conjugation geometry.

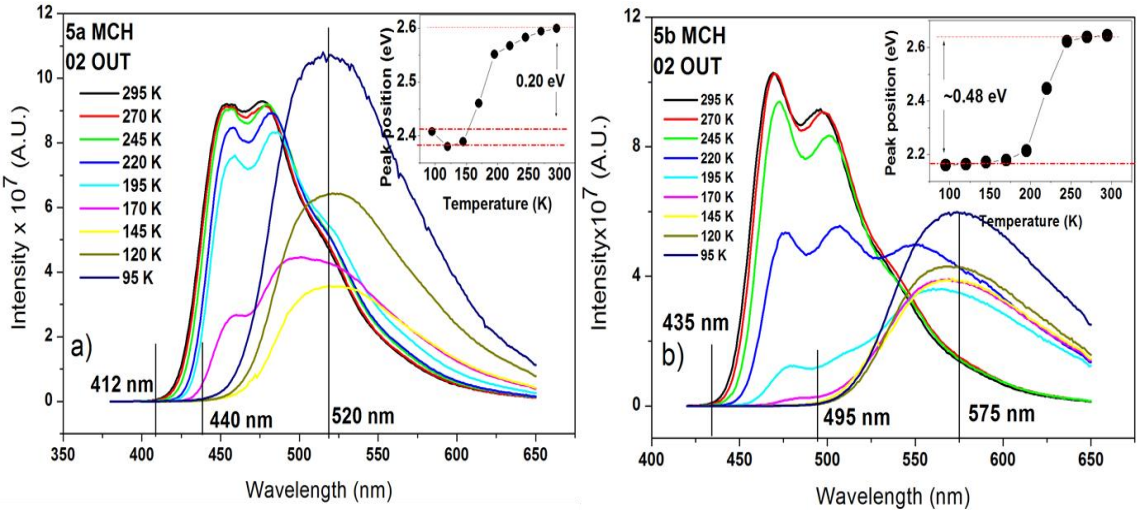

Figure 8.6 a) Temperature dependence of steady-state corrected phototoluminescence spectra in MCH **a)** 5a **b)** 5b. The isnet graphs show the change in energy peak position as a function of temperature. The energy change can be given from 295K to 90K is ~0.200 eV for 5a and for ~0.48 eV for 5b

Theoretically, if the linkage between the decoupled moieties is only one single covalent bond, then the relative conformational folding between $D^{\delta+}$ and $A^{\delta-}$ units is precluded because of limited degree of freedom in space, therefore, the internal rotational relaxations around the central bond are favored and concomitantly the $D^{\delta+}$ moiety takes an out of plane position with respect to the $A^{\delta-}$ moiety which results in a change in the electronic distribution by means of forming a relaxed excited state.[13] However, once the

temperature drops below the glass transition of MCH (<135 K), the rigid nature of matrix prevents any donor rotations around the single bond of phenyl ring which gives rise to complete disappearance of LE fluorescence band (collapse of the LE band as a function of temperature), thus, the fluorescence only originates from the TICT excited-state for 5a and from WICT excited state for 5b which can be considered as a final retention of twisted/wagged ground state conformation of molecules.

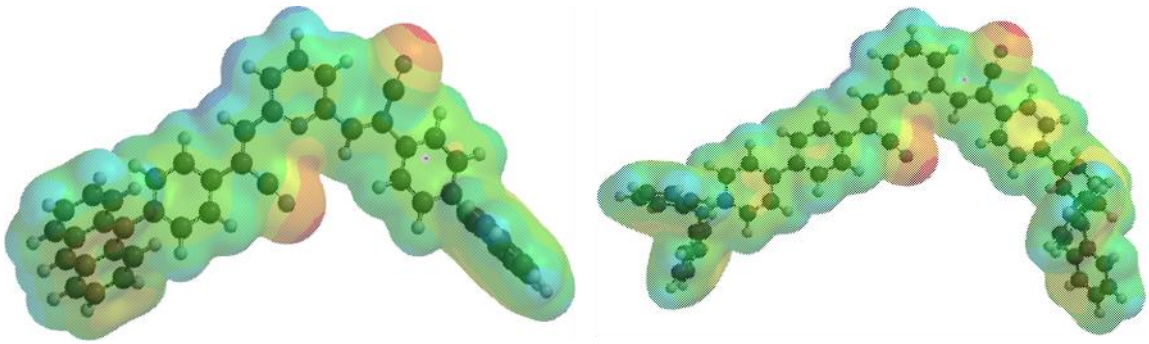

Figure 8.7 Charge distribution graphs for 5a and 5b showing perpendicularly positioned anthracene unit (5a) and pyramidal distortion (wagged) conformation of triphenylamine unit (5b) with respect to the phenyl ring. Adapted from Ref.[16]

8.3.3 Temperature dependence (thermochromism) of emission in 2-MeTHF

In order to better understand the strong thermochromism of the ICT fluorescence, the measurements were repeated in 2-methyltetrahydrofuran (2-MeTHF) solvent in the temperature range of 295K-95 K (see. Fig. 8.8). From the steady-state measurements in 2-MeTHF solution it was clear that the thermochromic red shift and associated decreasing quantum yield (also there was not significant triplet contribution to the ICT state, see Table 8.4) occur with decreasing temperature, indicative of further relaxation of the excited-state geometric distortion and increased charge transfer strength as the temperature decreases. The fluorescence spectrum red-shifts through the glass transition temperature (~135 K), and nearly covers the whole visible region, in this case the

fluorescence has taken place after full solvent-relaxation, but then, upon cooling the temperature further (<135 K) the spectra start shifting to the blue again (see in Fig 8.8). The peak-to-peak positions show dramatical change in energy which are 0.38 eV for 5a and 0.36 eV for 5b molecule and onset-to-onset shifts are ~40 nm.

Below 135 K, intramolecular rotations about the single C-C bond are inhibited because of the increasing rigidity of the 2-MeTHF matrix environment. At low temperatures the solvent shows high viscosity and there is less thermal activation of molecular vibrations which plays a significant role on solvation dynamics. Once the solvent freezes (e.g. at 90 K), a very large blue-shifted fluorescence peak is observed (*ca.* 478 nm for 5a and *ca.* 520 nm for 5b) however, the band is still a unstructured Gaussian shape (to the red of the LE band seen in MCH) and so this is ascribed as a 'blue band' characteristic of the non-relaxed ICT state, in a rigid polar environment, corresponding to that seen in MCH at low temperature. These findings are in agreement with previous reports of 2-MeTHF solvent relaxation dynamics,[19–21] where a similar fluorescence behaviour trend upon decreasing temperatures were reported.

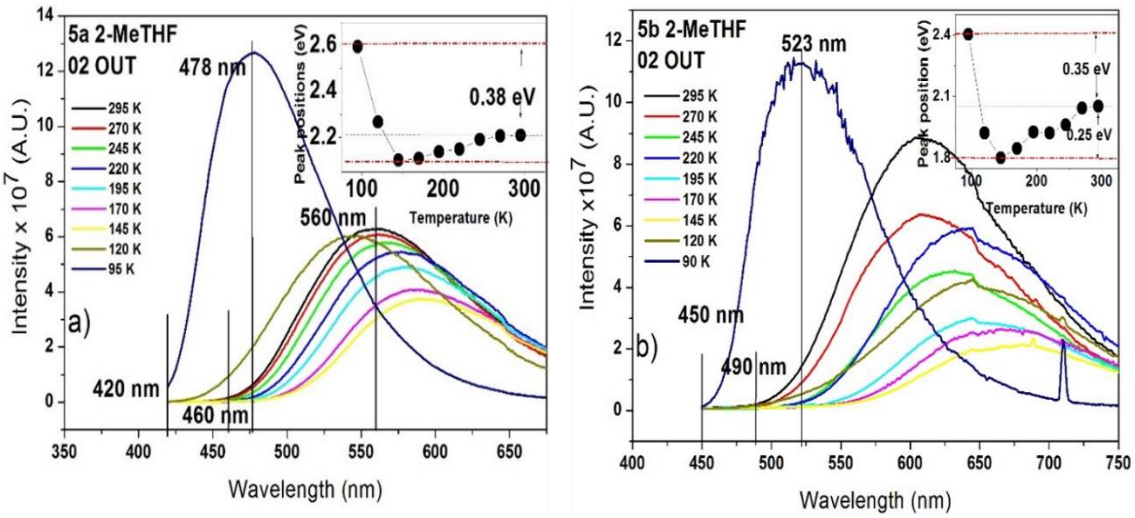

Figure 8.8 a) Temperature dependence of steady-state corrected phototoluminescence spectra in 2-MeTHF **a)** 5a **b)** 5b

The general conclusion from all this work is that the temperature has significant effect on the '*polarity and polarizability'* of 2-MeTHF solvent in the vicinity of solute, which results in decreasing '*permittivity*' of solvent as reported by Kawski *et al.*[22] In principle, the existence of dipoles in the solute give rise to charge orientations of solvent molecules in the vicinity of solute which appears as the ICT excited-state dipole moment reorientation (generally rotational relaxations) of the solvent dipoles giving rise to an increase in effective solvent polarity and a greater degree of charge stabilisation in the solute molecule, and this effect will be more enhanced as the temperature decreases.[20] According to Gorlach *et al*.[19] if the solvent reorientation occurs on a time scale which is comparatively as fast as the fluorescence lifetime of solute, then it is possible to observe gradually red-shifted fluorescence maxima (thermochromic shift) upon decreasing temperatures, therefore, between the fluid and glass temperature regime the spectra of these molecules show gradual thermochromic shift. However, once the temperature is lowered below 135 K, the thermochromic shift decreases due to the slowing of the re-orientation of the solvent molecules in the vicinity of the ICT excited-state dipole as the motion of the solvent molecules is slowed in the rapidly increasing viscous solvent shell. Below the freezing point, the solvent molecules can no longer reorient and the fluorescence 'dramatically' blue-shifts to the energy of the non-relaxed ICT state. The effect should also been observed by time dependent Stokes shift as measuring an increase in solvent (2-MeTHF) relaxation time from nanosecond range (>135 K) to seconds (<135 K, e.g. at 90 K).[19]

8.3.4 The ground and excited state geometry of films

In addition, photo physical investigations were also made in a rigid host matrix to understand the ground-state conformations of the molecules in the solid-state phase. Steady-state measurements were taken at RT using spin-coated films (including 10% CBP host material, see Fig.8.9). In such a rigid matrix, the molecules do not have rotational degrees of freedom, therefore, possible corresponding rotations about the C-C bond will be prevented, and the emission spectrum should not exhibit the effect of significant structural reorganisation. Spectra confirm that the ground-state conformations

of the solid-state phases have twisted/wagged geometry as the emission peak positions (*ca.* 524 nm for 5a and *ca.* 580 nm for 5b) are in very good agreement with the emission positions of the ICT excited-state observed in the rigid MCH matrix (*ca*. 520 nm for 5a and *ca.*575 nm for 5b) at 90 K. The solid-state spectra also only showed slight temperature dependent behaviour (slightly red-shifted) comparing at RT and 25 K again confirming no increased structural relaxation as a function of decreasing temperature, as will be represented in time-resolved spectroscopy measurements section below.

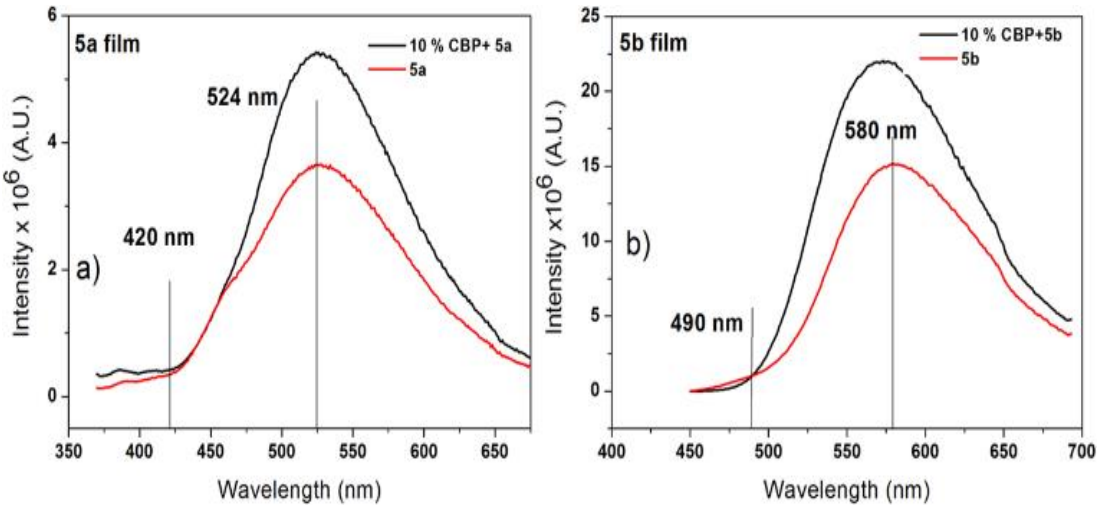

Figure 8.9 The steady state spectra of spin-coated film including 10 % CBP host material a)**5a** b) **5b**

8.3.5 The fluorescence lifetimes of LE and ICT states

In 2-MeTHF, the twisted excited state can be stabilized with respect to a planar local excited state, hence, the emission spectrum shows strongly red-shifted and broadened fluorescence which arises from excited-states of the molecules having strong charge transfer character. The fluorescence lifetimes were measured (see Fig 8.10) by time correlated single photon counting (TCSPC) method for 5a and 5b under varying conditions (in MCH and 2-MeTHF) to assess the relative importance of solvent polarity on the fluorescence decays. The molecules in MCH solution were excited at 368 nm and the emission from the LE state was collected at 450 nm and 475 nm for 5a molecule and 470 nm and 500 nm for 5b molecules. The LE emission of molecules shows biexponential

decay components, one long lasting and one fast decay (Table 8.3). The large lifetime differences between the two components indicate that they are of different origin. The long lasting component (~9 ns for 5a and ~5.5 ns for 5b) corresponding to the LE emission and the fast components (~ 0.1 ns for both of the molecules) may result from partially twisted geometry of the molecules giving rise to a fast non-radiative decay channel.

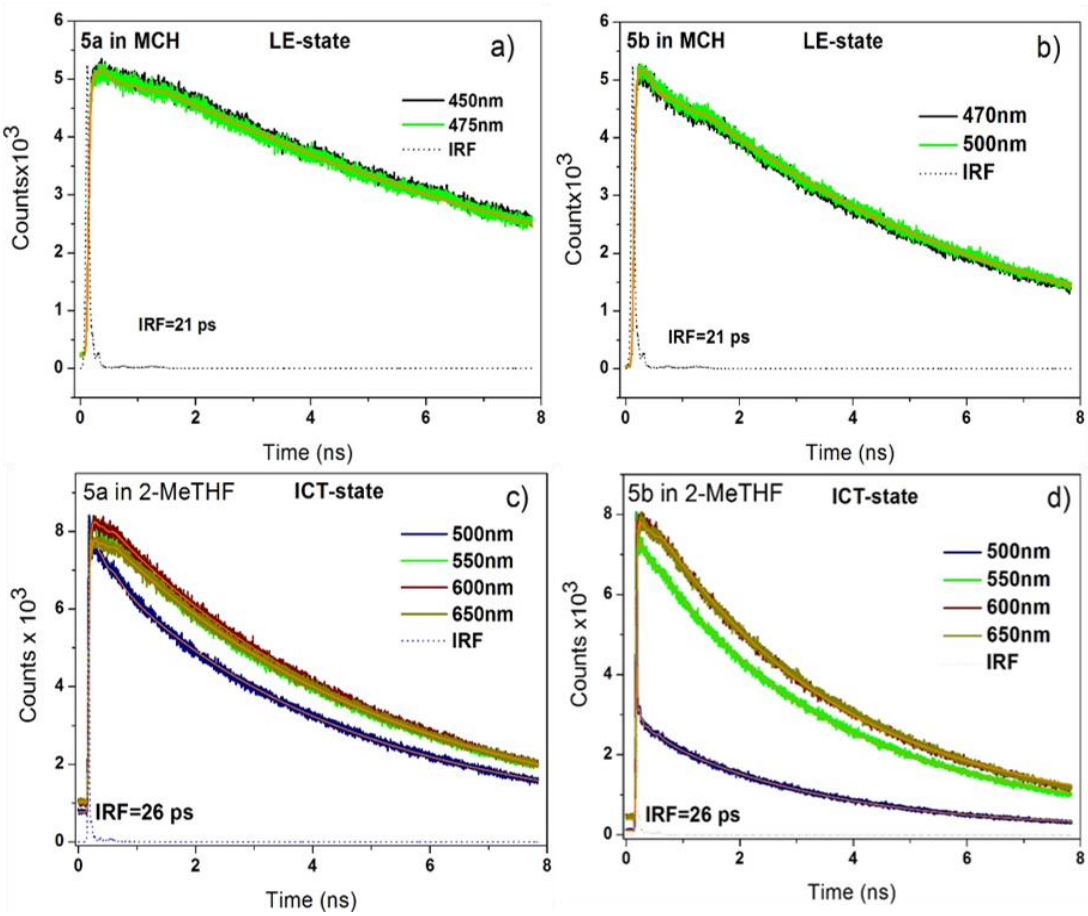

Figure 8.10 The fluorescence lifetime decays were collected by using single photon counting technique at different wavelength positions in degassed MCH (**a** and **c**) and 2-MeTHF solutions (**c** and **d**) at RT. The Orange segmented lines are exponential fits

Table 8.3 The fluorescence decay dynamics of LE state were recorded in degassed MCH solution

Materials in MCH **LE-state dynamics**	**λ_{ex}=368 nm**	
	450 nm	**475 nm**
5a	**τ_1=9.02 ns** **A1=0.18** **τ_2=0.094 ns** **A2=0.04** **χ^2= 1.1**	**τ_1=8.98 ns** **A1=0.18** **τ_2=0.16 ns** **A2=0.028** **χ^2= 1.18**
	470 nm	**500 nm**
5b	**τ_1=5.52 ns** **A1=0.24** **τ_2=0.13 ns** **A2=0.059** **χ^2= 1.1**	**τ_1=5.57 ns** **A1=0.24** **τ_2=0.12 ns** **A2=0.065** **χ^2= 1.09**

The ICT lifetimes of molecules were measured in 2-MeTHF solution exciting at 402 nm and the emission was collected at 500 to 650 nm for both molecules and the results are represented in Table 8.4. Obviously the fluorescence decay of molecules in a polar environment has a different nature due to the difference in arrangement of molecular geometries. The measurements clearly indicate that the lifetimes of ICT excited state have reduced significantly comparing the lifetime decays in MCH which is expected behaviour from ICT excited state decaying faster than the LE state,[23] and also the quantum yields show reduces values. The ICT fluorescence shows triexponetial decay components (at 500 and 550 nm) for 5a molecules, then turns into biexponential at 600 and 650 nm. The slow component can be associated with the TICT state and the rest of the fast components are of diffent origins. And similar behaviour was observed with 5b molecule, triexponential decay components turn into biexponential at 650 nm. And, the fast

components at shorter wavelengths may be associated with rapid quenching of the molecules that do not reach the stabilised CT geometry.

Table 8.4 The quantum yields and fluorescence lifetime decays of ICT excited-state were measured for 5a and 5b in 2-MeTHF solution, and triplet state contribution on total fluorescence was elucidated by degassing the solution

Materials In 2-MeTHF ICT-state dynamics	**Quantum Yields (Φ_{ICT}) In 2-MeTHF in Air saturated/ Degassed And Quantum yield (Φ_{ILE}) In MCH Air saturated/ Degassed (%)**	**λ_x= 402 nm**			
		500 nm	**550 nm**	**600 nm**	**650 nm**
5a	**27.5 ± 3 / 35.6 ± 4 And 48.2 ± 1 / 57. 8 ± 3.1**	**τ_1= 3.76 ns A1=0.25 τ_2= 0.25 ns A2=0.05 τ_3= 6.4 ps A3=0.43 χ^2= 1.12**	**τ_1= 3.92 ns A1=0.23 τ_2= 0.1 ns A2=0.03 τ_3= 8.8 ps A3=0.02 χ^2= 1.17**	**τ_1= 4 ns A1= 0.24 τ_2= 0.06 ns A2=0.02 χ^2= 1.2**	**τ_1= 4.04 ns A1=0.23 τ_2= 0.04 ns A2=0.014 χ^2= 1.22**
5b	**20.7 ± 2 / 26.2 ± 3.6 And 31.6 ± 1.2 / 40. 3 ± 4.2**	**τ_1= 3.04 ns A1=0.30 τ_2= 0.22 ns A2=0.08 τ_3= 3 ps A3=5.85 χ^2= 1.08**	**τ_1= 3.18 ns A1=0.30 τ_2= 0.15 ns A2=0.05 τ_3= 6.3 ps A3=0.44 χ^2= 1.1**	**τ_1= 3.28 ns A1=0.30 τ_2= 0.08 ns A2=0.04 τ_3= 4.5 ps A3=0.01 χ^2= 1.15**	**τ_1= 3.32 ns A1=0.30 τ_2= 0.08 ns A2=0.03 χ^2= 1.2**

8.3.5 Time-resolved measurements

The nanosecond gated time resolved spectroscopy technique was employed to measure the decay dynamics in MCH solution and the results compared with the spin-

coated films. By way of this technique it is possible to record more than 12 orders of magnitude in intensity and more than 10 decades of time in one single experiment, therefore, it is possible to measure lifetime decays with totally covering both prompt (PF) and delayed fluorescence (DF) regimes simultaneously (in one curve) as shown in double logarithmic scales in Fig. 8.11.

In general, the initial fast part of the decay is assigned to PF, and the long slower decay component is assigned to DF, in particular, Fig. 8.11 a and b. include the lifetime decay of 5a and 5b either in degassed MCH solution (at RT and 90K) and spin-coated thin film (at RT and 25 K). In MCH, at RT, the lifetimes of PF were measured as 4.1±0.07 ns for 5a and as 3.5±1 ns for 5b which were emitting from the LE state as identified from the structured spectra of the emission as $^1(\pi\pi^*)$-PF (see Fig. 8.12 a and b), note that at RT, the DF was only measured for 5b material in MCH as 49.85 ±0.8 ns, but not for the 5a material. At 90 K, as seen in the steady state spectra, the molecules have a stabilised twisted/wagged geometry which can be confirmed with the time resolved spectra showing an unstructured, red-shifted and much broadened CT type emission comparing with the structured spectra at RT, clearly emission emanating from the TICT/WICT excited states at all decay times. This red-shifted emission was attributed to the DF, but not phosphorescence (PH), the reason is that the DF spectra appears energetically very close to PF emission in solid films (very good spectral overlap observed, see Fig. 8.12), so if the long-lived emission would belong to PH, the energy gap between locally excited singlet and triplet states should be high and will not arise from the same energy level of PF. Therefore, the emission totally arises from the ICT states. At 90 K, the measured lifetime decays represented the dynamics of the ICT states, resulting in biexponential PF (TICT/WICT-PF) decay dynamics; $\tau_{1=}$ 7.8± 0.5 ns, τ_2=53.46±1.8 ns for 5a and $\tau_{1=}$ 4.39± 0.28 ns, $\tau_{1=}$ 30.47± 1.9 ns for 5b. Then the decays transform into a power law (decay) regime ($I_{DF} \sim t^{-m}$) at longer times with an exponent of -1.2 for 5a and -3.2 for 5b. No phosphorescence emission could be observed for both of the materials at 90 K.

The spectra of spin-coated thin films are also represented in Fig. 8.12 a.b for 5a and 5b materials at RT and 25 K, where no significant time evolution was observed on spectra except for slight shifts of PF emission of 5a film at 25 K (the red unstructured curve rapidly evolve into unstructured spectra). And the lifetimes of PF (TICT/WICT-PF) were

measured as $\tau_{1=}$ 4.88 ±0.28, $\tau_{2=}$ 15.17± 0.93 ns for 5a and $\tau_{1=}$ 6.76± 0.49 ns, $\tau_{2=}$ 31.82± 1.27 ns for 5b at RT. The DF follows a biexponential lifetime decay for 5a at RT with $\tau_{1=}$ 111.2 ±3.9 ns and τ_2 = 430.74 ± 11.7 ns decays (which is distinctive, because no DF was observed for 5a in MCH solution at RT, but not surprising considering the packed nature of molecules in solid films), whereas the DF from 5b follows two power law regimes with the exponent of -3.2 then turns to -1.2 at later times at RT.

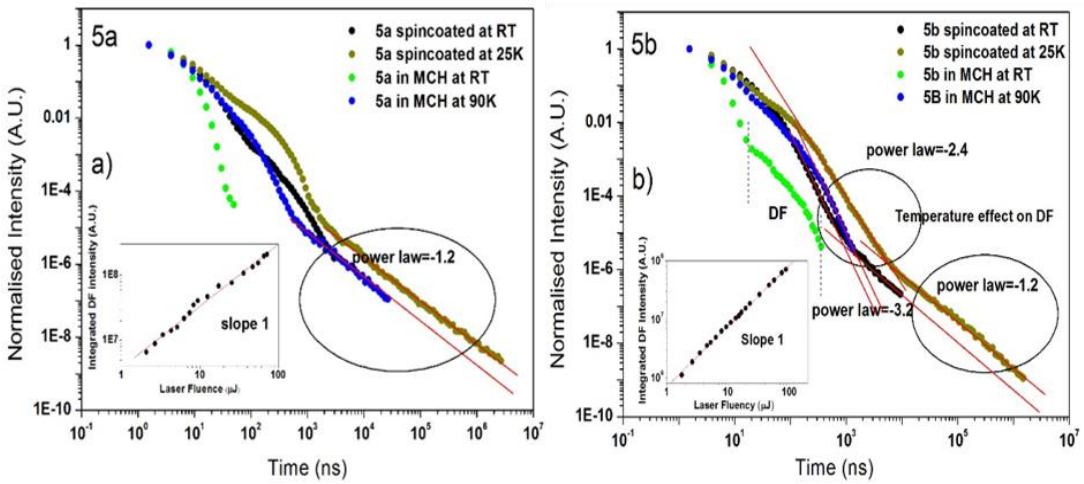

Figure 8.11 Log-log scale the lifetime decays **a)** 5a in MCH solution (both at RT and 90 K) and spincoated film (both at RT and 25 K) **b)** 5b in MCH solution (both at RT and 90 K) and spincoated film (both at RT and 25 K)**,** the laser fluence dependence of DF were inserted into the graphs

Once the temperature was lowered to 25 K, the PF lifetimes increased showing biexponential dynamics τ_1=11.55 ±0.73 ns, τ_2=165.54 ±3.97 ns for 5a and τ_1=5.81±0.34 ns, τ_2=62.8±2.86 ns for 5b. The DF of 5a decays following the transition from biexponential to power law regime ($I_{DF} \sim t^{-m}$) with an exponent of -1.2 (which is intriguing point to note as it is so similar a power law behaviour compared with the frozen solution at 90 K). The DF decay of 5b again follows two power law regimes; decays with the exponent of -2.4 at early times of the regime and then turns into -1.2 at later time ranges. Once again no phosphorescence emission could be observed with spin-coated films at 25 K.

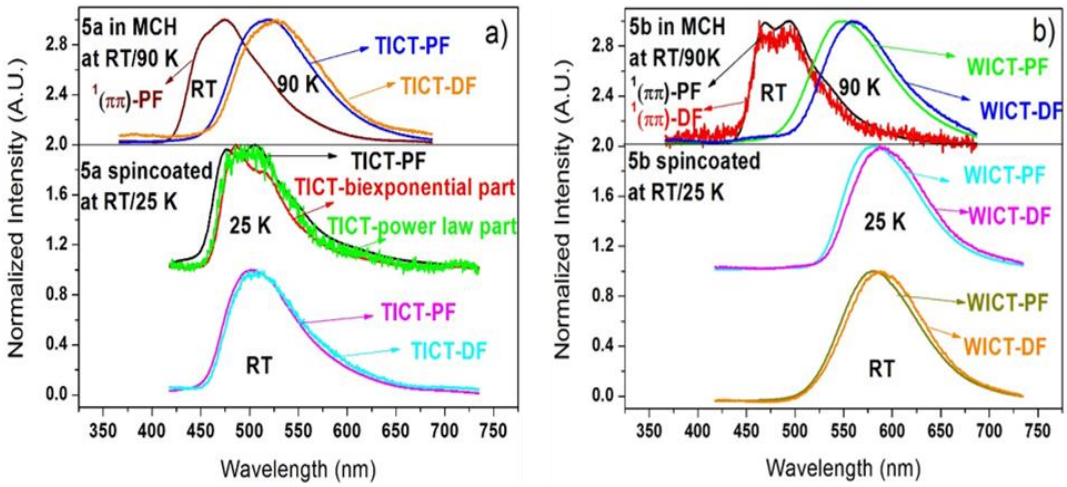

Figure 8.12 Time-resolved spectra of materials in MCH (at RT and 90 K) and spincoated film (at RT and 25 K) **a)** 5a **b)** 5b

In Fig. 8.12 a and b, the spectra observed at different delayed times. At room temperature both 5a and 5b PF and DF are nearly identical, clearly ICT in nature. The DF spectra show a hint of a red shoulder that shifts the peak of emission to the red. There exist no clear spectral separation of this feature so it is difficult to ascribe it to a phosphorescence component for example, it may be emission from a slightly different geometric ICT state. At 25 K, 5b yields the same behaviour as at room temperature, whereas 5a gives more complex structured PF and DF emission which appears to be some combination of species but well red shifted from the LE emission, this tends to shift more to fully ICT emission at longer times. In principle, the appearance of long-lived DF emission (power law regime) at low temperatures could be attributed to enhanced triplet state contribution upon total ICT emission[24] giving rise to DF via two possible mechanisms: triplet-triplet annihilation (TTA) or geminate-pair recombination (GPR).[25–28] In practice, the best way to distinguish these phenomena is either comparing the decay pattern of PH and DF, or measuring the DF intensity dependence upon the laser excitation intensity. If the (delayed) singlet excitons originate from the TTA then the DF decays either exponentially at half the PH lifetime or it shows t^{-2} power law decay dynamics as a result of the dominant bimolecular annihilation process, in addition, singlet generation via TTA mechanism, the DF emission should follow a quadratic (excitation) intensity

dependence, at low intensities ($I_{exc} \leq 10\ \mu J$) and then turn over into a linear law at high intensities($I_{exc} \geq 10\ \mu J$).[26] As here, the PH lifetime cannot be measured, therefore, only the DF intensity dependence on laser fluence could be recorded, covering the DF power law regime for spin-coated films at 25 K (2 µs- 70 µs for 5a, 10 µs- 80 µs for 5b) and frozen MCH solutions (1 µs- 10 µs for 5a, 0.1 µs- 1 µs for 5b). In all cases a linear (slope 1) dependence upon laser fluency was found (see Fig. 8.11 as inserted graph integrated DF intensity as a function of laser fluence) concomitant with a monomolecular decay process, not bimolecular processes as triplet-triplet annihilation.

Alternatively, monomolecular DF can arise from the decay of geminately bound electron-hole pairs (as happens in Chapter 4). According to Monte Carlo simulations upon geminate pair recombination phenomena[29,30] the electron-hole pairs show dispersive characteristics within their mutual coulombic potential and therefore result in time dependent power law decay $I \sim t^{-m}$ with m=1..1.3 for the delayed fluorescence which is in good agreement with the measured time dependence of 5a and 5b spin-coated film featuring a power law with the exponent of -1.2 at 25 K. In addition, if the geminate pair is generated as a result of bimolecular process, e.g. triplet-triplet annihilation, the DF intensity dependence should follow quadratic to linear intensity dependencies (which is not the case here). The electron-hole pairs here are generated as a result of a monomolecular process, i.e. dissociation of an excited state, with intensity dependence of the DF linear on excitation intensity (from low to high I_{exc} conditions). This behaviour was observed in spin-coated thin films at 25 K as well as in dilute frozen solutions with the same linear power-law dependency of the DF predominantly observed at low temperatures. To confirm the origin of the DF, the laser fluence dependence of DF for 5b material in dilute MCH solution was measured at RT, again it showed the same linear dependency upon I_{exc}. Thus, the major primary dissociation mechanism of excited states into geminate electron-hole pairs in these ICT states is an intramolecular process as reported by Vissenberg *et al*.[31] This also can explain why the quantum yield of emission reduces as the ICT state relaxes (to lower energy). With increased excess energy (the difference between the initial photo created state and the final ICT state), it will be easier for the delocalised electron hole pair to escape their mutual coulomb attraction and dissociate, if the geminate (and possible non-geminate) recombination process has a poor

radiative efficiency then with increasing relaxation the total emissive yield will decrease as the rate of dissociation increases.

8.4 Conclusion

The excited-state photophysical properties of novel family of donor-acceptor pyridine molecules with anthracene and triphenylamine donor units were investigated where the ground states have a large degree of rotation around the phenyl C-C bond in the ground state. Significant differences in emission spectra properties were observed as a function of temperature (from 295 K to 90 K) in non polar MCH and polar 2-MeTHF solutions. In particular, in MCH, as the temperature was lowered dual fluorescence appeared and, at RT, the emission only arose predominantly from the locally excited state where the ground-state geometry of the molecules have partially twisted or pyramid-shaped of D-A orientations. However, the observation of a resolved emission in MCH at RT showing a planarization in the excited state geometry, therefore, no CT-type emission is observed. However, once the solvent was frozen, and the geometry could not relax a broad, CT-type emission is observed confirming that perpendicular arrangement of ground state D-A is stabilised in the excited state.

By contrast, in 2-MeTHF the fluorescence was always that of the ICT state and the spectrum gradually red-shifts through the glass transition temperature (~135 K), but then, upon cooling the temperature (<135 K) the spectra significantly shifted to the blue resulting in ICT emission from an unrelaxed molecular geometry, but not the LE state. Thus, only at high temperature and in non polar solvent is the ICT emission not observed, a result also confirmed from solid state measurements where again only ICT emission was observed. This highlights the key role of specific solvent-solute interactions in the vicinity of solvation dynamics where vibrational excitation of the molecule at high temperature coupled with the lack of solvent polarity destabilises the twisted molecular structure to allow planarisation and conjugation to over come ICT formation. In addition, the investigations revealed that the twisted ground-state molecular conformations were retained in spin-coated thin films ensuring ICT stabilisation and emission as required for dominant ICT emission in a device setting. Delayed fluorescence predominantly

originated from monomolecular recombination of the geminately bound electron-hole pairs and it is believed that this can be a major loss mechanism of quantum yield in ICT systems and particularly as the ICT state moves to lower energy the competition with dissociation becomes acute. It is clear that to achieve ICT excited states in the solid state, the active emitter molecule must have a ground state configuration that stabilises the charge transfer state and this must be ‘locked-in’ in the solid state.

8.5 References

1. Lakowicz, J. R. *Principles of Fluorescence Spectroscopy*. (Springer US, 1999).
2. Rettig, W., Braun, D., Suppon, P., Vauthey, E., Rotkiewicz, K., Luboradzki, K. & Suwinska, K. Molecular-Conformation and Excited-State Dipole-Moments of Di-Methylaminobenzonitrile and Tetramethylaminobenzonitrile (dmabn and Tmabn). *J. Phys. Chem.* **97,** 13500–13507 (1993).
3. Mataga, N., Kaifu, Y. & Koizumi, M. Solvent Effects Upon Fluorescence Spectra and the Dipolemoments of Excited Molecules. *Bull. Chem. Soc. Jpn.* **29,** 465–470 (1956).
4. Grabowski, Z. R., Rotkiewicz, K. & Rettig, W. Structural changes accompanying intramolecular electron transfer: Focus on twisted intramolecular charge-transfer states and structures. *Chem. Rev.* **103,** 3899–4031 (2003).
5. Lippert, E. Dipolmoment Und Elektronenstruktur Von Angeregten Molekulen. *Z. Naturforschung Part -Astrophys. Phys. Phys. Chem.* **10,** 541–545 (1955).
6. Rotkiewicz, K., Grellman, K.H., & Grabowski, Z.R. Reinterpretation of Anomalous Fluorescence of "Para-N,n-Dimethylamino-Benzonitrile. *Chem. Phys. Lett.* **19,** 315–318 (1973).
7. Rettig, W. Charge Separation in Excited-States of Decoupled Systems - Tict Compounds and Implications Regarding the Development of New Laser-Dyes and the Primary Processes of Vision and Photosynthesis. *Angew. Chem.-Int. Ed. Engl.* **25,** 971–988 (1986).
8. Li, W., Liu, D.D., Shen, F.Z., Ma, D.G., Wang, Z.M., Feng, T., Xu, Y.X., Yang, B. & Ma, Y.G. A Twisting Donor-Acceptor Molecule with an Intercrossed Excited State for Highly Efficient, Deep-Blue Electroluminescence. *Adv. Funct. Mater.* **22,** 2797–2803 (2012).
9. Chandross, E. A. & Thomas, H. T. Intramolecular exciplex formation in naphthylalkylamines. *Chem. Phys. Lett.* **9,** 393–396 (1971).
10. Brooks, P. R. Electron transfer, harpooning, reagent orientation, and chemical intuition. *Mol. Phys.* **110,** 1729–1738 (2012).
11. Shephard, M. J. & Paddon-Row, M. N. Electrostatically driven geometry changes accompanying charge separation in supposedly rigid bichromophoric systems. *J. Phys. Chem. A* **104,** 11628–11635 (2000).
12. Goes, M., de Groot, M., Koeberg, M., Verhoeven, J.W., lokan, N.R., Shephard, M.J. & Paddon-Row, M.N. Temperature dependence of charge-transfer fluorescence from extended and U-shaped donor-bridge-acceptor systems in glass-forming solvents. *J. Phys. Chem. A* **106,** 2129–2134 (2002).
13. Grabowski, Z. R., Rotkiewicz, K. & Rettig, W. Structural changes accompanying intramolecular electron transfer: Focus on twisted intramolecular charge-transfer states and structures. *Chem. Rev.* **103,** 3899–4031 (2003).

14. Bangal, P. R., Panja, S. & Chakravorti, S. Excited state photodynamics of 4-N,N-dimethylaminocinnamaldehyde: A solvent dependent competition of TICT and intermolecular hydrogen bonding. *J. Photochem. Photobiol. Chem.* **139,** 5–16 (2001).
15. Ladanyi, B. & Foriero, A. A numerical solution of cavity expansion problem in sand based directly on experimental stress-strain curves. *Can. Geotech. J.* **35,** 541–559 (1998).
16. Aydemir, M., Haykir, G., Turksoy, F., Gumus, S., Dias, F.B., Monkman, A.P. Synthesis and investigation of intra-molecular charge transfer state properties of novel donor-acceptor-donor pyridine derivatives: the effects of temperature and environment on molecular configurations and the origin of delayed fluorescence. *Phys. Chem. Chem. Phys.* **17,** 25572–25582 (2015).
17. Raikar, U. S., Tangod, V. B., Mannopantar, S. R. & Mastiholi, B. M. Ground and excited state dipole moments of coumarin 337 laser dye. *Opt. Commun.* **283,** 4289–4292 (2010).
18. Dubroca, C. Temperature Effect Upon Uv Absorption-Spectra of Aniline Derivatives. *Chem. Phys. Lett.* **15,** 207- (1972).
19. Gorlach, E., Gygax, H., Lubini, P. & Wild, U. Solvent Relaxation of Oxazine-4 in 2-Methyltetrahydrofuran. *Chem. Phys.* **194,** 185–193 (1995).
20. Damrauer, N. H. & McCusker, J. K. Variable-temperature emission studies of solvation dynamics: Evidence for coupling of solvation to chromophore structural dynamics in the evolution of charge-transfer excited states. *Inorg. Chem.* **38,** 4268–4277 (1999).
21. Bublitz, G. U. & Boxer, S. G. Effective polarity of frozen solvent glasses in the vicinity of dipolar solutes. *J. Am. Chem. Soc.* **120,** 3988–3992 (1998).
22. Kawski, A., Kuklinski, B. & Bojarski, P. Temperature influence on dual fluorescence of 4-(dimethylamino) benzaldehyde in 1,2-dichloroethane and ethyl acetate. *Chem. Phys. Lett.* **455,** 52–54 (2008).
23. Pereira, R. V., Ferreira, A. P. G. & Gehlen, M. H. Excited-state intramolecular charge transfer in 9-aminoacridine derivative. *J. Phys. Chem. A* **109,** 5978–5983 (2005).
24. King, S. M., Matheson, R., Dias, F. B. & Monkman, A. P. Enhanced triplet formation by twisted intramolecular charge-transfer excited states in conjugated oligomers and polymers. *J. Phys. Chem. B* **112,** 8010–8016 (2008).
25. Rothe, C., Hintschich, S. I. & Monkman, A. P. Violation of the exponential-decay law at long times. *Phys. Rev. Lett.* **96,** 163601 (2006).
26. Hayer, A., Bassler, H., Falk, B. & Schrader, S. Delayed fluorescence and phosphorescence from polyphenylquinoxalines. *J. Phys. Chem. A* **106,** 11045–11053 (2002).
27. Koehler, A. & Baessler, H. Triplet states in organic semiconductors. *Mater. Sci. Eng. R-Rep.* **66,** 71–109 (2009).

28. Aydemir, M., Jankus, V., Dias, F. B. & Monkman, A. The key role of geminate electron-hole pair recombination in the delayed fluorescence in rhodamine 6G and ATTO-532. *Phys. Chem. Chem. Phys.* **16,** 21543–21549 (2014).
29. Ries, B. & Bassler, H. Monte-Carlo Study of Dispersive Charge-Carrier Transport in Spatially Random-Systems with and Without Energetic Disorder. *Phys. Rev. B* **35,** 2295–2302 (1987).
30. Nikitenko, V. R., Hertel, D. & Bassler, H. Dispersive geminate recombination in a conjugated polymer. *Chem. Phys. Lett.* **348,** 89–94 (2001).
31. Vissenberg, M. & deJong, M. J. M. Theory of exciton migration and field-induced dissociation in conjugated polymers. *Phys. Rev. Lett.* **77,** 4820–4823 (1996).

CHAPTER 9: CONCLUDING REMARKS AND FUTURE WORK

Throughout the course of this thesis, the origin of delayed fluorescence (DF) was investigated in variety of organic molecules including dye molecules, a polymer and small molecules. Each of the molecules was particularly chosen for the purpose of developing new perspectives on structure-DF relationships by way of comparing the molecules in a variety of environments. Considering that a number of general conclusions can be drawn from the various chapters.

In Chapter 4, the origin of DF is investigated in Rh6G and ATTO-532. It was systematically shown how the origin of DF can be distinguished from previously suggested DF mechanisms. For this purpose, the typical characteristics of triplet-triplet annihilation (TTA) and thermally activated delayed fluorescence (TADF) mechanisms were represented and compared with experimental findings taken from Rh6G and ATTO-532. In this way, a general picture was determined experimentally of typical DF behaviours, then, this chapter was used as a "model chapter" for the rest of the thesis. According to the findings, it was shown that a monomolecular process was operative behind the DF. This process was designated as "geminate-pair recombination (GPR)". The GPR results from optically generated electron-hole pairs on dimer species rather than TTA or TADF. Consequentially, for the first time the origin of DF was clarified in these dye molecules.

In Chapter 5, the complex excited state dynamics of polyspirobifluorene (PSBF) were investigated as a function of temperature in two solvents of differing polarity. It was shown that "inter/intrachain" interactions were significantly affected by solvent polarity and viscosity. Then the type of interactions between polymer chains were designated as the key factors behind the formation of charge transfer (CT) states. Active roles of CT states were found to reduce the singlet-triplet energy gap, thus allowing the exciton to cycle between the excited states. In this way, the CT state was involved in total fluorescence by means of taking an active role in a mixed DF mechanism (CT+ TTA), which was confirmed by calculating the empirical value of the quantum yield of delayed fluorescence (Φ_{DF}). Consequentially, the findings of this chapter helped to make a good

interpretation of the up-conversion data obtained from by PSBF/Zeonex film in Chapter 6.

In Chapter 6, a two-pulse-pump excitation method was used to get a better understanding of possible photophysical mechanisms in PSBF/Zeonex film, which result in a high Φ_{DF} value (0.34). According to the energy states of PSBF ($2xE_{T_1} > S_1$ and $2xE_{T_1} > E_{T_N}$), the maximum contribution to Φ_{DF} from TTA was limited by 0.2 (only TTA contribution), and an additional contribution of 0.14 was attributed to an induced TADF contribution, arising from the decay of upper excited triplet states (T_N) to the ^{3}CT state rather than directly to the $^3(\pi,\pi^*)$ state. Consequentially, according to the findings in this chapter, the TTA can generate singlets in two ways; first of all *via* triplet fusion, where the encounter complex gains sufficient singlet wave function character that two triplets become a singlet state. Secondly, a distinct process requiring an intermediate charge transfer state. The normally unused T_N state formed *via* the TTA triplet channel under conditions of 2x $E_{T_1} > T_N$ then decay by electron transfer to ^{3}CT, giving rise to triplets which are harvested *via* TADF mechanism through the emissive ^{1}CT state. This intensity enhancement was observed to as a DF signal arising from the ^{1}CT state. To understand the T_N state contribution to a mixed DF mechanism (TTA+TADF), the requirement carrying out a two-pulse-pump experiment was highlighted.

In Chapter 7, triplet properties of novel anthracene derivatives were investigated using a sensitizer-acceptor based up-conversion mechanism. According to the findings, an understanding was developed of the molecular structures of anthracene based novel acceptor molecules where structural modifications can be made to improve the efficiency for the next generation or up-conversion applications. With these results the question of how the side groups having different electron donating, withdrawing or neutral units affect the triplet-triplet annihilation efficiency and triplet energy transfer efficiency were also clarified. Comparing the results the best triplet transfer efficiency was observed with the molecules including electron donating groups, which suggest that the molecules having electron donating groups might be alternative molecules which could be used to obtain high quantum efficiency from up-conversion. In addition, the presence of a mixed triplet harvesting mechanism (TTA+TADF) was found in one of the materials, which was

in good agreement with the findings in Chapter 6. This particular mechanism was highlighted as a desirable alternative system to get high efficiency in potential devices.

In Chapter 8, the formation of TICT/WICT states was investigated in donor-acceptor-donor type pyridine derivatives. The investigations revealed that the twisted ground-state molecular conformations were retained in spin-coated thin films ensuring ICT stabilisation and emission as required for dominant ICT emission in a device setting. Delayed fluorescence predominantly originated from monomolecular recombination of the geminately bound electron-hole pairs and it was believed that this can be a major loss mechanism of quantum yield in ICT systems, particularly since as the ICT state moves to lower energy the competition with dissociation becomes acute. It was clear that to achieve ICT excited states in the solid state, the active emitter molecule must have a ground state configuration that stabilises the charge transfer state and this must be 'locked-in' in the solid state.

9.1 Future Work

The investigations presented in this thesis developed a deeper understanding of structure-DF relationship in particularly chosen molecules. They can be used as reference materials to design novel molecular structures to get a high contribution to the total fluorescence *via* delayed fluorescence phenomena.

The mixed DF (both TTA and TADF operative) mechanism was highlighted as one of the desired alternative systems to obtain high efficiencies in potential device applications. Therefore, it would be interesting to study the molecular geometry of the molecules, in order to determine whether a rigidly perpendicular arrangement of donor-acceptor units is the key factor behind the operative TADF or dynamic rocking about orthogonality gives rise to a larger TADF contribution. To understand this, X-ray crystallographic data might be useful to investigate. In addition, the cycling process between charge transfer states (^{1}CT-^{3}CT) was reported as an important mechanism behind the TADF. Therefore, it would be also interesting to carry out computationally the vibronic coupling dynamics between ^{1}CT-^{3}CT states, so that an understanding can be

developed of how this coupling mechanism effects the reverse intersystem crossing rate (k_{rISC}). Such modelling studies will give more insight into the dynamical mechanisms for highly efficient TADF and open design routes for the future development of high performance systems.